# POST-IRRADIATION EXAMINATIONS OF WWER-440 FA PROVIDED WITH STAINLESS STEEL SPACER GRIDS

A.V. SMIRNOV, V.P. SMIRNOV, D.V. MARKOV,
V.S. POLENOK, B.A. KANASHOV, V. SHISHIN
State Scientific Center "Research Institute of Atomic Reactors",
Dimitrovgrad, Russian Federation

**Abstract**

The WWER-440 fuel assembly (FA) design incorporates 4158 junctions at the place of contact between fuel rod and spacer grid (SG) cell. That is why examination of cladding fretting is of importance for prediction and assurance of its serviceability in case of long-term operation period. An integral criterion, which characterizes the FR tightening in the spacer grid cells of spent fuel assemblies, is the force of their extraction from the bundle. The analysis revealed that steel spacer grids ensure a reliable tightening of FR claddings up to the average fuel burnup of ~50MW·day/kgU over the fuel assembly. As a rule, fretting tracks on FR claddings of WWER-440 leak-tight fuel assemblies looked like shallow scratches or insignificant abrasion at the place of contact with the spacer grid cells. The post-irradiation examinations of WWER-440 untight fuel assemblies revealed fretting tracks to be significant in depth (right up to through-the- thickness ones) at the place of contact with cells of the lower steel SG-1-SG4. The deposits on fuel rods and spacer grids are the most probable cause of this phenomenon because of the primary circuit contamination.

## 1. INTRODUCTION

Fretting of fuel rods claddings under the spacer grids is one of the main reasons leading to failure of FR claddings in LWR. So according to the data published in paper [1], currently the causes of PWR fuel rod damage are as follows:

- Fretting of fuel rod claddings under the spacer grids (grid-rod fretting) - 40-45%;
- Interaction between fuel rod claddings and debris in the coolant flow (debris-fretting) - 40-45%;
- Undetermined causes and causes conditioned by violation of the fuel production technology- the rest.

As the WWER-440 fuel assembly incorporates 4158 junctions at the place of contact between fuel rod and spacer grid, the study of cladding fretting phenomenon is of importance for prediction and assurance of its serviceability in case of fuel cycle prolongation or increase in their number. Vibrations, which are inevitably occur in the pressurised water reactors, can induce propagation of cladding fretting at these particular places of junction under the adverse conditions.

In general fretting (sometimes "fretting-corrosion" term is used) is in the aggregate the processes of mechanical wear of contact surfaces during their cyclic sliding with each other or impact and chemical interaction of the surface layers with the environment. The following factors can be distinguished among those ones that induce fretting of FR claddings under the spacer grids:

- vibration frequency and amplitude,
- pressing force of contact surfaces,

- period of exposure,
- quality of FR fixation in the bottom support plate,
- quality of spacer grid fixation on the central tube.

Some factors directly depend upon the quality of FA fabrication and ability of FA components to retain geometrical stability during operation. Moreover, the coolant flow and pressure fluctuations caused by either the operation of the main circulation pumps (blade-impulse frequency) and the character of the coolant flow affect the FA and its components in the reactor. The system of coolant stream separation in the assembly, spacer grids and other devices cause pressure fluctuations in the flow. These power sources can induce and sustain vibration of fuel rods.

In 1996 Russian WWER-440 fuel manufacturers turned to manufacturing FA with zirconium spacer grids. Implementation of zirconium spacer grids was accompanied with the problems, which mainly were overcome. Currently wide experience in post-irradiation examination of FA with zirconium spacer grids was accumulated. Nevertheless, it is expedient to renew the results of operation of FA with stainless steel spacer grids in order to compare them with the results of operation of FA with zirconium spacer grids.
The present report presents the results of WWER-440 FR cladding state analysis at the place of their contact with the stainless steel spacer grid. The conclusions are made based on the experimental data obtained in SSC RF RIAR, Novovoronezh NPP and «Loviisa» NPP in the course of post-irradiation examinations of spent fuel assemblies. In particular at SSC RF RIAR 10 spent WWER-440 FA were examined. 8 FA of them were with stainless steel spacer grids and 2 FA with zirconium spacer grids.

## 2. FUEL ROD FIXATION IN WWER-440 SPENT FUEL ASSEMBLIES

The operation lead to the increase in diameter of the spacer grid cells and decrease in diameter of FR claddings that has immediate effect upon the fixation of fuel rods in the bundle. A force applied for removal of fuel rods from the bundle is the integral parameter that characterizes fixation of fuel rods in the spacer grid cells. Fig.1 shows this parameter versus fuel burnup for fuel rod bundles with the stainless steel and zirconium spacer grids. The given data suggest that both types of spacer grids assure fixation of fuel rods up to the average fuel burnups of ~ 50 MWd/kgU over the fuel assembly.

All fuel rods subjected to examination were effectively fastened with pin wire in the bottom support plate. Fixation of spacer grids on the central tube corresponds to design requirements. Attachment points didn't have any visible defects. There were no noticeable material wear on the central tube at the place of spacer grid attachment.

## 3. EDDY-CURRENT TESTING AND RESULTS OF VISUAL INSPECTION OF CLADDINGS AND SPACER GRIDS

The SSC RF RIAR applied two techniques to reveal fretting marks. They are eddy current testing and visual inspection using optical systems. Some fuel assemblies were subjected to the complete inspection of claddings using the pulse-type EC-defectoscopy during the bundle dismantling. The inspection was run in the continuous mode with the use of EC-detector of through-flow type. According to the results of EC-defectoscopy fuel rods with abnormal eddy-current signals were selected for visual inspection.

As a rule, fretting marks on the fuel rod claddings of the WWER-440 leak-tight fuel assemblies looked like shallow scratches or slight abrasions at the places of contact with the spacer grid cells at fuel burnups of ~50 MW·day/kgU [2].

As an illustration we refer to Fig.2 where marks of cladding fretting are shown for fuel rods of WWER-440 fuel assembly that has been operated during three fuel cycles in the fourth unit of Novovoronezh NPP up to the average fuel burnup of 34.1 MWd/kgU. All fuel rods of this FA exhibit the marks of contact interaction with the spacer grids. The marks of such interaction were located at three points along the perimeter of fuel rod at the place of contact with the spacer grid cells. The marks of contact interaction were partially covered by white spots on some fuel rods (Fig. 2b).

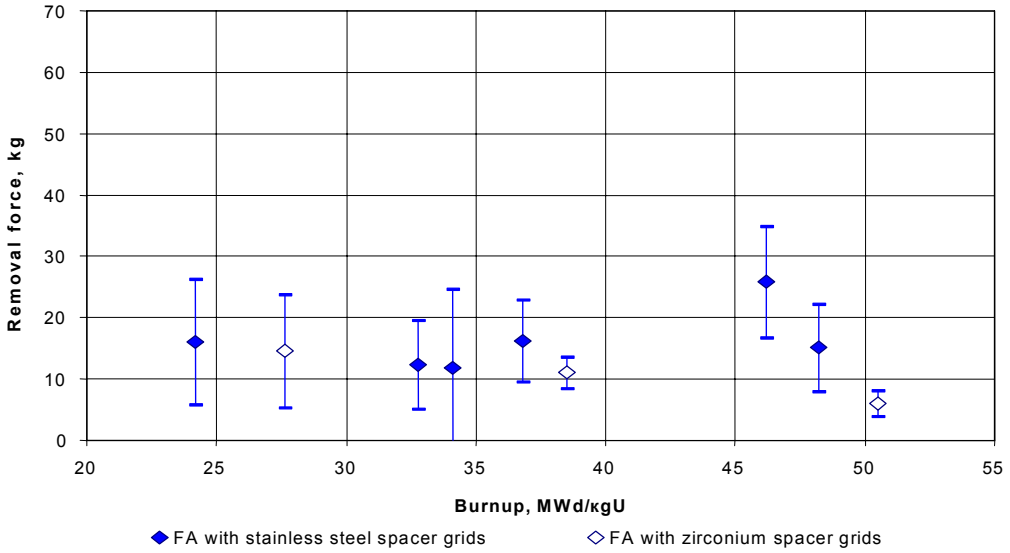


*FIG.1. Force applied for WWER-440 fuel rod removal versus fuel burnup*

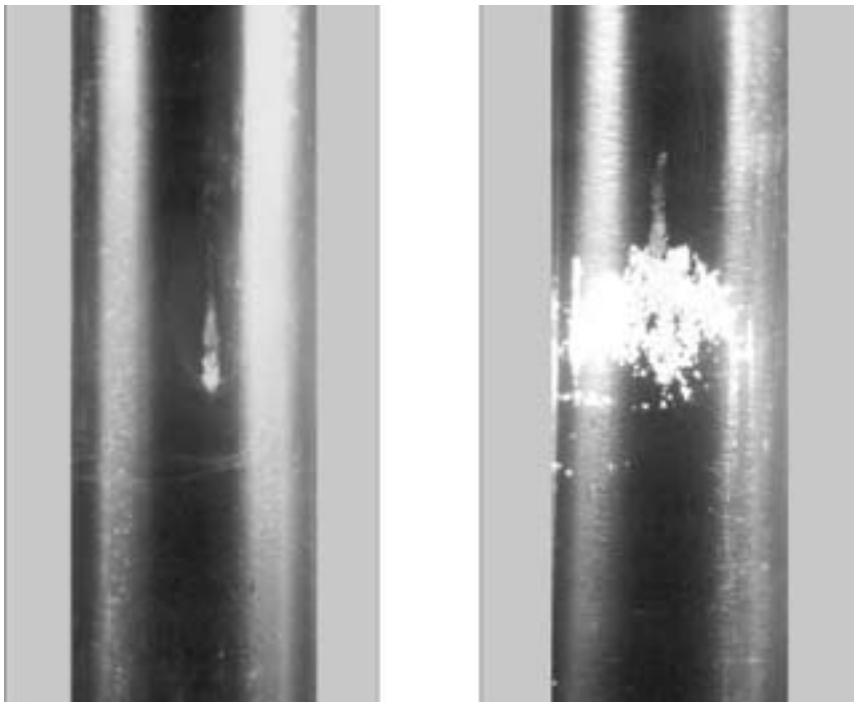

*FIG. 2. Typical marks of contact interaction of WWER-440 fuel rods with spacer grids*

The post-irradiation examinations of WWER-440 untight fuel assemblies operated at Novovoronezh and «Loviisa» NPPs [3, 4] revealed considerable marks of fuel rod cladding fretting, which differ in depth and wear rate (up to the through-the-thickness ones) at the place of contact with the bottom stainless steel spacer grid (from SG1 to SG4).

In 1989 some FAs were manufactured for the3d unit of Novovoronezh NPP. Stainless steel spacer grids of the same batch were used there. Based on the results of tightness test all FAs were tight. However on one of them became leaky during the 4th year of operation fretting traces were detected both on spacer grid cells and claddings. Places of interaction between spacer grids 1-4 and fuel rods of this FA have wearing of different degree. Especially severe wearing is observed on spacer grids №1, 2 (fig3). As a whole the examined grids revealed that the preferred orientation of cells to be subjected to greater fretting was absent. However each spacer grid revealed the preferred orientation of the cell to be subjected to the least fretting. But this orientation is different for different types of spacer grids.

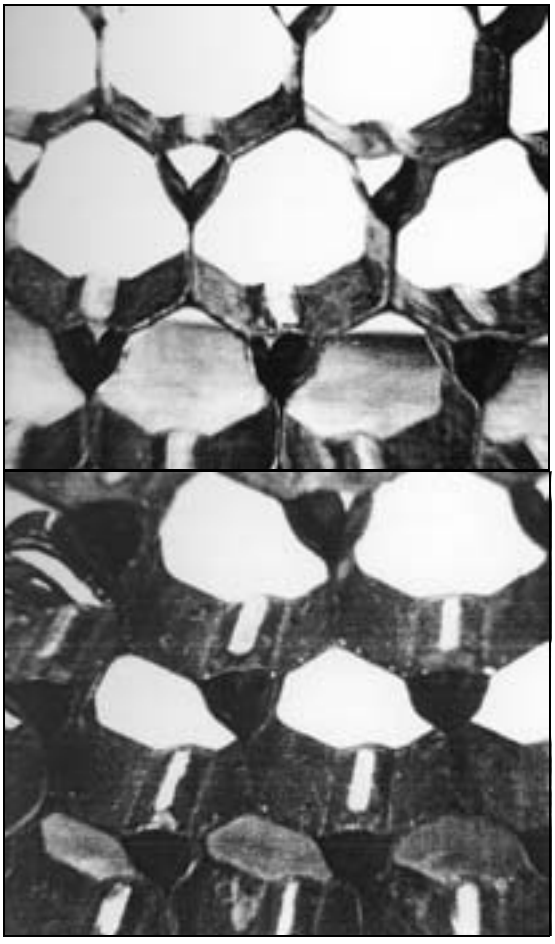


*FIG.3. Visual appearance of spacer grid 1 (a) and spacer grid 2 (b)*

All fuel rods exhibited abrasion of claddings that was different in depth at the place of contact with spacer grid 1 and spacer grid 2 (Fig.4). Some fuel rods exhibited marks of fretting at the place of contact with other spacer grids (SG3, SG4). Two arbitrarily selected fuel rods (No. 14 and 94) were subjected to measurement of the maximal depth of cladding fretting that constituted ~0.43mm. Fuel rod No. 72 and fuel rod No.105 exhibited the through-the-thickness abrasions (up to the fuel pellet) of cladding at the place of contact with spacer grid 1.

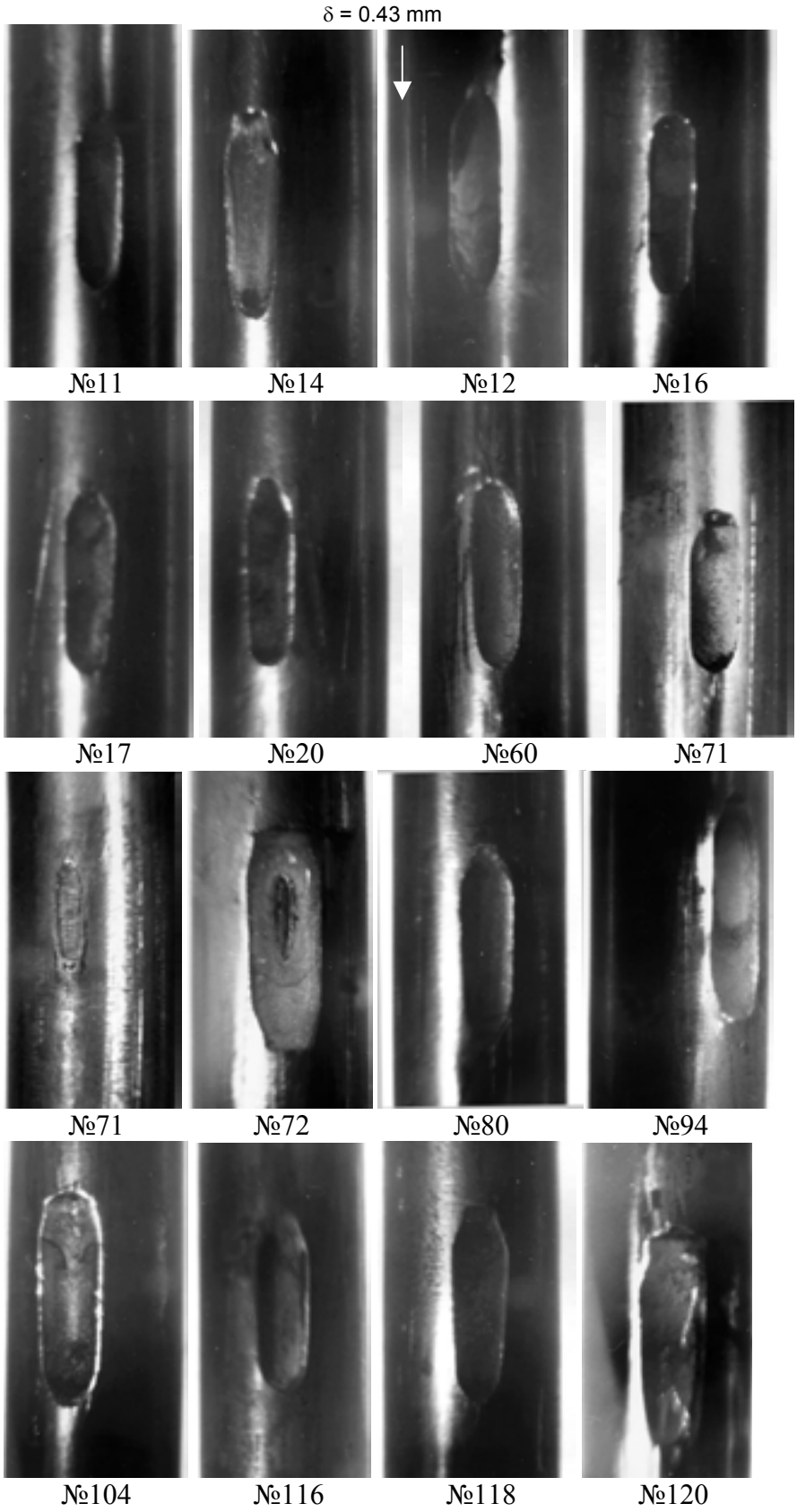


*FIG.4. Visual appearance of cladding fretting at the places of contact with spacer grids*

Ten fuel rods exhibited greater degree of fretting were subjected to inspection to estimate the preferred azimuthal orientation of abrasions. The size of abrasions and their positional relationship under all spacer grids were the subject of estimation. The inspection didn't reveal any preferred azimuthal orientation regarding the location of defects. The greatest degree of abrasion was found out throughout the fuel rod height without any definite orientation. The results of fuel rod inspection are in good agreement with the results of visual inspection of spacer grids, which in their turn haven't revealed the preferred orientation of abrasion for the spacer grid cells.

Moreover it might be well to point out that the greater part of FR cladding surface and spacer grids was covered with a thin layer of deposits, which are black in color and exhibit the maximal degree of darkening at the place of spacer grid location. The primary circuit contamination during the maintenance between the refueling procedures is among the possible causes of such deposits.

Some fuel assemblies provided with the stainless steel spacer grids became untight during the primary circuit washing out of the «Loviisa-2» NPP. The PIE and inspection of assemblies were carried out in Finland using the inspection rig.

The performed examinations revealed that the fuel rod bundles and the spacer grids of assemblies particularly, which were operated after the primary circuit washing out, were covered with corrosion products. As for fretting of failed fuel rod claddings it was similar to abrasion of fuel rod claddings in Novovoronezh NPP FAs. Spacer grids of №SG1–SG3 were covered with the definite deposit layers, which showed partial exfoliation on the walls of the outer cells. Abrasion of claddings was found on the fuel rods. Its marks were beyond the height of spacer grid cells (10mm) and extended above and below the spacer grids. Through holes were discovered on the claddings during examinations. They were arranged along the axis at the centre of abrasion marks under the spacer grid 2 cells. According to the results of examination at least seven fuel rods in the outer row of this FA were unsealed. The similar results were obtained for another FA that incorporated eight unsealed fuel rods in the outer row of the bundle.

In doing so the most probable cause of higher vibration of fuel rod bundles in this and other case is the presence of deposits on the fuel rods and spacer grids resulted from the primary circuit contamination.

## 4. CONCLUSION

The following conclusions on fretting corrosion of WWER-440 fuel rod claddings can be made according to the analysis results. The examination of ten fuel assemblies (1260 fuel rods) provided with either the stainless steel and zirconium spacer grids at the SSC RF RIAR didn't reveal any case of seal failure due to fretting-corrosion. All fretting defects found at the place of rod-grid junction were small in depth. The stainless steel spacer grids ensure the reliable fixation of fuel rods in the bundle in the course of long-term operation up to five fuel cycles. Additional examinations are required to make such conclusions related to zirconium spacer grids. The most probable cause of fuel rod depressurization according to the fretting mechanism occurred at Novovoronezh and "Loviisa-2" NPPs is the primary circuit contamination.

## REFERENCES


[1] Yu. TVELOV, Rate and causes of fuel rod failures in power reactors, Atomnaya Technika za rubezom, 1 (2000) 22-26 (in Russian).

[2] E. BECK, A. ENINE, A. IVANOV et. al. Atlas "State of the VVER spent fuel rod cladding", Novosibirsk 1999.

[3] A.K. PANJUSHKIN, E.G. BECK, V.A. TSIBULJA, et al, Definition of untightness of working assembly №13634250, irradiated 4 years at the Unit 3 of Novovoronezh, Report presented at the Russian-Finnish Seminar on exchange of experiencein operation of VVER-440 assemblies, Helsinki, Finland (1999).

[4] R. TERASVIRTA, Fuel design and operational experience in Loviisa NPP, future trends in fuel issues, Report presented at the international Conference on WWER Fuel Performance, Modeling and Experimental Support, Albena, Bulgaria, 1-5$^{th}$ October, 2001 (to be published).

# CHANGES IN GEOMETRY OF CLADDINGS AND FUEL COLUMNS OF SPENT WWER-440 AND WWER-1000 FUEL RODS UNDER STEADY-STATE AND TRANSIENT OPERATING CONDITIONS

B. KANASHOV, S. AMOSOV, G. LYADOV, D. MARKOV,
V. OVCHINNIKOV, V. POLENOK, A. SMIRNOV, A. SUKHIKH
State Scientific Center "Research Institute of Atomic Reactors,
Dimitrovgrad, Uljanovsk Region

Ye. BEK
JSC "Mashinostroitelny zavod, Electrostal, Moscow Region

A. YENIN
JSC “Novosibirsk Chemical Concentrates Plant”, Novosibirsk

V. NOVIKOV
JSC "TVEL", Moscow

Russian Federation

**Abstract**

The report represents the main results of post-irradiation examinations of WWER-440 and WWER-1000 high burnup fuel rods operated in commercial reactors during 3-5 fuel cycles under steady-state operation conditions up to the maximal fuel rod burnup of 62.3 and 57.8 MWday/kgU. The results of fuel rod testing in research reactors during single and graduate power changes within the range of linear power of 100-400 W/cm and 100-500 are considered. The main concern is given to the changes in geometry of the cladding and the fuel column and mechanical interaction between them. Thermomechanical fuel-cladding interaction after 4 and 5 fuel cycles doesn't limit WWER cladding efficiency. Fuel rod testings under transient conditions at high levels of linear power confirmed this conclusion: all of the tested fuel rods remained tight and the cladding diameter changed insignificantly. High capability of WWER-440 and WWER-1000 fuel rods to resist swelling fuel column impact is illustrated both in steady-state and transient operation conditions.

## 1. INTRODUCTION

The degree of geometry variability of fuel rods (FR), cladding and fuel column is one of the most important characteristics of their serviceability. But on the other hand the geometrical parameters influence much on other FR characteristics such as fuel temperature, fission gas release, fuel-to-cladding interaction and cladding stress strained state as well as degree of interaction with the FA skeleton elements and skeleton rigidity.

The geometrical parameters of WWER-440 and WWER-1000 cladding and fuel column don’t’ differ considerably as (they) delivered from the factory. The principal difference is the value of the central hole diameter. The central hole diameter for WWER-440 pellet is 1.2mm and for WWER-1000 is 2.4mm. More than that the outer diameter of the WWER-440 pellet is 7.59 mm at the initial state and as for the WWER-1000 pellet it is 7.55 mm [1]. At the same time the design operating conditions of WWER-440 and WWER-1000 fuel rods differ [2,3]: the average linear power is 129 and 167 W/cm$^2$, coolant temperature -312 and 335°C and coolant pressure -12.5 and 16 MPa for WWER-440 and WWER-1000, respectively. Coolant-

fuel rod pressure difference is also higher for WWER-1000 core. So, the operation conditions for WWER-1000 fuel rods are severe.

Nevertheless, the post-irradiation examinations of WWER-440 and WWER-1000 fuel assemblies and fuel rods operated 3 fuel cycles under the design basis conditions don't reveal any considerable differences in the geometrical parameters changes in FR components. Rates of FR elongation, cladding diameter decrease, fuel column swelling are practically indistinguishable within the limits of statistical dispersion.

Differences in WWER-440 and WWER-1000 FR state become apparent at a burnup higher than 40 MWd/kgU that is the fourth year of operation. They were confirmed by the results of high burnup FR testing in the MIR reactor under transient conditions. The present report is dedicated to the peculiarities of geometrical parameters changes in WWER-440 and WWER-1000 claddings as well as fuel column at high burnups.

## 2. OPERATION CONDITIONS

### 2.1. Subjects of examination

Spent fuel assemblies are chosen for post-irradiation examination (PIE) at annual meetings with participation of experts of the branch, manufacturers, users, designers and fuel researchers. By the present the full-size examinations of 10 WWER-440 fuel assemblies and 20 WWER-1000 fuel assemblies have been carried out.

All WWER fuel assemblies of standard type were investigated in RIAR hot cells to evaluate fuel serviceability after 3, 4 and 5 fuel cycles under normal operation conditions. Some investigated fuel assemblies achieved fuel burnup exceeding the designed burnup and were of deep interest. The most attention was paid to new potentially negative phenomena, which may occur at higher burnups.

This amount of fuel assemblies were used as the base for summarizing and conclusions on behaviour of WWER-440 and WWER-1000 high burnup fuel rods operated in power reactors.

### 2.2. Change in cladding outer diameter

It has been known that the outer diameter of WWER FR claddings decreases [4] because of coolant-fuel rod pressure difference and Zr-1%Nb alloy creep. The axial profile of the cladding outer diameter represents the axial distribution of neutron-flux density and temperature up to the moment of fuel-to-cladding contact. The maximum decrease of the cladding diameter was noticed in the central part of fuel rod. Difference ($\Delta d_1$) in the average diameters of the cladding in the region of gas plenum and maximum linear power one was taken to estimate the diameter decrease. Fig.1 demonstrates the change in difference according to the fuel burnup in WWER- 440 and WWER-1000 fuel rods. As may be seen from the diagrams, the decrease in the cladding diameter for WWER-440 and WWER-1000 fuel rods follows nearly the same law up to burnups of 40-45 MWd/kgU. As for WWER-440 fuel rods, the cladding diameter stops decreasing at the burnups higher than 50 MWd/kgU. The data for this particular range of burnups are absent for WWER-1000 fuel.

The local changes in diameter of the cladding (so-called "ridgings") appear at a burnup of 40-45 MWd/kgU those spacing is a multiple of the fuel pellet length (that is an average of 11-12mm). Such "ridgings" appear in the central part of fuel rod mainly. The height and number

of “ridgings” noticed on the diagram of the outer diameter (Fig.2a) can be characterised by the periodogram peak amplitude (Fig.2b.) that in its turn can be used as a qualitative characteristic of fuel-to-cladding interaction degree. Fig.2c shows the outer diameter profile for cladding in the central part of fuel rod provided with pellets having facets. The local changes in diameter are associated with the joints of fuel pellets. The minor decrease in the cladding diameter is noticed in the middle part of the pellet.

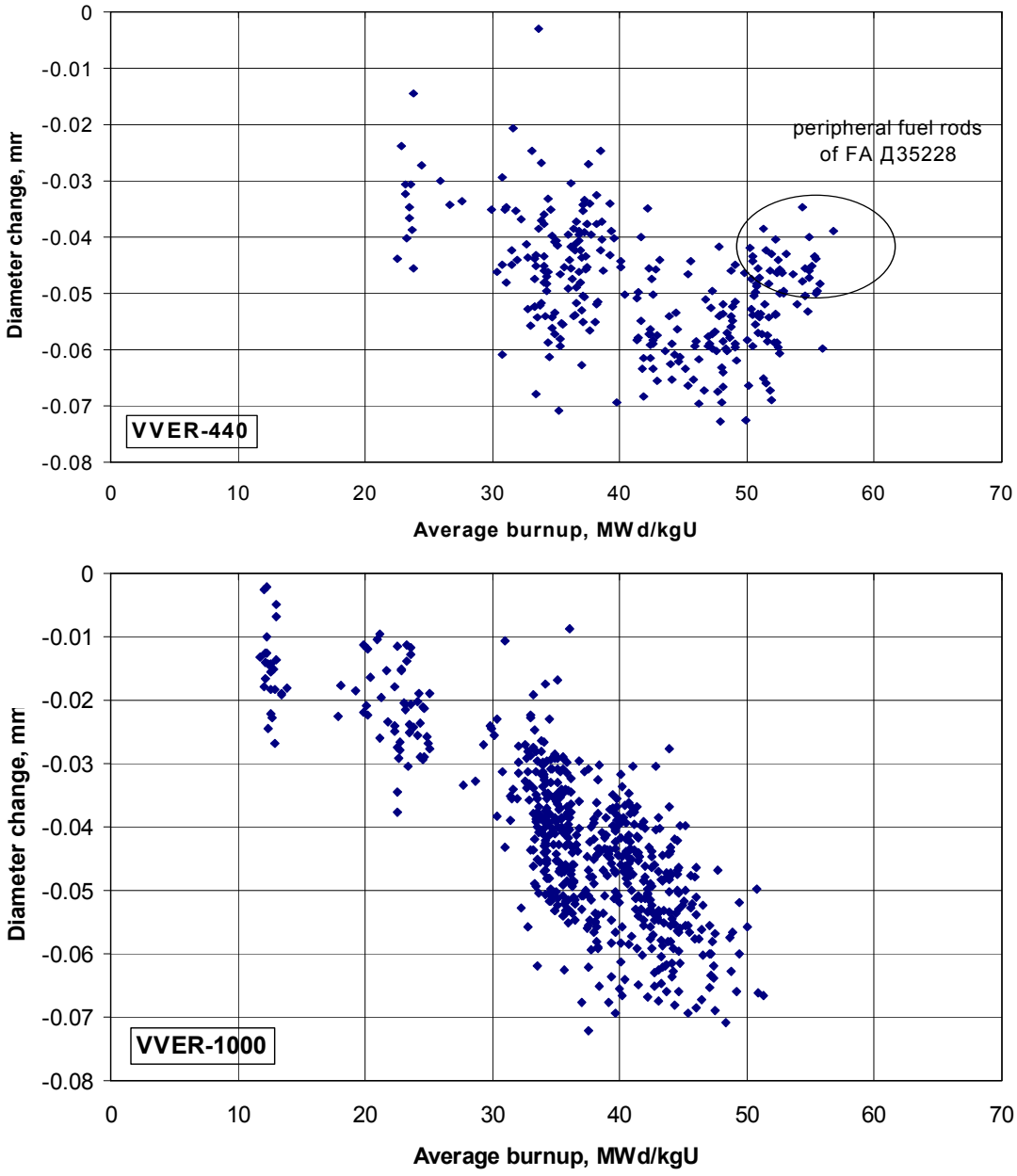


*FIG. 1. WWER cladding outer diameter change vs fuel burnup.*

Fig.3 gives peak amplitude on the periodogram as a function of fuel burnup for WWER-440 and WWER-1000 fuel rods. All examined fuel rods are broken down into two groups: fuel rods equipped with the old type pellets (without facets) and fuel rods equipped with standard pellets (with facets). As may be seen from the diagrams, firstly, amplitude of peaks for WWER-440 fuel rods is 4 times more than for WWER-1000 fuel rods at the same fuel bur-

nup. Secondly, the diagrams bear out the beneficial effect of facets on the mechanical fuel-to-cladding interaction for both types of fuel rods. According to the results of outer diameter analysis as well as results of metallographic study of WWER-1000 fuel rods operated under the design-basis conditions 4 fuel cycles show that the mechanical interaction between the fuel column and cladding is either at the initial stage or it is absent at all [5].

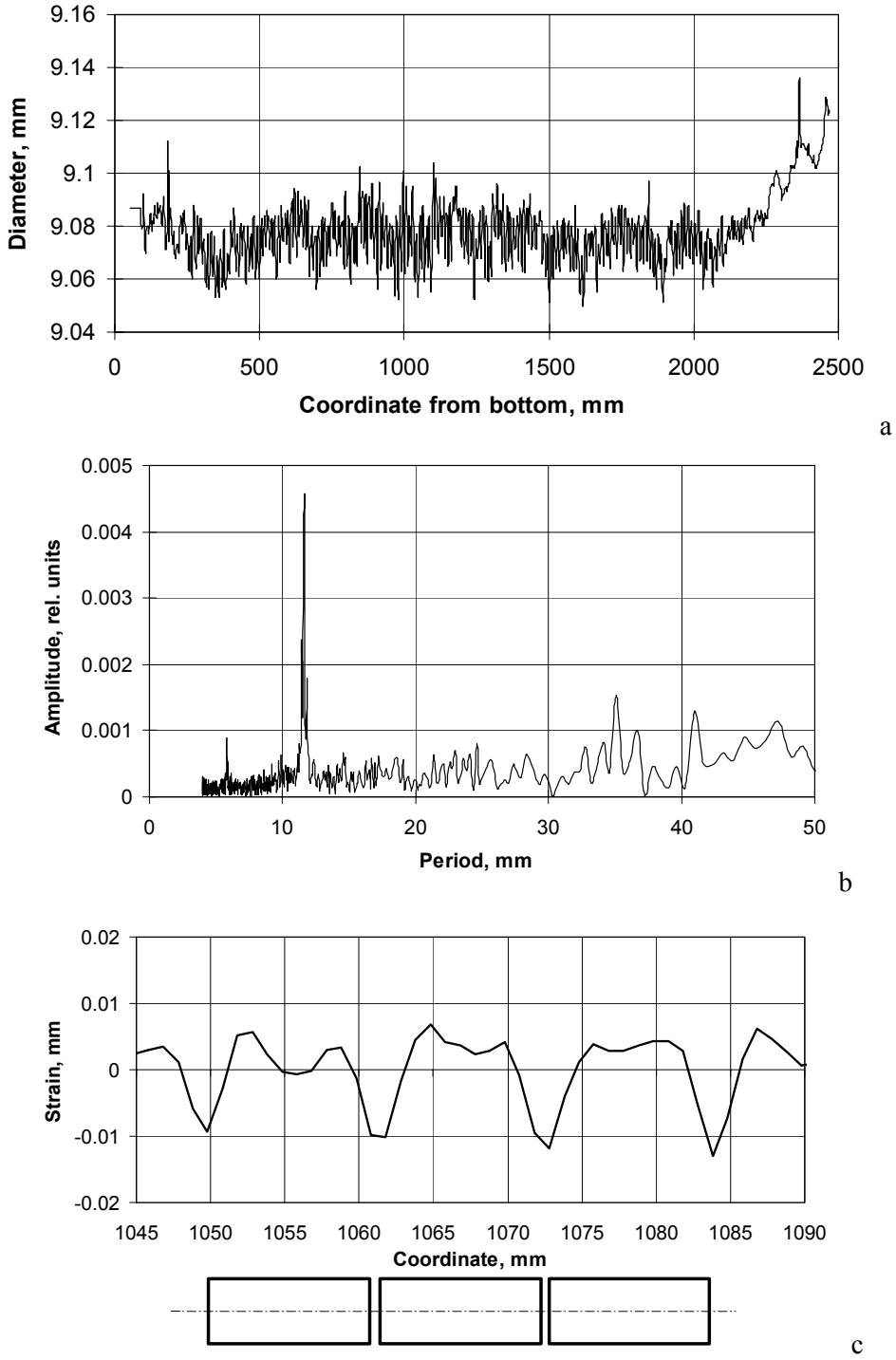


*FIG. 2. Cladding outer diameter profile of WWER-440 fuel rod after 4 fuel cycles (a),cladding outer diameter periodogram of WWER-440 fuel rod after 4 fuel cycles (b),cladding local strain of WWER-440 fuel rod at maximal linear power area after 4 fuel cycles (c).*

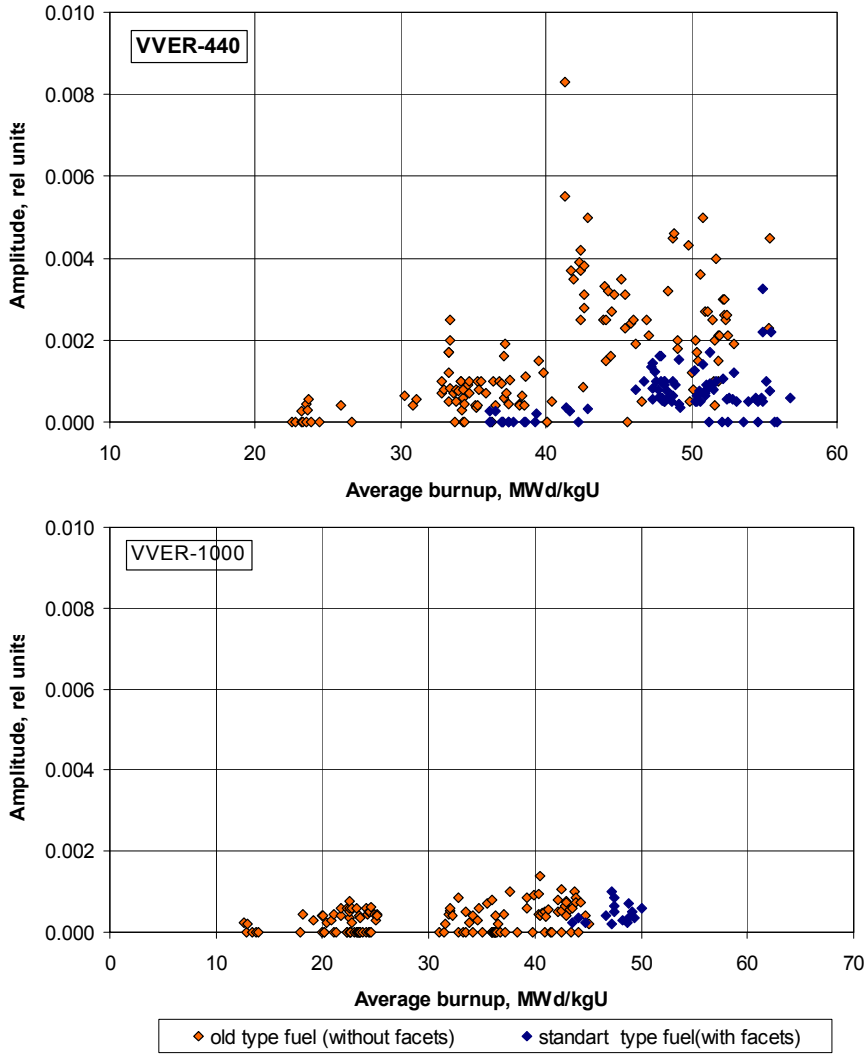


*FIG. 3. Peak amplitude (11 mm) at outer diameter periodogram of WWER fuel rods vs average burnup.*

A change in stress sign in the cladding takes place in central part of WWER-440 fuel rods at higher burnups (>50 MWd/kgU) under the influence of swelling fuel column. The stresses gain the tensile character and the outer diameter of cladding begins increasing [3]. Thus for example, the number of fuel rods demonstrating the same effect is three times as much in WWER-440 fuel assembly operated 5 fuel cycles than in WWER-440 fuel assembly operated 4 fuel cycles under the same conditions. The maximum value of the reverse diametrical stress for fuel rods of this particular fuel assembly is no more than 30μm.

## 2.3. Fuel column swelling

The change in volume swelling of the fuel column is studied adequately [3,5] up to fuel burnups of 63 MWd/kgU (WWER-440) and 50 MWd/kgU (WWER-1000). It is revealed that the rate of fuel swelling for WWER-440 and WWER-1000 fuel rods in the first linear approximation differs insignificantly. Based on fuel sintering through at the initial stage of operation (0.2-0.5% of the initial volume) this coefficient take on a value of 0.8% per 10 MWd/kgU over the range of 30 to 65 MWd/kgU (Fig.4).

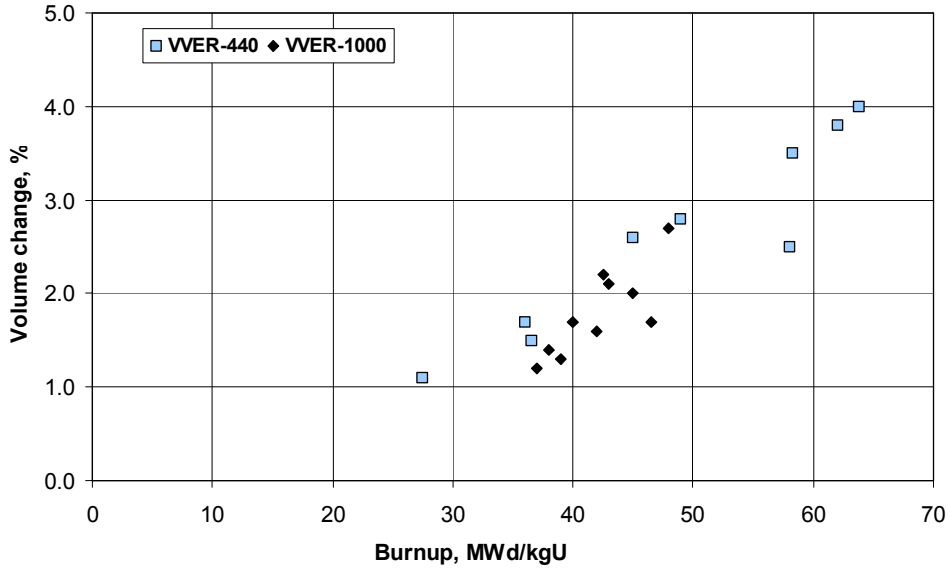


*Fig. 4. Dependence of WWER fuel swelling on local fuel burnup [5]*

## 2.4. Change in fuel-to-cladding gap

The diametrical fuel-to cladding gap was measured with the use of compression technique [6]. The gap measurement is in error of ±10 μm. The distinctive features of the technique didn't make it possible to measure the diametrical gap over 130 μm. The axial distribution of fuel-to-cladding gap demonstrates the largest decrease of the gap in the region 500 to 2000 mm for WWER-440 fuel rods. As for WWER-1000 fuel rods, the largest decrease is noticed in the region 500 to 3000 mm from the lower part of the fuel rod. Fig.5 demonstrates the simultaneous axial distribution of the outer diameter and fuel-to-cladding gap of WWER-440 and WWER-1000 fuel rods. The average gap was found for each fuel rod in the above-mentioned regions. The average fuel-to-cladding gap as a function of fuel burnup is given in Fig.6. The figure confirms the disappearance of fuel-to-cladding gap at a burnup of 42-45 MWd/kgU for WWER-440 fuel rods and 47-50 MWd/kgU for WWER-1000 fuel rods.

## 2.5. Fuel rod elongation

The cladding material creep in WWER fuel rods together with the radiation growth result in FR cladding elongation. Fig.7 gives the specific elongation of WWER-440 and WWER-1000 fuel rods as a function of average fuel burnup. All fuel rods are broken down into two groups: a) fuel rods, where fuel contact with cladding was absent during the whole period of operation; b) fuel rods, where fuel contact with cladding was noticed at the final stage of operation. Two techniques were used for contact finding that are the compression technique and deformation markings of local strain noticed on the outer diameter diagram. But it was assumed that if the average gap is less than 12μm in the middle part of fuel rod in the cold state, such fuel rod had a tight fuel contact with cladding at the operating temperature. According to the comparison of pictures the elongation rate for WWER-440 fuel rods is slightly higher as of WWER-1000 fuel rods. So WWER-440 fuel rods elongate by 0.45% and WWER-1000 fuel rods by 0.4% at a burnup of 50 MWd/kgU. More than that the pictures demonstrate that fuel rods operated under the conditions of fuel contact with the cladding elongate to the greater degree than fuel rods, where the contact was absent.

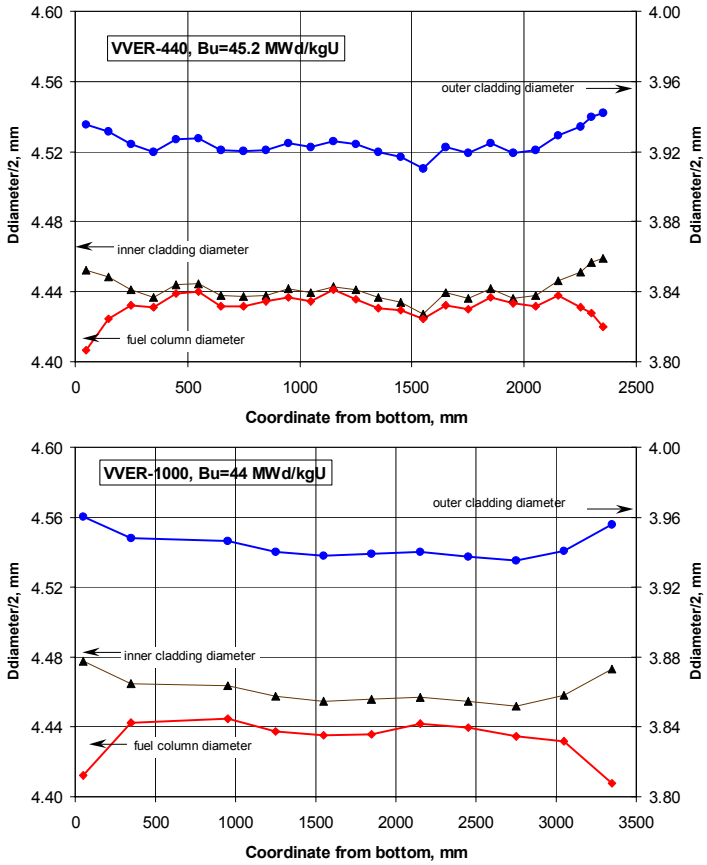


*FIG. 5. Axial profile of cladding outer and inner diameter and fuel column outer diameter for WWER fuel rods.*

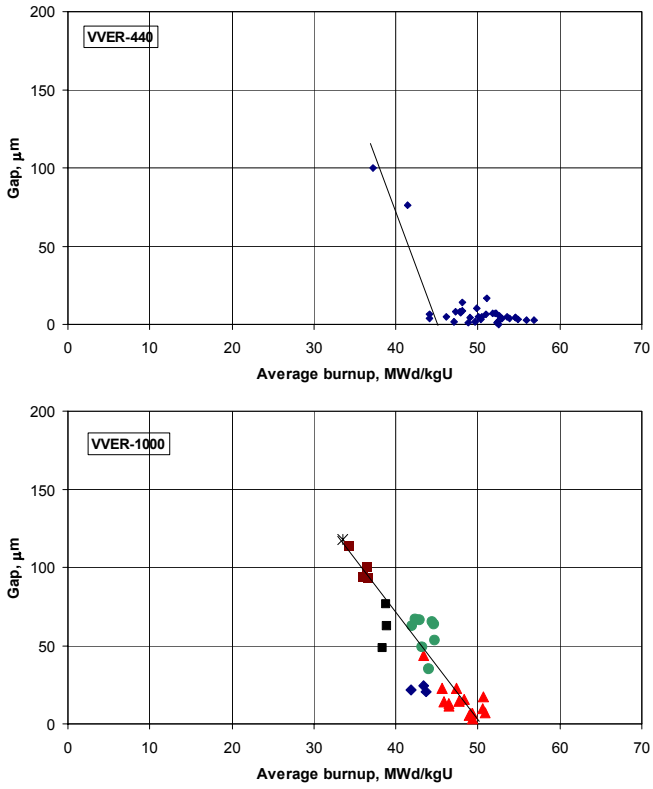


*FIG. 6. Dependence of WWER fuel-cladding gap on average burnup.*

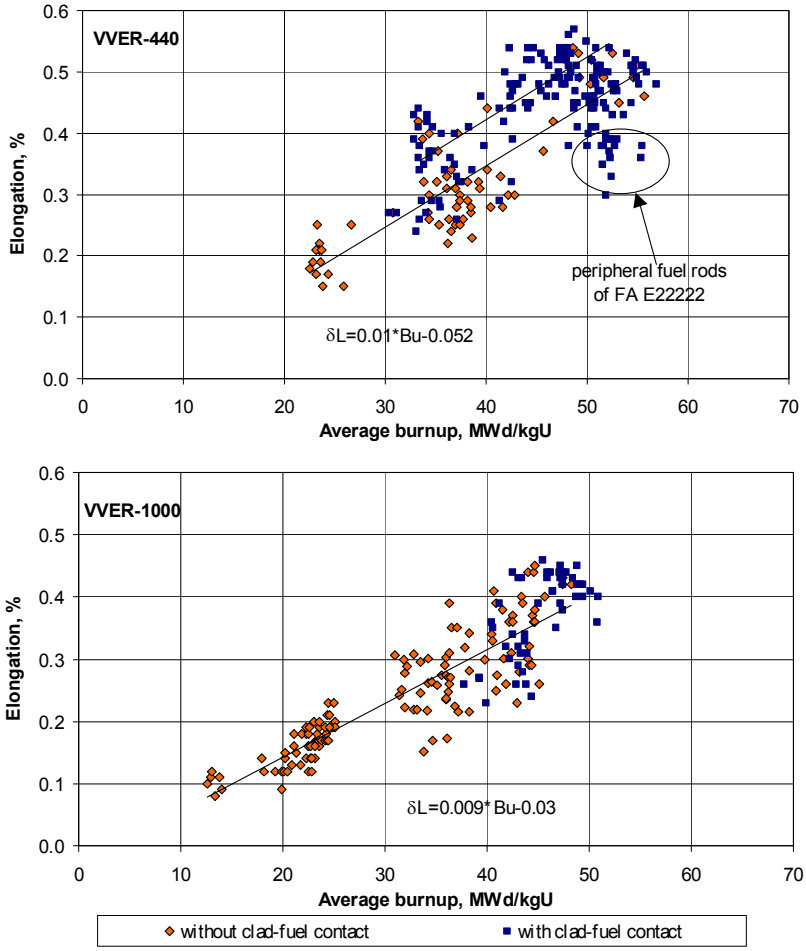


*FIG. 7. WWER fuel rod relative elongation vs average burnup.*

The only exception is the peripheral fuel rods in FA E22222, where the elongation was less in comparison with fuel rods in FA Д35228 in spite of the presence of fuel-cladding contact. The fuel burnup was the same. According to the analysis all fuel rods of this particular group were equipped with claddings making one lot and mechanical properties of claddings in this lot were better than in other FR lots. The ultimate strength and yield stress in the cross direction were higher by 5-7% for claddings of this particular lot than for other claddings at a testing temperature of 380°C. But at the same time the yield stress in the axial direction doesn't differ from the yield stress of claddings taken from the other lots.

In this way the state of WWER-440 and WWER-1000 fuel rods differ as regards the change in geometrical parameters of the cladding and fuel column after operation under the design-basis conditions up to burnups more than 45-50 MWd/kgU differs. Thermo-mechanical interaction between fuel and cladding occurs to a greater degree in WWER-440 fuel rods than in WWER-1000 fuel rods, which reached the same fuel burnups. There are more fuel rods with the close fuel-cladding contact in WWER-440 fuel assembly. Never the less, the change in the cladding diameter because of hoop tensile strain is no more than 30μm for WWER-440 fuel rods operated up to a burnup of 60 MWd/kgU. The material structure and mechanical properties of WWER-440 claddings are satisfactory and they don't differ from the material structure and cladding properties of WWER-1000. The specific elongation of WWER-440 fuel rods is greater by 10-12% in comparison with elongation of WWER-1000 fuel rods. As for volume swelling of the fuel column it doesn't differ considerably.

# 3. TRANSIENT TESTING

## 3.1. Subjects of examination and testing conditions

A set of transient tests for spent WWER-440 and WWER-1000 fuel rods was carried out in SSC RF RIAR in 1995-1999. The tests were run in transient conditions by single and gradual change in power [7,8,9]. The range of fuel burnup was 30-60 MWd/kgU for WWER-440 fuel rods and 27-50 MWd/kgU for WWER-1000 fuel rods. Fuel rods with the same U-235 enrichment (4.4%) and nearly the same fuel burnup of 46-51 MWd/kgU were chosen from the whole set of rods to analyse the differences in behavior of two types of fuel rods in the present paper. It has been already mentioned that the state of WWER-440 and WWER-1000 fuel rods reached the specified burnup was different. The main difference was the size of "cold" fuel-to-cladding gap. It was 10-20μm for WWER-440 fuel rods (Fig.8). This leads to the close fuel-cladding contact when the starting linear power of ~100W/cm was brought to. The "cold" fuel-to-cladding gap was 50-90μm for the WWER-1000 fuel rods reached the same burnup. When the starting linear power of 180-200W/cm was brought to, the fuel-to-cladding was different from zero. The second difference between the tested WWER-440 and WWER-1000 fuel rods consists in undergoing of initial stage of so-cold reverse strain by WWER-440 FR claddings by the time of test run beginning. WWER-1000 claddings were not subjected to this effect.

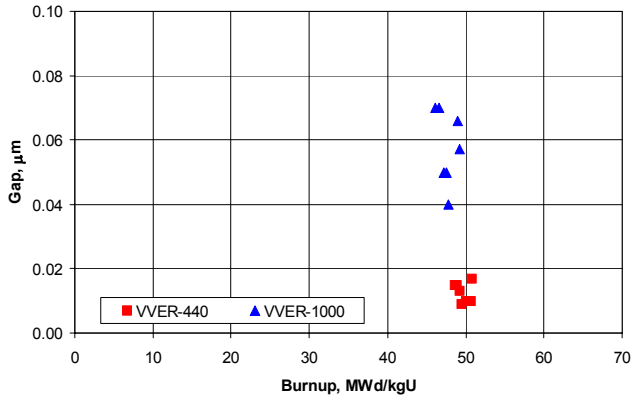


*FIG. 8. Fuel-cladding gap of WWER fuel rods before transient testing.*

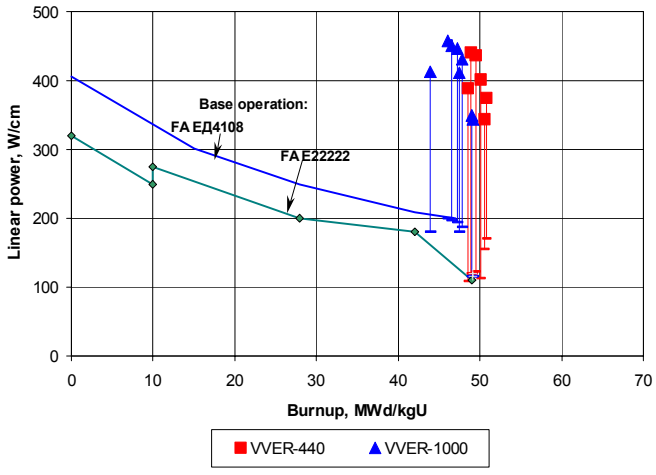


*Fig. 9. Transient test parameters for WWER fuel rods.*

The range of linear power was chosen for the tested fuel rods (Fig.9) with due regard to starting level simulate the FR operating conditions at the final stage of their operation and the maximum linear power exceed the permissible level laid down in specifications. The picture also demonstrates that test conditions for WWER-440 and WWER-1000 fuel rods didn't differ significantly with regard to linear power. The coolant temperature and pressure simulate the operation conditions in the appropriate reactors.

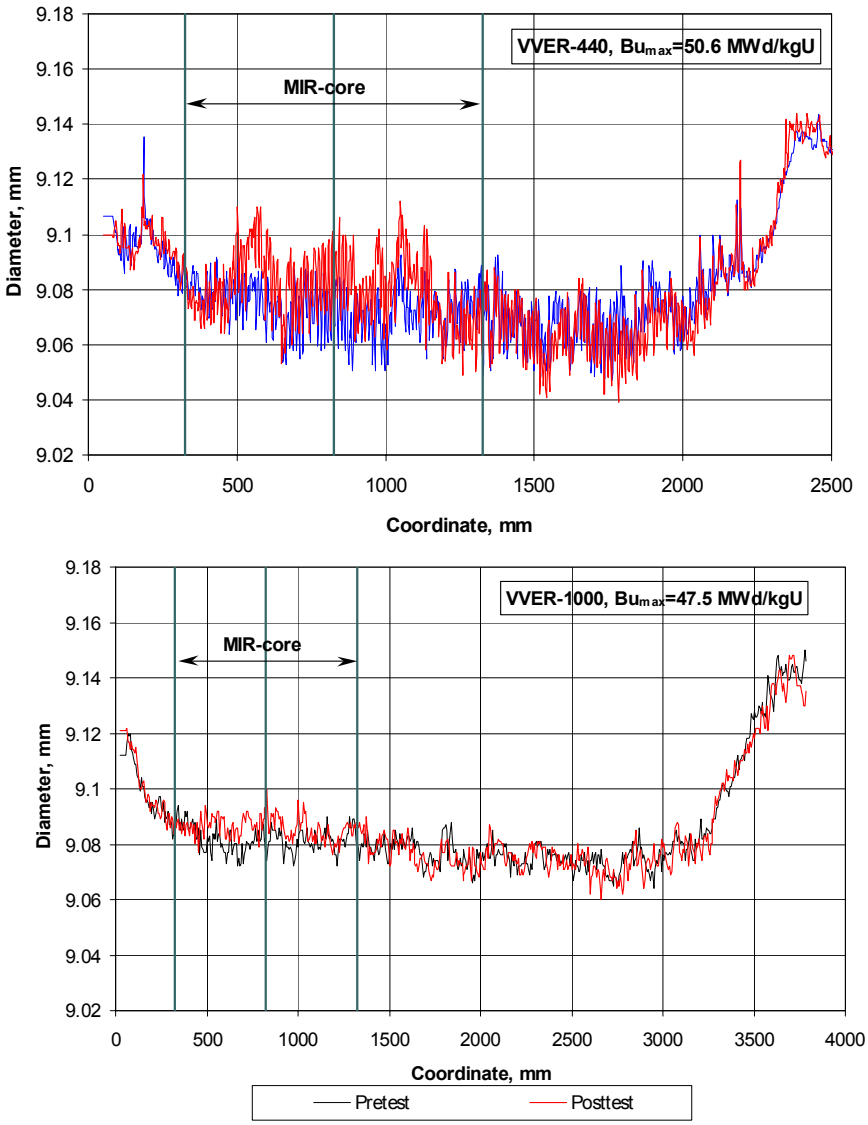


*FIG. 10. WWER cladding outer diameter profile before and after RAMP test.*

### 3.2. Change in the outer diameter of claddings

The typical diagrams made before and after the reactor tests show the outer diameter of claddings (Fig.10) for one WWER-440 and WWER-1000 full-size fuel rod reached a burnup of ~50 MWd/kgU. Their analysis revealed an insignificant increase in the outer diameter of the cladding in the area of the maximum linear power for WWER-440 fuel rods but the outer diameter of WWER-1000 fuel rods didn't change at all. The character of the local cladding

strain was the same in both cases in other words there was no additional fuel-cladding interaction at the place of pellet junction. Fig.11 gives the change in the outer diameter of claddings as a function maximum linear power. The picture confirms the difference in behaviour of WWER-440 and WWER-1000 fuel rods having a burnup of 50 MWd/kgU over the studied linear power range. The increase in the outer diameter of WWER-440 FR claddings was 22-33 μm. As for WWER-1000 fuel rods it was up to 10μm.

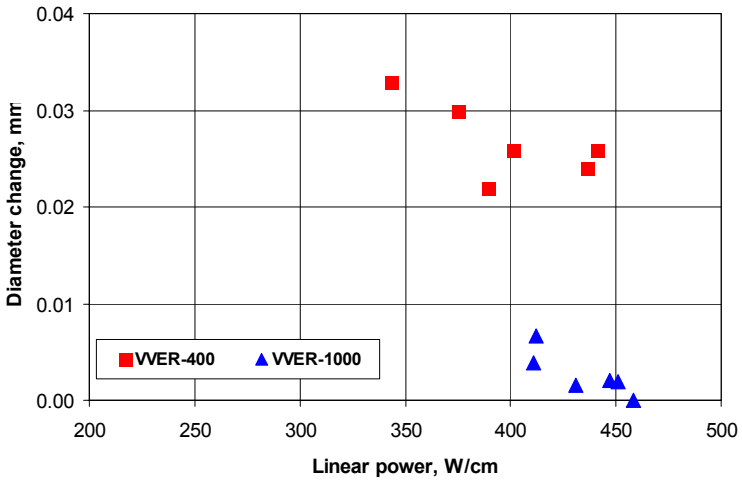


*FIG. 11. WWER cladding outer diameter change after transition test.*

The results presented in Fig. 11 were obtained for the central area of fuel rods, where the linear power was the maximum one at the final stage of testing. There also the regions on the full-size fuel rods, where the linear power varies between zero to maximum values. This fact allows for establishing the relationship between the change in the outer diameter of claddings and linear power over the whole range of its variation practically when data for one fuel rod are available only. In order to exclude the influence of the "ridgings" the length of region for averaging was taken equal to the length of several fuel pellets.

Fig.12a and 13a show the typical diagram of the outer diameter change together with the linear power profile along WWER-440 and WWER-1000 FR length. The outer diameter was in error of ±0.01mm. The relationship between the above-mentioned parameters is plotted in Fig.12b and 13b for each fuel rod.

Fig.12b demonstrates that a cladding strain for WWER-440 fuel rod begins at a level peculiar to the final fuel cycle under the operation conditions of power reactor (~100 W/cm). It should be noted that this particular fuel rod didn't have any essential fuel contact with cladding before the testing. The cladding strain is proportional to the linear power up to 250 W/cm in the first approximation. On the average, the outer diameter of WWER-440 FR claddings was constant over the thermal power range >300 W/cm. In its turn WWER-1000 FR diameter (Fig.13b) didn't change within the limits of measurement error.

### 3.3. Fuel-to-cladding gap

Fig.14 presents the values of average gaps measured in normal conditions after the reactor tests. The picture demonstrates the fuel-to-cladding gap in the region of maximum linear power is 40-65 μm after testing of WWER-440 fuel rods (the tight contact was noticed before testing). The gap decrease by no more than 20 μm was noticed for WWER-1000 fuel rods.

### 3.4. Change in the outer diameter of fuel column

Based on the available data on the outer diameter of the cladding, fuel-to-cladding gap for a separate sections of each fuel rod it is possible to define the axial distribution of the fuel column outer diameter and establish its relationship with the linear power.

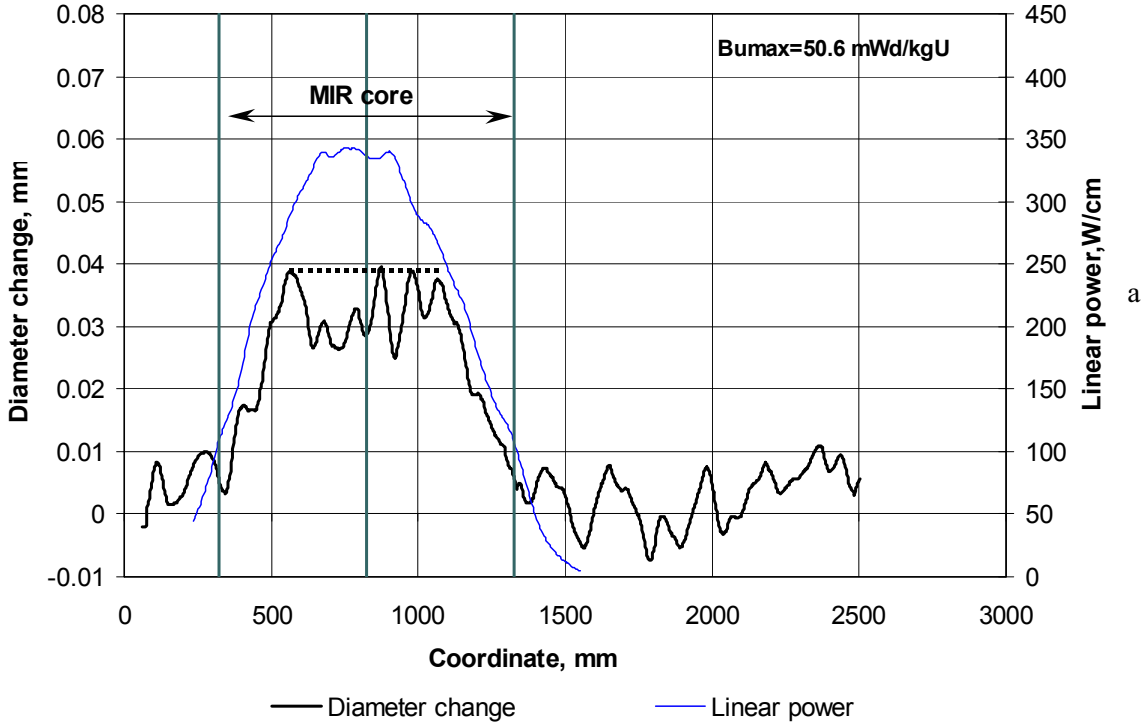


a

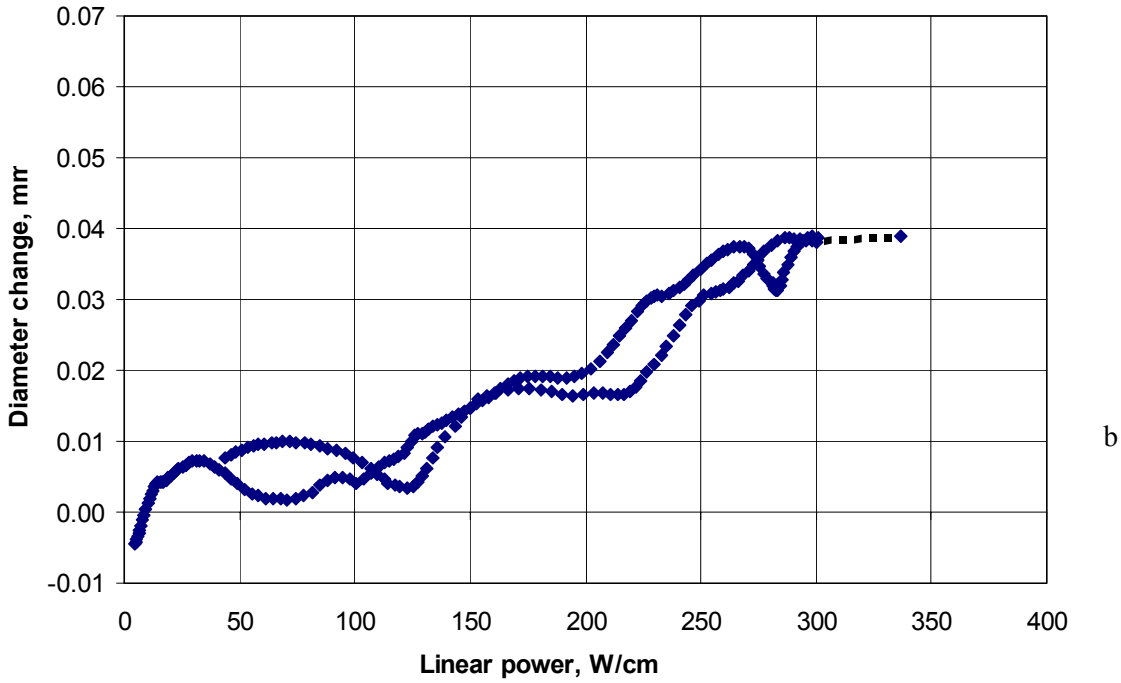


b

*FIG. 12. Cladding outer diameter and linear power distribution for WWER-440 fuel rod after transient test (a), coupling between linear power and cladding diameter change for WWER-440 fuel rod after transient test (b).*

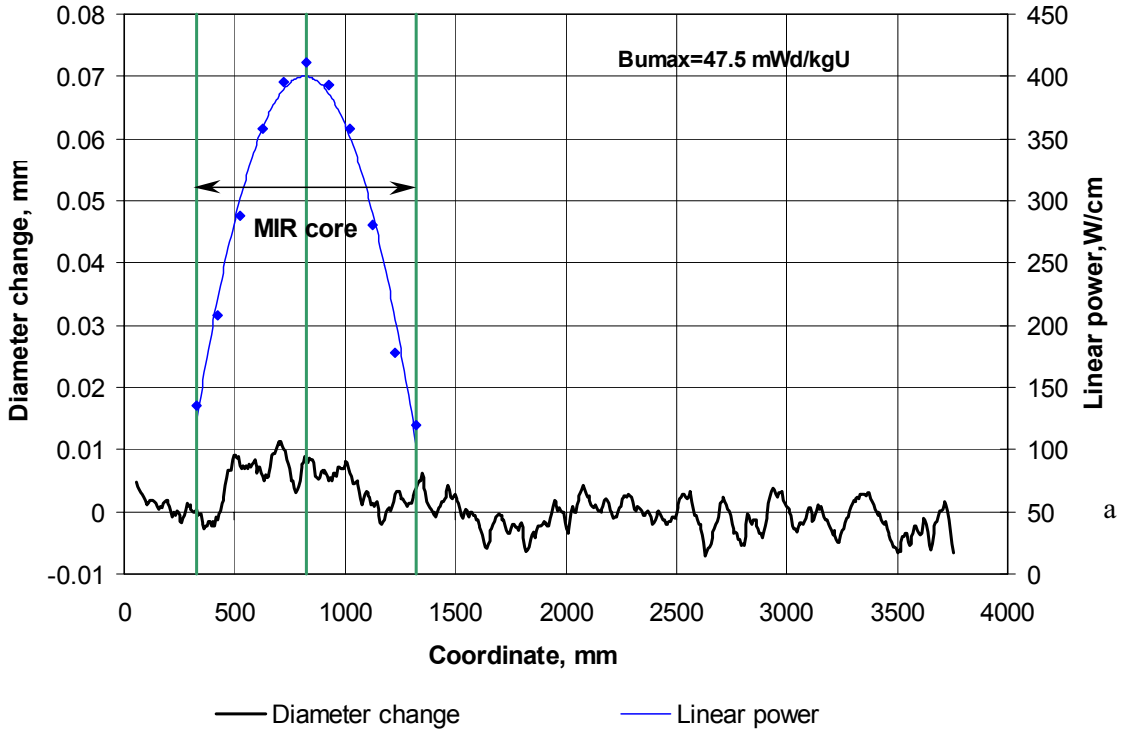


a

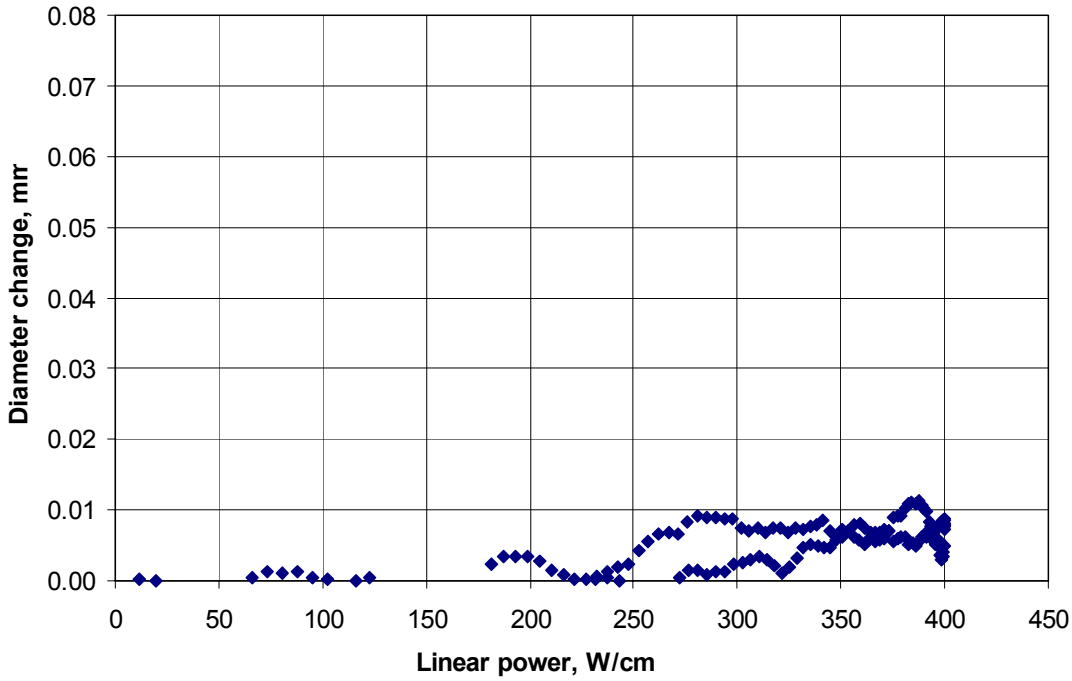


b

*FIG. 13. Cladding outer diameter and linear power distribution for WWER-1000 fuel rod after transient test (a), coupling between linear power and cladding diameter change for WWER-1000 fuel rod after transient test (b).*

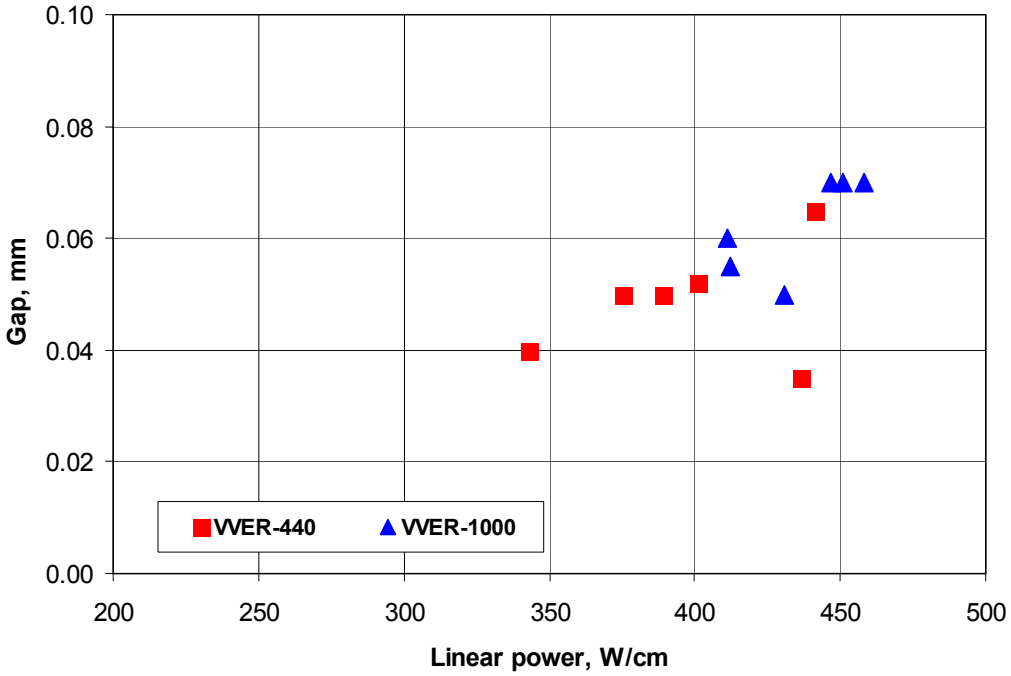


*FIG. 14. WWER fuel-cladding gap after transient test.*

Fig.15a and 15b show the profiles of the outer and inner diameter of the cladding as well as outer diameter of the fuel column for WWER-440 and WWER-1000 fuel rods after the testing. As indicated in these pictures, the region of the outer diameter averaging conforms to the pace of fuel-to-cladding gap measurement (50 mm). Fig.15a demonstrates that the outer diameter of the cladding increases insignificantly for WWER-440 fuel when a linear power of 343 W/cm has been reached. The maximum linear power region is characterized by a large fuel-to-cladding gap and the fuel column diameter is less in this region in comparison with the adjacent regions. The diameter of the fuel column increased in the WWER-1000 fuel rod over the region of the MIR reactor core, the cold gap became less and the cladding diameter increased insignificantly (fig.15b). So the fuel column is touched to the cladding in the hot state.

The central hole diameter starts decreasing when the linear power is ~230÷250 W/cm. When the linear power is 340-360 W/cm, the central hole disappears completely and a new central hole has appeared in one of the cross-sections of WWER-440 fuel rod when $q_l$=440 W/cm. Such behaviour of the central hole as compared with the decrease in the fuel column diameter draw to the conclusion that there is a certain relationship between them when the linear power is higher than 300 W/cm. The diameter of the fuel column was sensibly constant at the cross-sections that are free from the central hole. Correspondingly the change in cladding diameter was minimal (~25 μm) at these particular cross-sections. At the same time diameter of the fuel column increased at the cross-sections where the central hole diameter didn't change or changed insignificantly. The cladding diameter increased respectively.

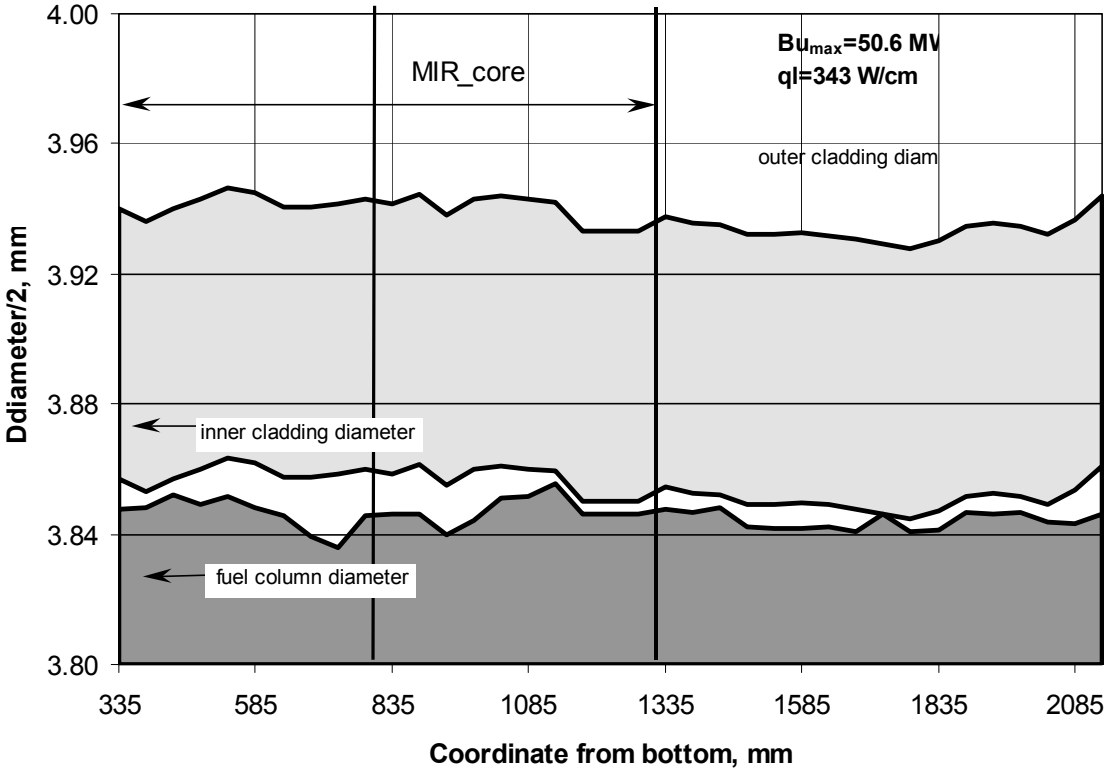


a

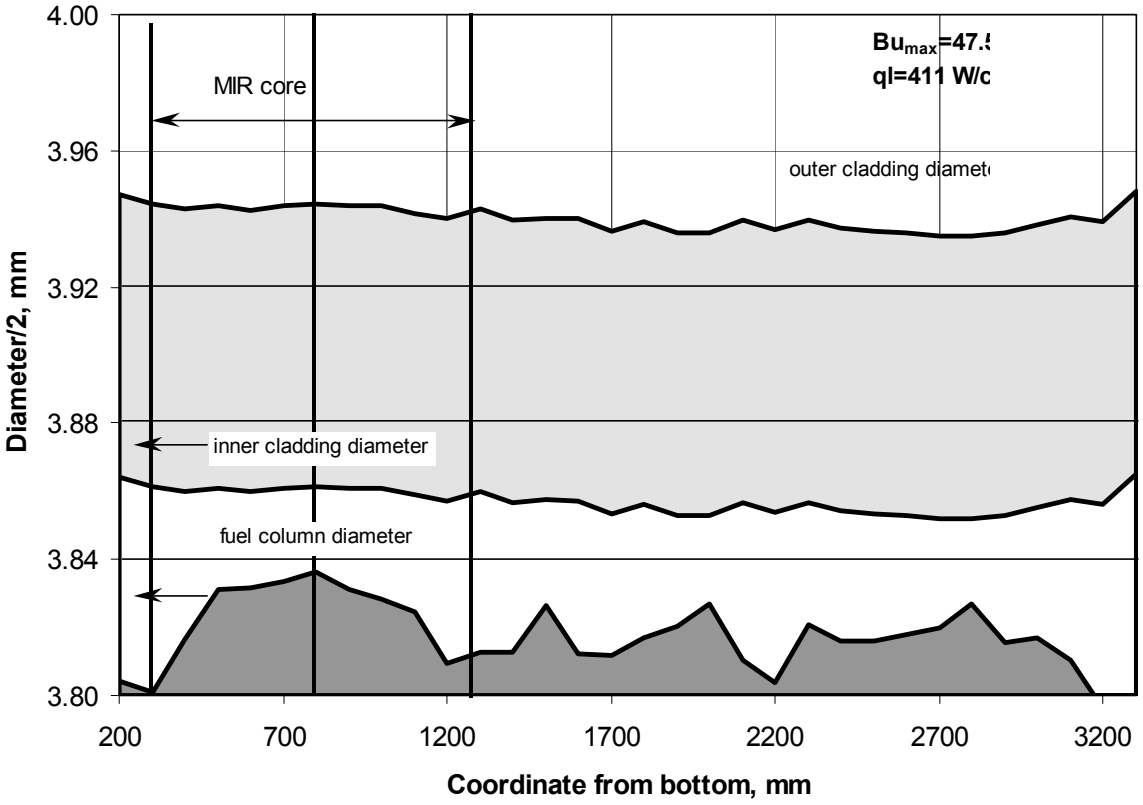


b

*FIG. 15. Axial profile of cladding outer and inner diameter and fuel column outer diameter for WWER-440 fuel rod after RAMP test (a), axial profile of cladding outer and inner diameter and fuel column outer diameter for WWER-1000 fuel rod after RAMP test (b).*

## 4. CONCLUSIONS

The following conclusions can be drawn based on the study of geometric parameters changes of WWER-440 and WWER-1000 claddings and fuel column in operation conditions and transient testing:

- WWER-440 cladding is subject to tensile stress under the influence of fuel column at burnups of 42-45 MWd/kgU. However, the value of hoop strain isn't high ($\Delta d_2$ is no more than 30 μm) and it doesn't lead to the mechanical property changes of cladding.

- WWER-1000 fuel rods are characterized by the less degree of thermomechanical interaction after the operation conditions up to a burnups of 45-50 MWd/kgU in comparison with the WWER-440 fuel rods reached the same burnup. The fuel-pellet contact in WWER-1000 fuel rods occurs at higher burnups compared to WWER-440 fuel rods.

- Testing of high burnup WWER-1000 fuel rods in transient conditions over the linear power range of 180 to 400 W/cm demonstrates that the geometric parameters of WWER-1000 cladding are practically constant, fuel-to-cladding gap doesn't disappear, cladding strain is absent.

- In their turn, WWER-440 fuel rods having the same burnup and close fuel-cladding contact before the testing were subjected to considerable hoop cladding strain in testing up to 300 W/cm. But the hoop strain don't grow due to the structural changes in fuel column and decrease in central hole diameter occurred when the power is higher.

## REFERENCES


[1] YU. BIBILASHVILI, V. VELYUKHANOV, A. IOLTUKHOVSKI, O. NIKISHOV et al., Operation Experience of VVER Fuel Including Abnormal Conditions. Proceeding of the Second International Seminar "VVER Reactor Fuel Performance, Modelling and Experimental Support", 21-25 April 1997, Sandanski, Bulgaria.

[2] A. NOVIKOV, V. PAVLOV, A. PAVLOVICHEV, V. PROSELKOV, V. SAPRYKIN, Status and Prospects of VVER In-Core Fuel Management Activities. Proceeding of the International Seminar on VVER fuel performance, modeling and experimental support, Varna, 7-11 November 1994.

[3] A. SMIRNOV, V. SMIRNOV, B. KANASHOV et al., Behaviour of VVER-440 and VVER-1000 Fuel in a Burnup Range of 20-48 MWd/kgU. Proceeding of the Second International Seminar "VVER Reactor Fuel Performance, Modelling and Experimental Support", 21-25 April 1997, Sandanski, Bulgaria.

[4] D. MARKOV, A, SMIRNOV, V. POLENOK, V. KUZMIN, A. NOVOSELOV, Validation of VVER-1000 Fuel Rod Efficiency at Operation during Four Fuel Cycles. Third International Seminar on VVER Fuel Performance, Modelling and Experimental Support, Pamporovo, Bulgaria, 4-8 October 1999.

[5] V. KUZMIN, V. GOLOVANOV, G. MAJORSHINA, et al., Changes in VVER fuel rods occurred under irradiation till 40-60 MWd/kg U, 5th Conference on Reactor Materials, Dimitrovgrad, Russia, 1997, RIAR (1997) (In Russian).

[6] S. AMOSOV, Determination of the Fuel-to-Cladding Gap of Fuel Rods by Nondestructive Method, Technical Committee on Advanced Post-Irradiation Examination Techniques for Water Reactor Fuel. May 14-18, 2001, Dimitrovgrad, Russian Federation, INTERNATIONAL ATOMIC ENERGY AGENCY, Vienna (2002).

[7] YU.K. BIBILASHVILY, A.B. MEDVEDEV, V.V. NOVIKOV et al., Studies into VVER fuel rod behavior at high burn-up in power ramps. HPR-349: "Enlarged HPG meeting on high burn-up fuel performance, safety and reliability and degradation of in-core materials and water chemistry effects and man-machine systems research". OECD Halden Reactor Project. Halden, Norway, Lillehammer, 15-20 March 1998.

[8] SMIRNOV A., SMIRNOV, V., KANASHOV, et al, Investigation of behaviour of high burnup VVER-440 fuel rods under transient conditions, 5th Conference on Reactor Materials, Dimitrovgrad, Russia, 1997, RIAR (1997) (In Russian).

[9] SMIRNOV A., KANASHOV B., OVCHINNIKOV V. et al, Study of behavior of VVER-440 fuel rods of higher fuel burnup under transient conditions. Enlarged Halden Programme Group Meeting on High Burn-up Fuel Performance, Safety and Reliability and Degradation of in-core Materials and Water Chemistry Effects and Man-Machine Systems Research, Volume II, HPR-349/43, Lillehammer, 15th-20th March 1998.

[10] SMIRNOV A., KANASHOV B., LYADOV G. et al, Examination of fission gas release and fuel structure of high burnup VVER-440 rods under transient conditions. Third International Seminar on VVER Fuel Performance, Modelling and Experimental Support, Pamporovo, Bulgaria, 4-8 October 1999.

# FAILURE ROOT CAUSE OF A PCI SUSPECT LINER FUEL ROD

F. GROESCHEL*, G. BART*, R. MONTGOMERY**, S.K. YAGNIK***

* Paul Scherrer Institute, Switzerland
** Anatech, United States of America
*** Electric Power Research Institute, United States of America

**Abstract**

Zirconium-lined claddings reveal increased PCI resistance of fuel rods and provide large flexibility in reactor operation by allowing faster power ascension rates. Nevertheless a liner fuel rod failed after 3 cycles of operation and an approximate burn-up of 26 MWd/kgU in a Swiss Boiling Water Reactor, after a power transient following a control blade manoeuvre. Poolside inspection of the rod showed a primary defect in the shape of a small axial crack (X-mark). A PCI type failure was therefore suspected, although operating limits had not been exceeded. This paper describes the hot cell examinations, which were undertaken to investigate the root cause of the failure. Standard NDT methods, high resolution neutron radiography with "fuel-in" condition, and detailed metallography were applied to assess the status of the pellets and the cladding at the location of the defect. The findings were compared to the characteristics of a sibling sound rod. The investigation revealed a pellet with a missing surface at the origin of the cladding crack, which had not been rejected during the manufacturing process. A similar case had been observed in a US reactor before and the size of the defect in the pellets was comparable. PCI analysis using the EPRI-FREY code showed that due to the missing pellet surface local stresses are generated in the cladding during such power transients, which are considered large enough to trigger ISCC. A second important effect is the degraded transfer across the large pellet-cladding gap associated with a missing pellet surface. This condition raises the fuel pellet surface temperature and promotes the migration and transport of volatile fission products conducive to ISCC towards the cladding. The presence of these reactive fission products further stimulates the ISCC process in the zirconium liner and then through the remainder of the cladding wall. The results from the FREY-01 analysis demonstrate that the PCI-type crack observed in heat KLG072 Rod B4 was probably caused by ISCC of the zirconium liner and then exposure of the Zr-2 cladding wall to the volatile fission products. Further propagation of the crack occurred as a consequence of the high hoop stresses in the Zr-2 cladding wall. These conclusions are supported by the metallographic findings in the vicinity of the X-mark crack in Rod B4 which revealed a multi-branching through-wall crack in the Zr-2 portion of the cladding, characteristic of PCI cracks observed in older non-barrier rods. Thus missing pellet surfaces increase the PCI failure propensity, although they are not a necessary or sufficient requirement for such failures.

## 1. INTRODUCTION

Successful fuel operation is essential to the safe, reliable, and economic power production by commercial nuclear reactors. Fuel failures during operation represent a major threat towards that goal.

Active fuel failures have been categorized according to the following mechanisms [1]:

- Pellet-Cladding Interaction (PCI)
- Crud-Induced Localized Corrosion (CILC)
- Debris Fretting
- Undetected Defects during Manufacturing

In the past, manufacturers have continuously improved fuel design features, manufacturing processes, and quality inspection methods and developed mitigation actions to reduce the number of failures and achieve the ultimate goal of zero fuel failures. This endeavour has turned out to be very successful up to now and the majority of failures to date are due to debris fretting [2].

PCI fuel failures result from the combined action of fuel pellet expansion-imposed stresses in the cladding and the presence of an aggressive fission product environment. With the introduction of the zirconium liner (barrier) fuel the resistance of the rod to PCI-type failure was considerably improved and the PCIOMR (Pre-Conditioning Interim Operating Management Recommendations) constraints could be lifted, which were imposed for non-barrier fuel to mitigate PCI risk. This provided large flexibility in reactor operation by allowing faster power ascension rates. The barrier fuel concept proved to be very successful, since no PCI-type failures have been reported up to date [3, 4].

Undetected Manufacturing Defects resulting in fuel rod failures have been tubing reduction flaws and end plug weld defects. In one case, a pellet missing cylindrical surface was reported as the primary failure cause [2]. The unsupported cladding section can be subjected to significant bending stresses during a power increase. In addition, higher fuel pellet temperatures in the vicinity of the chipped area were assumed, which contributed to higher local concentrations of fission gas in the enlarged gap thus increasing the propensity to Stress Corrosion Cracking attack on the cladding [5].

Although no characteristic PCI failure has been identified in barrier fuel, some concern exists, in particular when the fuel rods were operating in control cells and the failure occurred during a control blade withdrawal [6]. Inspection of failed rods and investigation of the root cause is therefore necessary to assess the principal failure mechanisms.

During cycle 10 of Kernkraftwerk Leibstadt (KKL) rod B4 of assembly KLG072, which operated in a Control Cell, failed during a control blade manoeuvre and a PCI-type failure was suspected. Since the cycle was interrupted shortly afterwards, the rod was not degraded after unloading and the perspectives were considered promising to be able to elucidate the cause of the primary failure by post-irradiation examination.

## 2. PLANT OPERATION

Assembly KLG072 operated uncontrolled during cycle 8 and 9 [7]. Durng the first cycle, rod B4 and its sibling rod D2 reached a maximum linear heat generation rate (LHGR) of about 45 kW/m in the bottom part of the rods for a short period. The shuffling from cycle 8 to 9 resulted in a peak nodal power change of about 30 kW/m in the bottom part and a maximum power level of about 42 kW/m. Both rods reached a burnup of about 23 MWd/kgU at the end of the cycle.

For cycle 10, the assembly was moved to a control cell and operated with the control blade fully inserted for most of the cycle, I.e. at low nodal power level. A partial control blade withdrawal resulted in a local power increase in the upper half of the rods with peak power change of 25 kW/m and a peak power level of 38 kW/m. Fig. 1 shows the axial power shapes of rod B4 during control blade withdrawal [8]. The axial position of the X-mark observed in rod B4 during poolside inspection corresponds to peak power experienced by the rod.

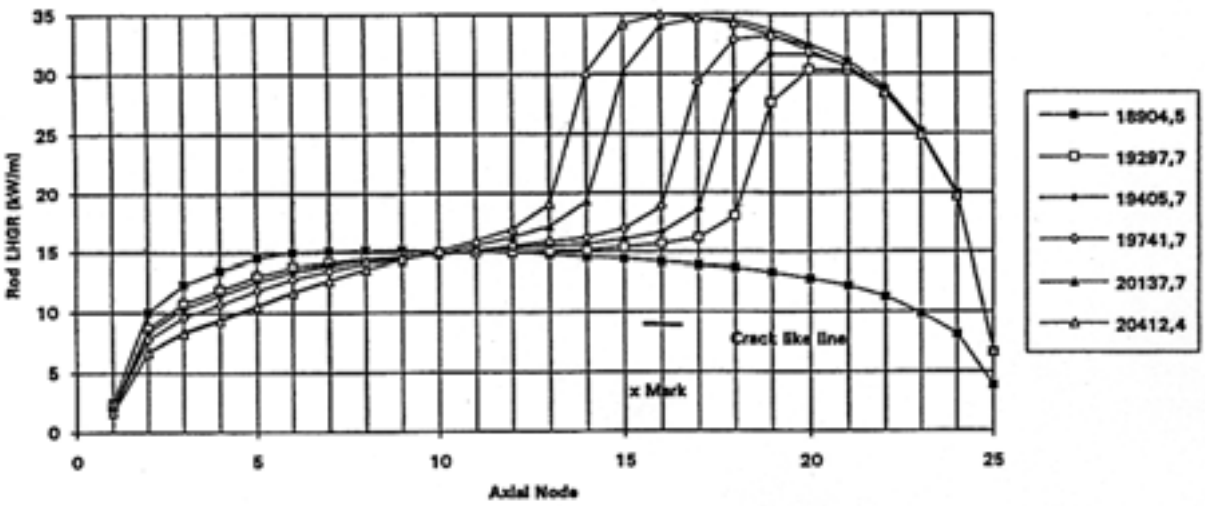


*FIG. 1. Axial power in rod B4 during control blade movement.*

## 3. POOLSIDE INSPECTION

Inspection of the rod B4 by eddy current (EC) indicated a small defect at the inside of the cladding, typical for a PCI-type crack, about 14 cm below spacer 5 (about 2450 mm elevation). Visual inspection revealed a tiny longitudinal crack about 1-2 mm long, decorated at both ends with discoloration lines, forming an angle of 90° between them, a so called "X-mark". In addition, a hydride bulge about 40 cm above the lower end plug and several small hydride blisters up to spacer 3 were observed. Ultrasonic testing confirmed that the rod was filled with water [8].

## 4. POST-IRRADIATION EXAMINATION

The defective rod B4 was shipped to PSI in 1996 together with its sibling sound rod D2 for post-irradiation examination to reveal the root cause of the failure. Table 1 summarizes the characteristics of the two rods and Fig. 2 shows the positions of the two rods within the bundle, which had been fabricated in 1988.

Table 1. Rod Characteristics

| Bundle | Rod | F/A Burnup [Mwd/kgU] | Cycles | Unloading |
|---|---|---|---|---|
| KLG072 | B4, D2 | 27.3 | 3 | May 94 |

PIE of rod B4 consisted in:

- re-identification of the primary defect and its position by NDT-methods
- assessment of the rod condition at the X-mark by neutron radiography (NR)
- characterization of the defect and of the state of the pellet by metallography
- comparison of the results with those of the sound rod D2.

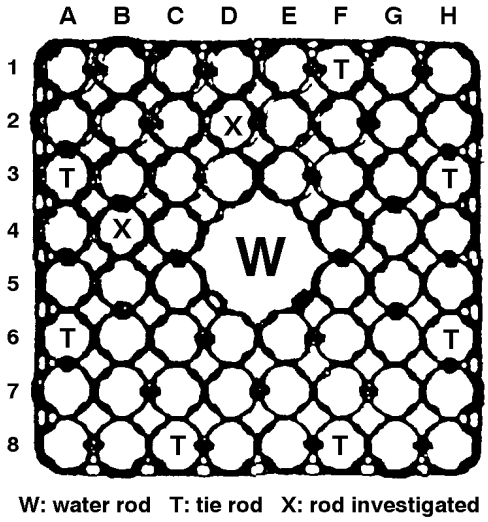


*FIG. 2. Positions of rod B4, D2 within bundle KLG072.*

### 4.1. NDT-measurements

Axial μ-scans of rod D2 showed a flat activity profile with strong Cs-peaks at the pellet gaps in the 2nd, 5th and 6th span, indicative of a high fuel temperature. The profile of B4 is similar in shape without Cs-peaks. A slight decrease in total activity in the 5th and 6th span extending around the X-mark location is evident. This decrease is entirely due to Cs, which was probably washed away, whereas other nuclides showed no change in profile. A strong Cs-peak is associated with the bottom blister indicative of a perforation. Fig. 3 compares the total gamma profiles of the two rods. The difference in absolute values is due to differing collimator lit widths.

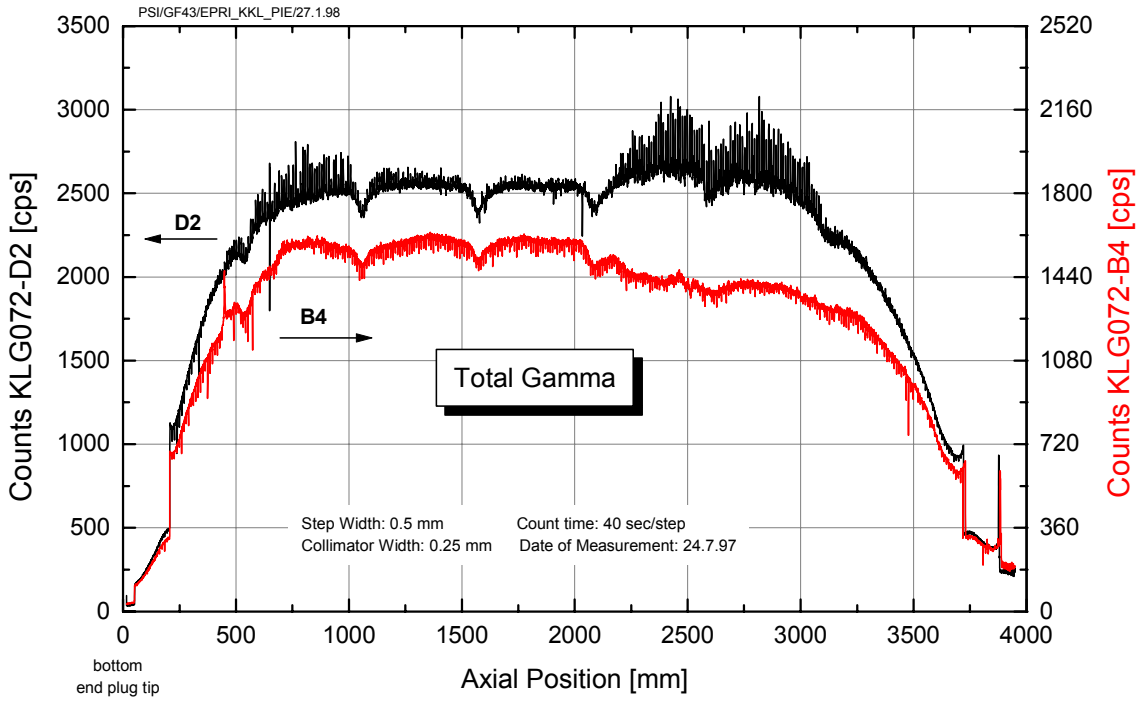


*FIG. 3. μ-scan of rods B4 and D2 (energy window 100 – 2000 keV).Collimeter width setting: x mm.*

The diameter profiles of both rods were very similar showing a creep-down of about 60 μm vs. the nominal diameter (Fig.4). Two remarkable, although rather faint peaks were observed:

- a broad peak around elevation 800 mm, which is attributable to crud accumulations resulting in a EC lift-off signal of about 60 μm
- a similar peak around elevation 2500 mm.

The EC oxide profile shows a constant 10 μm reading, which corresponds to the expected crud/oxide layer thickness. The diameter increase could therefore well be indicative of the pellet swelling during the power transient.

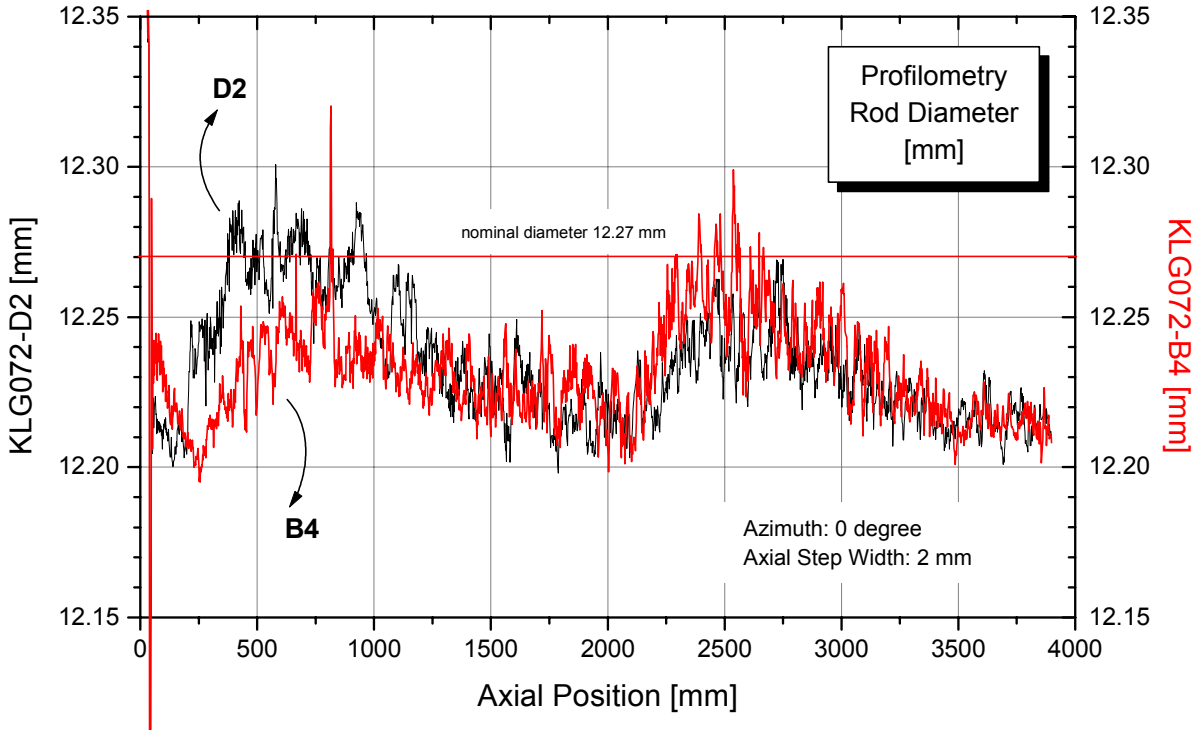


*FIG. 4. Diameter profiles of rods B4 and D2.*

Finally, the encircling coil (eddy current) method yielded a clear signal of a longitudinal defect at the X-mark position of rod B4, which was located at 2456 mm elevation. The blisters in the bottom part gave also strong indications. Fig. 5 compares the EC-signal of rods B4 and D2.

Visual inspection was able to identify a feature at the X-mark position indicated by the above methods (Fig. 6a), but the aspect differed from the image obtained during poolside inspection. Some doubts therefore remained whether this location really corresponded to that of the X-mark. A leak test of the above rod segment showed that a wall penetration existed in that area. By applying a dye penetrant test, the location could be confirmed and the dimension of the defect could be estimated. Fig. 6b shows the area after dye application and the position of the crack is marked by the red dye sipping out of the crack and penetrating the white developer. After removal of the developer, the size of the defect became apparent (Fig. 6c), which amounted to about 1.5 mm and corresponded well to that estimated from the poolside inspection. Fig. 6d gives the final positions of the defect.

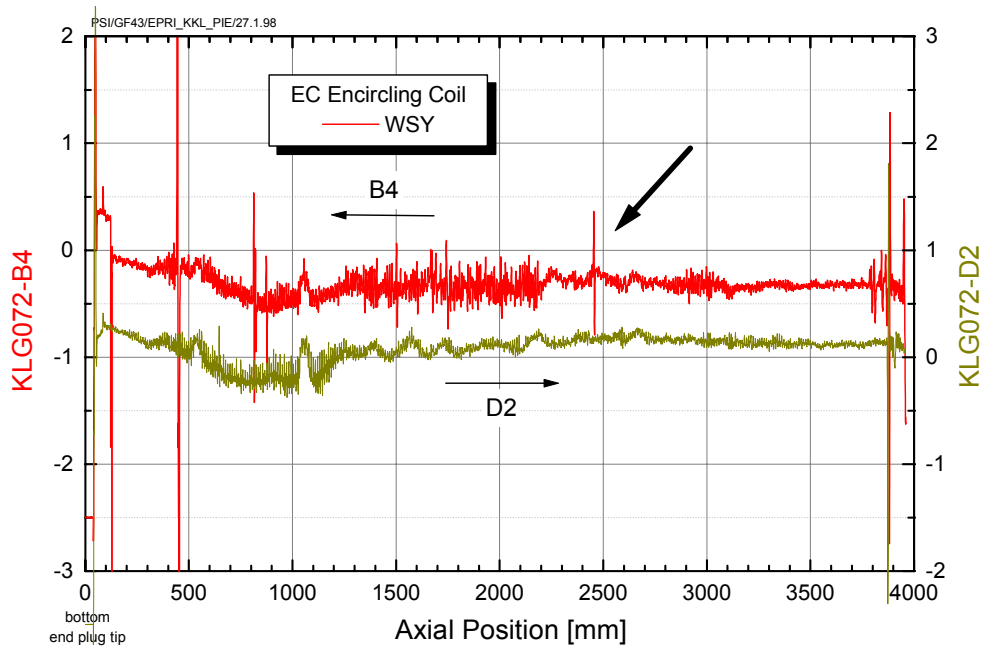


*FIG. 5. Encircling coil measurement of rods B4 and D2.*

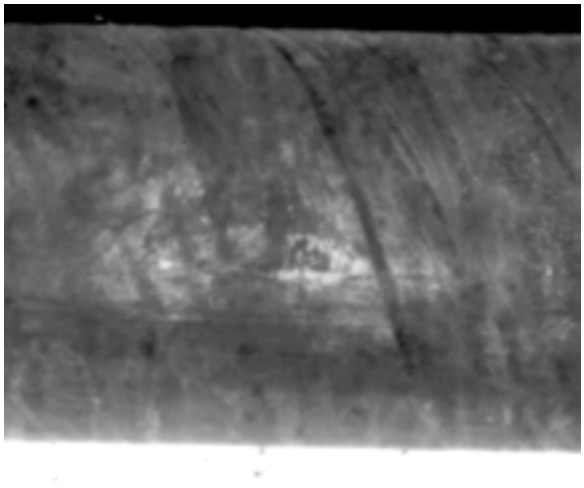

a) as received

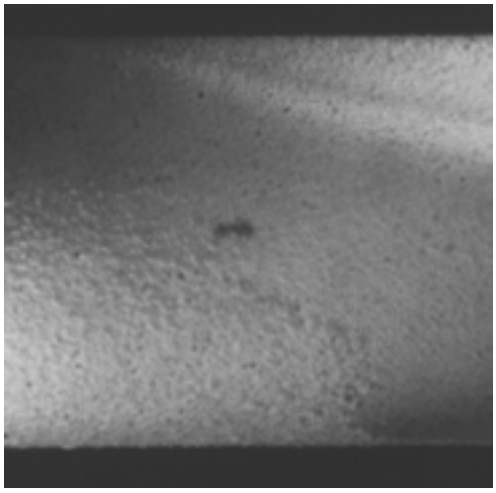

b) during dye-penetrant test

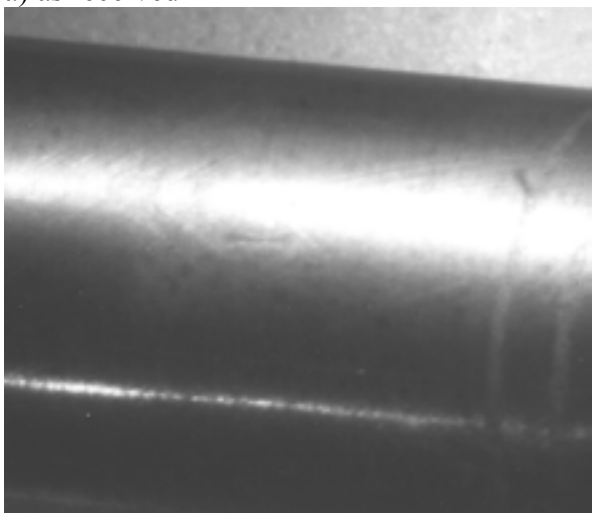

c) after dye-penetrant test

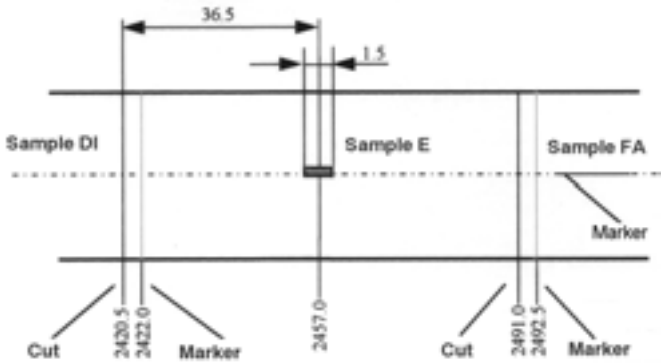


d) sketch of defect position

*Fig. 6. Aspect of X-mark.*

### 4.2. Neutron radiography of the X-mark segment

A rod segment of about 700 mm length containing the X-mark was neutron radiographed in order to assess the condition of the fuel pellet beneath the primary defect. For comparison, the same segment of the sibling sound rod D2 was also investigated. Radiography was carried out at the NEURAP facility of the PSI spallation neutron source [9]. The characteristic beam properties are given in Table 2.

Table 2: Beam Properties at the NEURAP position

| Distance from aperture blind | Beam Diameter | Neutron Flux | L/D ratio | Cd-ratio |
|---|---|---|---|---|
| mm | mm | $cm^{-2}s^{-1}mA^{-1}$ | - | - |
| 7292 | 290 | $5 \cdot 10^{6}$ | 350 | 100 |

The mean neutron energy was 25 meV and the flux amounted to $4 \cdot 10^{6}$ $n/cm^2s$ at a proton current of 820 μA. Images were taken using the track-etch method (boron coated nitro-cellulose film CN85 Type B) and an exposure time of 15 minutes. The films were processed according to the manufacturer prescription. The negatives were digitised in the reflective mode using a CCD camera and processed with standard image processing software.

Neutron radiography images were taken of both of the segments from three different angular positions 45° respectively. Rod D2 only showed a small chipped area at a pellet edge and a slight gap at one pellet-pellet intercept. In rod B4 no indication of a defect could be detected at the location of the X-mark (elevation 2456 mm) under all three angles. Fig. 7 shows a detail of the corresponding radiographs. The pellets exhibit transversal and some longitudinal cracks but otherwise appear in perfect shape. About 60 mm below the X-mark position a small chipped area was detected in the cylindrical surface at the pellet edge as shown in Fig. 8. It extended about 2.4 mm in axial direction. It is difficult to estimate the dimensions in radial and circumferential direction since the defect was not visible in the two other views and these two dimensions cannot be determined from only one image. A second rather peculiar defect was observed at elevation 2509 mm, which is 50 mm above the X-mark. Two adjacent pellets showed missing cylindrical surfaces on the pellet edges at the same intercept but about 180° opposite to each other. The size of these chipped areas were considerable and amounted to 3.2 and 4.0 mm in axial direction respectively. Again, the defects were not visible in the two other views rotated by 45° on either side.

Further away from the X-mark position, additional small chipped areas were observed in rod B4. The quality of the pellets in this rod seemed definitely inferior to that in rod D2. The defects were always emanating from the pellet edge, which is typical chipping during the manufacturing process. The defects were only visible in one of the three images taken from the segment. They can be assumed to be rather shallow and the difference in transmissivity compared to the sound cross section is therefore so small that they are only visible when located at the rim of the pellet cross section being radiographed.

Not having found any indication at the X-mark position raised the question whether the fuel stack was not displaced versus the cladding in the cold condition due to the difference in thermal expansion of Zircaloy and uranium oxide. A simple estimate, however, yields that the displacement should not exceed about 8 mm. Clamshell opening of the rod segment just above the X-mark showed that the axial positions of the pellet intercepts and the corresponding

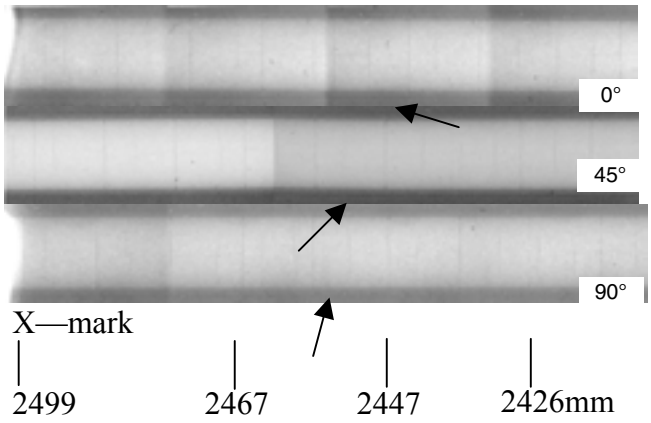


*FIG. 7. Neutron radiographs of the segment of rod B4 containing the X-mark viewed from three different angles 45° apart; X-mark position at elevation 2454-2456 mm.*

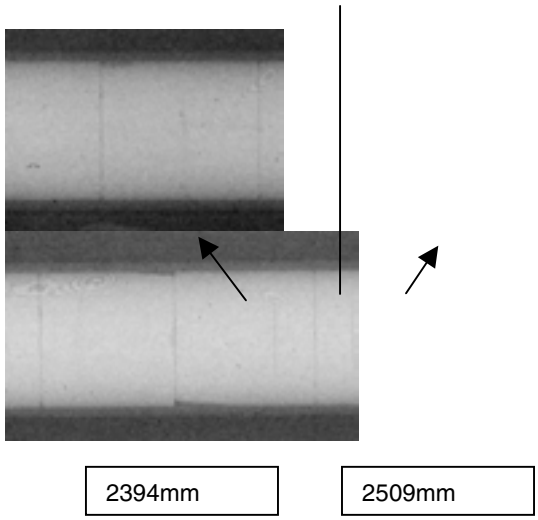


*FIG. 8. Pellets with missing surfaces close to the X-mark.*

markers at the inside of the cladding differed by less than 1 mm. The pellet found beneath the X-mark in the investigation thus corresponded to that during operation and being involved in the PCI event.

Assuming a pellet defect of similar size or slightly larger than the defects observed in NR and mentioned above, it seems highly probable that the defect could not be detected if its azimuthal orientation was situated between the imaging positions chosen. Not having found a defect thus not necessarily excludes its existence.

### 4.3. Metallography

Careful metallography was applied to finally reveal the conditions at the X-mark location. A rod segment of 13.5 mm length containing the defect was extracted and starting far above the presumed X-mark position, consecutive cross sections of the rod were prepared first 1.5 mm apart and later only 0.5 mm apart, when the defect appeared covering an axial distance of about 8 mm total. The preparation in each step consisted in grinding with SiC-paper of 220 to 4000 grit and polishing with a diamond suspension down to 0.25 μm. The cross sections were imaged using a Reichert Telatom 62. No hydride etching was applied.

Preparation started in the pellet above the X-mark location. The pellet was fragmented and showed some large radial cracks. The gap between the pellet and the cladding was completely filled with oxide (10-20 μm thick). At some locations around the circumference, the inner liner showed a pit-like attack with a penetration depth of up to about half the liner thickness.

Having removed the above pellet, at the edge of the underlying pellet, a missing cylindrical surface extending about 2.1 mm in circumferential and 0.21 mm in radial direction appeared. The cladding was still sound and only exhibited the pit-like attack at the inner liner. Consecutive preparation showed that the missing surface extended about 4 mm along the axial direction of the pellet. The pellet itself showed a large radial crack ending into the chipped area.

After about 2 mm from the intercept, a crack in the cladding appeared over a length of about 1.3 mm. Fig.9 shows the cross section of the rod with the missing surface at the top and the crack nearly penetrating the cladding (elevation 2458.6 mm). The crack is completely oxidized and shows only little branching as shown on the insert.

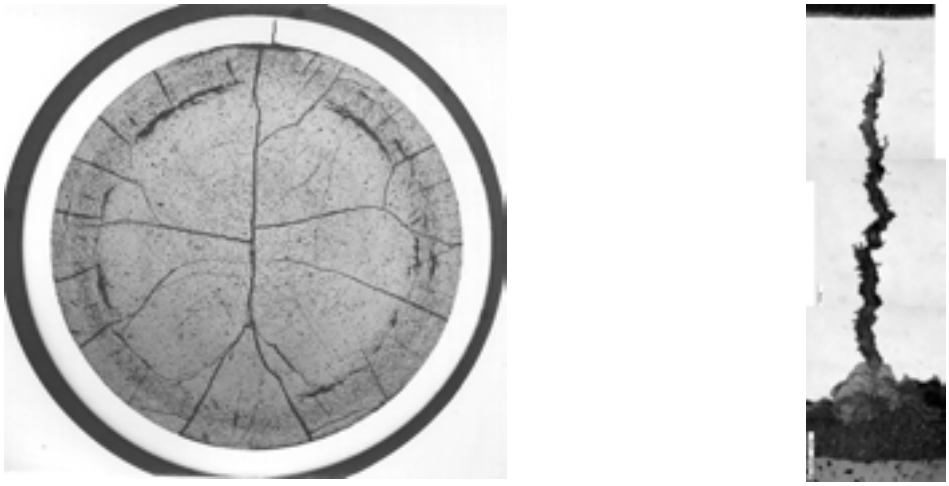

*FIG. 9. Cross section at the X-mark location with a small missing cylindrical surface on the pellet. The crack in the cladding starts from the chipped area and almost penetrates the cladding.*

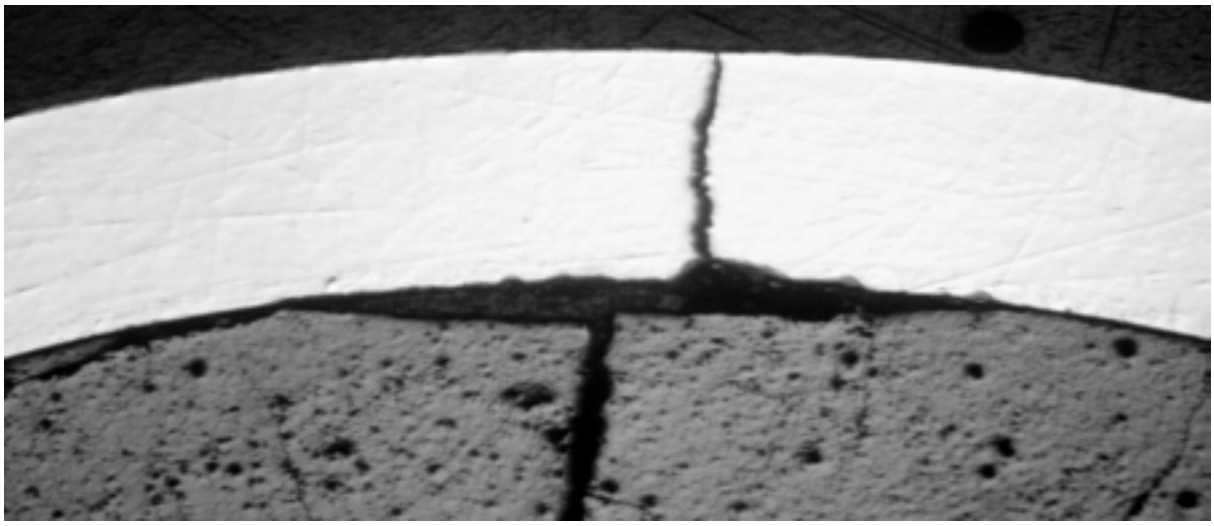

*FIG. 10. Missing pellet surface with fully penetrated crack in the cladding.*

## 5. DISCUSSION

A schematic of the missing pellet surface is shown in Figure 11 together with a 3-dimensional representation of a fuel pellet. The missing surface extended approximately 4 mm (~1/3 of the overall pellet height) along the axial direction starting at the upper end of the pellet. At the location of the cladding crack, the width and depth of the missing pellet surface was approximately 2 mm and 0.15 mm, respectively. These dimensions indicate that the missing pellet surface is slightly concave as shown in Figures 11 a) and b).

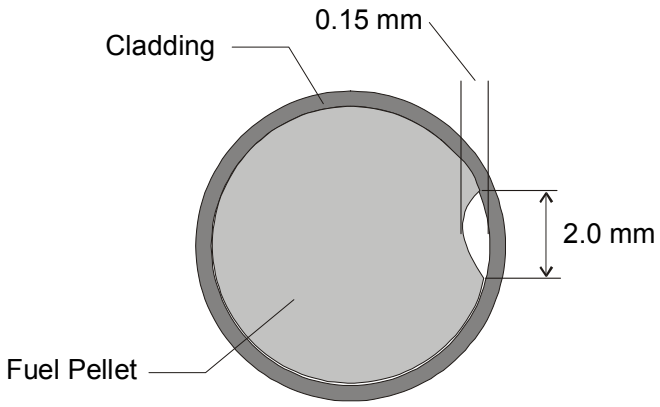


*FIG. 11 a. Schematic of Missing Pellet Surface in Rod B4 at crack location.*

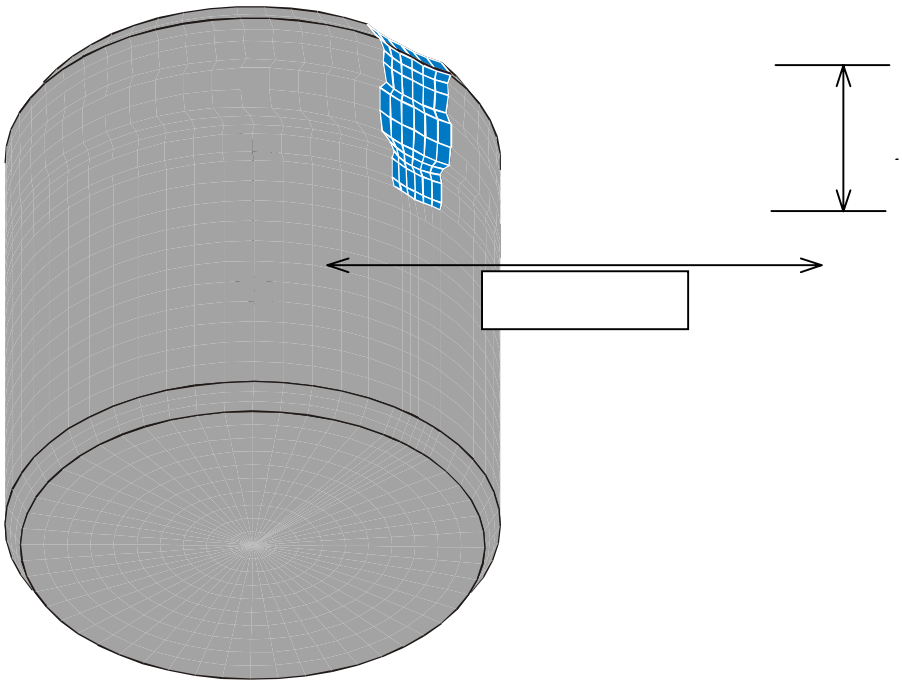

*FIG. 11 b. 3-D Representation of Missing Pellet Surface.*

A local PCI analysis was conducted using the unique r-μ geometric modeling capabilities of the FREY-01 fuel behavior analysis program [10, 11] to evaluate the impact of the missing pellet surface on the potential for cladding failure for KKL Rod B4. This capability allows for a detailed calculation of the cladding stress and strain response in the vicinity of the missing pellet surface during and following the power increase coincident with failure.

FREY-01 utilizes the finite element methodology (FEM) to represent the fuel pellet, cladding and pellet-cladding gap. The versatile geometric modeling capability of FREY allows for explicit representation of the missing pellet surface within the FEM model. The local special effects model, based on nominal 8x8 fuel rod dimensions, is shown in Figure 12 for the defected KKL rod B4. The model is a 30º r-Φ slice at the axial elevation of the PCI-type crack and in the vicinity of the missing pellet surface. The model also includes a series of elements to represent the zirconium liner on the cladding inner surface. Symmetry boundary conditions

are used at the 0º and 30º locations in the model. Previous sensitivity studies have shown that this model size is sufficient to eliminate any end effects arising from the symmetry boundary conditions. Coolant conditions (temperature and heat transfer coefficient) at full power were used at the cladding-coolant interface. The pellet and cladding geometry, fill gas pressure, and fill gas composition at the time of the control blade withdrawal were obtained from a full-length fuel rod analysis of Cycles 8, 9 and 10.

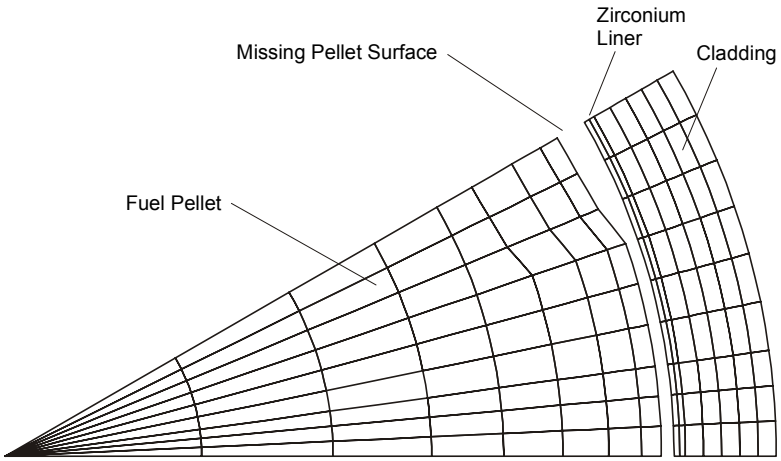


*FIG. 12. Finite Element Used in PCI Analysis of Missing Pellet Surface.*

The local power during Cycle 10 in the vicinity of the PCI-type cladding crack is shown in Figure 13. As shown, Rod B4 started Cycle 10 under controlled conditions, with the local power near 4 kW/ft. At approximately 163 EFPD's into Cycle 10, the control rod in the vicinity of assembly KLG072 (Gang-38) was withdrawn several notches at a time. This caused the local power to increase slightly to about 6 kW/ft. The local power then displays a sharp increase to near 10.5 kW/ft when the control blade uncovers this region at 200 EFPDs. The assembly continued to operate for another 37 EFPDs until the mid-cycle shutdown.

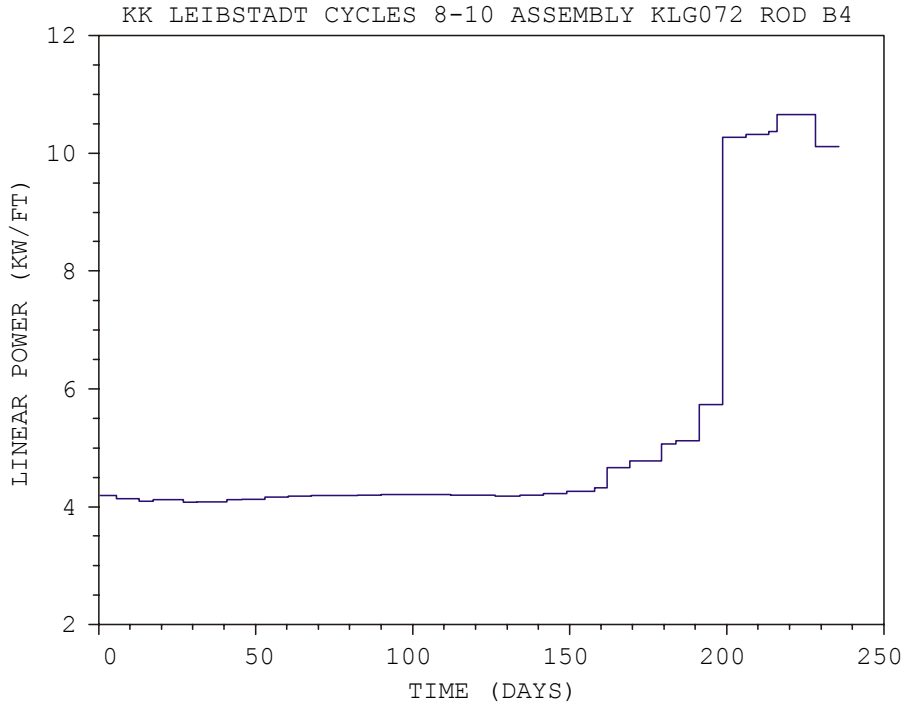


*FIG. 13. Local Linear Power at 96" (2458 mm) Elevation During Cycle 10.*

The PCI analysis focused on the power change at 200 EFPD to evaluate the cladding stress and strain response in the vicinity of the missing pellet surface. The fuel rod conditions just prior to the power change were obtained from the full-length analysis and were used to initialize the PCI analysis. A power ramp of ~45 kW/ft/hr (~150 kW/m/hr) was used to model the power change associated with the control blade withdrawal of 4 notches. This value was determined by assuming the power rise associated with a control blade withdrawal occurring in 0.1 hours.

ISCC leading to cladding failure is a function of the fission product environment, the material composition, and the cladding stress level [12]. The burnup level of Rod B4 insures that sufficient fission product inventory was available to support ISCC. As mentioned, Rod B4 had a zirconium liner, which was developed specifically to protect the cladding from ISCC. Ramp tests have been performed previously by GE and others to demonstrate the effectiveness of a zirconium liner to minimize PCI failures [13, 14]. A small fraction of these tests did exhibit cladding failure by PCI at peak power levels above >52 kW/m, showing that the zirconium liner is susceptible to ISCC, but only under the most demanding of cladding stress conditions. Therefore, the assumption stated above is not groundless, and as will be shown by the FREY-01 analysis, the environmental and stress conditions were sufficiently high to cause ISCC in Rod B4.

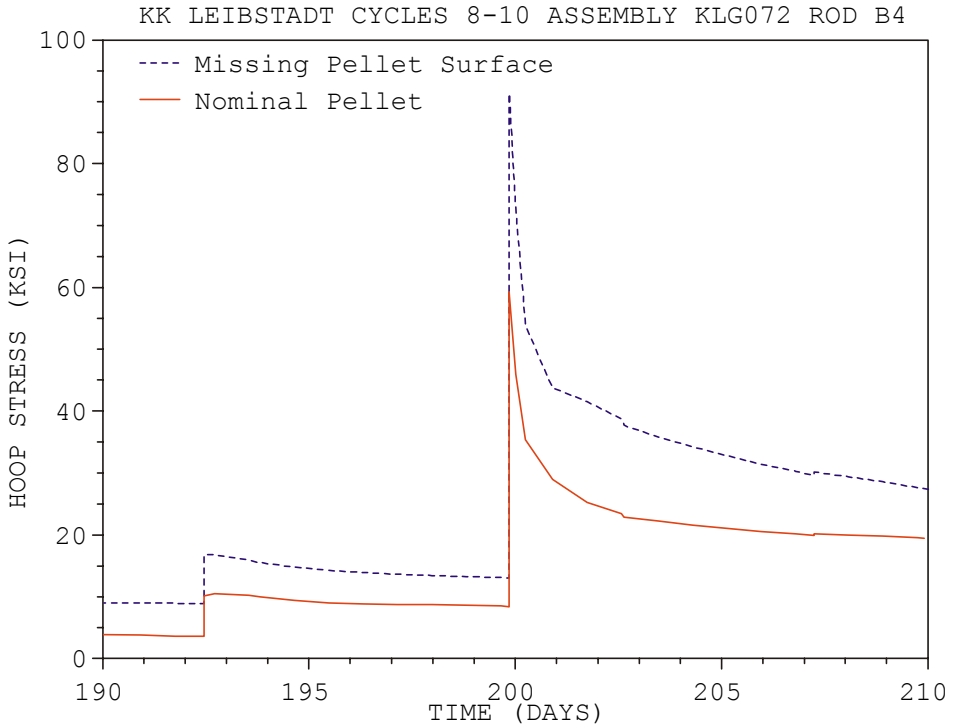


*FIG. 14. Comparison of Cladding Hoop Stress Near Zr/Zr-2 Interface.*

A key element in the PCI process is the magnitude and duration of the stress level in the cladding following a power change. The analysis results show that the hoop stress in the Zircaloy portion of the cladding increases significantly in the region adjacent to the missing pellet surface. Figure 14 is a plot of the cladding hoop stress near the Zr/Zr-2 interface (location of maximum stress) at the mid-point of the unsupported cladding ligament. Also shown for comparison is an analysis where the pellet is assumed to be cylindrical without any defects. As can be seen, the cladding hoop stress at the end of the power ramp is approximately 60% higher for the missing pellet surface case. This situation arises because the unsupported cladding ligament experiences an additional bending stress component as this

region attempts to straighten and conform to the non-circular geometry of the pellet. The additional bending component increases the magnitude of the hoop stress and decreases the rate of creep relaxation of the stresses following the power increase as compared to a nominal pellet. A contour plot of the cladding hoop stress is shown in Figure 15 for both cases analyzed.

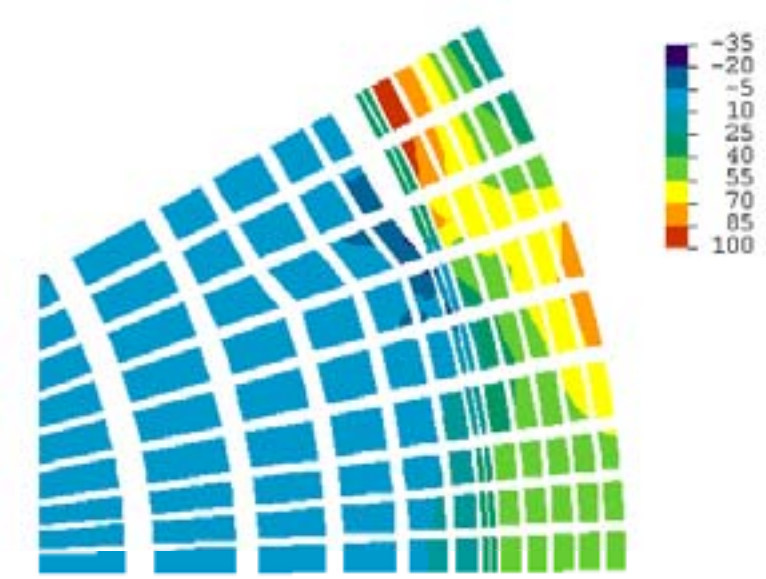


*FIG. 15. Hoop Stress Contour Results for Rod B4.*

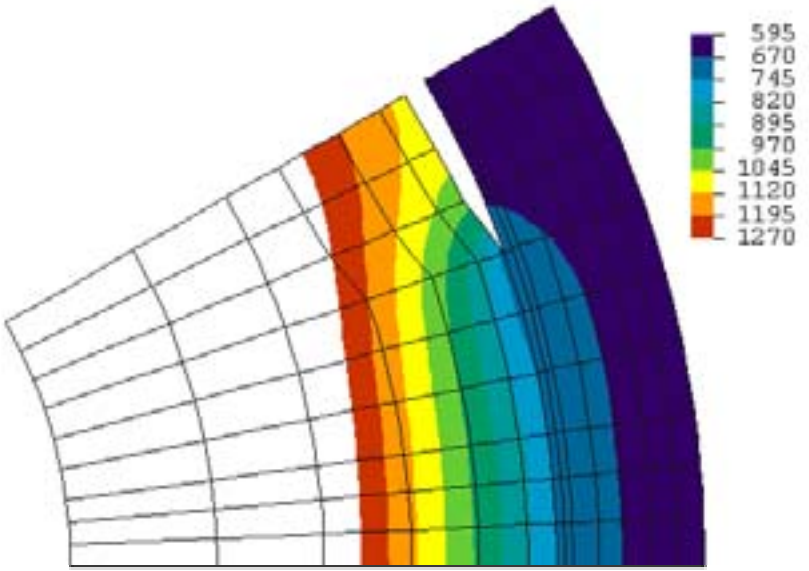


*FIG. 16. Temperature Contour in the Pellet and Cladding.*

A second important impact of the missing pellet surface is on the local fuel and cladding temperature distribution. The calculated results are highlighted in Figure 16. The wider gap between the pellet and cladding produces a lower gap conductance in the region of the missing pellet surface. As a consequence, the fuel pellet surface temperature is increased by 220ºC and the cladding temperature decreases slightly. The locally higher fuel temperatures may promote

the release or transport of volatile fission products such as Cs, I, and Cd to the region of the missing pellet surface. These are the primary fission products suspected to produce ISCC in Zircaloy cladding. Combined with the elevated cladding hoop stress caused by the missing pellet surface, the increase in volatile fission products establishes an aggressive environment for ISCC of the liner and is probably the main cause of failure in Rod B4.

## 6. SUMMARY

Detailed PIE on the defected KKL rod B4 of assembly KLGO72 showed that the fuel below a cladding X mark defect at elevation 2456 mm revealed a missing surface. The cladding defect occurred after a control blade withdrawal which exposed the pin position of height 2456 mm to a rapid power increase from 18 kW/m to ~ 35 kW/m.

The local effects PCI analysis of the mentioned rod during the KKL Cycle 10 Gang-38 control blade withdrawal sequence shows that the presence of the missing pellet surface caused a significant increase in the cladding hoop stress as compared to a normal (circular) pellet. A second important effect is the degraded heat transfer across the large pellet-cladding gap associated with a missing pellet surface. This condition raises the fuel pellet surface temperature and promotes the migration and transport of volatile fission products conducive to ISCC towards the cladding. The presence of these reactive fission products would further stimulate the ISCC process in the zirconium liner and then through the remainder of the cladding wall.

The results from the FREY-01 analysis demonstrate that the PCI-type crack observed in KLG072 Rod B4 was probably caused by ISCC of the zirconium liner and then exposure of the Zr-2 cladding wall to the volatile fission products. Further propagation of the crack occurred as a consequence of the high hoop stresses in the Zr-2 cladding wall. These conclusions support the metallographic examinations in the vicinity of the X-mark crack in Rod B4 which found a multi-branching through-wall crack in the Zr-2 portion of the cladding, characteristic of PCI cracks observed in older non-barrier rods.

## REFERENCES


[1] G.A. POTTS, R.A. PROEBSTLE: Recent GE BWR Fuel Experience; Int. Topical Meeting on LWR Fuel Performance, West Palm Beach, 1994, 87-95.

[2] G.A. POTTS: Recent GE BWR Fuel Experience; Int. Topical Meeting on LWR Fuel Performance, Portland, 1997, 261-271.

[3] J.S. ARMIJO: Performance of Failed BWR Fuel; Int. Topical Meeting on LWR Fuel Performance, West Palm Beach, 1994, 410-422.

[4] G.A. POTTS: Recent GE BWR Fuel Experience; Int. Topical Meeting on LWR Fuel Performance, Park City, 2000, 95-107.

[5] S.K. YAGNIK, O. OZER, B.C. CHENG, R.L. YANG, R.O. MONTGOMERY, Y.R. RASHID, J.H. DAVIES, E.V. HOSHI, R.B. ADAMSON: Assessment of BWR Fuel Degradation by Post-Irradiation Examinations and Modeling in the Defect Code; Int. Topical Meeting on LWR Fuel Performance, Portland, 1997, 329-336.

[6] D.J. SUNDERLAND, M.W. KENNARD, J.E. HARBOTTLE: An Evaluation of the Potential for PCI in BWR Barrier Fuel Failures; Int. Topical Meeting on LWR Fuel Performance, Portland, 1997, 372-376.

[7] H.G. HAGER: KKL - Neutronenphysikalische Unter-suchung der Stableistungsgeschichte von in Zyklus 10 defekt gewordenen Brennstäben; PSI TM-41-99-01, 1999 (private communication).
[8] H. KNAAB, M.W. KENNARD, S. LUNDBERG, H.G. WEIDINGER: KKL Cycle 10 Fuel Failure Evaluation; 1994.
[9] F. GROESCHEL, P. SCHLEUNIGER, A. HERMANN, E. LEHMANN, L. WIEZEL: Neutron radiography of irradiated fuel rod segments at the SINQ; Nucl. Instr.&Methods in Physics Research A424 (1999) 215-220.
[10] RASHID, Y. R., MONTGOMERY, R. O., ZANGARI, A. J., "FREY-01: Fuel Rod Evaluation System, Volume 1: Theory Manual," EPRI NP-3277, Revision 3, August 1994.
[11] RASHID, Y. R., ZANGARI, A. J., AND LIN, C. L., "Modeling of PCI Under Steady State and Transient Operating Conditions," IAEA Technical Committee Meeting on Water Reactor Fuel Element Computer Modeling in Steady State, Transient and Accident Conditons, IAEA-659/IWGFPT/32 Preston England, pg. 91-101, September 18-22, 1988.
[12] ROBERTS, J. T. A., et. al., "A Stress Corrosion Cracking Model for Pellet-Cladding Interaction Failures in Light-Water Reactor Fuel Rods," Zirconium in the Nuclear Industry, ASTM STP 681, June 1978.
[13] ROWLAND, T. C., "Demonstration of Fuel Resistant to Pellet-Cladding Interaction: Phase 2 Final Report," GEAP-25163-10, UC-78, November 1984.
[14] OHARA, H., et al., "Fuel Behavior during Power Ramp Tests," Proceedings of the ANS Topical Meeting on LWR Fuel Performance, West Palm Beach, Florida, p. 674, April 1994.

# MODEL DEVELOPMENT OF FUEL FAILURE IN WATER REACTORS DUE TO CLADDING HYDROGENIZATION

E.YU. AFANASIEVA[A], I.A. EVDOKIMOV[A], V.V. LIKHANSKII[A],
A.A. SOROKIN[A], V.V. NOVIKOV[B]

[A] State Research Center "TRINITI", Troitsk Institute for Innovation and Fusion Research
[B] JSC TVEL,

Moscow, Russian Federation

**Abstract**

The present paper is focused on modelling the growth of a massive hydride at inner surface of Zr claddings. A mechanistic model of massive hydriding has been developed which takes into account the following key processes: fuel rod thermal behavior, $UO_2$ fuel oxidation in steam-hydrogen atmosphere under irradiation, hydrogen diffusion in zirconium and in the hydride, growth of the hydride phase. Fuel rod thermomechanical behavior is calculated with an integral fuel code RTOP. An oxidation model has been implemented to the RTOP code to represent the effects of temperature dynamics and temperature profile along fuel axis and radius on fuel/cladding oxidation as well as on hydrogen accumulation inside the fuel element. Along with ordinary thermal dissociation of $H_2O$ molecules the oxidation model also deals with steam radiolysis due to fission fragments. Hydrogen transport in zirconium cladding is modeled with account for thermodiffusion. Calculation of the massive hydride growth is performed in 2-D geometry. The present numerical module allows the self-consistent calculations of thermomechanical fuel behavior under conditions of varying power, varying composition of the gas phase inside fuel rod, inhomogeneous fuel oxidation. The module is able to predict hydrogen redistribution in Zr cladding and growth of the hydride "blister". Preliminary results are presented on numerical prediction of possible cladding failure owing to formation of the through-cladding massive hydride in fuel rod with residual moisture.

## 1. INTRODUCTION

Fuel element failures at operating NPPs are repeatedly reported in literature. Cladding failures cause release of fission products into coolant and penetration of steam inside the rod. Formation of primary defects in cladding is generally attributed to original cladding defects, to process of fretting corrosion (in presence of rubbing areas on cladding), to nodular corrosion, to impact of extraneous particles on cladding ("debris" particles), to pellet-cladding interactions [1,2]. Probability of primary defect formation in cladding also depends on in-reactor water chemistry and hydrogen (water) content in fresh fuel.

As a rule considerable cladding failures take place on the stage of secondary defect formation under fuel normal operation conditions. Secondary defects in most cases are axial or circumferential splits. Fairly long axial splits have been observed – more than ten centimeters in length. However, some data evidence the possibility of cladding failures which are not related to primary defect but are caused by redundant moisture in originally intact fuel rod.

It is believed that the key processes governing dynamics of fuel element failures under normal operation conditions are as follows:

- fuel oxidation in steam atmosphere and hydrogen generation,
- oxidation of inner cladding surface with hydrogen production,
- hydrogen adsorption by cladding and formation of zirconium hydride phases,

- through-cladding growth of massive hydride,
- increase of fuel specific volume due to oxidation and mechanical pellet-cladding interaction leading to initiation and progression of cracks.

Each of these processes is controlled by many interconnected physical phenomena. For instance, the rate of fuel oxidation and hydrogen generation depend on fuel stoichiometry and temperature, on pressure and composition of gas mixture, on heat generation rate in fuel and flux density of fission fragments in gas phase. In its turn, fuel temperature is affected by composition and pressure of gas inside the fuel rod (fuel oxidation is accompanied by increased release of fission products); fuel thermal diffusivity (a function of stoichiometry, temperature and burnup); gap width between pellets and cladding. Gas composition is governed by the rate of fuel and cladding oxidation. Also fuel microstructure may be changed in course of oxidation; along with thermal expansion this may have a considerable impact on process of pellet-cladding interaction.

It should be noted that the problem is of essentially nonlocal nature. Many of basic parameters are functions of axial and radial position in fuel rod. This fact necessitates modelling the distributed system. In presence of redundant moisture in fuel the process of cladding failure may follow the below scenario.

While fuel rod is put to operation for the first time, fuel temperature is increased, available moisture emerges as steam and fills the gas volume inside the fuel rod. In regions of higher temperature steam dissociates with production of hydrogen and oxygen. Hydrogen produced due to dissociation and radiolysis of steam is efficiently taken up by the cladding. Generally this process is hindered by an oxide film over the cladding inner surface [3]. Pellet-cladding interactions may result in cracking of the oxide. Besides, dissolution of the oxide layer may take place on cladding inner surface if hydrogen content in gas phase exceeds a certain threshold level [4]. After the oxide layer is locally cracked, rapid penetration of gaseous hydrogen into metal starts in this location. Hydrogen concentration in near-surface region is increased and for high partial pressure of $H_2$ may exceed the solubility limit in zirconium at local temperature. In this case massive hydride will grow on cladding inner surface (so-called “blister”). Massive hydrides of similar type were observed experimentally [1,5]. Grown up to a size of order of cladding thickness “blisters” may cause substantial fuel element failures.

The present report is devoted to modelling of the just described scenario for massive hydride initiation and growth. Preliminary results on model development and numerical prediction of cladding failures due to formation of the through-cladding massive hydride in fuel element with residual moisture are discussed.

## 2. THE MODEL OF MASSIVE HYDRIDING

For purposes of modelling the massive hydride growth in zirconium cladding the model has been developed which gives an account of interconnected physical processes and comprises the following modules:

- Thermomechanical behavior of fuel element.
- Fuel oxidation and dynamics of gas phase composition inside the rod.
- Hydrogen penetration through the oxide layer on the cladding inner surface.
- Hydrogen diffusive transport in cladding.
- Growth of the massive hydride initiated on the cladding inner surface.

The sequence of calculations is schematically shown in Fig.1. It implies the following key steps:

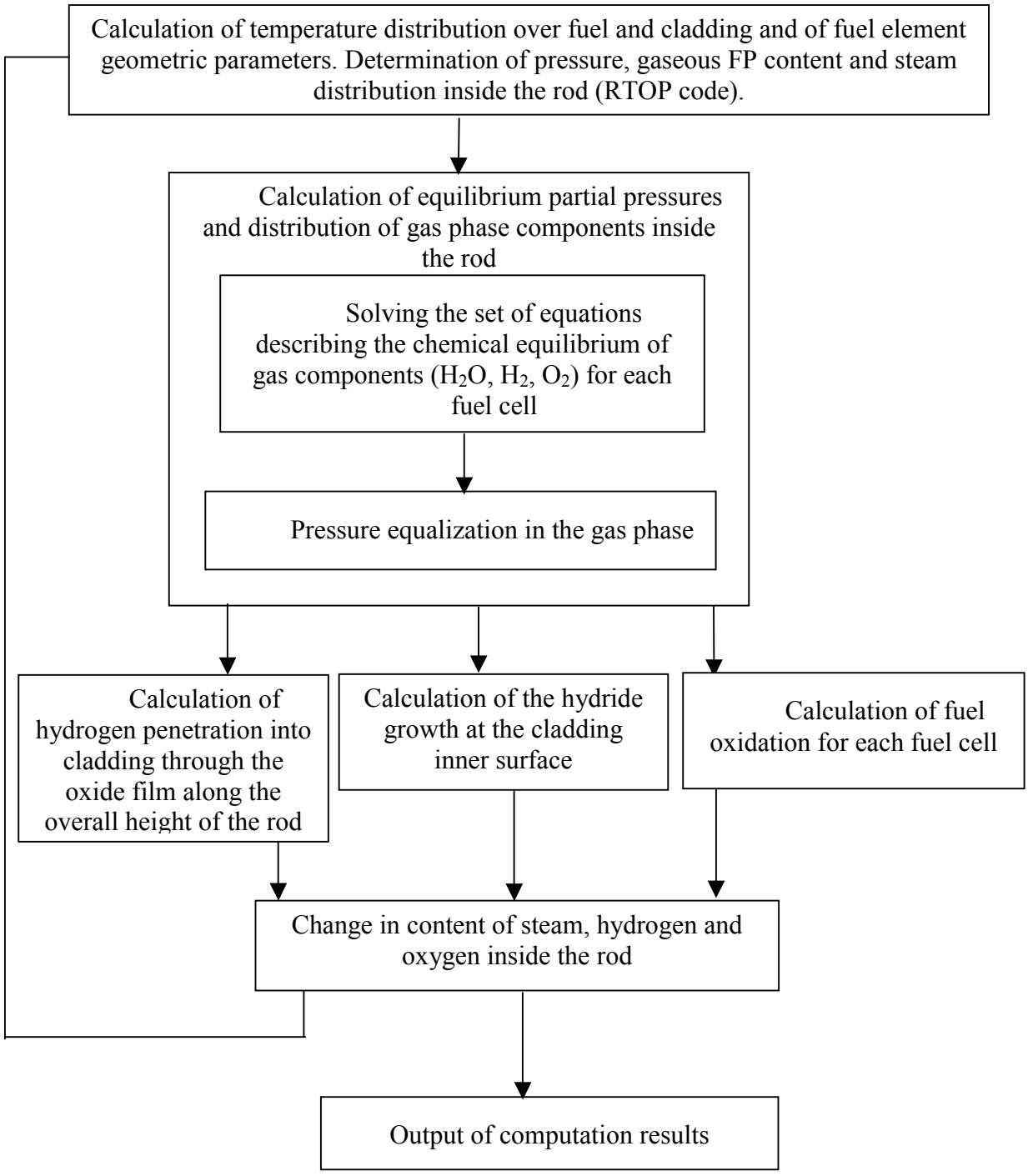


*FIG. 1. The calculation sequence.*

I. Fuel rod thermomechanical behavior is calculated with the integral fuel code RTOP [6-8]. These calculations take into account power distribution in fuel, the release of gaseous FP, the change in content of gas mixture inside the rod, dependence of fuel properties on burnup, stoichiometry and temperature. Thermomechanical calculations take into account geometrical parameters of the fuel and cladding, temperature distribution over the fuel rod. The calculated temperature profiles both axial and radial

are used in computational module which describes the dynamics of fuel oxidation and hydrogen generation.

II. Fuel oxidation and current composition of the gas phase is calculated using the model developed in papers [9,10]. The model accounts for radiolysis of water molecules under irradiation. Radiolysis parameters were chosen according to data [10]. The key factor governing the rate of oxidation under irradiation is the decomposition of water molecules in the gas phase caused by fission fragments. Within the current level of understanding of the complex radiation chemistry, the overall radiolysis effect may be reduced to decomposition of water molecules with production of equal amounts of hydrogen and hydrogen peroxide [10]. The peroxide production rate is proportional to the fission rate density (fissions $m^{-3}$ $s^{-1}$). Due to high reactivity of hydrogen peroxide it efficiently oxidizes the fuel and leads to the enhanced oxidation rate. The present computational module makes possible to calculate the dynamics of fuel stoichiometry change due to oxidation in steam-hydrogen atmosphere depending on temperature and composition of the gas mixture.

III. Modelling of hydrogen penetration through the oxide film on the cladding inner surface is based on correlation [11] which accounts for two mechanisms of hydrogen penetration into metal. The first mechanism is hydrogen diffusion through the oxide film, the second one is hydrogen penetration along defects in the oxide film.

IV. Hydrogen transport in zirconium cladding is modeled in 2-D approximation taking into account the effect of thermodiffusion and dependence of hydrogen diffusivity on temperature.

V. Model of the massive hydride growth on the cladding inner surface in the location of the cracked oxide film is based on experimental data on hydriding of zirconium samples [12]. It is assumed that micro-cracking of the hydride layer occurs when it have grown up to a certain thickness. Micro-cracking results in rapid hydrogen penetration through the cracks and in drastic increase of the hydride growth rate. The model parameters were chosen on the base of available experiments.

## **3**. COMPUTATION RESULTS

The massive hydride growth was calculated for different initial levels of residual moisture in fuel – in the range of 0.1 up to 10 ppm (by mass). Average linear power for the fuel rod was varied from 15 to 30 kW/m with maximum to average ratio of ~ 1.25. The dissolution process for the oxide film on the cladding inner surface in hydric atmosphere is not taken into account in the current code version. Calculations were performed for given initial sizes of cracks in the oxide film. Parameters on temperature dependencies were chosen according to data from: [12] – for hydrogen diffusivity in zirconium cladding, [13] – for hydrogen diffusivity in zirconium hydride, [14] – for the Sievert's constant, hydrogen solubility limit in zirconium alloys and equilibrium hydride stoichiometry in hydric atmosphere. Calculations showed that radiolysis effect on the fuel oxidation rate is temperature dependent as long as temperature governs the relation between the rate of thermal reactions (steam dissociation, recombination, adsorption) and the rate of radiolysis of water molecules under irradiation. Figs.2-3 show the examples of calculated dynamics of hydrogen generation during oxidation of uniformly heated fuel at different temperatures. Calculations were carried out both with and without account for steam radiolysis.

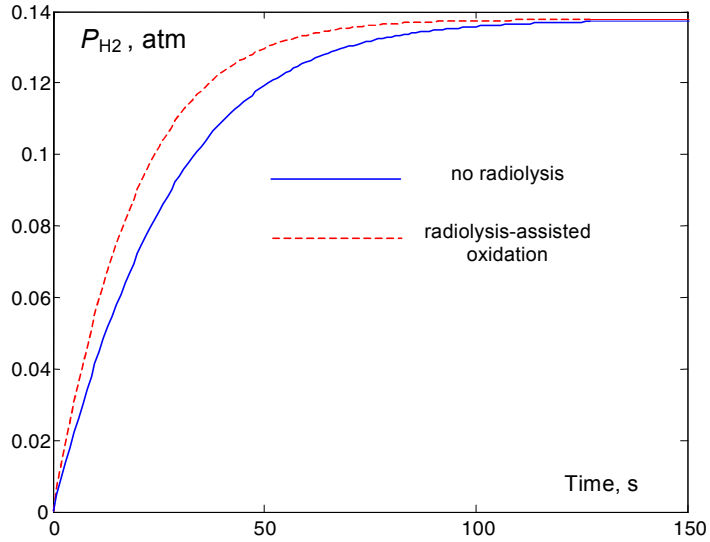


*FIG. 2. Dynamics of hydrogen partial pressure inside the fuel rod. Example of calculation for fuel oxidation at 1200$^0$C.*

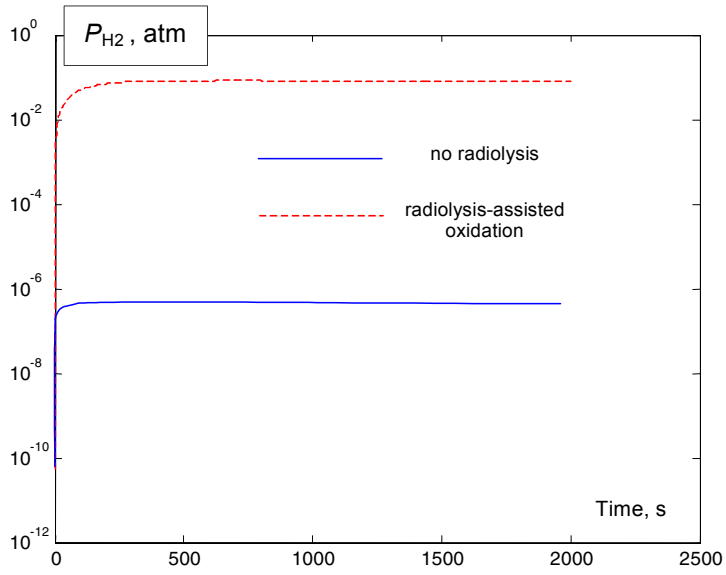


*FIG. 3. Dynamics of hydrogen partial pressure inside the fuel rod at 450$^0$C.*

At high temperatures (central regions of a fuel pellet) the effect of radiolysis is not pronounced but it goes more and more important at lower temperatures (pellet periphery).

Calculations at Figs.2-3 were performed for the fission rate density of $10^{19}$ $s^{-1}m^{-3}$ at initial steam content inside the rod of 0.7 ppm. Values for parameters characterizing interaction between fission fragments and molecules in the gas phase were chosen according to [10]. At high temperature (Fig.2) the rate of thermal reactions is high and even high fission rate density is not sufficient to make radiolysis contribution to fuel oxidation quite noticeable. As temperature goes down the radiolysis effect is increased. At low temperature (Fig.3) in absence of irradiation the rate of fuel oxidation is several orders lower. The established level

of hydrogen partial pressure in the gas phase (solid line in Fig.3) corresponds to thermal equilibrium for hydrogen concentration in the gas mixture $H_2O$–$H_2$–$O_2$ at $450^0$C.

Implementation of the oxidation model to the RTOP code makes possible to calculate kinetics of stoichiometry distribution change along the height and the radius in the fuel rod with account for its real geometry and for arbitrary given power dynamics. Examples of such calculations are shown in Figs.4,5. Fig.4 shows the final stoichiometry distribution along the fuel rod height ($L$) and radius ($R$) in absence of steam radiolysis. Fuel stoichiometry distribution for radiolysis-assisted oxidation is shown in Fig.5. Average linear power for these two variants was 17.5 kW/m, maximum to average ratio was 1.25 and total oxidation time was 9 months.

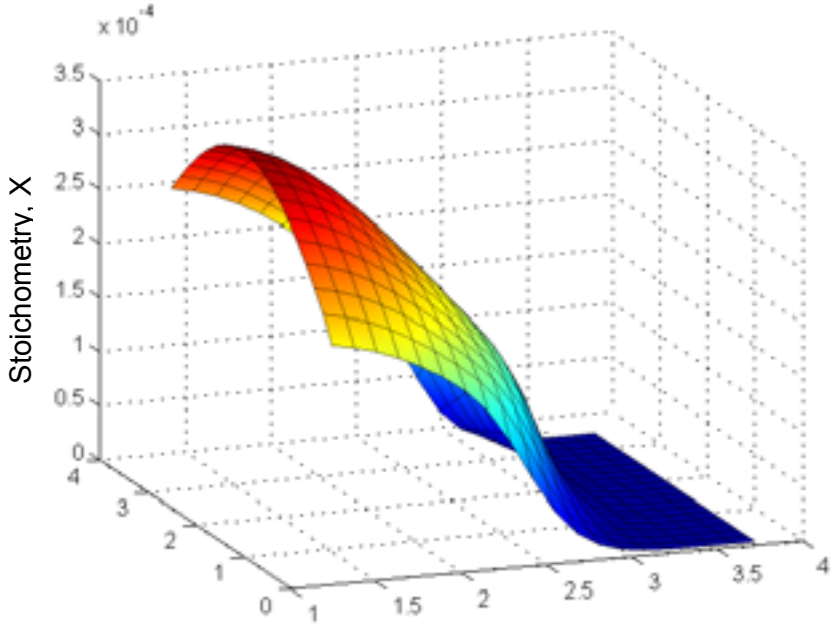


*FIG. 4. Fuel stoichiometry distribution without effect of radiolysis.*

A substantial difference should be noted between stoichiometry distributions calculated with and without account for steam radiolysis. In absence of radiolysis maximum of oxygen content in fuel is reached (for chosen parameters) in the central hot part of a pellet. This is a consequence of the higher steam dissociation rate in this region. Calculations of the radiolysis-assisted oxidation lead to just the reverse oxygen distribution across the pellet. For conditions of Fig.5 maximum of oxygen content in fuel is reached at the pellet periphery. The reason of the reverse behavior is that equilibrium stoichiometry deviation is higher at lower fuel temperature for close values of oxygen potential in the gas phase. Stoichiometry deviation is an important parameter for calculation of FP release kinetics as long as diffusivity of fission products is a steep function of oxygen content in the fuel. Stoichiometry deviation at given level of residual moisture in the sealed fuel rod is not large (for parameters of Figs.4,5) and has a negligible effect on FP release from fuel. However, in the case of the defective rod steam entry through a defect site may result in considerable oxygen accumulation in the fuel. This may cause a noticeable impact both on fuel properties and FP release [1,15].

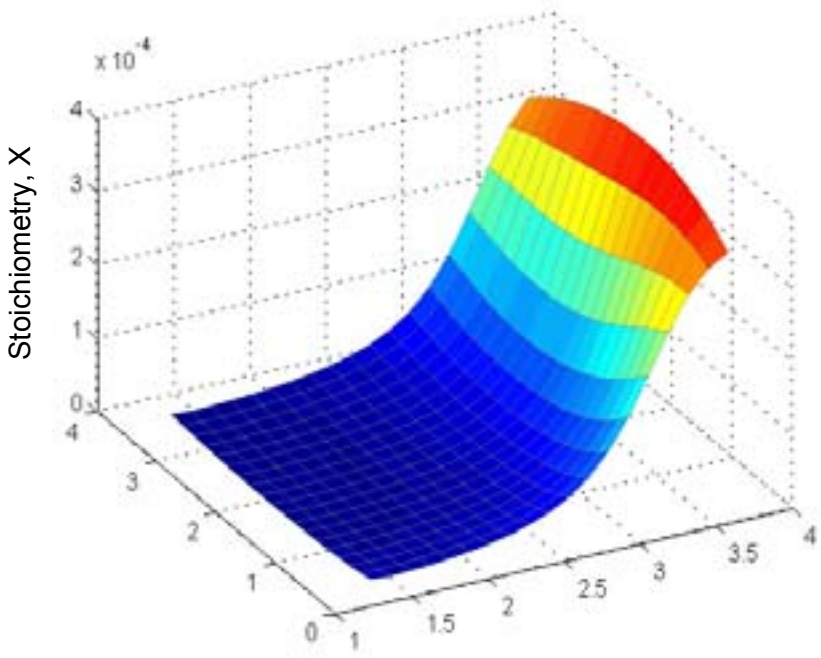


*FIG. 5. Fuel stoichiometry distribution with account for radiolysis.*

In the framework of modelling the kinetics of massive hydride growth, a critical size of a circular inoculating area (free from zirconium oxide) on the cladding inner surface was found. This critical size determines the possibility of massive hydride growth. If the area of direct contact between zirconium metal and the gas phase is not large enough (below the critical value), hydrogen inflowing into metal is rapidly carried away from the surface by diffusion and growth of the massive hydride is inhibited.

The change in shape of the growing hydride was calculated with 2-D computational module. This calculation included an effective diffusive withdrawal of hydrogen from the front of the hydride phase both in the direction of hydride growth and in the transverse direction. Because of hydrogen lateral transport hydrogen concentration profile near the hydride front remains relatively steep till size of the hydride goes close to cladding thickness. The model incorporates the change of hydrogen diffusivity in zirconium and in zirconium hydride due to temperature variation in course of hydride front progression. The thermodiffusion effect on hydrogen redistribution in cladding is also considered.

The modeled growth of the 2-D massive hydride is shown in Fig.6 as an example. Calculation was performed for the fuel rod at 20 kW/m linear power and initial steam content in fuel of 0.7 ppm (by mass). Average cladding temperature is 330 $^{o}$C, temperature drop is 30 $^{o}$C, thickness of the oxide film is 1 μm. The calculated hydride shape is in a qualitative agreement with the shape of massive hydrides observed in experiments (Fig.7). Calculations for higher level of residual moisture in fuel (7 ppm) give the through-cladding hydride, Fig.8. The hydride growth is accompanied by an increase of the hydride-zirconium and hydride-gas interface areas. This leads to increase of the rate of hydrogen uptake from the gas phase. Dynamics of hydrogen pressure for two initial steam contents in the fuel rod is shown in Fig. 9.

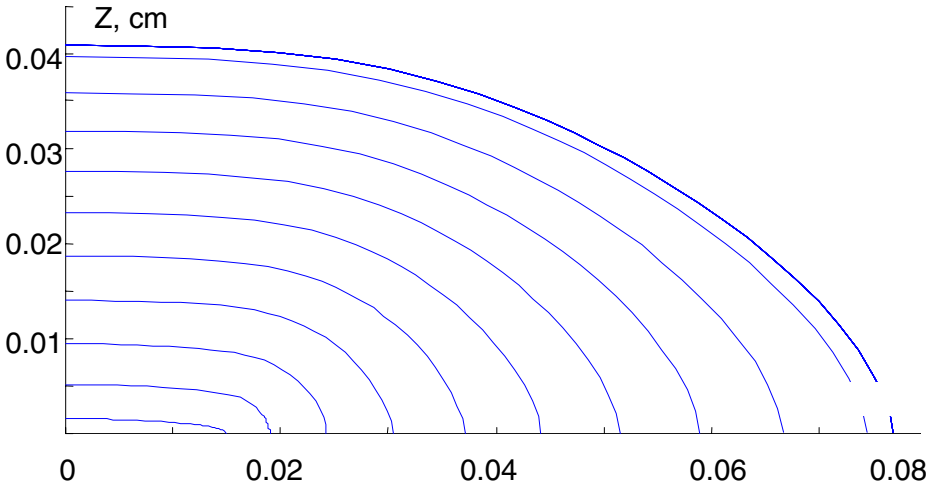


*FIG. 6. Hydride shape calculated in intervals of 5000 s, steam content – 0.7ppm.*

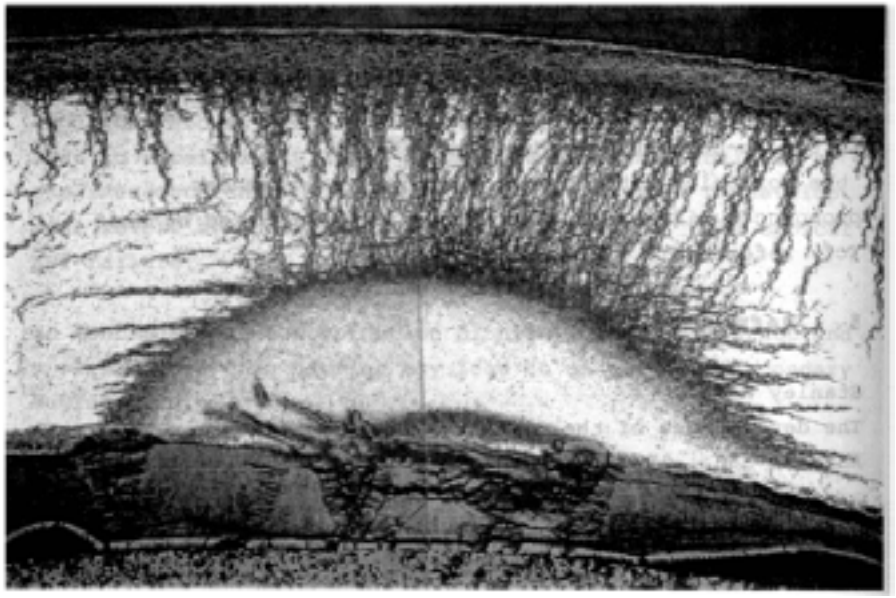

*FIG. 7. Shape of the massive hydride observed experimentally [2].*

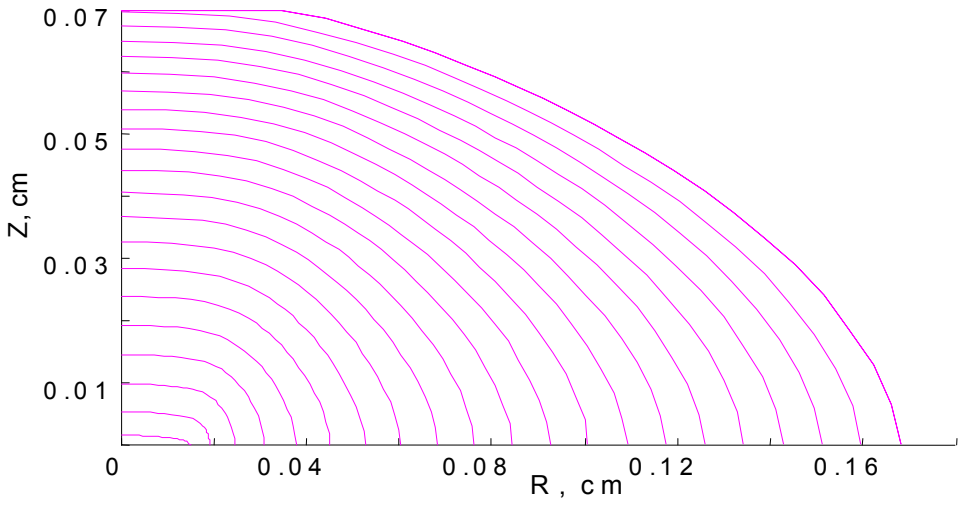


*FIG. 8. Hydride shape calculated in intervals of 5000 s, steam content – 7ppm.*

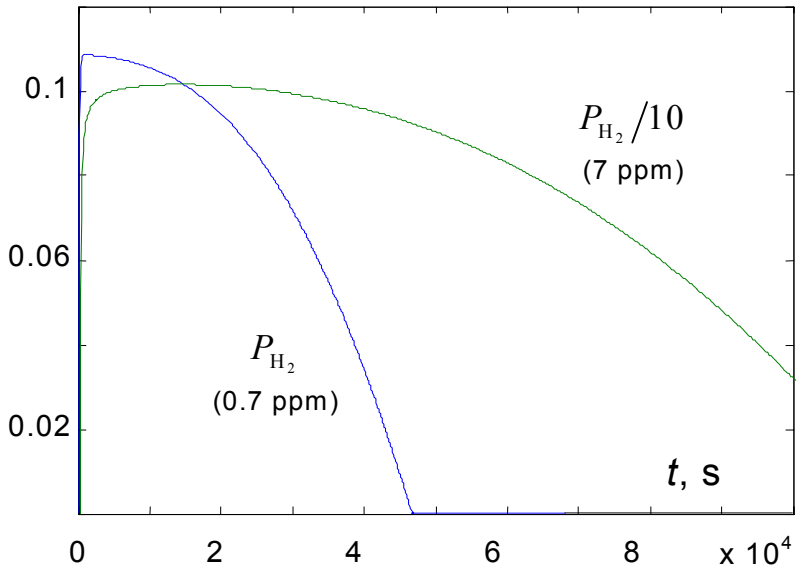


*FIG. 9. Dynamics of hydrogen pressure (atm) inside fuel rods with different initial steam content*

Fig.10 shows an influence of thermodiffusion on hydrogen concentration profiles (related to solubility limit) at different stages of hydride growth. The role of thermodiffusion at the initial stage of hydride growth is minor since gradients of hydrogen concentration are high. With increase of hydride size characteristic concentration gradients decrease and the effect of thermodiffusion on hydrogen redistribution becomes noticeable. Thermodiffusion leads to increase of hydrogen content near cold outer surface of the cladding.

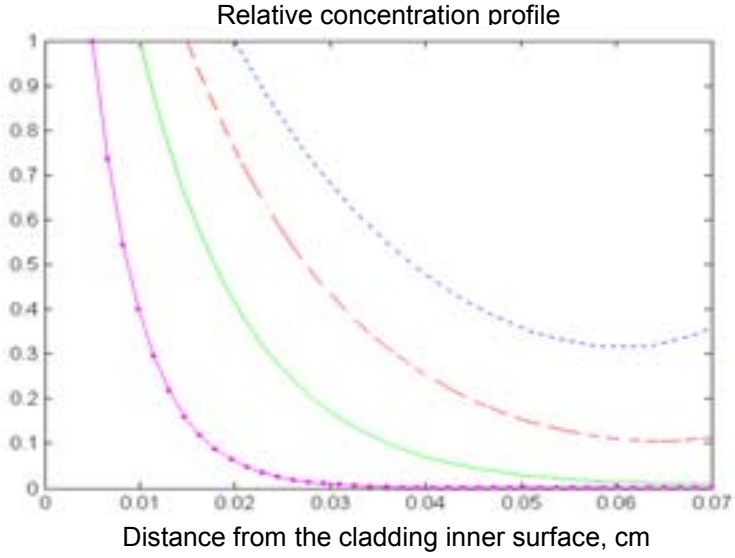


*FIG. 10. Thermodiffusion influence on hydrogen concentration profiles in zirconium at different stages of hydride growth.*

## 4. CONCLUSION

Numerical code has been developed for description of massive hydride growth in Zr cladding of hermetic fuel element. The model is based on following interconnected physical processes: temperature and mechanical behavior of the fuel element, fuel oxidation and dynamics of gas phase composition inside the rod, hydrogen penetration through the oxide layer on the cladding inner surface, hydrogen diffusive transport in two dimensional cladding geometry, growth of the two-dimensional massive hydride initiated on the cladding inner surface.

The analysis of the calculation results shows that there are threshold values of initial steam content inside the intact fuel rod which lead to possibility of through-cladding hydride growth. These threshold values depend on oxidation state of the cladding inner surface, axial linear power profile in the fuel rod, fuel rod geometry, cladding temperature conditions and hydrogen diffusivities in zirconium and zirconium hydride.

After development of a few models and their validation on experimental data the present computational module is supposed to be used for prediction of the defective rod behavior.

*The work was partially supported by Russian Fund for Basic Research (projects No.02-02-16494, 02-02-06670)*

## REFERENCES

1. KIM Y., LEE M., KIM K. *et. al.*, "Hydriding Failure Analysis Based on PIE Data", Proc. Intern. Topical Meeting "LWR Fuel Performance", April 10-13, 2000, ANS (2000) 193-202.
2. EDSINGER K., "A Review of Fuel Degradation in BWR", Proc. Intern. Topical Meeting "LWR Fuel Performance", April 10-13, 2000, ANS (2000) 162-179.
3. ZAIMOVSKII A.S., NIKULINA A.V., RESHETNIKOV N.G., "Zirconium alloys in nuclear industry," Moscow, Energoizdat, 1994 (*in Russian*).
4. KIM Y.S., WANG W.E., OLANDER D.R., YAGNIK S.K., "High Pressure Hydriding of Sponge-Zr in Steam-Hydrogen Mixtures", J. Nucl. Mater, 1977, v.246, pp.43-52.
5. MEYER G., KOBRINSKY M., ABRIATA J.P., BOLCICH J.C., "Hydriding Kinetics of Zircaloy-4 in Hydrogen Gas", J. Nucl. Mater., 1996, 229, pp.48-56.
6. DOBROV B.V., KANUKOVA V.D., KHORUZHII O.V., LIKHANSKII V.V., KOURCHATOV S.YU., SAKHAROV B.B., "The development of a mechanistic code on fission product behavior in the polycrystalline $UO_2$ fuel" Nuclear Engineering and Design, v.195, n.3, 2000, pp.361-371.
7. KANUKOVA V.D., KHORUZHII O.V., KOURCHATOV S.YU., LIKHANSKII V.V., L.V.MATWEEV "Mechanistic modelling of gaseous product behaviour in $UO_2$ fuel by RTOP code." Proc. of International Seminar on Fission Gas Behaviour in Water Reactor Fuels, 26-29 Sept, 2000, Cadarache, France.
8. KANUKOVA V.D., KURCHATOV S.YU., LIKHANSKII V.V., L.V.MATWEEV., SOROKIN A.A., KHORUZHII O.V., "Performance capabilities of the RTOP-2 code in modelling the behavior of nuclear fuel and fuel rods under nominal, transient and accident conditions", Trans. II National Conf. – *Safety Assurance of NPP with WWER*. Podolsk, 19-23 November 2001 (*in Russian*).
9. DOBROV B.V., LIKHANSKII V.V., OZRIN V.D., et. al. "Kinetics of $UO_2$ oxidation in steam atmosphere", J. Nucl. Mater, 1998, v.255, pp.59-66.

10. LEWIS B.J., SZPUNAR B., “Modelling of fuel oxidation behavior in operating defective fuel rods,” Proc. of International Seminar on Fission Gas Behaviour in Water Reactor Fuels, 26-29 Sept, 2000, Cadarache, France.
11. SMITH T., “Kinetics and Mechanism of Hydrogen Permeation of Oxide Films on Zirconium”, J. Nucl. Mater, 1966, 18, pp.323-336.
12. SHMAKOV A.A., BIBILASHVILLY YU.K., KALIN B.A., SMIRNOV E.A., “Prediction of possibility of hydride cracking in zirconium claddings of fuel rods”, MEPhI Preprint 003-99, 1999 (*in Russian*).
13. ANDRIEVSKII R.A., “The metallurgy of hydrides,” Moscow, Metallurgy, 1986, (*in Russian*).
14. DOUGLASS D.L., “The metallurgy of Zirconium,” Atomic Energy Review, IAEA – Vienna, 1971.
15. LEWIS B.J., “Fuel Oxidation Behaviour in Defective Fuel Rods”, Proc. Intern. Topical Meeting “LWR Fuel Performance”, April 10-13, 2000, ANS (2000) 203-215.

# MITIGATION OF FAILURES/DEGRADATION BY PLANT OPERATION

## (Session 4)

# DEVELOPMENT OF FUEL PERFORMANCE CODE FEMAXI-6 AND ANALYSIS OF MECHANICAL LOADING ON CLADDING DURING POWER RAMP FOR HIGH BURN-UP FUEL ROD

M. SUZUKI, H. UETSUKA
Department of Reactor Safety Research,
Japan Atomic Energy Research Institute,
Ibaraki-ken, Tokai-mura, Japan

**Abstract**

A fuel performance code FEMAXI-6 has been developed for the analysis of LWR fuel rod behaviors in normal operation and transient (not accident) conditions. The code uses FEM for mechanical analysis, and has incorporated thermal and mechanical models of phenomena anticipated in high burn-up fuel rods, such as fuel thermal conductivity degradation and pellet-clad bonding. In the present study, PCMI induced by swelling in a high burn-up BWR type fuel rod has been analyzed by the FEMAXI-6 code. During a power ramp for the high burn-up fuel, instantaneous pellet swelling can significantly exceed the level that is predicted by a "steady-rate" swelling model, causing a large circumferential strain in cladding. This phenomenon has been simulated by a new swelling model to take into account the fission gas bubble growth, and we found that the new model can give satisfactory predictions on cladding diametral expansion in comparison with measurements in test rod. The bubble growth model assumes an equilibrium between bubble size and external pressure on the bubble, and simultaneous solution is obtained with both bubble size determination and diffusion equation of fission gas atoms. In addition, a pellet-clad bonding model which assumes firm mechanical coupling between pellet outer surface and cladding inner surface predicts an elevated tensile stress in the axial direction of cladding during ramp, indicating the generation of bi-axial stress state in the cladding. These analyses by the FEMAXI-6 code enable us to predict the magnitude of mechanical loading on cladding during transient and also serve for failure investigation. Clearly, prediction by code calculation depends on the creep and stress-strain properties of highly irradiated cladding.

## 1. INTRODUCTION

High burn-up fuel rods of LWR share such features as pellet-clad gap closure, accumulation of large amount of fission gas in fuel matrix, reduced cladding ductility due to irradiation-hardening and hydrogen absorption, and pellet swelling enhances with burn-up to push cladding outward.

In these situations, mechanical loading on cladding gradually increases, and the cladding is always in a tensile hoop stress to some extent. If, during a normal operation, the fuel rod is subjected to a temporary power ramp, the cladding is anticipated to have enhanced stress. In particular, in the fuel rods which have generated firm bonding between pellet and cladding, mechanical loading on cladding by pellet stack expansion will be notable.

It is expected that the analysis and simulation by an integral fuel performance code will be very informative particularly in transient behaviors, because high burnup rod behavior is produced from much complicated interactions among a number of irradiation-induced phenomena.

On this ground, the present study has performed an analysis on the cladding mechanical loading by using FEMAXI-6 code which has some new models for high burnup rod.

In the study, analyses have been conducted in the power ramp test of BWR type high burn-up fuels and results have been evaluated on the basis of measured data, aiming to demonstrate the significance and validity of the FEMAXI-6 code prediction.

## 2. METHOD

### 2.1. Target Rod Irradiation

Nuclear Power Engineering Corporation (NUPEC) has carried out "The Verification Test on BWR High Burnup Fuel" for the purpose of safety and reliability confirmation of 8x8 fuel rods (BWR Step II Fuel) at high burnup[1][2]. In their test, a number of rods, one of which is a target rod of the present study, have been base-irradiated in assemblies in the core of Fukushima Daini Nuclear Power Station No.2 Unit, operated by Tokyo Electric Power Company under normal BWR conditions for 4 cycles, and then some rods were re-fabricated into a short segment rod and ramp-tested in Japan Material Testing Reactor (JMTR) using the Boiling Water Capsule.

The fabrication specification and irradiation condition of the target rod are listed in Table 1. NUPEC has also conducted such detailed PIE test as dimensional change and FGR measurements, and metallography observation for the fuel rods including the target rod [2].

Table 1. Specs and test conditions of the target fuel rod of FEMAXI-6 analysis

| |
|---|
| **Pellet:** Diameter : 10.4 mm<br>Density : 97%TD , Enrichment : 4.5 (w/o)<br>Stack length : 360. mm (in calculation) |
| Initial internal pressure : 0.484 MPa |
| **Cladding:** Outer diameter : 12.3 mm, Wall thickness : 0.86mm |
| **Burn-up** after base-irradiation : 56.2 GWd/tU |
| **Ramp** test coolant condition in JMTR:<br>Inlet temperature : 561 K, Pressure : 7.26MPa, Velocity : 0.38 m/s |

### 2.2. FEMAXI-6 Code

An overview of FEMAXI-6 functional system is given in Fig.1. FEMAXI-6, an advanced version of FEMAXI-V[3], has an internal structure in which FEM mechanical analysis of entire rod length and thermal analysis have a coupled solution using iteration in each time step for an accurate prediction of fuel behavior particularly in high burn-up region; i.e. the temperature and fission gas calculation use the gap size and contact pressure which have been obtained by the mechanical analysis of entire rod length. Here, users can perform a local PCMI analysis such as pellet ridging as an optional process. However, the present analysis conducts the entire rod length analysis only.

Figure 2 shows schematics of thermal analysis models, and Fig.3 describes the mechanical analysis system by FEM in a cylindrical geometry for the present calculation of rod deformation.

In Fig.2, one single rod is divided into several axial segments, and at each segment, linear heat rate is given, and temperature profile is calculated using burnup dependent materials properties such as thermal conductivity, and radial profile of heat generation density. This profile is obtained by an independent burning analysis code.

In Fig.3, the FEM element is a quad-angle 4-degree of freedom coaxial ring with quadratic approximation function.

*2.2.1. Fission Gas Bubble Swelling Model*

The swelling model in the FEMAXI-6 code has two mutually exclusive options: fission gas bubble swelling (GBS) model, and "steady-rate" swelling (SRS) model. The former calculates the contribution of fission gas bubble growth to swelling by combining the equilibrium bubble size model into the widely known fission gas diffusion and release model which originated in the White & Tucker + Speight model[4][5]. The latter determines the swelling rate as a function of burnup, and does not take into account the effect of bubble growth. The GBS model is described in the following sections.

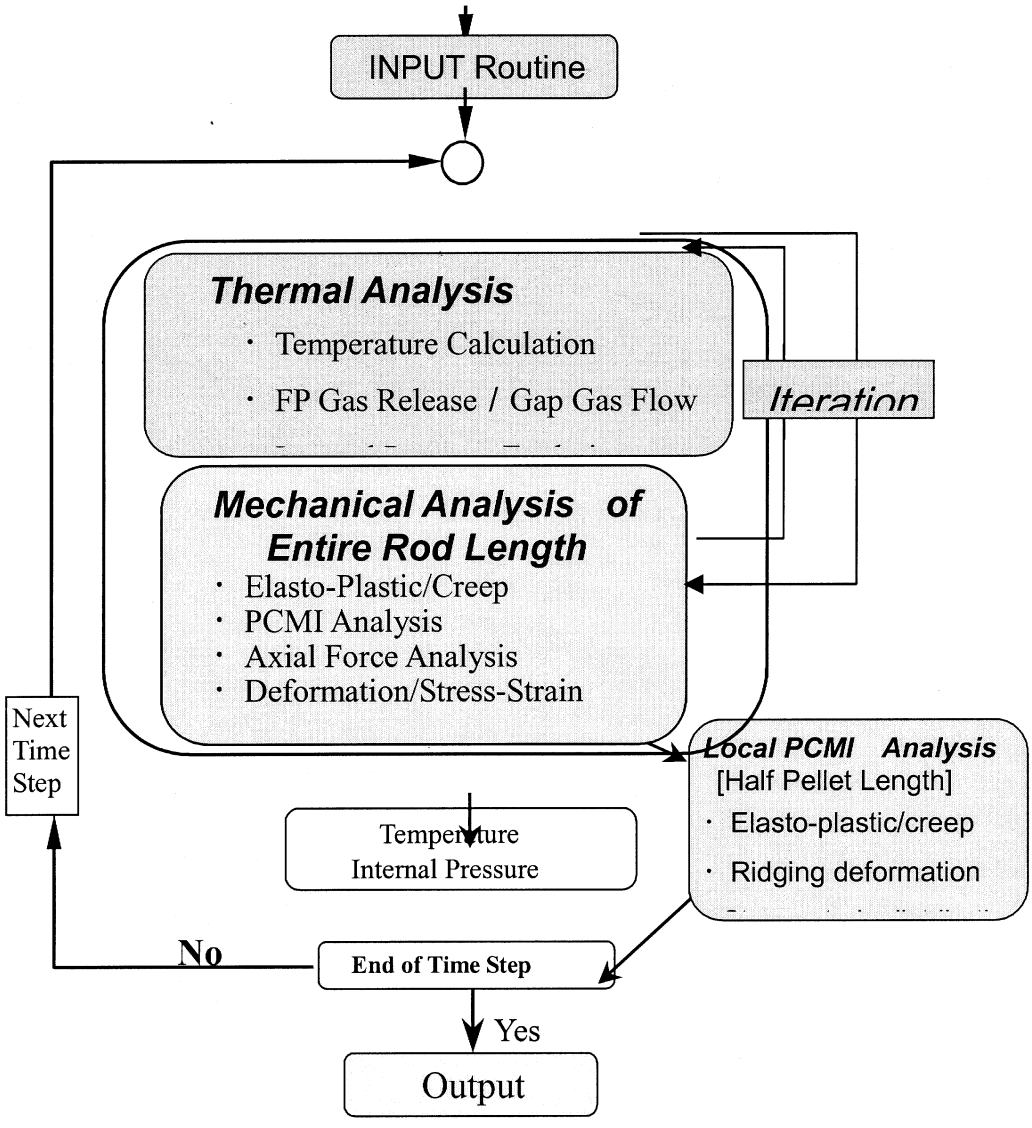


*FIG. 1. FEMAXI-6 analysis system.*

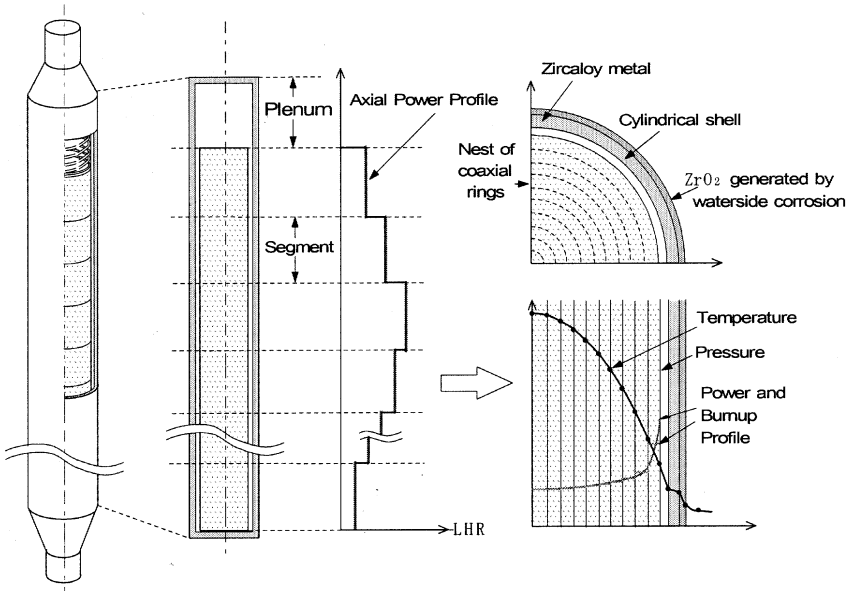


*FIG. 2. Geometrical model for thermal analysis of FEMAXI-6.*

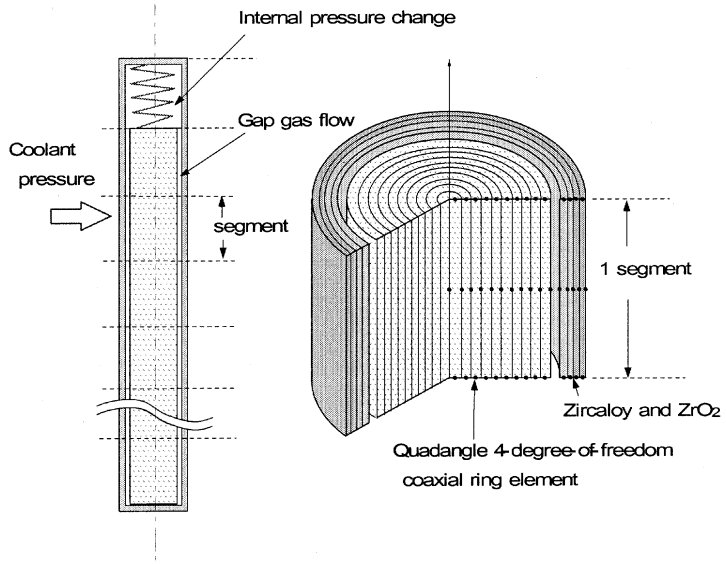


*FIG. 3. Entire rod length mechanical analysis system using cylindrical elements in FEMAXI-6.*

*2.2.2. Total swelling of pellet*

The total swelling of pellet, *Swell* , is defined as

$$Swell = S_{IG} + S_{GB} + S_{solid} \tag{1}$$

Here, $S_{IG}$, $S_{GB}$, and $S_{solid}$ are the fractions of swelling by intra-grain bubble growth, grain boundary bubble growth, and solid FP in the fuel matrix, respectively, and

$$S_{solid} = 0.0025 \quad \text{per } 10^{20} \text{ fissions/cm}^3 \quad (\fallingdotseq 0.66\% / 10\text{GWd/tU}) \tag{2}$$

is assumed.

The gas bubble swelling is defined as the fractional fuel volume increase induced by total gas bubble volume. The PIE metallograph of the target rod shows that the rim structure has appeared in the pellet peripheral [2]. However, the present study does not take into account the fission gas pore growth in the rim, because the pores exist in low temperature peripheral region.

*2.2.3. Equilibrium Method of Intra-grain Bubble Radius Calculation*

Calculation of intra-grain (IG) gas bubble is conducted on the following assumptions[4][5]:

(a) A relationship exists between gas bubble radius and number density of bubbles.

(b) The state equation is set to determine bubble radius, assuming the gas pressure is balanced with external pressure and surface tension of $UO_2$.

(c) Diffusion equation of fission gas atoms into grain boundary is set, assuming an instantaneous balance between trapping rate of fission gas atoms by intra-grain bubbles and re-solution of atoms from the bubbles into matrix. The fission gas atom generation and concentration inside the grain are determined from both power generation rate and diffusion to grain boundary.

A simultaneous solution of equations describing the above conditions (a) to (c) is performed at each time step. Therefore, a numerical solution of diffusion equation using FEM and intra-grain gas bubble radius, and its number density are inter-dependent and hold consistency as a whole.

Here,

(d) Coalescence of bubbles are not taken into account.

(e) It is assumed that the bubble does not shrink below a certain level even if power decreases.

*2.2.4. Calculation Method of Grain Boundary Bubble Volume*

The FEMAXI model calculates grain boundary bubble growth induced by diffusion of fission gas atoms to grain boundary, and fission gas release to free space is predicted on the following assumptions:

(a) Number density of grain boundary bubbles per unit surface area of $UO_2$ grain is assumed to be proportional to the square of the grain radius[6] and inversely proportional to the bubble radius. This indirectly reflects the effect of bubble coalescence.

(b) Equilibrium radius of grain boundary bubble is determined by the state equation until the bubble grows to have 0.5μm radius[4]. The bubble gas pressure is balanced with external pressure and surface tension.

(c) The threshold value (of fission gas atom accumulation in the grain boundary bubble) above which release of fission gas to free space is given by the method of the White & Tucker model. Here, the threshold bubble radius of 0.5 μm has proved to allow the FEMAXI code to predict FGR satisfactorily during normal operation and anticipated transients.

*2.2.5. Pellet-Clad Bonding Model*

It has been recognized that significant duration of pellet-clad contact will produce a bonding layer between them. FEMAXI-6 bonding model consists of "thermal bonding" and "mechanical bonding". These models are described below.

2.2.5.1. Bonding Progress

It is assumed that bonding reaction starts just after the beginning of contact between pellet and cladding. Here, bonding reaction progress, **BD**, is defined as:

$$\boldsymbol{BD} = \left( \int_{t_S}^{t} P_C dt \right) \Big/ X \qquad (0 \le \boldsymbol{BD} \le 1.0) \tag{3}$$

where

$Pc$ : Pellet-cladding contact pressure

$t_S$ : time of contact beginning

$X$ : empirically determined parameter (20,000 hour･MPa)

2.2.5.2. Mechanical Bonding

Upon **BD**=1.0, pellet outer surface and cladding inner surface are assumed to have a firm bonding with each other, and after that, displacement in the axial direction of cladding is set to be identical to that of pellet stack in the calculation.

2.2.5.3. "Thermal Bonding" for Gap Conductance

When 0<**BD**, thermal conductivity of bonding layer is approximated to be that of $ZrO_2$, considering that the main part of the layer consists of $ZrO_2$. Bonding state gap thermal conductance GC1 is expressed :

$$\mathrm{GC1}=(1-\mathbf{BD})\cdot\mathrm{OpenGC} + \mathbf{BD}\cdot\mathrm{BondGC}\ (\mathrm{W/cm^2K}) \tag{4}$$

Here, thermal conductance of $ZrO_2$ layer of 10μm thickness at the surface of pellet is BondGC, and gap conductance by the Ross_&_Stoute model[7] is OpenGC. When **BD**=1, heat is conducted through 10μm $ZrO_2$ layer from pellet to cladding.

*2.2.6. Material Properties*

Important models and materials properties of the code which are adopted in the present analysis are as follows:

(a) Pellet thermal conductivity: Halden model which has been derived on the basis of the in-pile measurement of rod temperature[8].

(b) Pellet thermal dilatation and creep: MATPRO-11model[9]. In the present calculation at above 1773K of pellet temperature, 1773K is always given to the model to obtain pellet creep rate, because 1) the model is based on the experiments that were conducted mainly up to 1300C, and 2) above around 1800K, the creep rate given by the model becomes unrealistically high.

(c) Pellet densification: FEMAXI-III model[10].

(d) Cladding thermal dilatation: MATPRO-11model. Creep: MATPRO-9 model[11].

(e) "Steady-rate" swelling (SRS) model: Studsvik model[12], as a comparative reference to the GBS model.

### 2.3. Input Power History

The FEMAXI-6 code calculation has been performed coherently along the power history and coolant conditions from BOL to EOL and ramp test, with manufactured specifications of rod. However, rod geometry in the calculation is a short segment of 360 mm throughout the irradiation. This segment geometry is sub-divided into three equal-length axial sub-segments, to which linear heat rate is given in the calculation. Power history in the base-irradiation is shown in Fig.4.

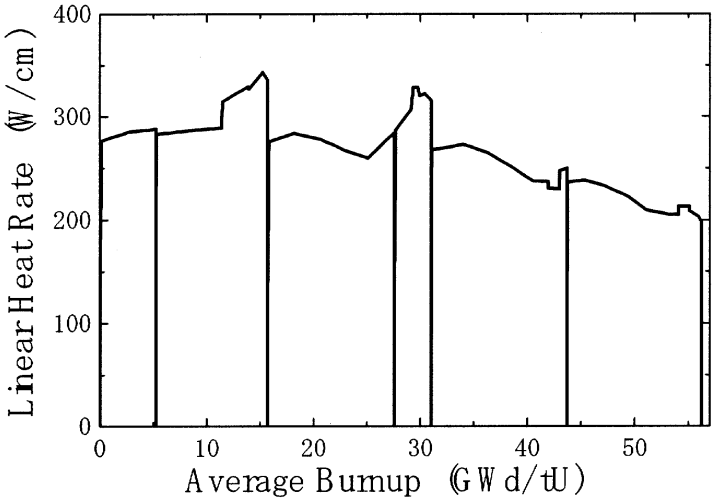


*FIG. 4. Input linear heat rate history during base-irradiation period.*

Heat generation density profile in the radial direction is calculated by a burning analysis code RODBURN[13] as a function of burnup and fed to the ten equally-spaced coaxial ring elements of FEMAXI (See Fig.2). Fast neutron flux is also given to input data. Total fluence has amounted to around $1.1 \times 10^{26} n/cm^2$ at the end of base-irradiation.

## 3. RESULTS AND DISCUSSION

### 3.1. Temperature and Deformation during Base-irradiation

#### *3.1.1. Temperature*

Pellet center temperature at the second (middle) sub-segment is shown in Fig.5. The temperature is not significantly elevated. Calculated FGR is around 10% at most at the end of base-irradiation, indicating a bulk portion of generated fission gas atoms is held in the fuel matrix.

*3.1.2. Deformation with GBS Model*

Figure 6 compares pellet diameter change of GBS model with that of SRS model. Difference between the two models increases after 30GWd/tU where fission gas bubble accumulation becomes significant.

Figure 7 shows changes of gap size and the bonding reaction progress **BD**, and Fig.8 shows cladding diameter change. In early period, cladding creeps down by coolant pressure inwardly to the open gap which is increased by pellet densification, and the gap is closed around 25GWd/tU. After the gap closure, pellet swelling becomes appreciable and cladding is pushed outward, its diameter gradually increases, and **BD** approaches to 1.0. At **BD**=1.0, bonding layer is completed. The bonding layer formation has been confirmed by the PIE metallography[2].

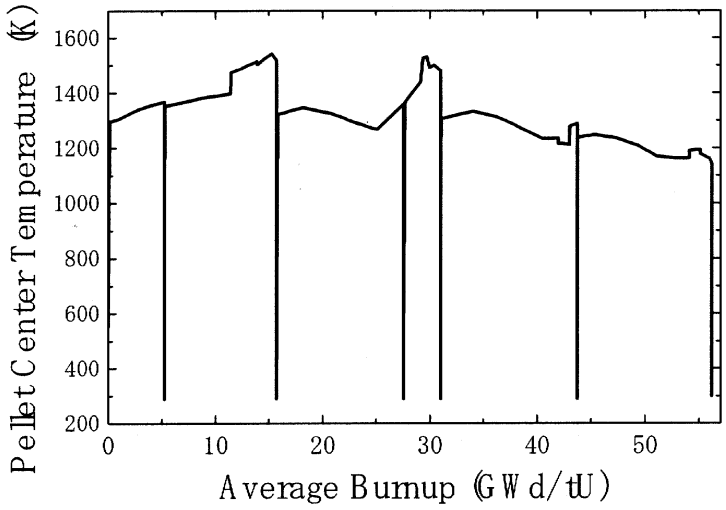


*FIG. 5. Calculated pellet center temperature during base-irradiation period.*

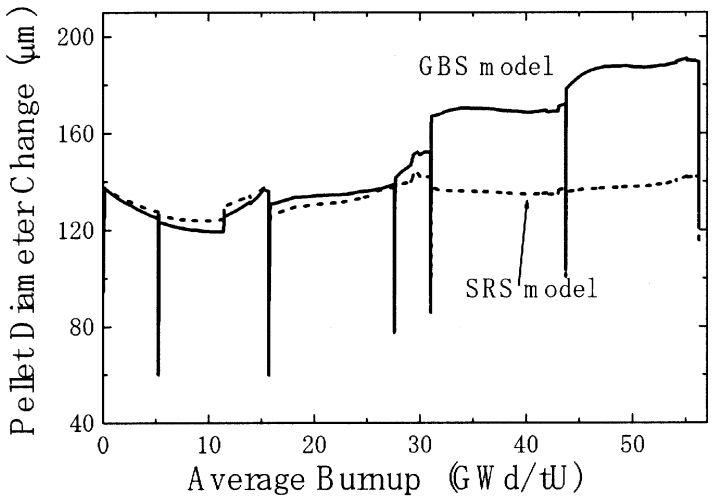


*FIG. 6. Comparison of calculated pellet diameter changes between FP gas bubble swelling (GBS) model and steady-rate swelling (SRS) model during base-irradiation.*

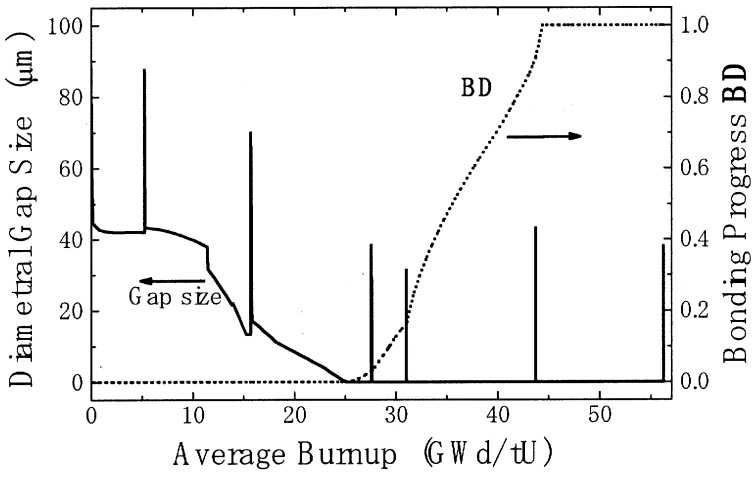


*FIG. 7. Diametral gap size change and bonding progress **BD** by GBS model during base-irradiation period.*

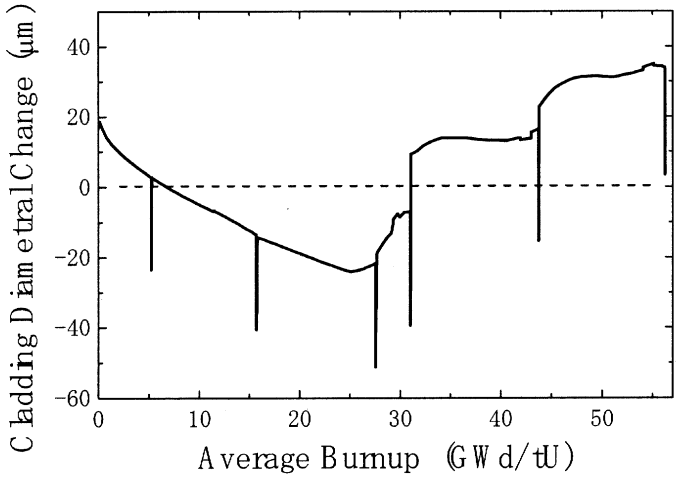


*FIG. 8. Cladding diameter change by GBS model during base-irradiation period.*

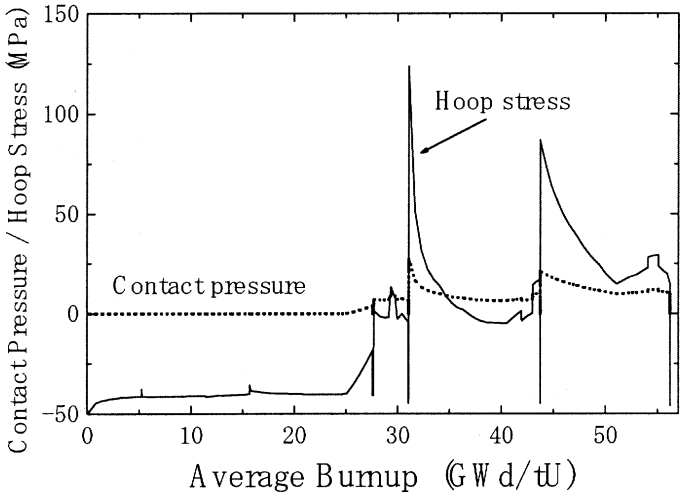


*FIG. 9. Contact pressure on the inner surface of cladding, and hoop stress in cladding by GBS model during base-irradiation period.*

The contact pressure on the inner surface of cladding and resulted hoop stress in cladding in these process is shown in Fig.9. The hoop stress is compressive during the cladding creep-down, but it is slightly tensile during the diameter increase by pellet swelling. It is noted that the hoop stress has a sensitive rise to a discontinuous increase of contact pressure at the start of power cycle, though the stress is not maintained at enhanced level due to the creep relaxation effect of both pellet and cladding.

Figures 10 and 11 show stress and elongation of cladding in the axial direction, respectively. Though the cladding is in a compressive state due to coolant pressure, it is in a tensile state by pull-up of axially elongated pellet stack after completion of the mechanical bonding. However, this stress is relieved owing to the stack creep.

Cladding axial elongation is produced by irradiation-growth up to 25 GWd/tU, after which the elongation has a temporary decrease due to a considerable cladding hoop strain increase induced by pellet swelling (See Fig.8).

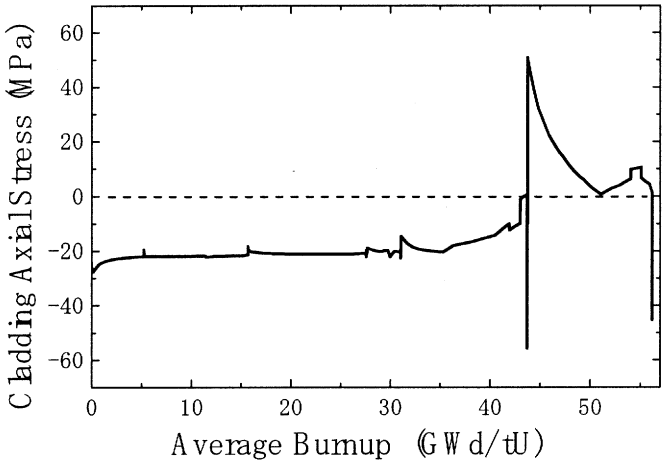


*FIG. 10. Axial stress of cladding with bonding during base-irradiation period.*

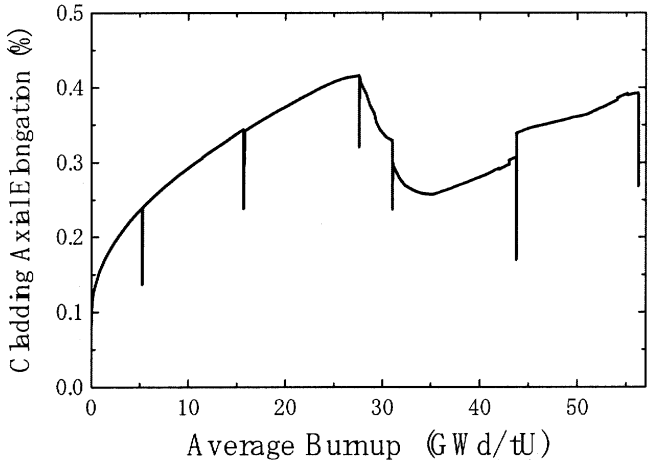


*FIG. 11. Axial elongation of cladding with bonding during base-irradiation period.*

### 3.2. Rod Behavior during Ramp Period

*3.2.1. Bubble Swelling Revealed by PIE Observation*

The PIE results[2] on which the present analysis is based as a reference observation are summarized as:

Rod diameter increased during power plateau period (see Fig.12). Namely, fuel swelling progressed during the plateau, keeping cladding hoop stress level. Rod diameter increase was more than 100μm.
Porosity of pellet after the ramp was 3 to 4 % larger than that before the ramp. The metallography indicates that this porosity increase was mainly attributed to the grain boundary gas bubble growth.

Therefore, it is strongly suggested that the swelling was generated by pellet thermal expansion and fission gas bubble growth.

*3.2.2. Calculated Temperature*

Figure 12 shows the power of the rod at three sub-segments during ramp. Axial difference of the power level has been derived from flux profile of the irradiation hole in JMTR. The power plateau level is around 550W/cm, which is remarkably high.

Figures 13 shows the calculated pellet center temperatures corresponding to the power ramp in Fig.12, and Fig.14 indicates radial profile of the pellet temperature at the power plateau. The pellet center temperature is 2487 K. However, it can be suggested that possibility of columnar grain formation in the pellet held at 2487K for 149min. is negligible in view of the threshold temperature rule that has been derived theoretically and verified by experimental data [14]. In accordance with this, the PIE metallograph of pellet cross section shows no image of columnar grain growth.

It is also found in the calculation that the "thermal bonding" model gives lower pellet temperature by around 40 K than the standard "Ross & Stoute" model [7].

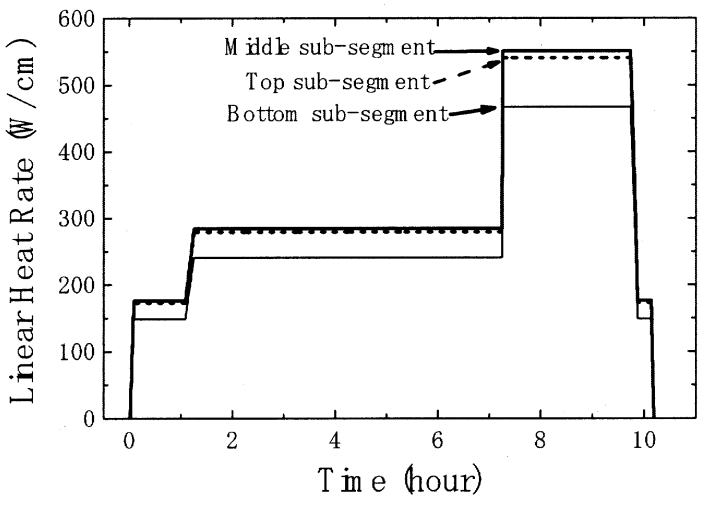


*FIG. 12. Input linear heat rate histories at three sub-segments of the rod during ramp.*

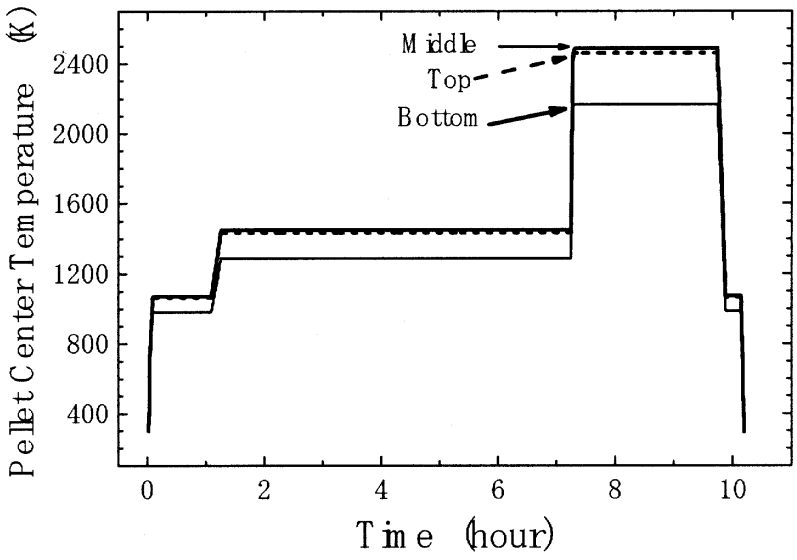


*FIG. 13. Calculated pellet center temperatures at three sub-segments during ramp.*

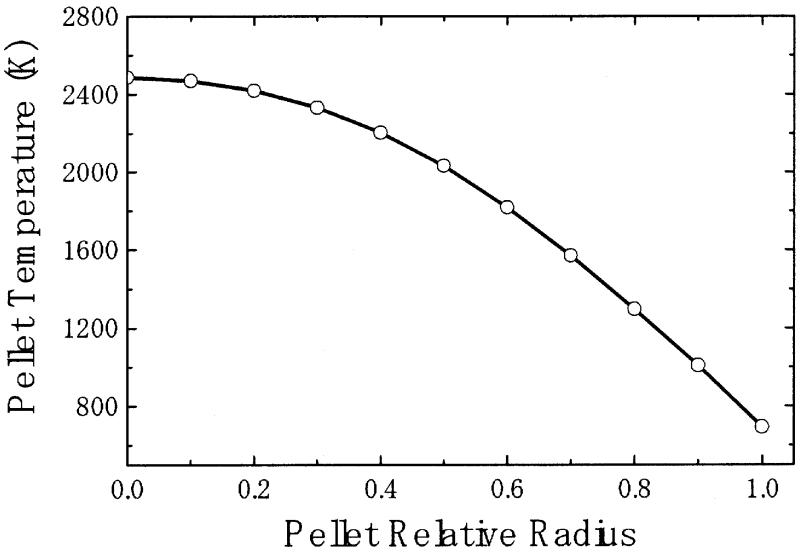


*FIG. 14. Radial temperature profile of pellet at the power plateau.*

*3.2.3. Adjustment of Gas Bubble Swelling Model to PIE Observation*

Since porosity increase of 3 to 4% during ramp was observed in PIE, simulations by FEMAXI-6 have been performed to obtain the identical amount of porosity increase by the bubble growth by setting the limit radius of grain boundary bubble growth to be 10 μm instead of the standard threshold limit of 0.5μm. In addition, in this first case there is no diffusion flux limit of fission gas atoms to the intra-grain gas bubbles. The results are shown in Figs.15 to 20. In Fig.15, the maximum bubble radius is around 6μm, and in Fig.16 pellet swelling after ramp (volumetric change in cooled state with respect to the pre-ramp state) is 3 to 4%, which is roughly identical to the PIE observations.

Also Fig.17 gives grain boundary bubble swelling, and Fig.18 intra-grain bubble swelling.

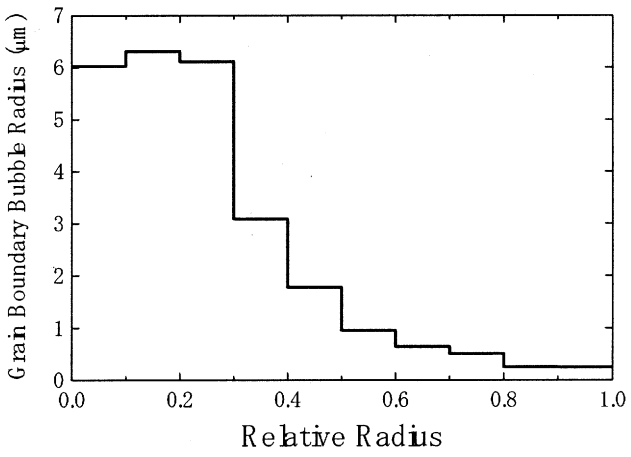


*FIG. 15. Grain boundary gas bubble radius of the rod at the end of ramp with threshold limit of 10 μm.*

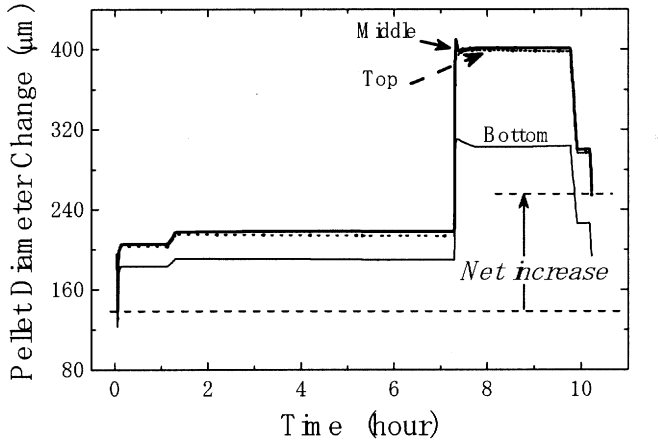


*FIG. 16. Diameter change of pellet at three sub-segments during ramp with no diffusion flux limit of FP gas atoms to intra-grain gas bubble growth.*

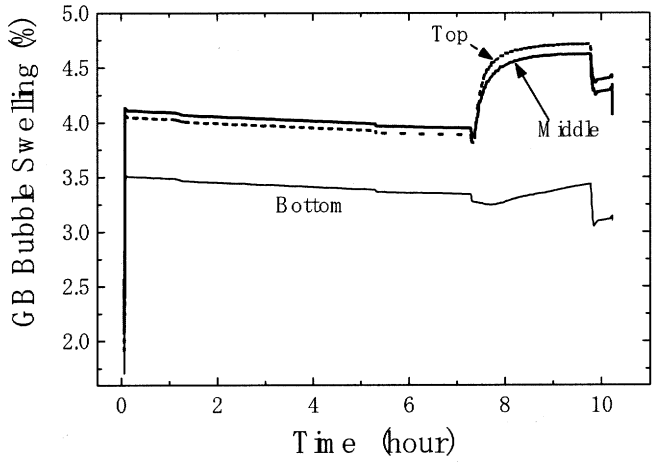


*FIG. 17 Swelling by grain boundary gas bubble growth at three sub-segments with no diffusion flux limit of FP gas atoms to intra-grain gas bubble growth.*

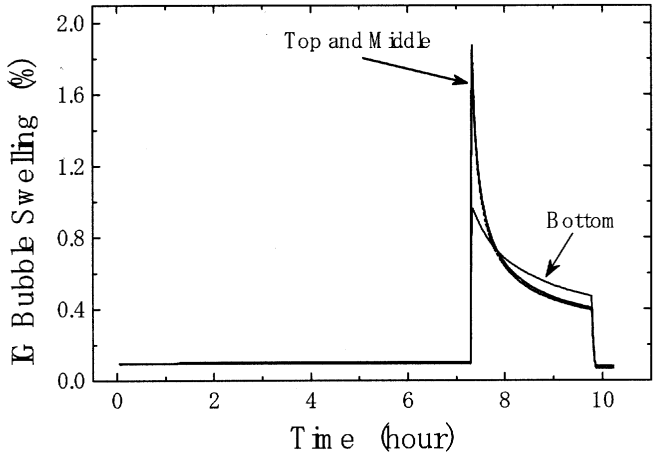


*FIG. 18. Intra-granular gas bubble swelling at three sub-segments during ramp with no diffusion flux limit of FP gas atoms to the bubble growth.*

These results indicate :

(a) Swelling by grain boundary bubble growth is significantly increased during the pre-conditioning period before the power plateau, and they still increase during the power plateau.

(b) Swelling by intra-grain bubble growth is much smaller than that by grain boundary bubble, but it sharply rises at the beginning of power plateau, and then attenuates.

This spike is attributed to the equilibrium radius calculation in which at the beginning of ramp fission gas atoms are heavily accumulated in the fuel matrix and diffusion is much accelerated by elevated temperature. Also, the sharp fall occurs by rapid attenuation of fission gas atom concentration due to fast diffusion to the grain boundary, and by enhanced re-solution of atoms from intra-grain bubbles to matrix. This spike expands the cladding so much at the initial instant that, as shown in Fig.19, the cladding hoop stress rapidly falls after the initial spike. As a result, cladding diameter does not increase during the plateau in the calculation, as shown in Fig.20. This result is contradictory to the PIE data.

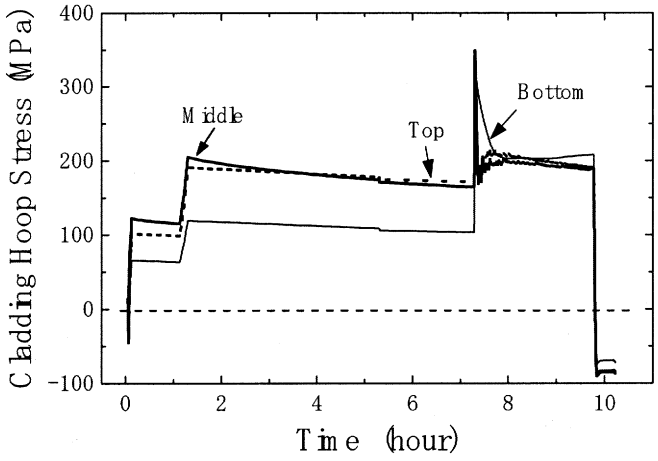


*FIG. 19. Cladding hoop stress at three sub-segments during ramp with no diffusion flux limit of FP gas atoms to intra-grain gas bubble growth.*

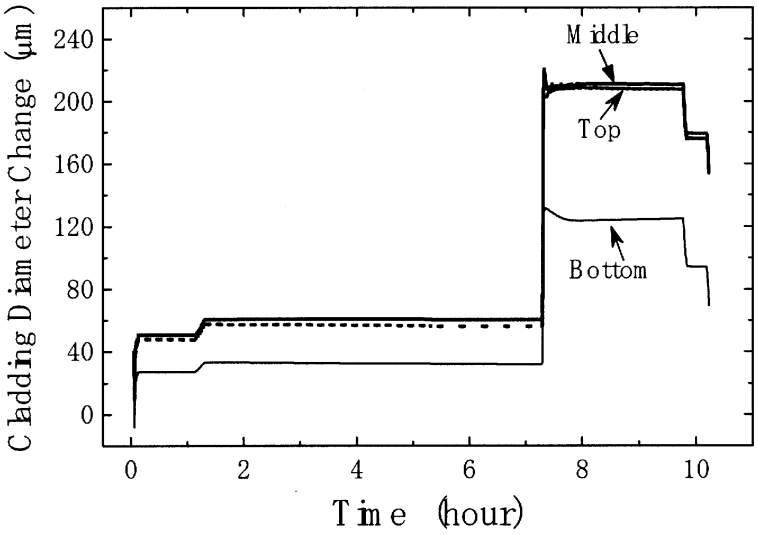


*FIG. 20. Cladding diameter changes at three sub-segments during ramp with no diffusion flux limit of FP gas atoms to intra-grain gas bubble growth.*

Then, to suppress this initial spike, an upper-limit for the diffusion of fission gas atoms to intra-grain bubbles has been added to the simulation conditions. Figures 21 to 24 shows the results of the second simulation calculation, where grain boundary bubble swelling is not shown because it is similar to that in Fig.17.

In Fig.21, magnitude of the initial spike is lowered by the upper-limit. In Figs.22, 23 diameters of pellet and cladding increase with time. In Fig.24, cladding hoop stress is kept at higher level of 260 to 300MPa than in Fig.19. The calculation suggest that, though swelling by intra-grain bubbles is almost negligible in comparison with that by grain boundary bubbles, even a small increase of pellet diameter will cause a large stress and strain of cladding at the beginning of power plateau when pellet and cladding has a considerable contact pressure.

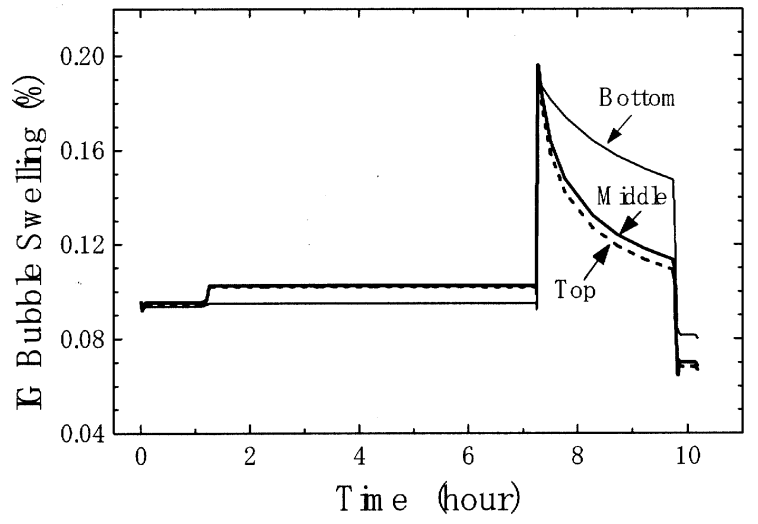


*FIG. 21. Intra-grain gas bubble swelling at three sub-segments during ramp with diffusion flux limit of FP gas atoms to the bubble growth.*

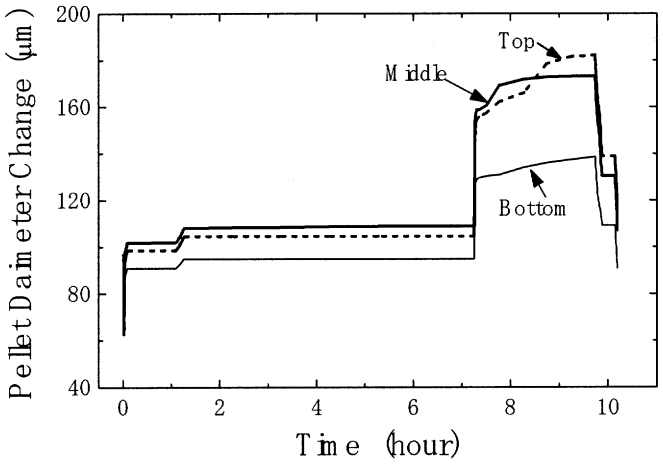


*FIG. 22. Pellet diameter changes at three sub-segments during ramp with diffusion flux limit of FP gas atoms to the intra-grain gas bubble growth.*

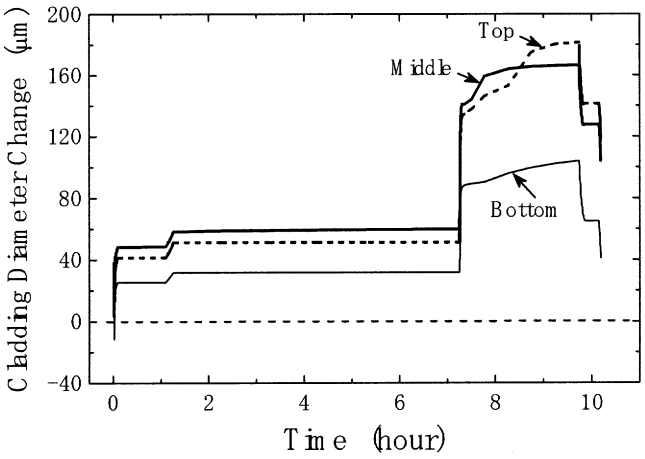


*FIG. 23. Calculated cladding diameter changes at three sub-segments during ramp with diffusion flux limit of FP gas atoms to the intra-grain gas bubble growth.*

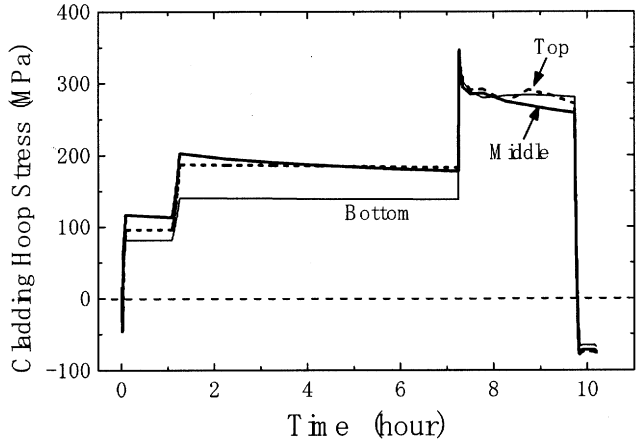


*FIG. 24. Calculated cladding hoop stress at three sub-segments during ramp with diffusion flux limit of FP gas atoms to the intra-grain gas bubble growth.*

In a number of trial calculations, variation of the upper-limit level changed the swelling by intra-grain bubble growth, but the initial spike follwed by attenuation is common to every case. This suggests that such trend as the rapid growth and reduction of intra-grain bubble size is predominant not only in the equilibrium model but also in actual situations. In the simulations, cladding hoop stress level is not sensitively changed with the variation of the upper-limit of the diffusion.

Therefore, such evaluation can hold that the present calculation is a reasonable first order approximation to the deformation of pellet and cladding, and that intra-grain bubble swelling has a negligible effect except at the initial stage of power plateau.

The calculated permanent diameter increase of cladding is shown in Fig.25 together with PIE data for comparison, where calculations by GBS model and by SRS model are described for three axial sub-segments. It is clear that the prediction by the GBS model reveals a reasonable agreement to the actual tendency, while the SRS model gives considerably lower value than the PIE data.

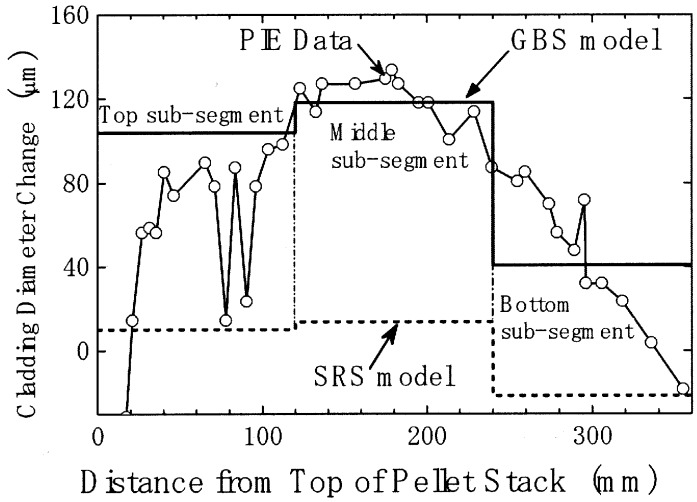


*FIG. 25. Comparison of cladding diameter increase after ramp; PIE data, calculations by GBS (gas bubble swelling) model, and SRS (steady-rate swelling) model.*

*3.2.4. Magnitude of Cladding Hoop Stress*

Calculated cladding hoop stress level shown in Fig.24 is 260 to 300 MPa. It is not sensitive to the magnitude of hoop strain. This level is attributed to the creep property model of cladding. The tensile stress corresponding to 0.2 to 1% strain of irradiated Zircaloy cladding at 617 K* is far above 300MPa; it is 1000 MPa by MATPRO-11 stress-strain model, and roughly 600 to 650 MPa according to the actual ring tensile test of irradiated cladding of high burnup rod [2]. Therefore, tensile stress of 300MPa cannot yield the cladding both in calculation and in actual material, not to mention that it is below the level of instantaneous cladding rupture. (* In the present calculation, the cladding temperature is 676 K at the inner surface and 598 K at the outer surface during the ramp.)

However, a tentative calculation with another creep model gave the results that the hoop stress during the power plateau was around 600MPa. This level is near the yield stress and clearly over-estimate. This suggests that an accurate creep property model derived from in-pile measurement is one of the important factors in numerical prediction.

*3.2.5. Bi-axial Stress State by Bonding*

In high burnup fuel rod, the mechanical bonding restrains pellet stack and cladding from free displacement in the axial direction. Free thermal dilatation of pellet stack in the axial direction is much larger than that of cladding because of high temperature of fuel. However, since the bonding reaction proceeds in normal operation with thermally dilated stack and cladding, thermal stress induced in the axial direction at the interface of pellet stack and cladding is not enhanced.

In addition, pellet thermal stress, which is compressive in a central region and tensile in peripheral region, is relieved by creep during extended irradiation time. Consequently, in normal operation conditions, stress level inside pellet and cladding is considered to be not elevated even with a complete bonding layer.

However, during ramp period, amount of fuel stack axial elongation by thermal dilatation and swelling far exceeds that of cladding, so that axial tensile stress is generated in the cladding wall and compressive stress is exerted on the periphery of pellet stack as a reaction force if mechanical bonding exists between the stack and cladding. Therefore, cladding is subjected to a bi-axial tensile stress state.

To compare this situation numerically, Figs.26 and 27 show the axial and hoop stresses of cladding of the rod with assumption of no bonding, and Fig.28 show also the axial stress of cladding with bonding. As shown in Fig.26, the cladding without bonding is in a compressive axial stress due to coolant pressure in normal operation. During ramp, the compressive stress is mitigated by fuel stack elongation which pushes the cladding top end through plenum spring, so that the cladding has substantially hoop stress only, i.e. uni-axial stress state.

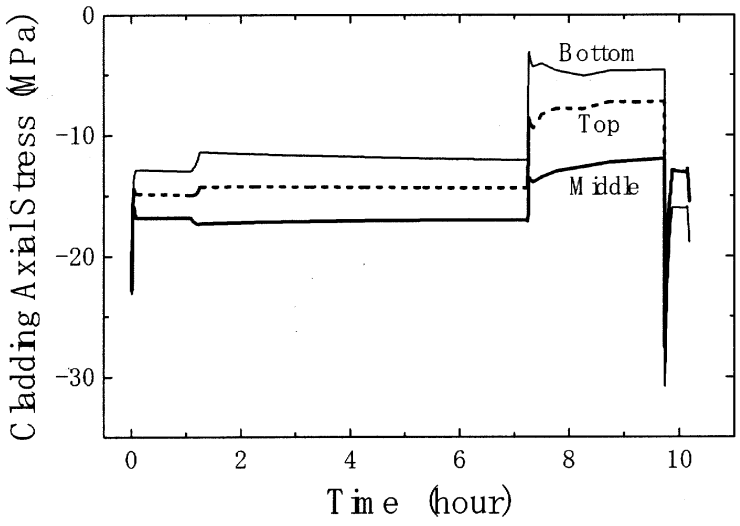


*FIG. 26. Cladding axial stress at three sub-segments calculated with no bonding assumption during ramp.*

On the other hand, comparing Fig.28 with Fig.24 indicates that the axial tensile stress of 200 MPa generated by bonding gives the ratio of axial stress to hoop stress of ； 0.7 . This is clearly bi-axial stress state. In general, bi-axial stress state facilitates the crack growth in comparison with uni-axial state. In addition, the axial stress also causes a larger hoop stress (Fig.24) by ； 17% than in the no-bonding cladding (Fig.27).

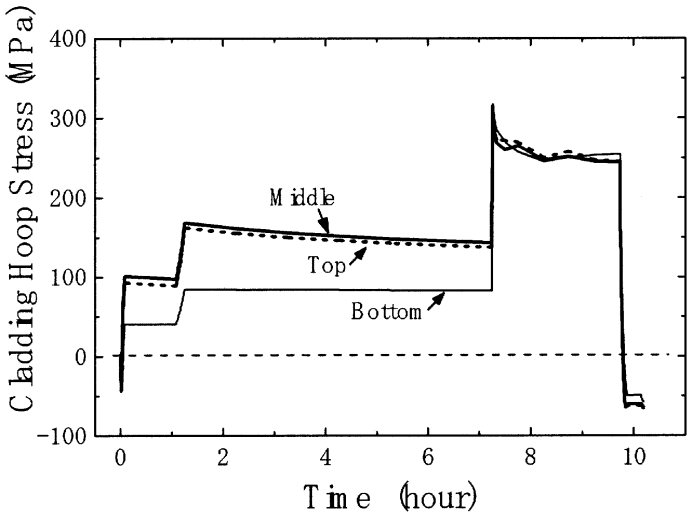


*FIG. 27. Cladding hoop stress at three sub-segments calculated with no bonding assumption during ramp.*

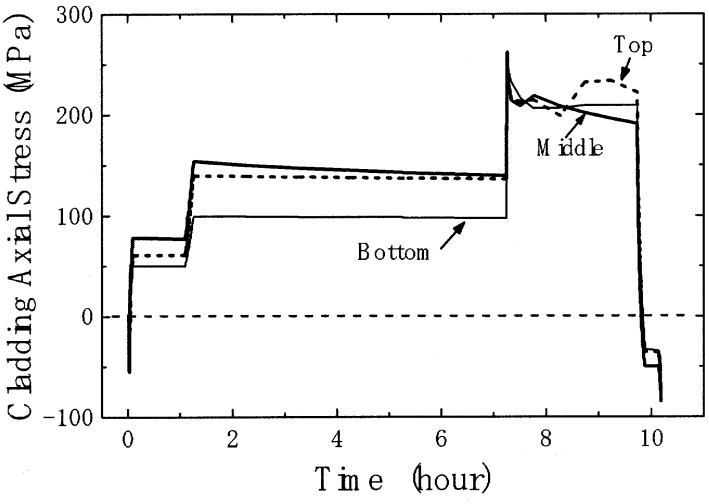


*FIG. 28. Cladding axial stress at three sub-segments calculated with bonding during power ramp.*

Figure 29 indicates the calculated axial elongations of cladding. The net increase of 1.5mm during ramp period is beyond the PIE data range of 0.2 to 1.2 mm, which suggests that the present analysis overestimates either the axial tensile stress or creep rate of cladding to some extent.

If crack is generated in the cladding with reduced ductility, duration of cladding hoop stress which is below the yield level can promote crack growth and propagation, because the crack top will yield by stress intensification effect. Moreover, in the bi-axial stress state, crack growth is more facilitated than in uni-axial stress state.

However, crack initiation and propagation in cladding is outside the coverage of FEMAXI analysis.

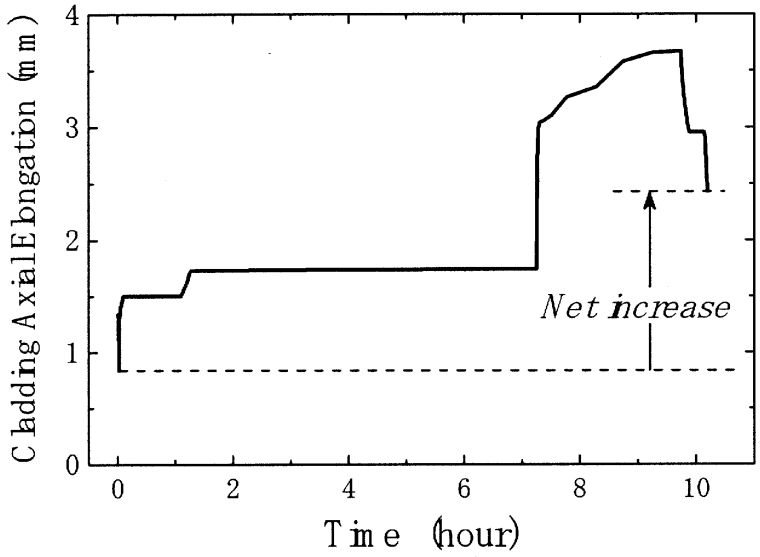


*FIG. 29. Axial elongations of cladding calculated with bonding during ramp.*

### *3.2.6. Alternative Account for Axial Stress of Cladding*

Cladding axial elongation during ramp can be alternatively accounted for by the hypothesis that local PCMI by pellet, i.e. ridging, exerts tensile force to the cladding in the axial direction. However, it is not clear if friction force generated by ridging PCMI would produce axial stress of 200 MPa level in the cladding.

In terms of analysis on the mechanical interaction between pellet stack and cladding in the axial direction, such equal displacement assumption as the present mechanical bonding model allows a reasonable simulation of the interaction. The model is also advantageous in that global rod behavior can be investigated at a time including the mechanical interaction among the axial sub-segments.

### *3.2.7. Response of High Burnup Rod to Power Ramp*

The discussion above indicates that the mechanical interaction between fuel stack and cladding imposes a crucial condition in the analysis of rod behavior during ramp. This interaction is prescribed by the accumulation of such irradiation-induced changes as deformation (densification, swelling, etc), fission gas diffusion and bubble growth, and irradiation-enhanced creep strain. In other words, it should be understood that the swelling and diameter increase during ramp is a response of these accumulated changes. Therefore, integral analysis of these phenomena by fuel performance code FEMAXI-6 is significant and informative.

However, crack initiation and propagation which may lead to failure is not included in the FEMAXI analytical capability. Instead, numerical predictions of stress and temperature resulted from FEMAXI analysis can be adopted as input data to other independent code which investigates crack behavior on the basis of failure mechanics with consideration to such metallurgical features of matrix as hydride precipitation.

## 4. CONCLUSION

Analysis has been conducted on the deformation behavior of BWR fuel rod during ramp by the fuel performance code FEMAXI-6 which has incorporated fission gas bubble swelling model and pellet-cladding bonding model. The results are that diameter increase of cladding and pellet stack has been reasonably predicted by taking into account of the fission gas bubble growth at grain boundary and inside grain during ramp.

Calculations have shown that cladding diameter increase is progressed by hoop stress, and its level depends on the creep property model used in the calculation. In addition, it was found that bonding between pellet stack and cladding generates axial tensile stress in the cladding, so that the cladding is subjected to bi-axial stress state.

Although analytical capabilities of FEMAXI-6 code does not directly cover rod failure, they give a quantitative insight into the complicated thermal and mechanical interactions in high burnup fuel rod, thus allowing to obtain useful pieces of information on the cladding mechanical loadings which can be adopted as a reliable reference for independent failure investigation.

## ACKNOWLEDGEMENT

The first author is indebted to Mr.Saitou of CRC Solutions Corp. for his much assistance in coding and improving the FEMAXI-6 source.

## REFERENCES

[1] H. SAKURAI, K.ITO, Y. TUKADA et al., Irradiation Characteristics of High Burnup BWR Fuels, ANS Topical Meeting, Park City, USA (2000), ANS (2000) 151.[2] Nuclear Power Engineering Corporation, The Annual Report on Irradiation Tests of High Burnup Fuels in FY 2001 -- Integrated Evaluation on Irradiation Behavior of BWR High Burnup Fuel --, March 2002 [in Japanese].

[3] SUZUKI M., Light Water Reactor Fuel Analysis Code FEMAXI-V (Ver.1), JAERI-Data/Code 2000-030 (2000).

[4] SPEIGHT M.V., A Calculation on the Migration of Fission Gas in Material Exhibiting Precipitation and Re-solution of Gas Atoms under Irradiation, Nucl. Sci.Eng.37 (1969) 180.

[5] WHITE R.J. AND TUCKER M.O., A New Fission Gas Release Model, J.Nucl.Mater., 118 (1983) 1.

[6] White R.J., The Development of Grain Face Porosity in Irradiated Oxide Fuel, NEA/NSC/DOC (2000)20, Seminar on fission gas behavior in water reactor fuels, Cadarache, France (2000).

[7] ROSS A.M. AND STOUTE R.L., Heat Transfer Coefficient between $UO_2$ and Zircaloy-2, CRFD-1075 (1962).

[8] WIESENACK W., VANKEERBERGHEN M. AND THANKAPPAN R., Assessment of $UO_2$ Conductivity Degradation Based on In-Pile Temperature Data, HWR-469 (1996).

[9] HAGRMAN D.L. AND REYMAN G.A., MATPRO-Verson11, A Handbook of materials for use in the analysis of light water reactor fuel rod behavior, NUREG/CR-0497, TREE-1280, Rev.3 (1979).

[10] NAKAJIMA T, ICHIKAWA M. et al., FEMAXI-III: A Computer Code for the Analysis of Thermal and Mechanical Behavior of Fuel Rods, JAERI-1298 (1985).
[11] MATPRO-9, A Handbook of materials properties for use in the analysis of light water reactor fuel rod behavior, USNRC TREE NUREG-1005 (1976).
[12] SCHRIRE D., KINDLUND A. AND EKBERG P., Solid Swelling of LWR $UO_2$ Fuel, HPR-349/22, Enlarged HPG Meeting, Lillehammer, Norway (1998).
[13] Uchida M. and Saito H., RODBURN: A Code for Calculating Power Distribution in Fuel Rods, JAERI-M 93-108 (1993) [in Japanese].
[14] NICHOLS F.A., Theory of Columnar Grain Growth and Central Void Formation in Oxide Fuel Rods, J.Nucl.Mater. 22 (1967) 214-222.

# OPERATION AND FUEL DESIGN STRATEGIES TO MINIMISE DEGRADATION OF FAILED BWR FUEL

P. RUDLING[1], T. INGEMANSSON[2], G. WIKMARK[1]
[1]Advanced Nuclear Technology, Uppsala, Sweden
[2]ALARA Engineering, Skultuna, Sweden

**Abstract**

Degradation of failed fuel may result in forced shutdown of the reactor to extract the failed fuel. If this occurs during a time when the price of electricity is high, the cost for this forced shutdown may be very costly. The objective of this paper is to point out the impact of fuel design and also operation strategy on the tendency of failed fuel degradation. The following number of items are discussed in the paper:

- *Failure causes*: The dominating causes are debris fretting, PCI and crud/water chemistry related defects. It is recommended to adopt the goal, maximum one defect per year per million rods in the core and to achieve the zero-failure goal for PCI.
- *Models* for secondary failure development: Two different secondary degradation scenarios can develop, circumferential cracks or breaks and axial cracks. Models for describing the propagation of secondary defects are given and discussed. The secondary degradation tendency can be delayed and minimized by using fuel cladding with improved corrosion resistance such as cladding with large secondary phase particles and high iron content in the liner layer. Also, the spacer design has a large impact on the tendency for transversal break formation. A spacer that catches the debris at the lower part of the fuel assembly will reduce the risk of getting transversal breaks. On the other hand a spacer that catches the debris in the upper part of the fuel assembly will result in a significant risk of developing transversal breaks in low and intermediate burnup fuel.
- *A new model for data analyses* - BwrFuelRelease: A new model, BwrFuelRelease, is presented. This model is an efficient tool for analyses of measured off-gas and reactor water data. The model can replace all currently used methods for analyses of fuel failures. By this model it is possible to detect very small defects, to quantify with high precision the amount of Fissile materials on the core surfaces during operation both with non-defected core and during operation with significant uranium dissolution. He BwrFuelRelease model can be used for assessing if the zero-failure goal has been achieved after a shutdown. The model is easy to use and interpret.

## 1. INTRODUCTION

A failed BWR fuel rod may degrade either by developing long axial cracks and/or transversal breaks or not degrade at all. The activity and fuel release from these degraded rods may be substantial. During the period 1992-1993 six plants in US and in Europe were actually forced into unscheduled outages because of concerns about failed BWR sponge Zr-liner fuel[1] degradation. In all these cases, the very high off-gas activites resulted from only one or two failed rods. Degraded fuel may result in very large utility costs. The tendency of failed BWR rods to degrade depends on the fuel design and reactor operation of the failed rod. The knowledge of the degradation mechanisms may be used to develop secondary degradation resistant fuel and/or to mitigate the degradation tendencies during operation of failed fuel.

[1] *Zr sponge liner fuel* consists of a liner produced from Zr sponge material. No alloying elements have been added to this material and its major impurities are oxygen (about 600-900 wtppm) and iron (about 150-500 wtppm).

The work presented in this paper is carried out in co-operation between ALARA Engineering and Advanced Nuclear Technology, ANT. The paper contains two main features. One part discusses mechanisms for primary defect generation and provides models for how secondary defects blisters, transversal breaks and axial splits develop. Fuel design features to get secondary degradation resistant fuel are listed and discussed. The second part is related to a new computer code, *BwrFuelRelease*, to analyze reactor activity data.

## 2. PRIMARY FUEL FAILURES

Primary defects in BWRs fuel since the early days of operation, are listed in Table 1. However, in reality most of the primary failure causes listed in Table 1 are rare, and a few causes are dominating. Due to changes in fuel design and operation, the same causes are not necessarily dominating for longer periods, but instead the most common causes change with time as illustrated in Table 2.

Table 1. Known primary failure causes for BWR fuel rods, [1, 2]

| Failure Cause | Short Description |
|---|---|
| **Primary Hydriding (Manufacturing)** | Moisture or organic material is present in the pellet or the rod after welding the top plug. The hydrogen released will be locally absorbed by the cladding, causing embrittlement and failure. |
| **Welding Defects (Manufacturing)** | The weld for the top or bottom end plug has some defect, allowing inflow of steam or water. |
| **End Plug Piping (Manufacturing)** | The end plug has an open or almost open channel (due to ingot piping) axially. The hole will immediately or with time allow intrusion of coolant into the rod. |
| **Cladding Tube Cracks (Manufacturing)** | The pilgering of the cladding tubes has caused incipient cracks, which will be weak points for any PCMI transient. |
| **Debris Fretting** | Debris in coolant frets a hole in the cladding |
| **Excessive Corrosion** | An accelerated general or local cladding corrosion causes penetration. Many different causes are known. |
| **PCI (SCC)** | Pellet Clad Interaction, a stress corrosion crack penetrates the cladding. Fission products, mainly iodine, are produces the aggressive chemical environment causing the failure. A significant power ramp or defect pellets are required for PCI. |
| **PCMI** | Pellet Cladding Mechanical Interaction. The rod 'cracks due to mechanical overload without environmental influence. |
| **Rod Bowing** | The fuel rod bows and failure occurs by fretting or other mechanical interaction between the rod and adjacent components (rods, fuel flow channels, etc,). Several causes for the elongation producing rod bow are known. |
| **Dry-out** | The local power is too high for the coolant flow, causing the cladding to be overheated. The overheating causes (local) corrosion penetration of the cladding. Only one case is known. |

Table 2. BWR fuel cladding failures in the US in 1990–1999 [3]

| Failure Cause | 1989 | 1990 | 1991 | 1992 | 1993 | 1994 | 1995 | 1996 | 1997 | 1998 | 1999 | Total | |
|---|---|---|---|---|---|---|---|---|---|---|---|---|---|
| **Debris fretting** | 2 | 2 | 17 | 2 | 6 | 4 | | 2 | 3 | 5 | 3 | 46 | *20%* |
| **Grid fretting** | | | | | | | | | | | | 0 | *0%* |
| **Fabrication failures** | 3 | 3 | 1 | 1 | 1 | 2 | | | | | | 11 | *5%* |
| **PCI**[1] | | 1 | | | 2 | | 2 | 2 | 1 | 1 | | 9 | *4%* |
| **Crudding/Corrosion** | | | | | | | | | | | **7** | **7** | *3%* |
| **CILC**[2] | 52 | 5 | 3 | | | | | | **3** | **46** | | **109** | *48%* |
| **Unknown/Uninspect.** | | 4 | 3 | 9 | 7 | 9 | 2 | 10 | 1 | 1 | 1 | 47 | *21%* |
| ***Annual total*** | ***57*** | ***15*** | ***24*** | ***12*** | ***16*** | ***15*** | ***4*** | ***14*** | ***8*** | ***53*** | ***11*** | | *100%* |

# 3. SECONDARY DEGRADATION

## 3.1. General

Under certain conditions the rod with a primary failure may degrade. Two different types of degradation scenarios have been identified, namely development of:

?? Transversal breaks (also called guillotine cuts or circumferential break), and,

?? Long axial cracks, i.e. axial splits[3]

Degradation of failed fuel is a situation when fuel dissolution occurs, Fig. 1. This may occur if the rods degrade to such a point that the water gets in contact with the fuel pellet. Steam may not dissolve the fuel pellet while the water phase can. Normally, utilities are much more concerned about fuel dissolution than high iodine and noble gas release. This, since it may take up to 10 years to clean the core from the tramp uranium resulting from the fuel dissolution. On the other hand, the high iodine and noble gas activities released from the failed rod will be eliminated when the failed rod is extracted from the core.

Literature data, e.g., [4 - 6], show that bng axial cracks only occur in conjunction with a power ramp of preferentially intermediate to high burnup rods. Thus, if a failed rod is not subjected to a power ramp, no axial split will form. It should be pointed out however, that power ramps must be performed in the reactor for other reasons and consequently, it will be impossible to run a plant without any power ramps.

1 Pellet Cladding Interaction-an iodine assisted stress corrosion cracking phenomenon that may result in fuel failures during rapid power increases in a fuel rod. There are three components that must occur simultaneously to induce PCI and they are: 1) tensile stresses - induced by the power ramp, 2) access to freshly released iodine-occurs during the power ramp, provided that the fuel pellet temperature becomes large enough and 3) a sensitised material – Zircaloy is normally sensitive enough for iodine stress corrosion cracking even in unirradiated state.

2 Crud Induced Localised Corrosion – an accelerated form of corrosion that have historically resulted in large number of failures. Three parameters are involved in this corrosion phenomenon, namely: 1) Large Cu coolant concentrations- as a result of e.g. aluminium brass condenser tubes, 2) Low initial fuel rod surface heat flux – occurs in Gd rods and 3) Fuel cladding that shows large initial corrosion rates - occurs in cladding with low resistance towards nodular corrosion.

3 Axial split is a term introduced by GE and represents a failed rod that either has an off gas level larger than 5000 ?Ci/s (185 MBq/s) or a total crack length that is larger than 152 mm (6 inches).

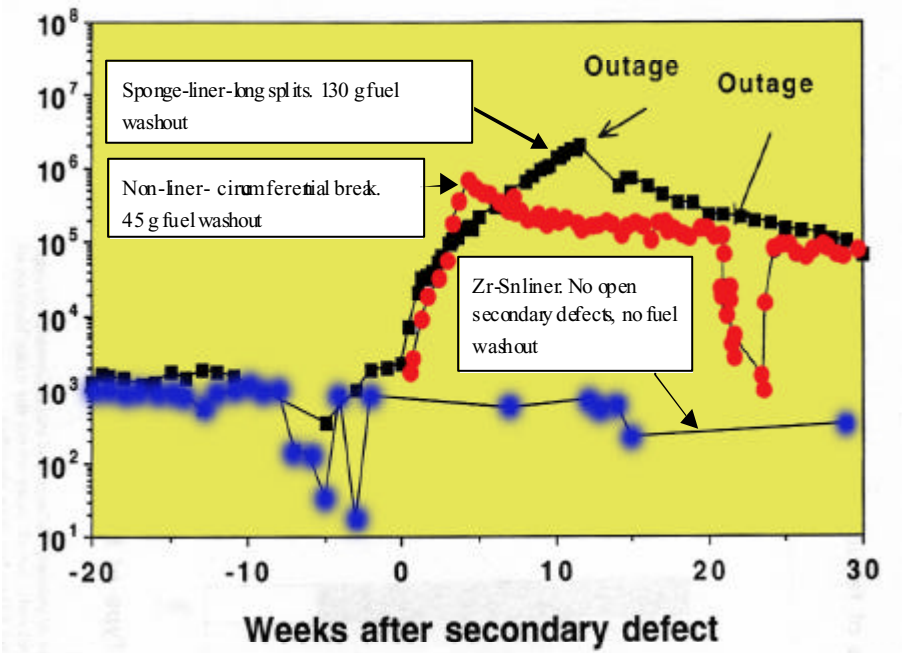


*FIG. 1. $^{239}Np$ activity (a measure of $UO_2$ dissolution during Normal Water Chemistry conditions) measured in the coolant before and after formation of: 1) a long split (1 rod with sponge Zr liner-black data points) and 2) a transversal break (red data points). A long split cause a significantly larger $UO_2$ dissolution than a transversal break. The blue data points refer to a rod that only had a primary failure and did not degrade. It is also apparent that primary failures normally do not result in fuel dissolution, [4].*

On the other hand, transversal break formation is not correlated to power ramping but can result during operation of a failed rod during constant power. Transversal breaks predominantly occur in low burnup fuel [4]. Sometimes, it seems that lowering of the reactor power to such an extent that the lower part of the rod may be filled with water, *waterlogging,* such as e.g. during a cold shut-down, may enhance the risk of getting a transversal break upon return to full power.

### 3.2. Transversal break formation

If the failed rod has low burnup, one may expect first, that the overall pellet-cladding gap is large and second, that this gap is much smaller at the lower part of the rod due to the downshift in power profile for these low burnup rods provided that:

– The ratio of hydrogen to steam partial pressure is large enough and,
– The protecting clad inner surface oxide is thin enough, massive hydrogen ingress into the cladding may occur.

When the hydrogen solid solution solubility in the fuel cladding has been exceeded, precipitation of hydrides will start with forming *hydride blisters,* Fig. 2. Once the attack starts the hydrogen flux entering the inner surface must exceed the rate of the diffusion to the colder outside surface for a massive local hydride to form. These local hydrides lead to high local tensile stresses in the outer part of the cladding due to the larger hydride specific volume of 16% compared to that of zirconium. The final leak path is then developed along radial fingers

of $ZrH_{1.6}$ that penetrates to the cladding outer surface. Once a hydride defect starts to leak then it may no longer continue to develop and there are cases when continued diffusion of hydrogen to the cooler cladding outer surface results in the zirconium hydride near the cladding inner surface reverts to zirconium. The *hydride blisters* may subsequently grow into massive hydrides throughout the cladding thickness along its whole circumference. Since zirconium hydrides are very brittle, the cladding zone that is completely transformed into zirconium hydride will be very brittle and may easily fracture even during operation at constant power. It seems that scram, shutdown and cold shutdown may result in large enough stresses to enhance the risk of getting transversal break of a failed rod.

The events resulting in a transversal break is schematically shown in Fig. 3, and the parameters impacting the transversal break tendency is shown in Fig. 4.

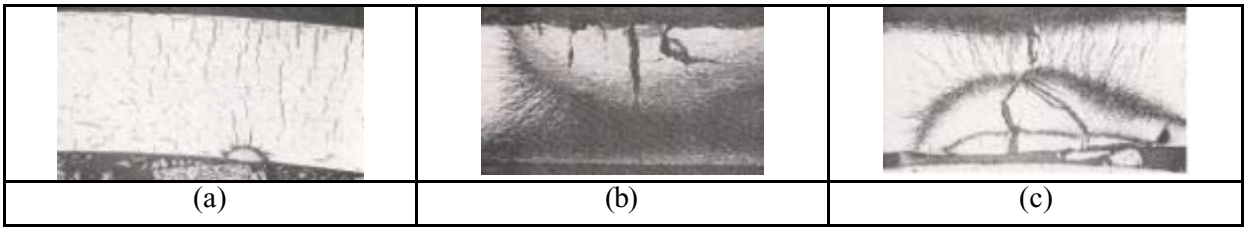


*FIG. 2. Primary hydride blisters, (a) early stage but stress effect on hydride orientation, (b) and (c) hydride blister with large leak showing beginning of hydride reconversion to Zr, [7].*

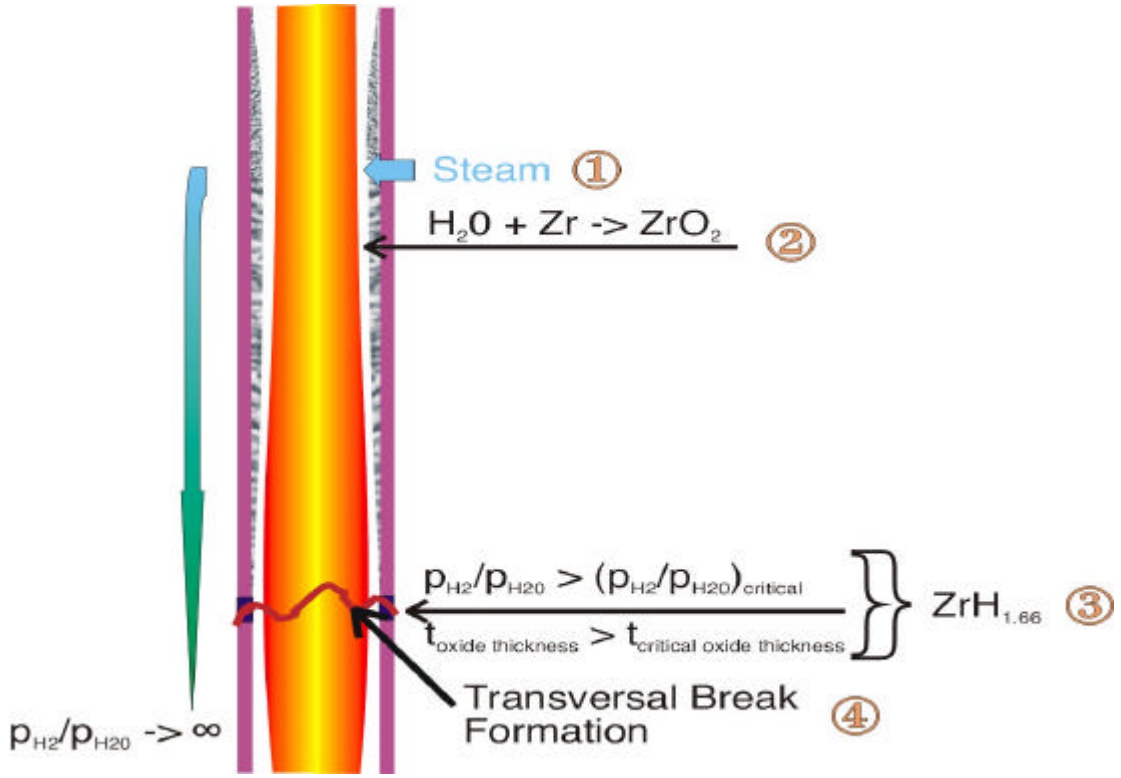


*FIG. 3. Schematics showing the events resulting in transversal break formation. The numbers in the figure relate to the sequence of the different events that may lead to a transversal break.*

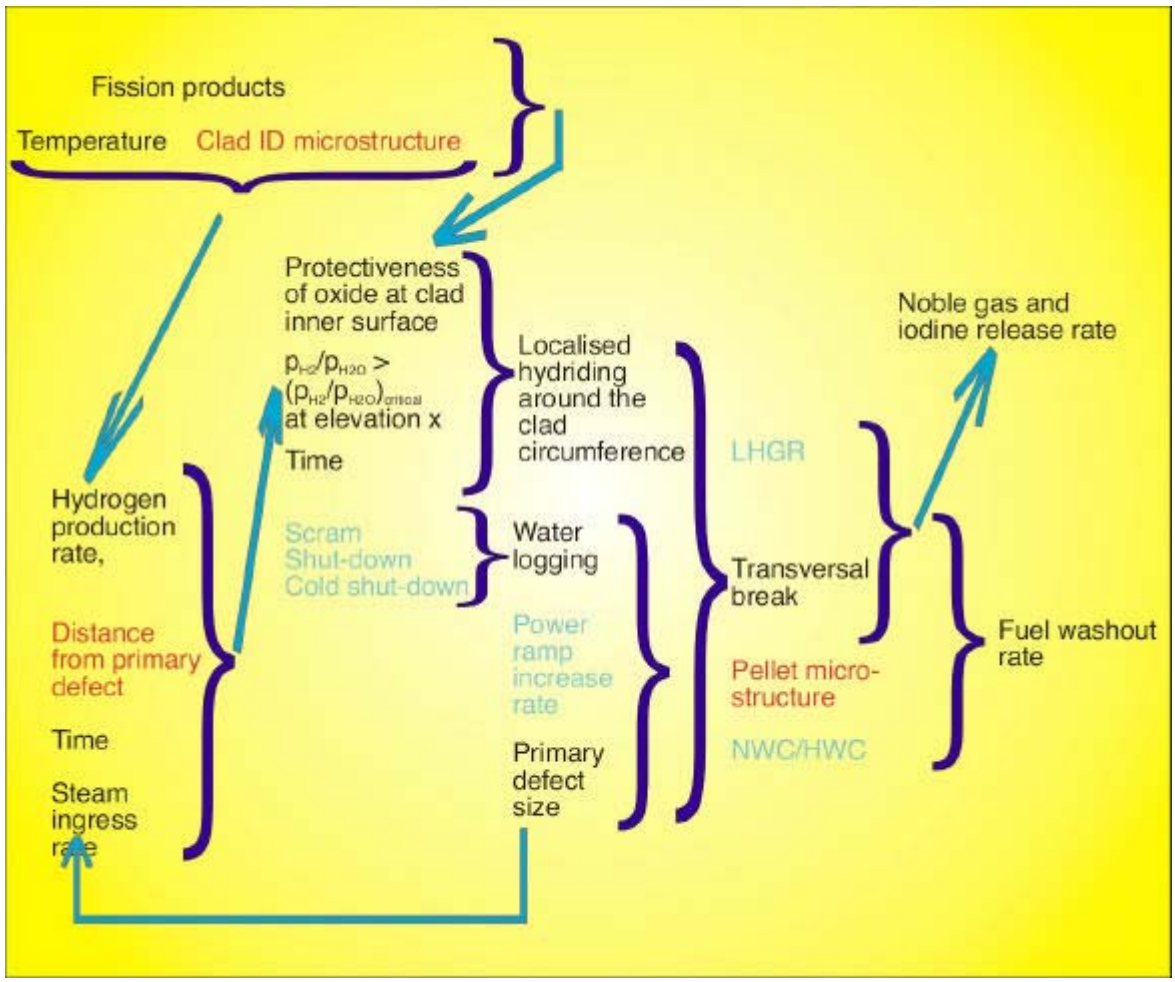


*FIG. 4. Schematics showing the parameters that may impact the transversal break tendency. The key parameter that is related to operation is in blue colour while the corresponding parameters related to fuel design is in red colour. The numbers related to the sections that follow that describes the parameter in detail*

### 3.3. Axial split formation

The fuel rod may in principal develop two different types of primary through- wall defects. The first type A defects consists of sharp through- wall cracks formed during a power ramp either by:

– Propagation of an existing non-through- wall manufacturing defect prior to the ramp

– Iodine induced stress corrosion cracking mechanisms resulting in PCI cracks.

The second type B defects consist of defects that may be regarded as blunt cracks formed due to corrosion, fretting, etc.

The type A defects are sharp enough to result in a stress intensity factor, $K$, which during a second ramp may be larger than the critical value for crack propagation provided that the hydrogen solubility in the material is exceeded. This situation may thus result in an axial split without forming any secondary hydriding. It is proposed that the mechanism for crack propagation is *Delayed Hydride Cracking, DHC.*

The type B defects are not sharp enough to be able to propagate by itself during a ramp. However, if conditions are such that the ratio of hydrogen to steam partial pressures is larger than a critical value and the clad inner surface oxide thickness is smaller than another critical value at a certain rod elevation, secondary hydriding may occur. Since the specific volume of the hydride is larger than that of the zirconium alloy a large local stress field will build up in and just outside the *hydride blister* and due to that the hydride is brittle, many sharp cracks will form within the *hydride blister* (*see Fig. 5*). Now as in the case of sharp type A cracks previously discussed, the hydride cracks in the *hydride blister* may propagate during a power ramp by the *DHC* mechanism as originally proposed by Schrire et al., 1994 [8].

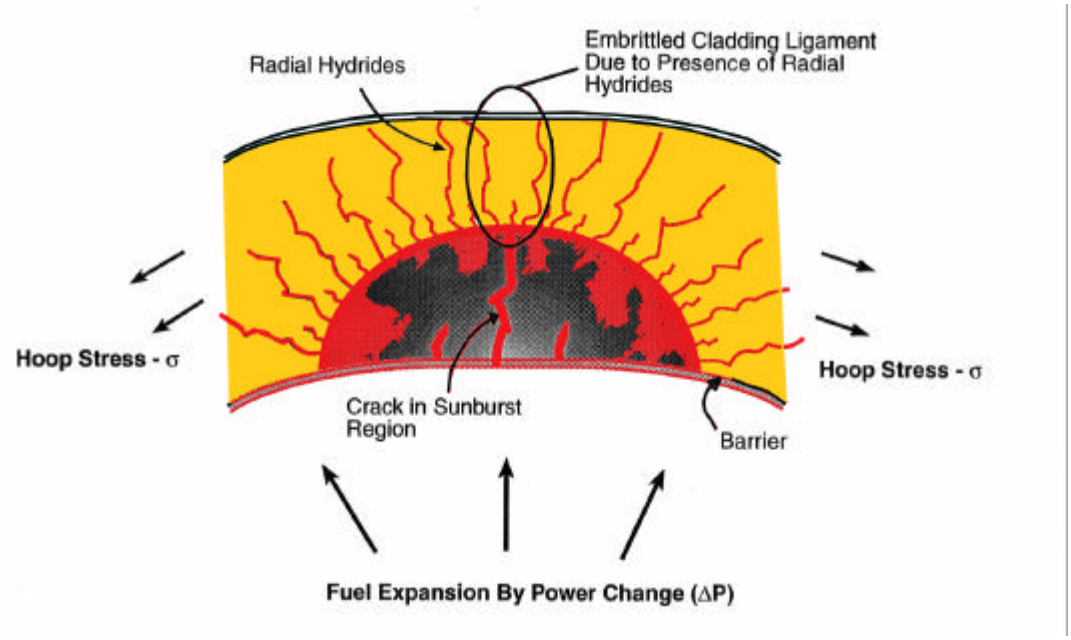


*FIG. 5. Stresses in hydride blisters during power ramping, [9].*

The axial split formation is schematically shown in Fig. 6. The events resulting in the formation of a long axial crack, axial spit, is schematically shown in Fig. 7.

## 4. DESIGN FEATURES IMPACTING SECONDARY DEGRADATION RESISTANCE

The following parameters have a significant impact on secondary degradation tendency:

– *Fuel temperature*: The lower fuel temperature the lower chemical activity. This make 10x10 more resistant towards activity release

– *The pellet itself*: The pellet as a barrier is an important parameter. Pellet performance may be monitored by the release rate of activity, specifically noble off-gas activity and fuel wash out, from two rods with about the same crack length or from two rods with circumferential breaks.

– *For liner fuel*, good corrosion properties of the liner are crucial to get good resistance towards formation of both long axial cracks and transversal breaks. Sn-addition seems to have only a minor effect on corrosion performance. The most potent alloying addition to achieve good corrosion performance is by adding Fe to the liner. It is recommended to have as much Fe as possible without deteriorating the PCI performance.

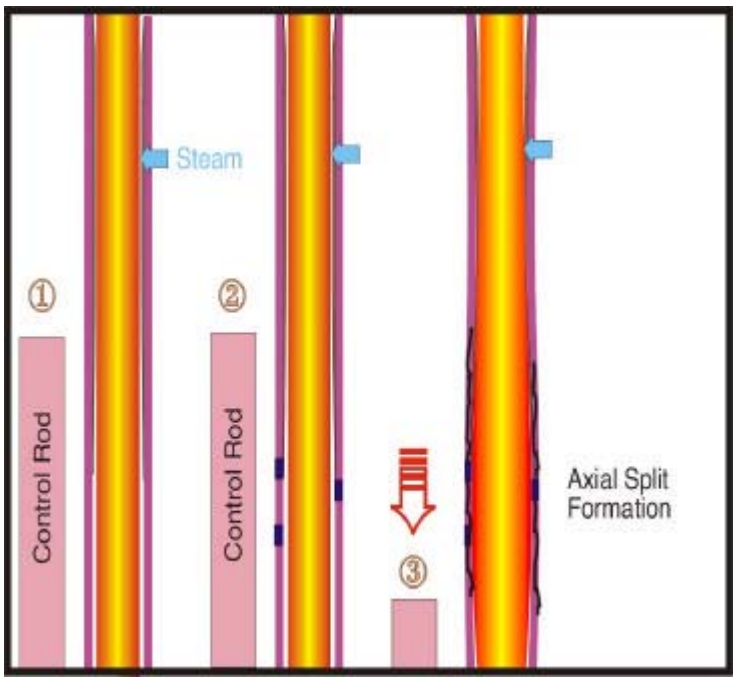


*FIG.6. Schematic showing the events resulting in axial split formation. The numbers in the figure relate to the sequence of the different events that may lead to an axial crack.*

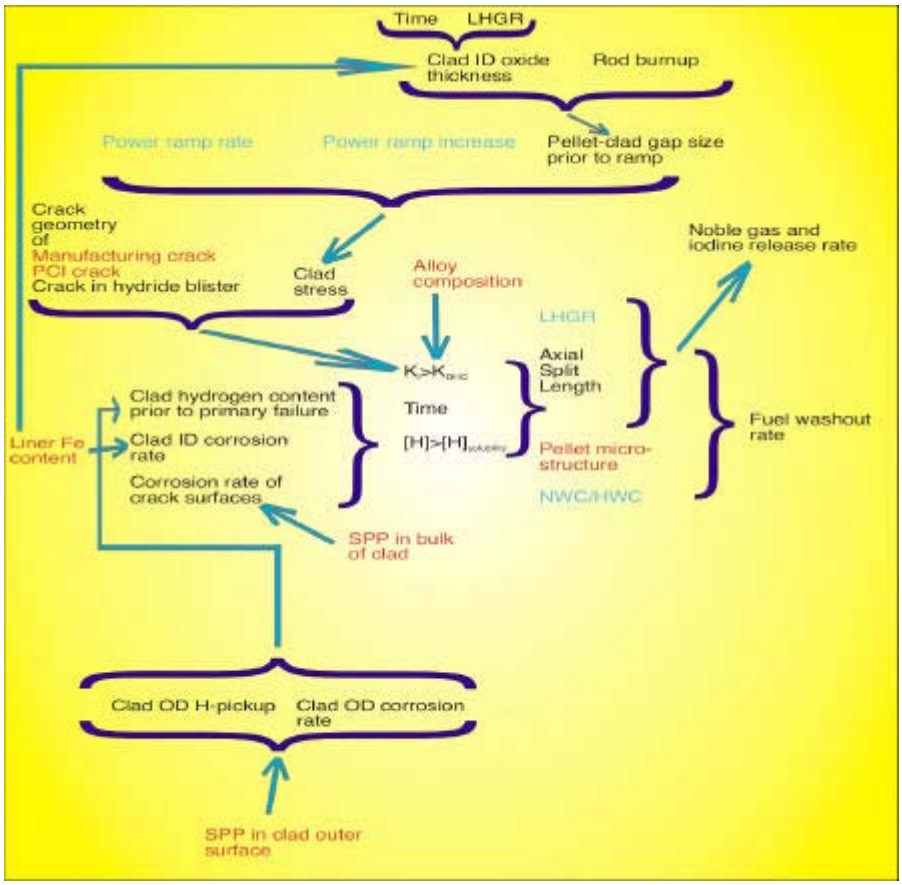


*FIG. 7: Schematics showing the parameters impacting axial split formation tendency. The key parameters that is related to operation is in blue colour while the corresponding parameters related to fuel design is in red colour. The numbers related to the sections that follow that describes the parameter in detail.*

?? *The size of the secondary phase particles in both liner and non-liner fuel:* Good corrosion properties of the bulk thickness of the fuel cladding will also reduce the risk of getting long axial cracks of failed fuel. Such good properties may be obtained by having second phase particles larger than 50-100 nm (assessed by scanning electron microscopy, SEM)

?? *Spacer design,* A design that catches the debris fretting failures in the lower part of the fuel assembly will reduce the risk of getting transversal breaks.

## 5. **BwrFuelRelease** – A NEW MODEL FOR ANALYSIS OF FUEL FAILURES

### 5.1. General

The BwrFuelRelease model is a plant specific model, and it is presented and discussed in this section.

The BwrFuelRelease model can be used to:

1. Detect very small defects.
2. Assess if the zero-failure goal has been achieved or not after refuelling.
3. Quantify with high precision the amount of FM, Fissile Material[4], during operation.

The BwrFuelRelease model can replace all currently used methods for analyses of fuel failure situations. The model is easy to use and evaluate and is also significantly more sensitive and has better precision than currently used methods and models.

### 5.2. Theoretical background for the BwrFuelRelease model

Several Nordic plants are applying Hydrogen Water Chemistry, HWC, i.e. hydrogen gas is injected into the feedwater. At HWC operation, reducing condition is achieved in many parts of the reactors, specifically in the reactor water sampling systems with large surface to volume ratios. At reducing conditions uranium and trans uranium nuclides will form complex, which will be deposited onto the system surfaces. As a result the Np-239 concentration in the coolant at the sampling point can decrease with a factor of 100 or more when hydrogen is injected into the feedwater. Consequently, by measuring the Np-239 coolant concentration under such conditions, the uranium dissolution from the degraded rods would be largely underestimated.

Since the Np-239 activity is not appropriate to monitor the Tramp Uranium[5] contamination of the core during HWC conditions, ALARA Engineering has developed the BwrFuelRelease

[4] *Fissile materials (FM):* There are three fissile nuclides in irradiated fuel, U235, Pu239 and Pu241. The term "fissile materials" is used for the sum of these. The amount of FM is used with the same meaning as TU (see below).

[5] *Tramp uranium (TU)*: Tramp uranium has the following meaning. If a specific nuclide, e g Xe133, is measured in the off-gas system in Bq/s it can be easily calculated how much uranium is needed for production of this activity. This amount of fuel is called TU. If the core is non-defected the origin is solely the fissile materials in the TU in the core. If the core is defected the amount of TU calculated from the "release rate" of Xe133 is the sum of the uranium in the core and in uranium in the defected rod(s) that is needed for this specific release rate. Thus the amount of TU represent *the amount of uranium that contributes to the activity release to the coolant*, the uranium can be said to be free.

model. This model can be used both for Normal Water Chemistry, NWC, i.e., no hydrogen injection and HWC conditions for estimation of the amount of FM and tramp uranium on the core surfaces. The BwrFuelRelease model can also with advantage be used for detecting small defects. Main advantages with this model is that it is

1. Simple to use and interpret.
2. Provides the amount of FM with very high accuracy based upon only one single reactor water analysis.
3. It is able to continuously monitor very small additional amounts of fissile materials on the core surfaces by use of reactor water sampling.
4. It can detect the first very small defect. One reactor water and one off-gas sample are required.
5. It can assess if the 0-failure goal has been achieved at start-up. One reactor water and one off-gas sample are required.

The BwrFuelRelease model must be able to separate the activity released from the core from that released from the defect(s). To be able to do this separation, the requirements of the nuclides to be included in the BwrFuelRelease model are the following:

— In Tables 3 and 4, krypton and xenon isotopes with decay chains, which may be useful for fuel defect monitoring purposes, are provided. Noble gas nuclides with long half-lives, longer than a couple of minutes can be sampled in the off-gas system. Noble gas isotopes with short half-lives, a few seconds, with water-soluble decay (daughter) products can also be used. For such nuclides the mean residence time in the reactor pressure vessel must be considered. The residence time is a function of vessel volume and steam flow rate.

— The water-soluble nuclide should have a "suitable" half-life. "Suitable" means that it should have such a long half-life that it is easy to measure but short enough that it should not have too long memory effect[6]. It is desirable that it reaches its equilibrium value relatively fast to be useful at all time when the reactor is operating. A half-life between one and couple of hours is optimal. The half-life of the mother nuclide shall be so short that the main amount decays within the Reactor Pressure Vessel, RPV, i.e., the half-life shall be less than a couple of seconds.

— An important quality is that the defect itself should not provide any contribution to the measured release rate in the off-gas system or to the reactor water concentration also during operation with open and degrading defects. This is the most limiting restriction for the selected nuclide(s) and makes it impossible to use any of the off-gas nuclides to estimate the amount of FM on the core surface during operation with defects. The off-gas nuclides have all too long half-lives and the defect itself is the main source for this activity. The only possibility is to use a water-soluble daughter product of selected noble gas nuclides.

6 The memory effect increases with increasing half life.

Table 3. Krypton isotopes tested for monitoring of fuel defects. The decay constants and the half-lives of the nuclides are provided.

| *Nuclide 1* | *? ($s^{-1}$)* | *$T_{1/2}$ (s)* | *Nuclide 2* | *$T_{1/2}$* | *Nuclide 3* | *? ($s^{-1}$)* | *$T_{1/2}$* |
|---|---|---|---|---|---|---|---|
| Kr-90 | 2.15E-02 | 32.3 | Rb-90 | 2.55 min | Sr-90 | 7.54E-10 | 29.1 y |
| Kr-91 | 8.09E-02 | 8.57 | Rb-91 | 58.4 s | Sr-91 | 2.02E-05 | 9.52 h |
| Kr-92 | 3.75E-02 | 1.85 | Rb-92 | 4.51 s | Sr-92 | 7.11E-05 | 2.71 h |
| Kr-93 | 5.64E-02 | 1.23 | Rb-93 | 5.70 s | Sr-93 | 1.58E-03 | 7.32 min |
| Kr-94 | 3.466 | 0.2 | Rb-94 | 2.70 s | Sr-94 | 9.10E-03 | 1.27 min |

Table 4. Xenon isotopes tested for follow-up of fuel defects. The decay constants and the half-lives of the nuclides are provided.

| *Nuclide 1* | *$T_{1/2}$ (s)* | *Nuclide 2* | *$T_{1/2}$* | *Nuclide 3* | *$T_{1/2}$* | *Nuclide 4* | *$T_{1/2}$* |
|---|---|---|---|---|---|---|---|
| Xe-139 | 39.7 s | Cs-139 | 9.3 min | Ba-139 | 1.38 h | La-139 | Stable |
| Xe-140 | 13.6 s | Cs-140 | 63.6 s | Ba-140 | 12.74 d | La-140 | 1.68 d |
| Xe-141 | 1.72 s | Cs-141 | 24.9 s | Ba-141 | 18.3 min | La-141 | 3.93 h |
| Xe-142 | 1.22 s | Cs-142 | 1.8 s | Ba-142 | 10.6 min | La-142 | 1.52 h |
| Xe-143 | 0.30 s | Cs-143 | 1.77 s | Ba-143 | 14.5 s | La-143 | 14.3 min |

If the above-mentioned requirements are applied to the nuclides in Tables 3 and 4, it appears that only nuclide Sr-92, alternatively Sr-91, and Xe-133 may be used on a routine basis to:

1) assess if the core contains a defect or not and,

2) quantify the amount of FM on the core surface.

When a defect occurs the calculated amount FM on the basis of Xe-133 will increase relative to that of Sr-91 and Sr-92. This depends on the fact that it is not only fissions on the core surfaces that contribute to Xe-133 but also a direct release of Xe-133 from the defect. Our analyses have shown that the Sr-91/Sr-92 concentration in the reactor water is *not significantly impacted* from small or large defects. *The dominating source for the Sr-91 and Sr-92 activity is only fissions on the core surfaces*. The precursor of Sr-91 and Sr-92, Kr-91 and Kr-92, respectively, does not have long enough half-life to be released from the fuel matrix to the coolant before they have decayed. The daughter products, Sr-91 and Sr-92, have such short half-life that also these nuclides decay before the fuel has dissolved.

In Fig. 8, the amount of FM in the core based upon measured Xe-133 in the off-gases and Sr-92 in coolant has been calculated by the BwrFuelRelease model.

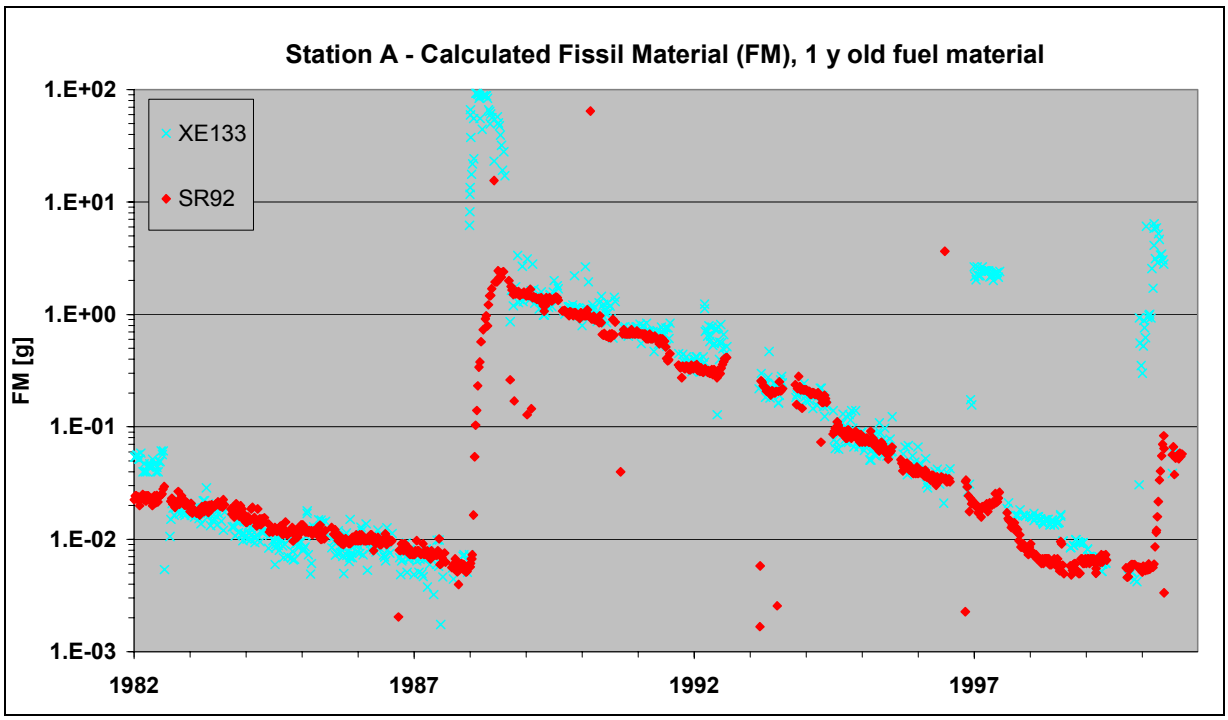


*FIG. 8. Plant A – With BwrFuelRelease calculated amount of fissile materials in the core with Xe-133 and Sr-92.*

Fig. 8 shows that:

- The calculated FM from Xe-133 and Sr-92 are similar during long periods. As an example, the averaged value of FM from July 1982 to September 1987, was estimated to 0.0130 and 0.0133 g with Xe-133 and Sr-92, respectively. The deviation is less than 3%. Since the calculated FM from Xe-133 and Sr-92 are similar, the core is defect-free.

- During the first half-year of 1988 the core was contaminated with 2.4g of FM, calculated based upon the Sr-92 activity. However, the corresponding amount based upon the Xe-133 activity, 100 g FM, is much larger. This discrepancy indicates that a failure has occurred.

- The memory of the defect is 10 years. Before the significant defect in 1988, the core inventory of FM was 6 mg and ten years had to elapse before the amount of FM decreased to this number again.

- During the year 2000 there is uranium dissolution again. The FM in the core increased from about 6 mg to 83 mg, corresponding to 4 g tramp uranium. It was not actually possible to estimate this small uranium contamination with any other used method. Plant A has been in operation with HWC for about 10 years. During operation from 2000 to 2001 with degrading fuel, the water chemistry was changed frequently between NWC and HWC conditions. However, the figure shows that the FM calculated based upon Sr-92 is not affected. It shows a constant increase in time. This indicates that this model can be used for estimation of the amount of FM and tramp uranium on the core surfaces both for both NWC and HWC conditions.

## 6. RECOMMENDATIONS WITH RESPECT TO POWER SUPPRESSION

Flux Tilting means that manoeuvring of single control rods changes the local power. Control rods can be manoeuvred in two ways, screwed or hydraulic manoeuvred. Screwed control rods can be manoeuvred at relatively high power without violation of thermal margins. In reactors with hydraulic manoeuvred rods single rod scrams is often recommended to protect the fuel from the significant power peaks that can be the result of the step movement with the hydraulic system. The main disadvantage with single rod scrams is that the Flux Titling results in poor resolution. It can be difficult to exactly locate the position of a core cell with the defected fuel bundle.

At insertion of the control rod the power in the surroundings of the neutron absorbing materials will decrease. This results in more water (more moderator) in the upper part of the fuel bundle. Thus the entire bundle power will decrease by the insertion of a control rod. The power change affects the release rate of noble gas. There are a number of ways to record the change of the off-gas flow. The supervision detectors in the off-gas system can be used; there can be on-line measurement with Ge- detector, or manually collected samples. It is recommended to use manually collected and analysed samples. The delay time from sampling to measurement ought to be at least one hour in order to reduce the background from short-lived radionuclides. The statistic scattering in the Xe-133 and Xe-135 peaks shall be kept below about 0.5%.

It is also strongly recommended to only manoeuvre one single control rod at time during Flux Tilting.

It is important to control the global power during a Flux Tilting investigation. If the power is increased in one core cell the power in the rest of the core may also increase by the increase of the main recirculation pumps if the reactor is in power control mode. This power increase may create increased leakage of noble gas from a defect randomly located in the core. Than a false signal can be generated. It is therefore recommended to keep the recirculation flow rate constant during a Flux Tilting investigation.

Power Suppression means that a control rod is inserted into the core cell with the defected fuel. The intent is to reduce the activity release and mitigate the secondary degradation tendency. There are however, a number of reasons for not adopting the Power Suppression method:

- It is difficult to exactly locate the core cell containing the defected rod. This is specifically difficult in plants with hydraulic manoeuvred control rods because these must 100% inserted. A large area around the core cell is affected with significant power exchange and there will be a significant probability of false signals.
- It is costly to have a control rod inserted for a long time. The reactor power will be lowered by about 5%.
- All fuel in the entire core will be unfavourably burnt up.
- The power (centre temperature) decrease in the power-suppressed fuel will be about 10%. The temperature decrease in the pellet-cladding gap will be less, may be 5-8%, which is about at the most 25°C. The temperature will at the most decrease from 350°C to 325°C. The chemical activity will not be significantly affected by this temperature exchange.

- If we look back we have a significant experience of the real significant power suppression. The centre temperature in old 8x8 fuel was at the most about 1800°C. In 10x10 rods the highest temperature is about 900°C. In 8x8 fuel the maximum centre temperature is about 1300 °C. When the old fuel was replaced the new fuel acts, as it was power suppressed, with about 50%. A further power decrease; about 10% is relative marginal compared to the outcome of the exchange of fuel type.

## 7. RECOMMENDATIONS FOR OPERATION WITH DEFECTS

When a defect has been detected. The following recommendations are suggested:

1. *Load following operation*: Load following operation shall, if possible, be avoided.

2. *Reactor power*: Keep the reactor power as constant as possible.

3. *At power changes*: At tests of components the reactor power is often decreased. These power decreases can be carried out as usual. The subsequent power increase, however, can initiate degradation if it is done in a fast way. Therefore it is recommended that the power is increased at a slower rate.

4. *Flux Titling and Power Suppression*: Avoid Flux Tilting and Power Suppression because of the risk that it initiates degradation. Flux Tilting may be done cautiously if the results are crucial.

## 8. SUMMARY AND RECOMMENDATIONS

Primary fuel defects can be initiated because of a number of reasons. The two dominating causes are debris fretting, about 70% of all failures, and historically PCI defects, about 10%. Also, there are some crud/water chemistry related fuel failures. For the remaining rods the failure cause has not been established.

When a rod has been subjected to a primary defect there is always a probability that a secondary defect develops. Two types of secondary defects can develop:

1. *Circumferential cracks or break.* This defect type may cause a limited amount of uranium fuel dissolution in the reactor water. The total amount of uranium from one single break has been estimated from measured data. At the most about 120 g uranium has been lost and 40% of this will accumulate in the core, about 40% in the RWCU system and the rest on the system surfaces.

2. *Axial cracks*. The axial cracks can be from a couple of centimetres up to the length of the rod. There is an unequivocal trend that this defect type has a significantly lower frequency for the modern 9x9 and 10x10 fuel. The old 8x8 fuel, and especially sponge liner, could develop very long axial cracks. The potential for uranium dissolution can be higher for this defect type than for circumferential breaks.

The fuel design has a significant impact on the resistance against degradation. The following factors have significant impact for modern fuel:

- *The size of the secondary phase particles in both liner and non-liner fuel:* Good corrosion properties of the bulk thickness of the fuel cladding will also reduce the risk of getting secondary degradation of failed fuel. Such good properties may be obtained by having SPPs larger than 50-100 nm (assessed by scanning electron microscopy, SEM).

- *For liner fuel*, the corrosion properties of the liner are essential to get good resistance towards secondary degradation. Sn-additions seem to have only a minor effect on corrosion performance. The most potent alloying addition to achieve good corrosion performance is by adding Fe to the liner. It is recommended to have as much Fe as possible without deteriorating the PCI performance. The fuel vendor must show that the Fe-doped liner has appropriate PCI performance by ramp testing.

- *Spacer design,* A design that catches the debris fretting failures in the lower part of the fuel assembly will reduce the risk of getting transversal breaks.

If the plant has high frequency of fuel defects it is recommended to carefully select such a fuel design to get the largest resistance towards secondary degradation.

A new model, *BwrFuelRelease*, useful for analyses of measured off-gas and reactor water data has been developed by ALARA Engineering. This model can replace all methods and models used to day. The model is useful nondependent of reactor chemistry, if the reactor is in operation with NWC (Normal Water Chemistry) or HWC (Hydrogen WC)

The model can manage the following items in a more sensitive way compared to the to day used:

- *Detect small failures*: It can detect a defect that releases about 10 kBq/s of Xe133 during operation.

- *Estimation of the amount of Fissile Materials (FM*): The model is able to quantify with significant precision the amount of, in the core during operation. It can easily detect uranium dissolution.

- *To assess the zero-failure goal:* It is important to achieve the zero-failure goal at start-up. If a defect is still in the core there is a significant probability that it will degrade. Of course it does not help to know if there is a defect at start-up but it is important to know this and learn why it could happen.

The following recommendations are provided regarding Flux Tilting and Power Suppression:

- *Flux Titling*: It is recommended to only use Flux Titling investigations only as an exception. It is always a risk to initiate degradation with the significant power impact during control rod manoeuvring.

- *Power Suppression*: It is not recommended to adopt the Power Suppression method. However, if power suppression is applied it is crucial that the core cell(s) have been located were the failed fuel are located to reduce risk of degradation.

## REFERENCES


[1] INTERNATIONAL ATOMIC ENERGY AGENCY, Review of Fuel Failures in Water Cooled Reactors, Technical Report Series no. 388, Vienna (1998).

[2] GARZAROLLI F., VON JAN R. AND, STEHLE H., “The main causes of fuel element failure in water cooled power reactors”, Atomic Energy Review, IAEA, Vienna, Vol 17 (1979) 31-128.

[3] YANG R. L., OZER O., AND ROSENBAUM H. S., "Current Challenges and Expectations of High Performance Fuel for the Millennium" Proc. ANS Int'l Topical Meeting LWR Fuel Perform, Park City, UT, USA, April 10-13, 2000, Vol. 1 (2000) 15-24.
[4] SIHVER L., HALLSTADIUS L. and WIKMARK G., Recent ABB BWR Failure Experience, Proc. ANS Topical Meeting on LWR Fuel Performance, Portland, Oregon, ANS (1997) 356.
[5] ARMIJO J. S., Performance of Failed BWR Fuel, Proceeding from Light-Water-Reactor-Fuel-Performance, West Palm Beach, Fl., April 17-21, 1994, ANS (1994) 410-422
[6] HÜTTMAN A., KETTLER M., SKUSA J., HECKERMANN H., RUDHOLZER G. and MANZEL R., Post-Irradiation Examination of Failed KKK-Barrier Fuel Rods, Proc. ANS Topical Meeting on LWR Fuel Performance, Portland, Oregon, 1997, ANS (1997) 350-355.
[7] D. O. PICKMAN, "Failure development in leaking LWR fuel rods – a literature survey", Studsvik Report NF(R)-89/83, 1989.
[8] D. SCHRIRE, G. LYSELL, G. FRENNING, G. RÖNNBERG, Å. JONSSON, „Secondary defect behaviour in ABB BWR fuel", ANS Light Water Reactor Fuel Performance, Proc: Int. Top Mtg., West Palm Beach, FL, ANS (1994) 398-409.
[9] O. OZER, "EPRI's Failed Fuel Degradation Program", Proc. Failed Fuel Degradation Workshop, Palo Alto, 1995.

# DETECTION AND MONITORING
## (Session 5)

# FUEL RELIABILITY OF BOHUNICE NPP

M. KAČMAR, J, BEŇA, I. SMIEŠKO
Bohunice NPP,
Jaslovské Bohunice, Slovakia

**Abstract**

Paper summarizes experience from last 15 years of operation at NPP Jaslovské Bohunice. During this period, leaking fuel assemblies have had been identified by in-core sipping method and verified by vendor specified canister sipping method. Methodology of operational and outage fuel integrity monitoring is described. Full survey of identified leaking assemblies is given. Fuel failure rates are calculated separately for V-1 (V-230 type) and V-2 (V-213 type) units. Systematic difference - significantly lower fuel failure rate at V-213 units exists for all period investigated. Analysis of potential fuel failure reasons and all related measures (planned and already implemented) are presented. Design, operation and fabrication features have been analyzed with the aim to identify dominant factors contributing to fuel failure. No unambiguous reasons have been found so far. It is believed that there is a superposition of several factors and differences causing higher failure rate at V-230 type units.

## 1. MONITORING OF FUEL INTEGRITY AND THE RESULTS OF EXAMINATION

The fuel gladding represents second, but the most important, barrier against release of the fission products beyond the nuclear plant. Fuel integrity monitoring is therefore principal for safe operation of the plant. Bohunice NPP has implemented following operational monitoring procedures:

- On-line gamma spectrometry of reactor coolant
- Laboratory analysis of reactor coolant, including radiochemical separation of isotopes $^{131}I$, $^{132}I$, $^{133}I$, $^{134}I$, $^{135}I$, $^{239}Np$, $^{239}Pu$, $^{242}Pu$
- Spiking effect monitoring during reactor power changes.

Activities of fission products are evaluated by installed calculating models that provide information on the probable number of fuel leakage. The relation $^{134}Cs/^{137}Cs$ and $^{238}Pu/^{239+240}Pu$ give data for leak fuel burn-up estimation.

If above-mentioned operation diagnostics indicate a leak all fuel assemblies are tested during refueling outage. These examinations include in-core sipping procedure and testing by canister sipping system in spent fuel pool. Till 1986 only chosen group of fuel assemblies were tested by canister sipping system and any assembly wasn't detected like a leaky though defected fuel had indicated by operational diagnostics.

Since 1986 the plant has used in-core sipping test bought from SIEMENS KWU. The reactor core checking by means of sipping system takes time 48 hours approximately. The leaky fuel assemblies identified by in core sipping test are once more checked by canister sipping system.

BOHUNICE NPP has four WWER-440 units in operation. The plant includes older reactor V-230 type on Unit 1 and 2 and advanced Unit 3 and 4 with V-230 type reactor. Totally 32 in-core fuel inspections were performed at Bohunice NPP from 1986 to 2001 identifying 49 leak assemblies. The number of occurrences for individual units is given in Table 1 and Figure 1. The relation between number of defective assemblies and fuel burn-up is shown on Figure 2.

Table 1. The distribution of leaking fuel assemblies at Bohunice NPP units

| | V-1 Unit | | V-2 Unit | |
|---|---|---|---|---|
| Year | Unit 1 | Unit 2 | Unit 3 | Unit 4 |
| 1986 | 2 | 1 | 0 | 0 |
| 1987 | 0 | 2 | 0 | 0 |
| 1988 | 0 | 2 | 0 | 0 |
| 1989 | 2 | 5 | 0 | 0 |
| 1990 | 1 | 4 | 0 | 1 |
| 1991 | 1 | 2 | 0 | 0 |
| 1992 | 0 | 1 | 0 | 0 |
| 1993 | 1 | 1 | 0 | 0 |
| 1994 | 1 | 0 | 0 | 0 |
| 1995 | 1 | 0 | 0 | 0 |
| 1996 | 0 | 4 | 0 | 0 |
| 1997 | 2 | 4 | 0 | 0 |
| 1998 | 3 | 2 | 0 | 1 |
| 1999 | 0 | 1 | 0 | 0 |
| 2000 | 1 | 0 | 0 | 0 |
| 2001 | 0 | 3 | 0 | 0 |
| Total | 15 | 32 | 0 | 2 |
| Total number | | 49 | | |

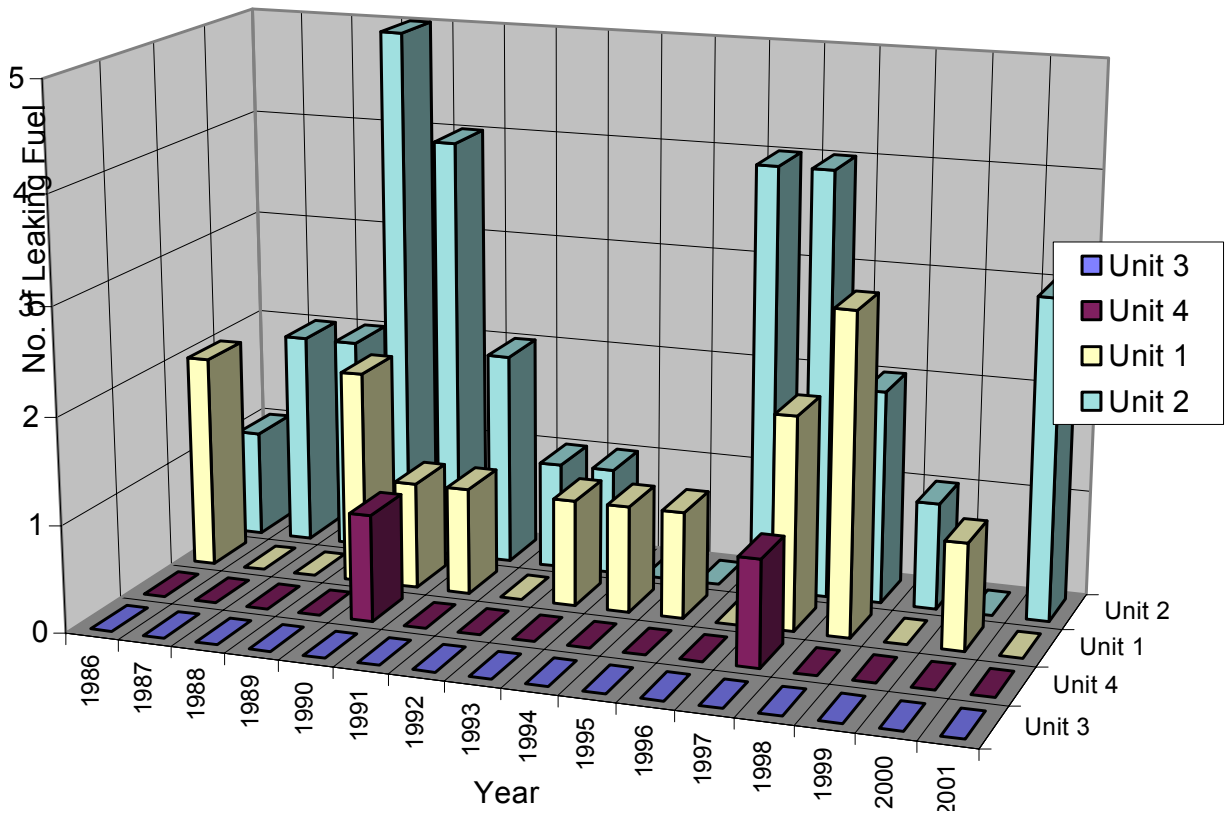


*FIG. 1. The distribution of leaking fuel assemblies at Bohunice NPP units.*

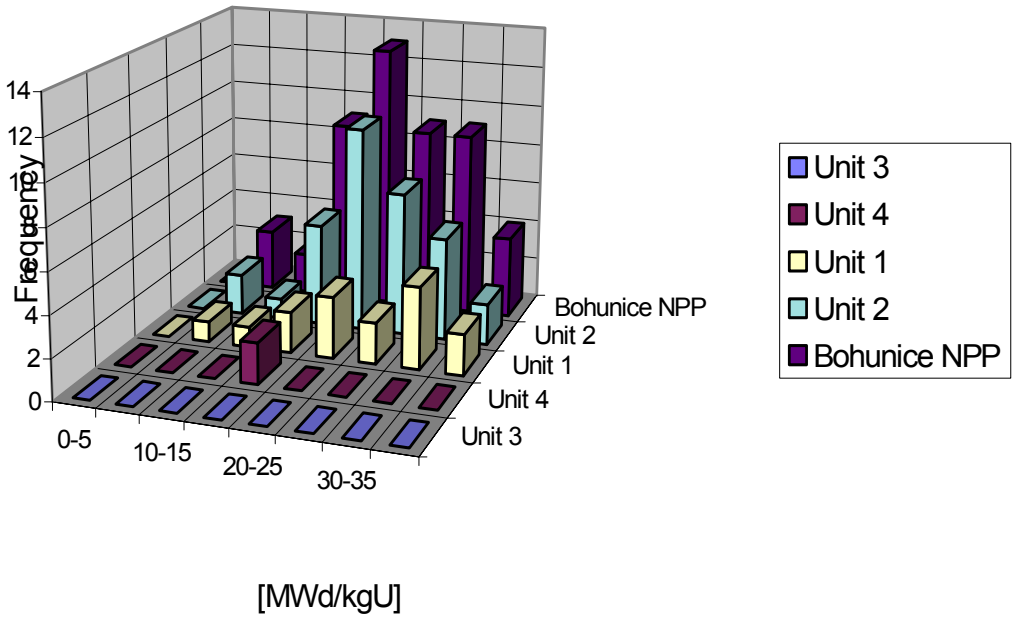


*FIG. 2. Burn up distribution of discharged Defective Fuel Assemblies at Bohunice NPP units.*

From the beginning of the fuel leaks systematic observation during reactors operation the differences in frequency of occurrences between V-1 and V-2 and between Unit 2 and Unit 1 as well were revealed. While the number differences of defective assemblies until 1989 could be considered as random fluctuation, the results from 1990 have confirmed that some parameters of Unit 2 are different from the other units.

## 2. ANALYSIS OF THE CAUSES OF FUEL LEAK AND LEAK FREQUENCES

Immediately after the leaks have been occurred in 1989 and 1990, the plant has implemented first steps to identify the causes of fuel leaks. As a first, operational parameters were analyzed and compared with allowed limits. This procedure did not provide solution. According to the calculation analysis leak fuel assemblies were selected for PIE testing in VNIIAR Dimitrovgrad. Due to extreme financial expenses and stabilization of the number of the occurrences in the following years, this idea has been left later on. The problem was activated again from 1996 when the second increase of occurrences of leaky fuel assemblies has bee indicated.

To find root causes of failures after 1996 the plant has summarized following facts:

- There is proven existing of statistic difference in probability of fuel cladding defects between V-1 and V-2 plants and between the 1$^{st}$ and the 2$^{nd}$ Unit as well.
- Two parameters sets exist that determine the probability of fuel defects: manufacturing and operation parameters. In reference to reality that all units of Bohunice NPP have used the same type of fuel, the reason of defects has been found out in the frame of operational parameters. Considering the different operational parameters of Unit 1 and Unit 2 are causing fuel defects, at the least one operational parameter of the units has to be different significantly.
- Among the set of different operational parameters on both units, at the least one operational parameter has relation to the probability of fuel defects occurrence.

Hereinafter activities and analyses have been made with regard to preceding considerations.

## 2.1. IDENTITA program

Main goal of this program was to find identity or differences in operational parameters of Unit 1 and Unit 2 and to analyze possible correlation of differences found and fuel leak appearances. Data collection, processing and analysis has been done for cycle 18-21 of Unit 1 and cycle 17-20 of Unit 2 [1].

Following parameters have been analyzed:

- activity of primary coolant
- model prediction of number and type of fuel leak.
- time based comparison of physical parameters
- core charts of heat-ups for all assemblies
- time based linear heat rate distribution
- time based evolution of PCMI margin of linear heat rate
- statistical processing of measured physical parameters in stable mode
- statistical processing of measured physical parameters in transient mode

Following conclusions were drown from this evolution:

- no systematic difference exists for analyzed set of physical parameter which can be relevant to fuel leaks appearance
- none of fuel assemblies reached PCMI margin in linear heat rate
- maximal power ramps of Unit 2 for high burn up fuel are lower than at Unit 1 and linear heat rate ramp limit valid for Bohunice NPP was never exceeded.
- none of fuel assemblies exceeded allowed values of limiting parameters for power distribution [2].

## 2.2. Dummy assemblies implementation

The dummy assemblies have been implemented at core periphery of V-1 reactors in order to protect the reactor vessel against fast neutron flux. The assemblies were implemented at Unit 2 in December 1985 on beginning of the $6^{th}$ fuel cycle and at Unit 1 in May 1992 on beginning of the $13^{th}$ fuel cycle. Consequently, the average power of assembly was increased from 3.94 to 4.39 MW and the mean linear power heat rate of fuel rod was increased from 129 to 144 W/cm.

From the dummy assemblies point of view the operation of Unit 1 and 2 can be divided:

- Period 1986-1991 - dummy assemblies implemented at Unit 2 only.
- Period 1992-2001 - dummy assemblies implemented on both units.

The cumulative frequency of failed fuel assemblies during period 1986-2001 is given on Figures 3 and 4. While the Figure 3 enforces on the opinion that the dummy assemblies implementation effected fuel defect occurrences, the Figure 4 disproves this opinion although the correlation between power increased and fuel defect occurrence cannot be excluded.

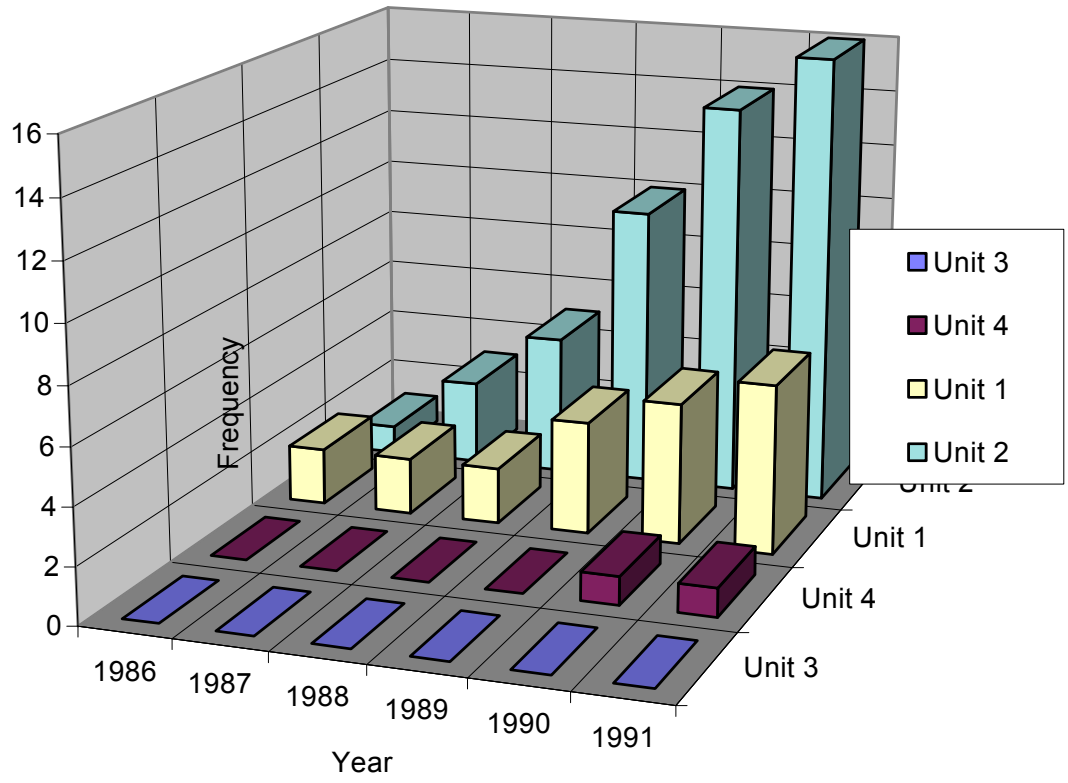


*FIG. 3. Cumulative frequency of failed fuel assemblies during period 1986-1991 (Dummy assemblies at Unit 2 only).*

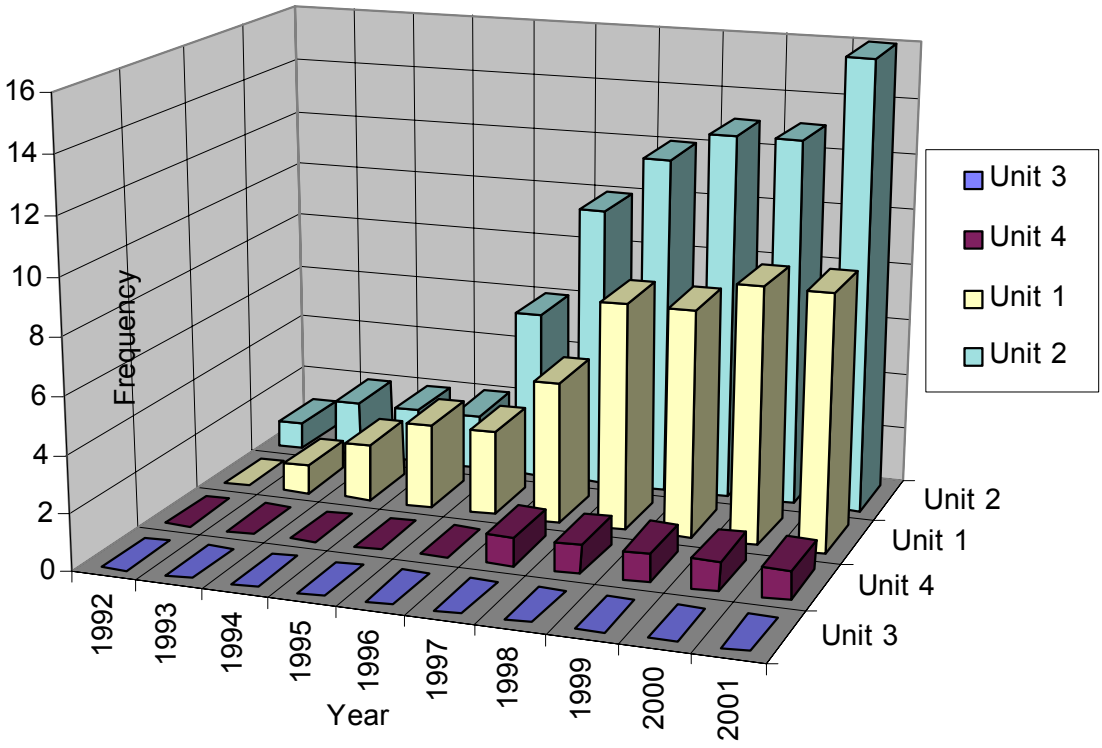


*FIG. 4. Cumulative frequency of failed fuel assemblies during period 1992-2001 (Dummy assemblies at both Units V-1).*

## 2.3. Data analysis systems PES and PEPA

The PEPA and PES systems [3] for leaking fuel monitoring have been implemented on all units Bohunice NPP. At the V-1 Units this exert systems have operated in off-line regime. At the V-2 Units the core monitoring system SCORPIO has been implemented in 2001 [4]. The SCORPIO is a computer system, based on modular design for on-line monitoring of reactor core. The complete system includes both PCMI-margin calculation (PES) and primary coolant monitoring (PEPA). The expert systems are working in the on - line regime.

## 2.4. In-core diagnostic system installation

For purposes to identify vibrations of in-core components the diagnostic system based on neutron noise was installed at V-1 and V-2 Units (SVRD V-1, SVRD V-2). Particular measurements on several reconstructed channels SVRD V-1 and SVRD V-2 were performed in order reveal vibrations of fuel rods. The measurements gave following results:

- In-core components vibrations are more intensive in V-1 Units compared with V-2 Units.
- The evaluation of analysis confirmed more significant fuel vibrations at V-230 reactors (V-1) compared with V-213 reactors (V-2).
- Long term monitoring of V-1 Units and comparison of both units confirmed higher vibration amplitudes of the basket at Unit 1, while the result of Unit 2 monitoring draw attention to more intensive frequency vibrations of in-core components. Beneficial information for explanation could be that Unit 1 has rigidly connected the basket with its bottom while at Unit 2 such connection does not exits.

## 2.5. Technological and/or physical difference between units:

Except of above differences between V-1 and V-2 Units (inserted dummy assemblies at V-1 Units, and connection of the basket with its bottom at Unit 1) there are occurred other two differences between V-1 and V-2 Units, which could contribute to higher frequency of fuel defects:

- The flat bottom of the basket at V-1 Units - it can affect the character of coolant stream in bottom part of pressure vessel and can contribute to more intensive vibrations of in-core components. The V-2 Units have semispherical bottom of the basket.
- The fuel assembly flow rate at V-1 Units is in upper part of range allowed by the Technical Conditions (100-130 $m^3.h^{-1}$) i.e. 125 $m^3.h^{-1}$. The V-2 Units have the flow rate 105 $m^3.h^{-1}$, which is in low part of allowed range [5].

## 2.6. Position of the leaking fuel assemblies in the core

With regard to the fact that movement of $6^{th}$ group of control assemblies has significant influence to power of neighbouring assemblies this effect was statistically evaluated as potential factor contributing to fuel leak development. Position of leaking assemblies of V-1 units is shown of Figure 5.

From total number of leaking assemblies 47, in the neighbouring cells 12 assemblies were loaded. From this statistic results fact when in the case that assembly is loaded for at least one cycle to the $6^{th}$ group neighbouring cell, fuel leak development probability is 2,2 higher compared to rest of assemblies. This is valid also separately for Unit 1 and Unit 2, so there is no difference between these units from this aspect.

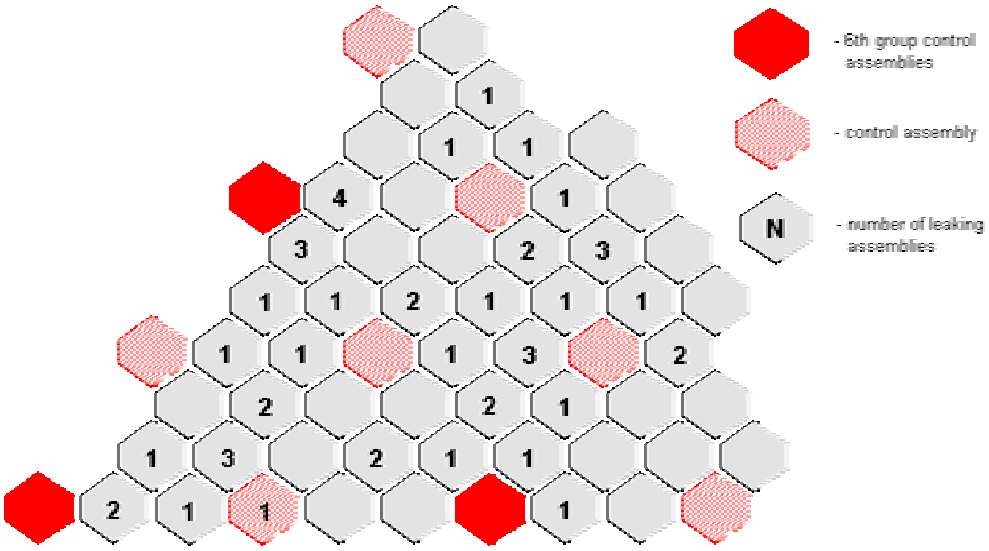


*FIG. 5. Leaking fuel assemblies - last cycle position.*

## 3. CONCLUSIONS

Providing one fuel rod within leaky assembly during 1986-2001, the average occurrence fuel rod failure rate of $7{,}98.10^{-5}$ have been achieved at V-1 Units. The occurrence frequency at V-2 Units is $3{,}99.10^{-6}$, which is less than PWR reactors worldwide average and this is close to $10^{-6}$ which is considered as a "zero failure goal".

The parameter or group of parameters responsible for different frequency of fuel failure is not known until now. It is supposed that such parameters will stay unknown, because the failure phenomenon is caused by other factors, which are not detectable with actual level of instrumentation.

The following factors are identified as possible contributors to different frequency of fuel leaks at V-1 and V-2 Units:

- Increasing of the assembly and rod average power in consequence dummy assemblies implementation in V-1 Units.
- Different shape of V-1 basket bottom compare with V-2 Units.
- Different fuel assembly flow rates at V-1 Units compared with V-2 Units. Increased coolant flow at fuel assembles of V-1Units.
- Rigid connection of the basket with its bottom at Unit 1.

More intensive vibrations of core components at V-1 Units are probably resulted from last three effects.

Position next to $6^{th}$ group of control assemblies increases probability of fuel damage.

Despite of unknown root causes of fuel failure the following corrective actions were carried out to reduce the frequency of fuel failure:

- V-1 Units have reduced trends of power changes.
- The suction of filling water pumps of V-1 Units are equipped by the screens to eliminate the intrusion of foreign materials into the coolant system.

- The improvement of diagnostic system SVRD V-1 was made to enable monitoring of fuel rods vibration.
- Bohunice NPP have ensured vendor quality inspections of fuel fabrication process.
- The project of fuel inspection stand is on progress.
- Some improvements have been implemented into in-core sipping instrumentation and methodology. Due to uncertainties related to proper sampling time, separate on line activity measurement system has been installed at each sampling line.
  Another module for measurement of liquid samples stripped gas activity is currently in development and will be tested during sipping at Unit 3 in July 2002.

## REFERENCES


[1] SEMMLER M., et al.: Primary circuit comparing 18-21 cycle Unit 1 and 17-20 cycle Unit 2 of V-1 Bohunice NPP. Summary report, CHEMCOMEX Prague, CCE-30-7-01528, Prague, July 2001.

[2] Technical Specification of Bohunice NPP, Slovak Republic, EBO, 2001.

[3] BARTA O., et al.: The application of the PES-PEPA Expert System at the Dukovany Power NPP, Techn.Comm.Meeting on Fuel Failure in Normal Operation of Water Reactors: Experience, Mechanisms and Management, 26-29 May 1992, Dimitrovgrad, Russian Federation.

[4] Reactor Core Monitoring System for Bohunice V2 Unit 3& 4. Phare Project No: PH 2.01.97, December 2000.

[5] A Set of Reactor VVER-440 Fuel Cassettes, 432.02.0000 KTC, Russia, Mashinostroitelny zavod, Dec. 2000.

# FAILED ROD DIAGNOSIS AND PRIMARY CIRCUIT CONTAMINATION LEVEL DETERMINATION THANKS TO THE DIADEME CODE

D. PARRAT, J.B. GENIN
DEN/DEC/S3C,
Saint-Paul-lez-Durance, France

Y. MUSANTE, C. PETIT
FRAMATOME–ANP/FFJE – 10,
Lyon, France

A. HARRER
EDF/SEPTEN/T/TR,
Villeurbanne, France

**Abstract**

Extended burn-up and longer fuel cycles are recently become key points of the fuel cycle economy, and are now operational strategies for fuel vendors and utilities. For plant operator, these evolutions necessitate to have a better understanding of the fuel reliability during the cycle. The presence of a specific alpha activity in the irradiated fuel more important than at low burn-up, or the risk of failure degradation during a long cycle constitute now two potential limiting factors for plant operation. In this context, it is very important to have reliable tools permitting to assess in operation defective fuel characteristics and primary circuit contamination for actinides and long half life fission products involved in health physics problems as well as in waste and decommissioning studies. With this aim, both theoretical and experimental studies have been carried out at the French Atomic Energy Commission (CEA) on the release of fission products and actinides from defective fuel assemblies in operation, and their migration and deposition in the PWR's primary circuits. Thanks to this large experience feedback, a Research and Development programme with the CEA, Electricité de France (EdF) and FRAMATOME-ANP permitted to develop and to qualify the DIADEME computer code. Physical equations and empirical correlations introduced in the code allow a correlation between noble gases, iodines and caesiums primary water gamma specific activities and the following parameters:

- the quantity of tramp uranium deposited on the cladding,
- the number and the seriousness of defects,
- the burn-up of the leaking rods,
- the type of failed fuel rod: $UO_2$ or MOX.

In case of tramp uranium, these characteristics allow to calculate the alpha activities present in the primary water, deposited on the primary circuit walls and on filters and resins of the purification circuit. It is also possible to extrapolate these results until the end of the cycle, in order to prepare the maintenance operations during the shutdown period in the best way. Moreover, when defective fuel assemblies have been reloaded, predictions of the primary activity levels and their future evolutions have been carried out with DIADEME. A good agreement has been obtained between predicted and measured activities, not only for gaseous fission products but also for long half life beta and alpha emitters.

## 1. INTRODUCTION

In many countries, the production and distribution of electric power has experienced a dual evolution over the last decade. Firstly, the construction and commissioning of new nuclear power plants decrease dramatically. Secondly, the liberalisation and deregulation of the sector introduced a harsh competition.

In order to improve effectiveness in the field of the fuel cycle economy, operators and fuel vendors are considering a variety of means to enhance plant performance and to reduce costs, introducing measures such as fuel burn-up extension, power up-rates, longer fuel cycles and plant life extension. This trend has taken place in the last several years, and is likely to continue in the long term. In fact, it can be seen as an enhancement of an evolution that Light water reactors (LWRs) started three decades ago. Among others, this evolution comprises following points:

- increasing the reactor power, from 900 MW(e) up to 1,400 MW(e),
- increasing the fuel assembly burn-up, from ~ 30 GWd/t up to 50-60 GWd/t,
- introducing new types of fuels, including MOX fuel in some countries, and new cladding materials,
- increasing the fuel cycle duration, from 12 months up to 18 or 24 months, moreover with more flexibility in the electric power output.

As a consequence of this evolution, fuel isotopic composition of the irradiated fuel has strongly evolved, with a presence of a alpha and long half-life fission products specific activities more important at the end of life. On the other hand, stronger stresses are applied to the cladding, due to fuel-clad interaction, external corrosion, or grid-rod interaction, which could impact the fuel reliability. This situation involves two potential consequences:

- new types of clad failure root causes, which occurrence probability was negligible in the past years, risk to emerge,
- the risk of a failure degradation during a long cycle constitutes now a potential limiting factors for plant operation.

The above mentioned radionuclides are notably involved in health physics problems, and in the activity level and composition in wastes, which obliges to a specific monitoring and management. They have also consequences in terms of plant operational surveillance, and radioactive source term in case of an accident. Finally, end of life problems are linked with the presence of such isotopes, i.e. long term fuel storage and plant decommissioning.

In this context, fuel reliability becomes an important point for the plant operator, and it is now necessary for him to have in hands reliable tools permitting to assess in operation failed fuel characteristics and primary water contamination for actinides and long half-life fission products. With this aim, both theoretical and experimental studies have been carried out at the Commissariat à l'Energie Atomique (CEA), in collaboration with Electricité de France (EDF) and FRAMATOME-ANP [1]. These studies deal globally with the release of fission products and actinides out of failed fuel rods in operation, and their behaviour in the PWR's primary circuits. Four main research topics can be identified:

- analytical in-pile experiments on short experimental failed fuel rods in a devoted irradiation loop [2], [3], and [4],
- power reactors primary activity monitoring and analysis, with comparison to fuel assemblies inspection results performed during the planned outage, mainly sipping tests and ultrasonic testing,
- modelling of the fission products and actinides migration and deposition in the primary and auxiliary circuits of a power reactor,
- modelling of the internal thermal-hydraulical behaviour of a failed rod at steady state and during transients,

## 2. DESCRIPTION OF THE DIADEME CODE

### 2.1. Aims and interest of the DIADEME code

Due to this large experience feedback, a Research and Development programme with the CEA, Electricité de France (EdF) and FRAMATOME-ANP permitted to develop and to qualify the DIADEME computer code. Thanks to physical equations and empirical correlations, the code allows a relation between gamma specific activities of noble gases, iodines and caesiums measured in the primary water and the following parameters:

- the quantity of tramp uranium deposited on the cladding,
- the number and the seriousness of defects,
- the burn-up of the leaking rods,
- the type of failed fuel rod: $UO_2$ or MOX.

In case of tramp uranium, these characteristics allow to calculate the alpha activities present in the primary water, deposited on the primary circuit walls and on filters and resins of the purification circuit. It is also possible to extrapolate these results until the end of the cycle, in order to prepare the maintenance operations during the shutdown period in the best way.

Moreover, the French failed fuel management policy allows the reloading of defective fuel assemblies when failures characteristics and activity release forecast are comprised beneath given limits [5], [6]. The main limits are the equivalent diameter of the defect obtained thanks to the quantitative sipping test [7], which represents the seriousness of the defect, and the absence of non-volatile fission products measured in the sipping cell water during the same test. When this situation occurs, the DIADEME code is able to predict the primary activity levels at the beginning of the following cycle, and forecasts their future evolution.

### 2.2. Input data for the DIADEME code

DIADEME is a Windows computer code running on PC computers and requires following input data:

- Radiochemical measurements of the primary water gamma activities for gaseous fission products (radioactive xenons and kryptons), iodines and caesiums, during steady state and operation transients; these measurements are performed either on primary water samplings or by on line gamma spectrometry.
- Average reactor power
- Purification system flow rate

These data can be obtained and used by three ways (see Fig. 1):

1 - The daily sampling and gamma spectrometry measurement of the primary water during a cycle, together with the reactor power and the purification flow rate values, are recorded on an EDF data base which is available on Windows files and which can be directly read by DIADEME.

2 - An on-line gamma spectrometry device can be used [8] and, in connection with a scope meter and an analog to digital converter for the power and the purification flow rate information, can be directly connected through a serial connection to the DIADEME computer.

3 - It is also possible to enter the data parameters through the DIADEME computer keyboard.

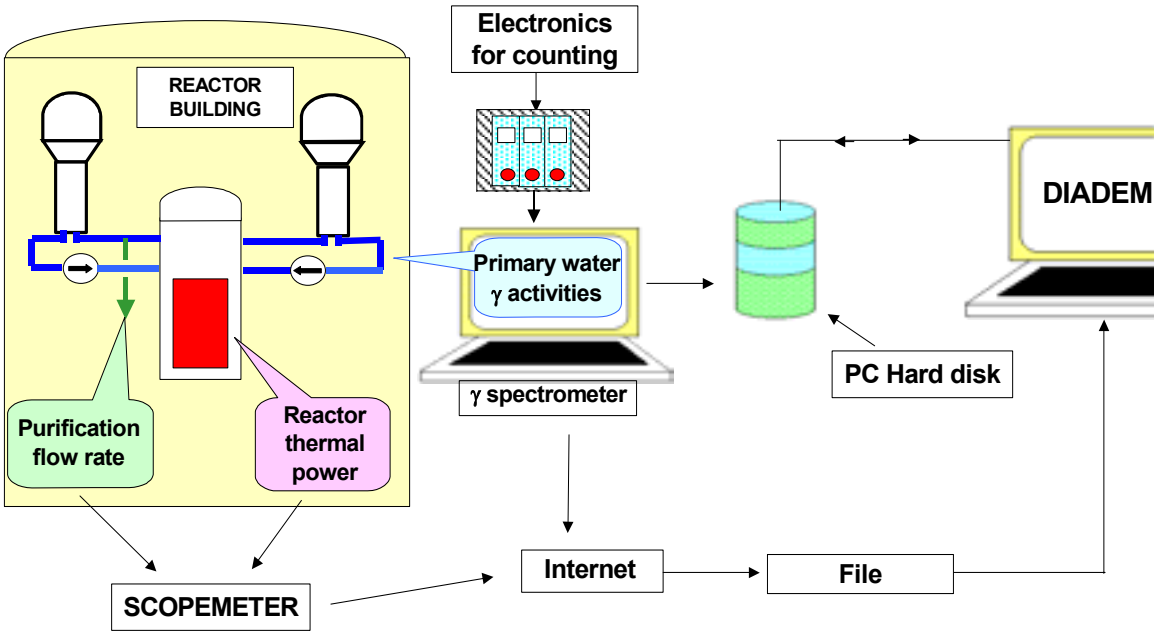


*FIG. 1. Schematic of the DIADEME input data network.*

## 3. FAILED FUEL RODS CHARACTERIZATION WITH DIADEME

The diagnoses are based on the analysis of the "release-to-birth" ratios (R/B) in the primary coolant of noble gases and iodines measured at steady state power level. In this ratio, R is the release of the fission products in the primary coolant, calculated in atoms/s. B is the birth term, i.e. the fission product creation rate in one rod operated at the average linear heat generation rate when the reactor is at nominal power. B is calculated at the radioactive equilibrium, this means including all ways of creation: direct fission, radioactive decay of a father, and neutronic capture. It is also calculated in atoms/s. The release-to-birth ratios are calculated from correlations with the primary water activities, the reactor power, the purification system flow rate and the average burn-up of the core.

Plotted versus the radioactive decay constant $\lambda$ of the measured radionuclides on a logarithmic scale, the release-to-birth ratios are located on two separate lines for iodines and for noble gases (see Fig. 2). The iodine release is generally lower than the noble gas line because of the trapping in the fuel-cladding gap.

The diagnosis consists of determining the main characteristics of the leaking rods. Physical equations and empirical correlations, already described in several papers [9], [10] and [11], allow a correlation of noble gases, iodine and caesium primary water activities to the following parameters:

a) quantity of tramp uranium deposited on the outer surface of the fuel rod cladding,
b) number of failures,
c) seriousness of defects in terms of defect size,
d) burn up of the leaking rods,
e) $UO_2$ or MOX failed fuel discrimination.

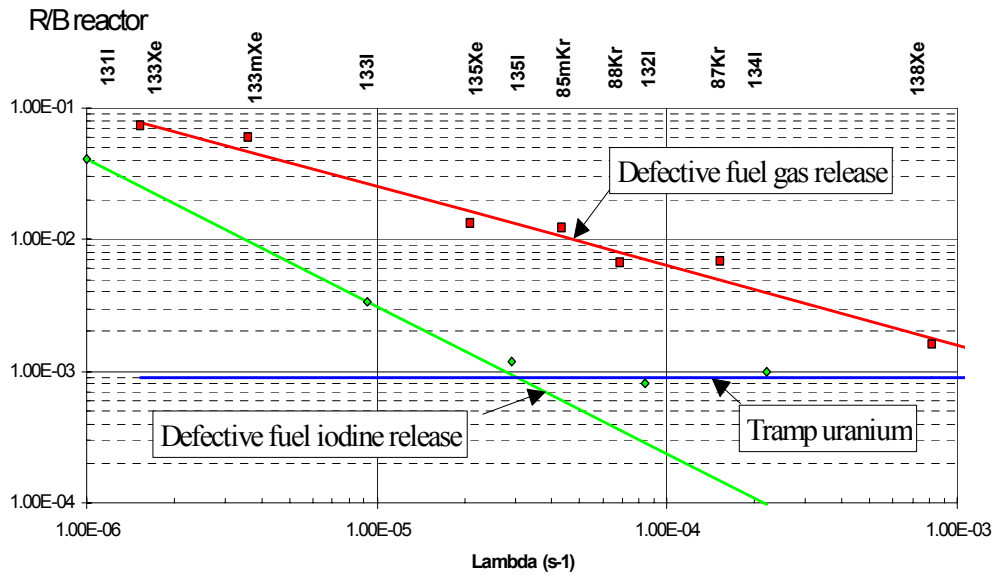


*FIG. 2. Noble gas and iodine release rates in the primary water versus the radioactive decay constant.*

### 3.1. Tramp uranium

The fission product release mechanism in the primary water from tramp uranium is due to recoil. Consequently a released fraction coming from tramp uranium is independent from the half-life of the nuclides and is equal to the measured released fraction of the short half-life iodines, such as $^{132}$I and $^{134}$I, generally not released by diffusion from the leaking fuel rods. Using the tramp uranium released fraction, it is possible to estimate the mass of fissile materials deposited on the fuel cladding and to forecast its evolution during the cycle.

A rough estimation of the tramp uranium mass is possible using the experimental data of the current cycle; but for a more accurate determination or for an estimation of the alpha activities in the primary circuit, DIADEME requires a complete set of fission product activities for the entire life of the reactor (especially when dissemination has occurred during a previous cycle).

### 3.2. Number of defects

From the release-to-birth ratio of the noble gases in the primary water, it will be possible to determine an average value of the number of defective rods, if we are able to estimate the individual source term for each defective rod.

This calculation is feasible thanks to the CEA code PROFIP. Physical models included in this code concern the release of fission products out of the defective fuel rods and include several mechanisms, such as the diffusion and knock out of the fission product atoms in the fuel oxide. These models have allowed parametric studies to be carried out, and correlations between the steady state released fractions of noble gases and the power of the fuel and the size of the defects. These models assume an instantaneous diffusion of the noble gases in the fuel-cladding gap up to the defect, that means that the release rate from the rod into the coolant is equal to the one from the fuel pellet into the gap, except for small defects (with an

equivalent diameter less than 20 micrometers obtained with quantitative sipping test). For this range of size, the low hydraulic conductance of the defect provokes a decay of the short half life isotopes in the fuel-cladding gap. The instantaneous diffusion in the fuel cladding gap is validate since the released fractions for short half life isotopes ($^{138}$Xe) as well as for middle half life isotopes ($^{133}$Xe) are well predicted with PROFIP oxide diffusion models.

One interesting result of these parametric studies is: for noble gases with decay constants λ between $10^{-3}$ to $10^{-6}$ $s^{-1}$ (meaning practically all the fission products gases measured by gamma spectrometry), the released fraction may be approximately expressed as:

$$R / B = k \cdot \lambda^{-n}$$

with n values between 0.35 and 0.7 depending on the fuel power (n increases with power) and defect size (n increases when the defect size decreases, due to the decay of the short half life nuclides in the gap, as explained above). It is not possible to determine these two parameters from the experimental value of n. Only an estimate of a bracket between the maximum defect number which can be calculated assuming a lower value for the individual defective rod R/B ($1.10^{-2}$ for $^{133}$Xe), and the minimum defect number which is calculated with a upper value of R/B, depending on the measured n (see Figure 3) can be made.

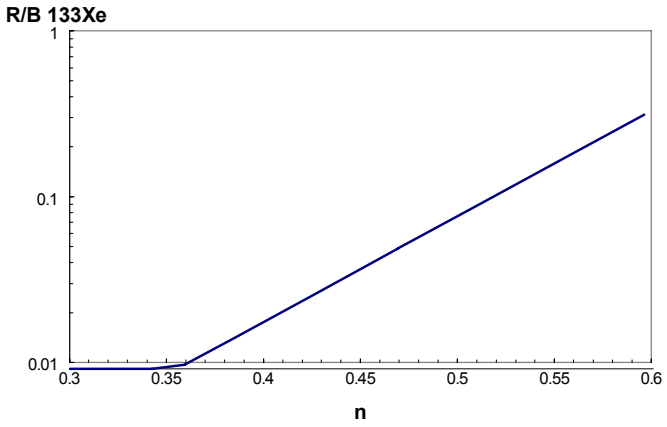


*FIG. 3. PROFIP correlation between $^{133}$Xe fuel rod released fraction and the noble gas slope.*

When defect equivalent diameter is larger than 20 micrometers, the slope n only depends on the defective rod power and a better estimation of the defect number can be given.

In 2001, cladding defects occurred on high burn up assemblies (> 40 GWd/t) on a few French units. In such cases, the fuel-cladding gap is closed and there is hard contact between clad and pellet. Once released from the pellet, the noble gases do not easily diffuse up to the defect. Thus, the DIADEME correlations are no longer accurate since the $^{133}$Xe R/B in the coolant is much lower than $1.10^{-2}$ (low power pellet R/B estimated with the PROFIP code) and DIADEME gives an underestimation of the defect number, even for the maximum defect number. The feedback has been used to improve the DIADEME diagnosis under such circumstances.

This event is clearly identified by the $^{133}$Xe coolant activity peak which occurs during a power transient and reveals the gas retention in the gap. In this case, the defect number evaluation may be more accurate with the DIADEME calculation of the total iodine release during the

transient, assuming that all the iodine trapped in the gap is released. By comparing the whole $^{131}I$ R/B in the coolant during the transient and the $^{131}I$ R/B from the fuel at nominal power (estimated with the PROFIP code), it is possible to provide a better estimation of the defect number.

### 3.3. Failure size

Up to now, no complete model has been developed for the fission products released from the fuel-cladding gap, taking into account the size and location of the defect. But the defect size has a greater influence on iodine release than on gas release. Therefore, the ratio of $^{131}I$ to $^{133}Xe$ released fractions was studied and using the experimental feedback from EDF (quantitative sipping test results and primary water activities), an empirical correlation between this ratio and the sipping test equivalent failure size was found. This correlation is represented on figure 4.

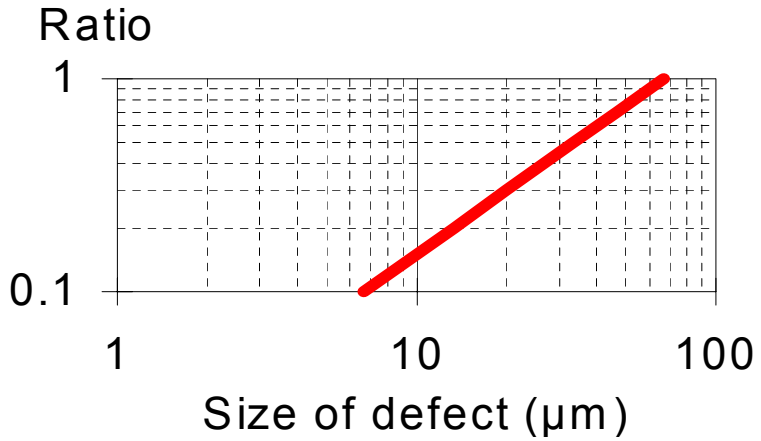


*FIG. 4. Empirical correlation between the ratio $^{131}I$ to $^{133}Xe$ released fractions and the equivalent diameter of the failure obtained by quantitative sipping test.*

### 3.4. Burn up of defective rods

The ratio of $^{134}Cs$ to $^{137}Cs$ activities in the oxide is directly related to the burn up of the rod. During a large power transient, cesium isotopes are released in the primary water and, due to the same chemical behaviour, the cesium ratio in the water is equal to that in the fuel. By comparing the measured values to the theoretical values of the cesium ratio (Fig. 5), it is possible to estimate the burn up of the defective fuel rods. This method is directly usable only if there is a few number of defective rods with nearly the same burn up. If different burn-up exist, one has to be careful with this analysis, and a more precise activity monitoring during the transient is needed (evolution of the ratio during the transient for example).

### 3.5. UO2/MOX discrimination

Because fission product yields in $^{235}U$ and $^{239}Pu$ are rather different for kryptons and similar for xenons, it is possible to discriminate $UO_2$ from MOX rod failures from the $^{85m}Kr$ to $^{135}Xe$ activity ratio in the primary coolant. Theoretical studies performed at the CEA show that this ratio is for any burn up greater than 12 for MOX fuel and smaller than 9 for $UO_2$ fuel, whatever the burn-up and le linear heat generation rate encountered in power reactors [12]. Fig. 6 shows a real example of ratios observed versus time for an $UO_2$ failed rod.

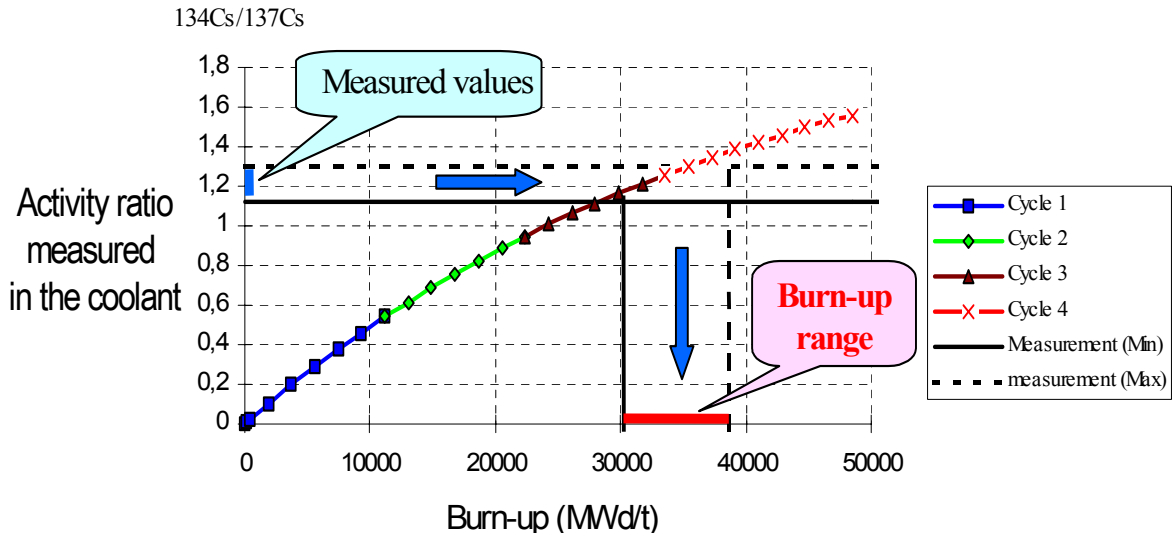


*FIG. 5. Evolution of the activity ratio $^{134}Cs/^{137}Cs$ for a $UO_2$ fuel rod versus burn-up.*

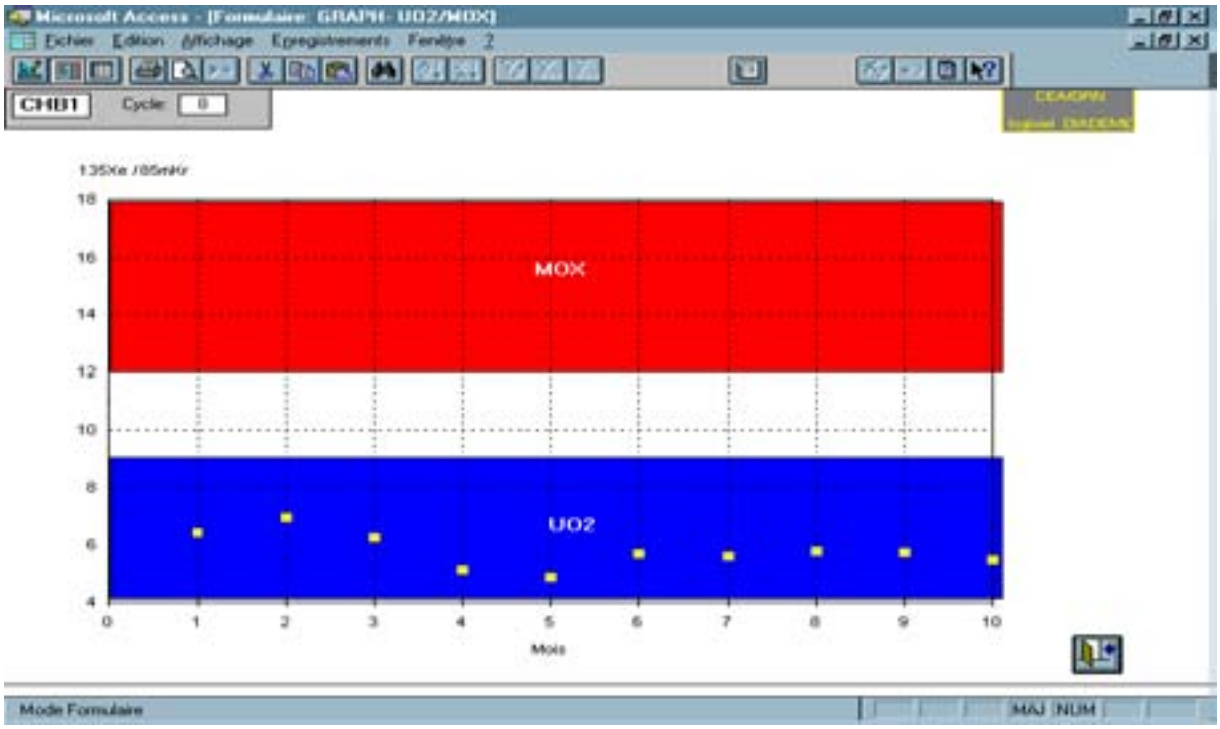


*FIG. 6. Example of a clad failure on an $UO_2$ rod: activity ratio $^{135}Xe/^{85m}Kr$ is always less than 9.*

### 3.6. General diagnosis

To avoid any fluctuation in the diagnosis due to measurement uncertainty, DIADEME calculates an average value for the parameters and primary water activities for each month of the cycle. The code then presents the diagnoses for each month of the cycle (see a fictitious case on Fig. 7).

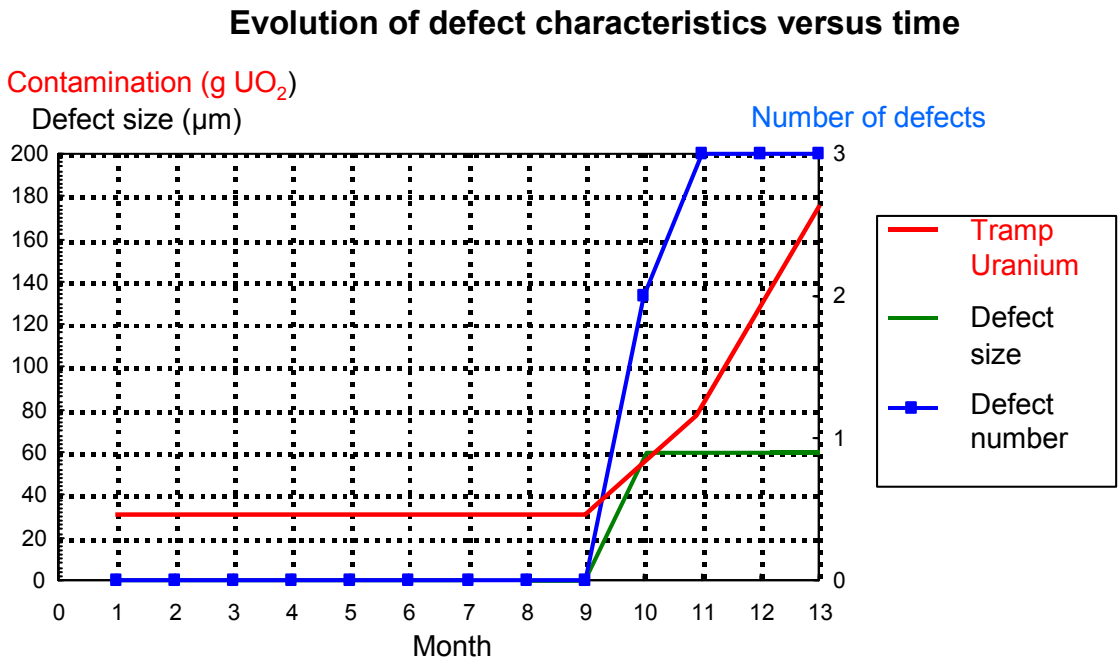


*FIG. 7. Failed fuel rod characterization with DIADEME during an entire reactor cycle.*

It is obvious that the assessment of the failed fuel characteristics is more accurate for a low defect number (1, 2 or 3). For a larger number, the diagnosis gives an average evaluation of the characteristics (burn up, defect size) with a larger uncertainty on the defect number. However it has to be noted that the average failure rate in French units is considerably less than 1 failed rod per reactor cycle.

## 4. PRIMARY CIRCUIT CONTAMINATION

### 4.1. Forecast of the primary circuit gamma activities when failed rods are reloaded

In addition to the defective fuel assembly characterization, DIADEME allows a prediction of noble gases and iodine primary water activities at the beginning of a cycle, when defective fuel assemblies are reloaded. A correlation is used in DIADEME to calculate $^{133}$Xe released fractions versus the linear power of a defective rod for different cycles during which the defect occurs.

The information needed for the diagnosis, which is not available "on-line", has to be provided by the operator to the processing unit before the beginning of the cycle. This information mainly concerns:

- the irradiation parameters for the assembly sets (meaning the linear power during the beginning cycle, the number of previous cycles for the set),
- the characteristics of reloaded defective fuel assemblies (number, size of the defects, linear power at reloading position).

All these parameters are entered in the processing unit by the operator by means of an easy graphic interface.

### 4.2. Calculation of the long half-life fission product and actinide activities

The defective fuel assembly characteristics, and mainly the determination of the quantity and the evolution of the tramp uranium, allow calculation of the activities of long half-life fission products and the alpha contamination in the primary water, deposited in the primary circuit and in the purification circuit on filters and resins [13], [14]. Up to now, the isotopes calculated by DIADEME are, $^{129}I$, $^{135}Cs$, $^{238}Pu$, $^{239}Pu$, $^{240}Pu$, $^{241}Am$, $^{242}Cm$ and $^{244}Cm$. The qualification of the code for these isotopes has been performed on several French power plants.

New developments are in progress in order to calculate $^{90}Sr$, as well as some activation and corrosion products ($^{59}Ni$ and $^{63}Ni$).

## 5. CONCLUSIONS

The methods and correlations used in the DIADEME processing for diagnosing and characterizing defective fuel assemblies during operation are currently being used satisfactorily by EdF, FRAMATOME-ANP and the CEA based on the primary water activity measurements performed through sampling by the laboratory of the nuclear plant. However, DIADEME must be considered as a tool for fission product primary water analysis and must only be used by specialists.

DIADEME has been qualified with a large database, including CEA measurement campaigns, EDF daily sampling measurements, and defective rod characteristics measured at the end of the cycle (sipping-test results). Concerning primary circuit contamination, a good agreement is obtained between the predicted and measured activities for gaseous fission products as well as for long half-life beta and alpha emitters.

An additional qualification on more than 50 recent reactors cycles is in progress, thanks to a close monitoring of the primary activity during operation, and thanks to complete inspection of the assemblies and of the failed rods during outage. Current improvements of the code concern mainly the high burn-up failed fuel analysis, this means when the fuel –clad gap is practically closed and limits the axial transfer of the noble gases.

In order to extend the qualification domain, DIADEME will be associated in 2002 to the FRAMATOME-ANP database SAFIR, which collects all the sipping-test results. The objective is exhaustive comparison between the defective rod diagnosis and experimental results.

## REFERENCES

**[1]** H. SEVEON, C. LEUTHROT, P. CHENEBAULT, R. WARLOP, JP. STORA, “Release of Fission Products by Defective Pressurized Water Reactor Fuel", *International Meeting on Nuclear Reactor Safety*, Karlsruhe, Germany, September, 10-13, 1984.

**[2]** D. PARRAT, Y. MUSANTE, A. HARRER, "Mixed Oxide Fuel in Defective Experimental Rod EDITHMOX 01: Irradiation Results and Metallographic PIE", *Proc. of the IAEA TCM on Fuel Failure in Normal Operation of Water Reactors*, Dimitrovgrad, Russia, May, 26-29, 1992, IAEA-TECDOC 709, Vienna (1993) 179.

**[3]** D. PARRAT, Y. MUSANTE, A. HARRER, "Failed Annular UO2 Fuel in PWR Conditions: The EDITH 03 Experiment", *Proc. of the 1997 International Topical Meeting on Light Water Reactor Fuel Performance*, Portland, Oregon, United States, March, 2-6, 1997, ANS, La Grange Park, Ill., USA (1997) 188.

**[4]** D. PARRAT, A. HARRER, "Failed high burn-up MOX fuel performance: The EDITHMOX 02 analytical irradiation", *Proc. of the 2000 International Topical Meeting on Light Water Reactor Fuel Performance*, Park City, Utah, United States, April, 17-21, 2000, ANS, La Grange Park, Ill., USA (2000).

**[5]** P. BOURNAY "Management of Failed Fuel during Operation - French Policy and Experience", *Proc. of the 1994 International Topical Meeting on Light Water Reactor Fuel Performance*, West Palm Beach, Florida, United States, April, 17-21, 1994, ANS, La Grange Park, Ill., USA (1994) 477.

**[6]** C. LEUTHROT, A. BRISSAUD, JP MISSUD, "Relationships between the characteristics of cladding defects and the activity of the primary coolant circuit. An aid for the management of leaking fuel assemblies in PWR", *Proc. of the 1991 International Topical Meeting on Light Water Reactor Fuel Performance,* Avignon, FRANCE, April, 21-24, 1991, ANS-ENS, SFEN (1991) 324.

**[7]** D. BEUNECHE, M. BORDY, P. BOURNAY, J. PELLETIER, D. PARRAT, R. WARLOP, "Overview of fuel sipping in French Power Plants", *Proc. of the 1988 International Topical Meeting on Light Water Reactor Fuel Performance,* Williamsburg, Virginia, United States, April, 17-20, 1988, ANS, La Grange Park, Ill., USA (1988) 304.

**[8]** D. PARRAT, R. WARLOP, F. MONTAGNON, "Permanent measurement of the primary coolant activity with the PIGAL experimental facility", *Proc. of the IAEA TCM on Post-Irradiation Examination Techniques for Water Reactor Fuel*, Workington, Cumbria, United Kingdom, September, 11-14, 1990, IAEA, Vienna, IWGFPT-37 (1991) 158.

**[9]** C. LEUTHROT, J.B. GENIN, P. RIDOUX, A. HARRER, "SADDAM, an on line computer code to assess in operation defective fuel characteristics and primary circuit contamination", *Proc. of the 1997 International Topical Meeting on Light Water Reactor Fuel Performance*, Portland, Oregon, United States, March, 2-6, 1997, ANS, La Grange Park, Ill., USA (1997) 365.

**[10]** J.B. GENIN, C. LEUTHROT, D. PARRAT, P. RIDOUX, A. HARRER, "DIADEME, a computer code to assess in operation defective fuel characteristics and primary circuit contamination", *Third International Seminar on WWER Reactor Fuel Performance, Modelling and Experimental Support*, IAEA, Pamporovo, Bulgaria, 1999, BAS-INRNE (2000) 73.

**[11]** P.BESLU, C.LEUTHROT, G.FREJAVILLE, "PROFIP code: A model to evaluate the release of fission products from a defective fuel in PWR", *Proc. of the IAEA meeting on the behavior of defective Zirconium alloys clad ceramic fuel in water coolant reactors* - Chalk River, CANADA, September, 17-21, 1979, IAEA, Vienna IWGFPT-6 (1980) 23.

**[12]** D. PARRAT, C. LEUTHROT, A. HARRER, D. DANGOULÊME, "Behaviour of a Defective MOX Fuel Rod in a PWR", *Proc. of the IAEA TCM on Recycling of Plutonium and Uranium in Water Reactor Fuel*, Newby Bridge, Windermere, United Kingdom, July, 3-7, 1995 - IAEA-TECDOC-941, Vienna (1997) 319.

**[13]** C. LEUTHROT, P. BESLU, “Distribution of actinides and solid fission products inside PWR primary circuits”, *Water chemistry for nuclear reactor systems, BNES*, London, 1986.

**[14]** C. LEUTHROT, K. CHEVALIER, P. RIDOUX, J.P. GHYSELS, “French codes for assessment of difficult to measure radionuclides in low level solid wastes in contaminated reactors materials”, *Int. Conference on Waste management*, Tucson, United States, March, 2-6, 1997.

# DISADVANTAGES OF MEANS AND METHODS OF FUEL FAILURE DETECTION

O.O. DEPENCHUK
Zaporizhzhe NPP,
Energodar, Ukraine

**Abstract**

The paper presents a view of a reactor operator on fuel failure detection techniques used presently at WWER reactors. Approaches on reduction of fuel failure rate are addressed to the fuel supplier and to the reactor operator. Close co-operation of fuel supplier and reactor operator is of special importance, especially in case of the use of modernized fuel or mixed cores.

## 1. FUEL FAILURE DETECTION

At present there are some deficiencies in the methods of fuel failure detection. The guideline on fuel failure detection provides for fuel rejection in accordance with the measured activity of such radioactive nuclides as I-131, Cs-134, and Cs-137. They are measured in samples of water taken from a circuit of a stand for failed fuel detection. Experience shows that fuel assemblies with visually marked defects (through holes in the fuel claddings) may be permitted for use in the course of reactor core operation. This might be done based on the results of water sample's analysis of specific activity of radioactive nuclides I-131, Cs-134, Cs-137 in accordance with the existing methodology.

In the presence of fuel failures classified as «direct contact» between fuel and coolant the activity of radioactive nuclide I-131 does not reach the rejection criterion.

The water samples taken from fuel cladding leak tightness monitoring stand contain Ba-140, Nb-95, Ru-103, Xe-131, Ce-141, Ce-144 and fuel fission products [1,2]. Example of activity monitoring of these radionuclides in the primary coolant in case of the core without fuel rod failure of «direct contact» type and in case of a such failure in a core are given in Figs 1 and 2. There is a need to determine fuel defectiveness degree based on the activity of these radioactive nuclides or provide alternative methods of fuel failure detection for the design.

The method of detection of the fuel element failures classified as «direct contact» between fuel and coolant has not been determined for the in-cask method. It is a problem for the VVER fuel operator. To improve the situation, R&D works are carried out jointly with Russian specialists. This issue is very urgent for Ukraine because of the facts given below.

1. The fuel assemblies with fuel failures, classified as "direct contact", contaminate the devices of cladding leak tightness monitoring with high-activity fission products. Due to this the need to implement continuous rinsing and decontamination arises, and for this period the operations on fuel cladding leak tightness monitoring shall be stopped. This might lead to delays and time period extension for power unit maintenance. An example of fuel failure detection of fuel assembly with visually marked defect (for comparison probe was taken from cask without fuel assembly, see the last line) is given in Table 1.

**Table 1. Fuel failure detection results .**

| | FISSION PRODUCTS ACTIVITY, KU/KG | | | | | | | | | | | | | | |
|---|---|---|---|---|---|---|---|---|---|---|---|---|---|---|---|
| | $I^{131}$ | $Cs^{134}$ | $Cs^{137}$ | | $Ce^{141}$ | $Ba^{140}$ | $Ru^{103}$ | $Xe^{133}$ | $Mn^{54}$ | $Nb^{95}$ | $Zr^{95}$ | $Co^{58}$ | $Co^{60}$ | $Fe^{59}$ | $Cr^{51}$ |
| | Fuel assembe with visually marked defect | | | | | | | | | | | | | | |
| FFD-1 The water sample №1 | 7.5E-6 | 6.8E-7 | 6.6E-7 | 1.03 | 3.1E-8 | - | 4.5E-8 | 2.8E-6 | 3.4E-8 | 9.3E-8 | 9.4E-8 | 7.2E-8 | 3.0E-8 | 1.3E-8 | 4.9E-7 |
| FFD-1 The water sample №2 | 7.2E-6 | 6.7E-7 | 6.5E-7 | 1.03 | 3.5E-8 | 1.0E-7 | 5.7E-8 | 2.8E-6 | 3.0E-8 | 8.4E-8 | 7.2E-8 | 6.1E-8 | 2.8E-8 | - | 3.9E-7 |
| FFD-2 The water sample № 1 | 9.4E-6 | 1.5E-6 | 1.3E-6 | 1.19 | 2.6E-8 | - | - | 2.7E-6 | 1.6E-8 | 5.6E-8 | - | 5.0E-8 | 2.4E-8 | - | 2.2E-7 |
| FFD-2 The water sample № 2 After filtering | 8.9E-6 | 1.5E-6 | 1.2E-6 | 1.25 | 2.4E-8 | - | - | 2.4E-6 | 1.7E-8 | 5.7E-8 | 9.8E-8 | 4.2E-8 | 2.6E-8 | - | - |
| FFD-2 The water sample № 1 After filtering | 9.1E-6 | 1.5E-6 | 1.2E-6 | 1.25 | 1.5E-8 | - | 2.8E-8 | 1.5E-6 | 1.5E-8 | 4.1E-8 | - | 2.2E-8 | 2.5E-8 | - | - |
| The water sample in-cask with out FA | 1.1E-6 | 7.6E-8 | 6.2E-8 | | 1.5E-8 | - | - | 8.6E-8 | 9.8E-8 | 3.9E-8 | 2.8E-8 | 2.2E-7 | 6.9E-8 | 3.7E-8 | 2.3E-6 |

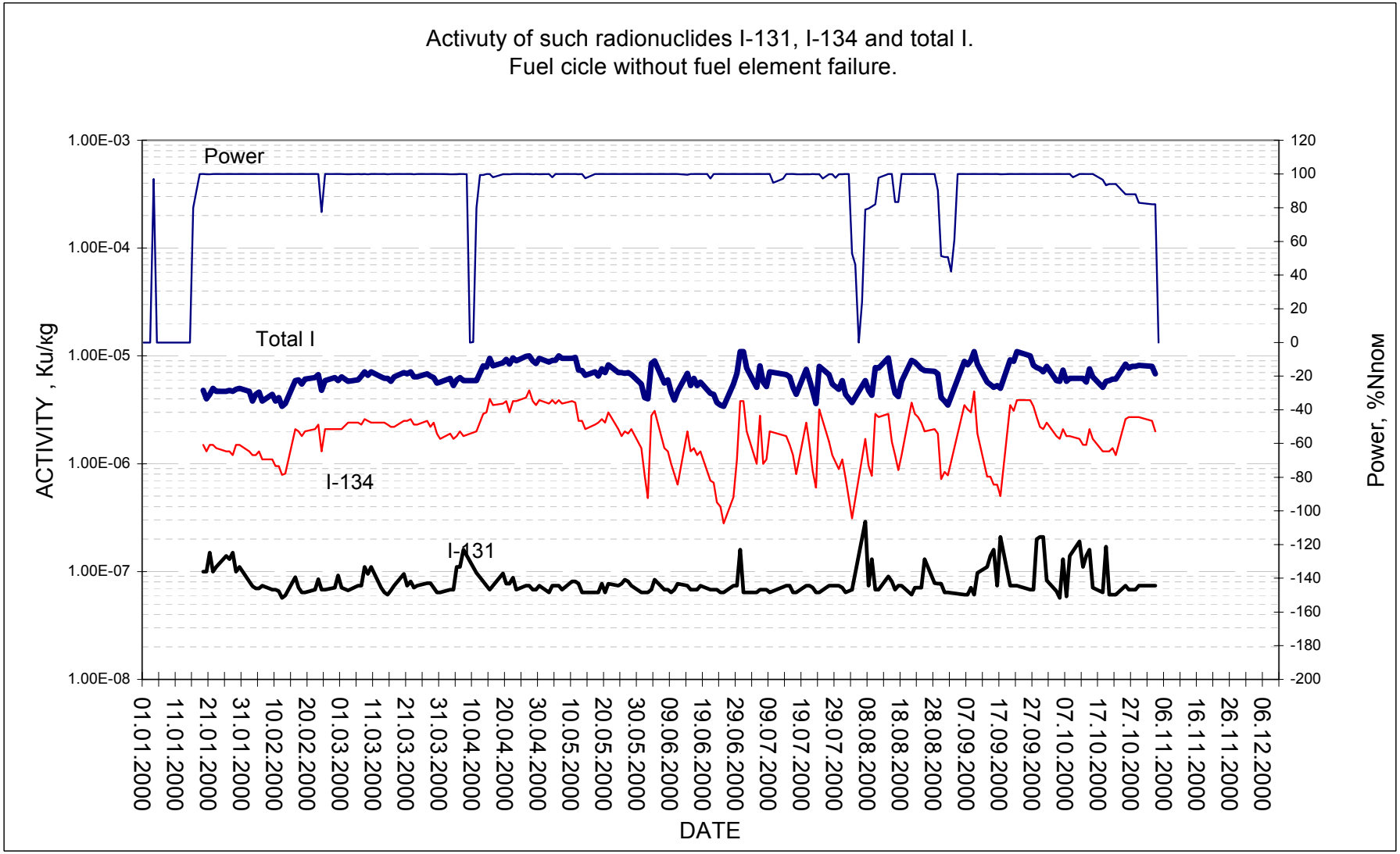


*FIG. 1. Coolant activity (I-131, I-134 and total I) in 2000 with no fuel element failure.*

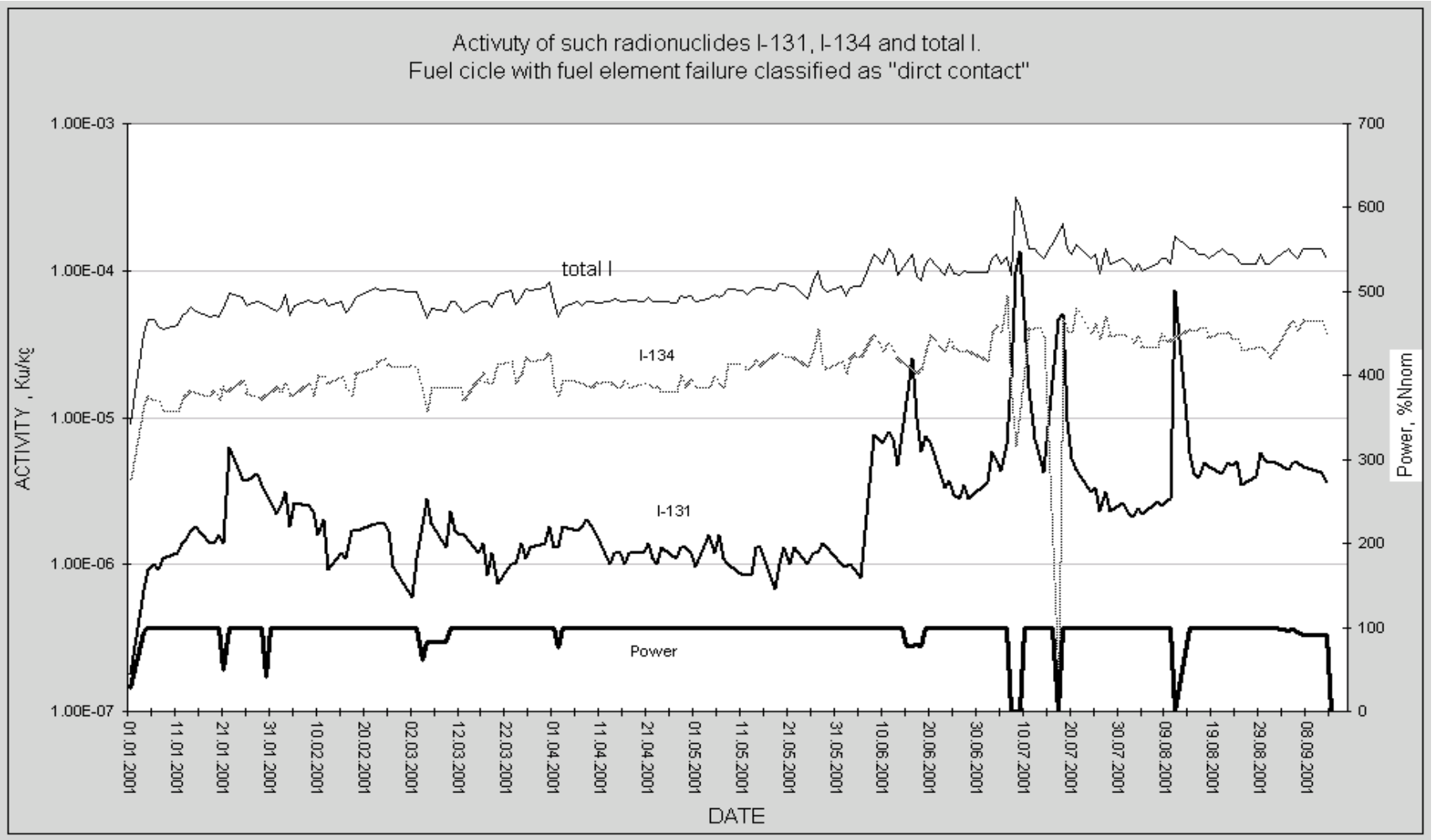


*FIG. 2. Coolant activity (I-131, I-134 and total I) in 2001 with failed fuel rod classified as "direct contact".*

2. Lack of the method of detection of the fuel element failures, classified as «direct contact», results in decreasing the Radiation Safety level, i.e. to the not necessary conservatism. If such a failure is not detected, this can lead to the loading of faulty fuel into reactor core for further operation. If an assembly is assigned to be unloaded for storage and failure is not detected due to method lack, such an assembly can be transported for storage to Russia. This action is considered to be a violation of the valid Norms and Standards on Nuclear and Radiation Safety.

If such failures are not detected, the radiation defense in-depth decreases. In fact, the loading into reactor core for further operation of an assembly with direct contact between fuel and coolant can lead to the weakness of the 1st and 2nd barriers on the way of active material release to environment. Radiation burden for maintenance staff increases.

The development of a method of cladding leak tightness monitoring can be a way out of the existing situation. The mentioned method can serve for unique detection of fuel failures classified as "direct contact", by activity of Ba-140, Nb-95, Ru-103, Xe-131, Ce-141, Ce-144 or availability of fuel composition in samples.

## 2. REDUCTION OF FUEL FAILURE RATE

The means dependent on designer and manufacturer include:

1. Improving the quality of fuel manufacture.
2. Implementing modernization and upgrading of fuel assembly design.

The means dependent on operation include:

3. Selecting fuel loading pattern with more uniform power distribution.
4. Developing and implementing new algorithms of reactor operation.
5. Maintaining fuel operation in the designed conditions.

Let's make an overview of the mentioned means.

1. Improving the quality of fuel manufacture.

### 2.1. Improving the quality of fuel manufacture

Maintaining fuel quality at the designed level is a part of the manufacturer's responsibilities. Improving the quality of manufacturing can be reached as a result of:

- Manufacturer Quality Assurance Audits held at a regular basis.
- Availability of several fuel suppliers or fuel manufacturers. A competition in fuel market and a possibility to select a supplier lead the manufacturers to the need to improve quality of goods supplied

### 2.2. Implementing modernization and upgrading of fuel assembly design

It should be noted that any modernization is to be implemented slowly and consistently in order to avoid mass fuel failures and, respectively, great economic losses in a case of any design deficiencies or errors.

In the world of commercial nuclear power engineering there are many known cases when, due to the fuel assembly design deficiencies, the fuel suppliers as well as operating organizations suffered economic losses. Nuclear power engineering has also suffered similar problems.

In my opinion, some design features of existing fuel assemblies may cause fuel failures.

In addition, it is necessary to consider an additional modernization for reactor design systems in a number of cases when upgraded fuel is to be put into operation. For example, in-core monitoring system is required for putting the control rods with different height absorbent characteristics into operation. In some cases the modernization of reactor refueling system and others can be needed.

Putting upgraded fuel into operation always requires implementation of a great scope of justifications, calculations for fuel behavior in the modes with normal operation violation and design basis accidents. Regulatory coordination of permissions for the implementation of such upgrades, state expertise of the validating documents also takes much time.

### 2.3. Selecting fuel loading pattern with more uniform power distribution

Power distribution uniformity of fuel loading affects the fuel operability and number of fuel failures. Fuel failures also make their impact on the possibility of uniform loading selection. Both aspects are interrelated.

In this connection it is worthwhile to note that upgraded fuel proposed by Joint-Stock Enterprise “TVEL” is provided with a more extensive set of fuel assembly initial enrichment. This can certainly lead to further reduction in fuel failure number.

An extensive set of fuel assembly initial enrichment is to facilitate selecting an equal replacement for the failed fuel assemblies in accordance with multiplying characteristics and consequently select a more uniform fuel loading.

### 2.4. Developing and implementing new algorithms of reactor operation

Considerable attention in Russian Federation is also being focused on developing and implementing new algorithms of reactor operation. The nuclear power plants in Ukraine are interested in these activities.

Upgrading algorithms of the control for height power distribution in the conditions of xenon accumulation allows avoiding core height power distribution that reduces the number of fuel loading cycles.

### 2.5. Maintaining fuel operation in the designed conditions

The Nuclear Safety Departments have been established at the nuclear power plants in Ukraine. One of the duties of mentioned departments is to develop NPP measures and technical documents in order to maintain fuel operation within the design limits and limits specified in the manufacturers’ technical documents. The NPP specialists are sufficiently skilled and experienced to prevent any possibility of fuel failure.

Considerable attention at NPPs focuses greatly on nuclear safety and the issues of preventing operational modes leading potentially to fuel failures.

The level of operation quality has not been changed essentially lately. Nevertheless, the failures classified by ZNPP specialists as “direct contact” between fuel and coolant and not observed before have occurred recently.

## 3. CONCLUSIONS

Investigation of fuel failures and determination of failure root causes are still very significant issues. In the course of fuel failure investigation the Ukrainian specialists faced the challenge of failure root cause determination, because the opinions of supplier and consumer are often different.

It should be also noted that the real cause of fuel failure might be not always determined, even after implementing full-scale post-irradiation examinations and fuel elements tests.

It is necessary to try classifying fuel failures, determining their characteristics and developing procedures and plans for cause determination. It will enable to regulate the relationship between suppliers, designers, manufacturers and users of nuclear fuel. The knowledge of fuel failure cause will allow minimizing the number of such failures by elaboration and implementation of the specific countermeasures.

In conclusion it is noteworthy to emphasize that:

- Development of new methods of leak tightness monitoring is required.
- Updating of the procedures on implementation of fuel design upgrade is required.

## REFERENCES

[1] Results of Cladding Leak Test Inspection, Reports of Zaporizhzhe NPP (1986-2002).
[2] Results of Visual Fuel Inspection, Reports of Zaporizhzhe NPP (2002).

# FUEL FAILURES AT PAKS NPP

A. KERKÁPOLY, N. VAJDA
Budapest University of Technology and Economics,
Institute of Nuclear Techniques,
Budapest, Hungary

A. CSORDÁS, Z. HÓZER
KFKI Atomic Energy Research Institute,
Budapest, Hungary

T. PINTÉR
NPP Paks.
Paks, Hungary

**Abstract**

The increase of the activities of fission and transmutation products in the primary coolant of the nuclear power plant indicates the presence of fuel rod failures. Methods were developed and improved for the identification and characterisation of the fuel failures in the four reactors of NPP Paks. The examinations of the primary water were carried out during normal and transient operation conditions. The activities of the iodine ($^{131}$I, $^{133}$I, $^{134}$I) and caesium isotopes ($^{134}$Cs, $^{137}$Cs) were experimentally determined in the primary coolant. The number and types (macro and micro) of failed fuel elements were estimated based on the measured activities of iodine isotopes during normal operation conditions. The surface uranium contamination of the core was determined from the concentration of short-lived $^{134}$I isotope. To model the behaviour of $^{131}$I during transient operation conditions spiking calculations were carried out. The spiking model was originally developed by EPRI and later applied for CANDU reactors and in the present examination it was adopted for WWER-440 reactors. With the determination of the ratio of the caesium and transuranium isotope activities, the burnup of the defected fuel was estimated. For failed fuels with macro leaks fuel fragments can be released into the coolant. In order to identify macro failures, individual particles (fuel fragments) of the primary coolant were filtered and examined by different microanalytical methods. The fuel particles were studied by autoradiography, alpha spectrometry and scanning electron microscopy. With the characterisation of individual hot particles originated from the primary water it becomes possible to examine several faulty fuel rods simultaneously. The above-mentioned techniques were applied to characterise fuel performances at all four reactors of Paks NPP. A statistical evaluation of failure rates of the fuel rods of NPP Paks is given.

## 1. INTRODUCTION

The increase of the activity of fission and transmutation products in the primary coolant of the nuclear power plant is connected to fuel rod failures. Evaluation of fuel performances is possible by on-line and off-line examination methods. Leaking into the primary coolant was examined by on-line methods during normal and transient operation conditions and the fuel particles released into the primary water were studied by off-line examination methods. To describe the leaking process during normal operation conditions a new model was developed, validated and compared with the concentration data of iodine isotopes determined experimentally. With these examinations the state of the nuclear fuel elements was estimated more exactly.

To describe the leaking process during the transient conditions an iodine spiking model was developed, which was suitable to estimate or predict the maximum activity of $^{131}I$ in the primary circuit using data measured under stable operation conditions.

The identification and analysis of individual fuel particles released into the primary water make possible to examine several faulty fuel elements simultaneously in the reactor.
New methods were applied and developed to characterise the distribution, morphology and isotope composition of the hot particles of the primary coolant.

## 2. ESTIMATION OF FUEL PERFORMANCE BY MEASURING ACTIVITY CONCENTRATION DATA

The determination of the number of failed fuel elements and the type of failures was based on the measurement of activity concentration of $^{131}I$, $^{133}I$ and $^{134}I$ during normal operation conditions. The type of failures, the number of the defected fuels and the surface uranium contamination were determined by means of a criterion coefficient and standard leak data. Failure sizes were estimated by calculating the amount of the fuel released into the primary water. The activity ratio of $^{137}Cs/^{134}Cs$ and transuranium isotopes measured during transient operation conditions were used to calculate the burnup of the defected fuel element.

## 3. THE IODINE SPIKING MODEL

The presence of defected fuel elements leads to the increase of the activity of iodine isotopes in the coolant during reactor shutdowns and power transients in comparison with the normal operation conditions. The iodine spiking model was originally developed by EPRI and later applied for CANDU reactors. The method was adopted for WWER-440 reactors using measured activity data of Paks NPP. This method can be used for the evaluation of the iodine isotopes as well as the noble gases (xenon and krypton isotopes).

The developed method consists of two main steps, of the steady state calculation and of the transient state calculation.

1. Steady state calculation: Using the release-to-birth ratio R/B of at least three iodine isotopes, the parameters of diffusion equation and the number of leaking fuel elements are determined during normal operation conditions. Simplex optimum calculation method is used for the numerical fitting of the parameters.
2. Transient calculation: The iodine spiking history is calculated considering the effects of power change ratio, increase rate of boric acid concentration and pressure decrease rate. Different coefficients are determined for each contributing effect and the correction takes into account the activity level before the transient.

### 3.1. Steady state model

The first step of the calculation is used for the determination of release-to-birth ratio R/B for unit volume of the primary water on the basis of activity measurements:

$$\left(\frac{R}{B}\right)_{measured} = \left(\frac{\lambda+\beta}{\lambda}\right)\frac{C_m V_L}{FY}\exp(\lambda T_r) \qquad (1)$$

R – release rate (atom/s)
B=FY – birth rate (atom/s)
F – fission rate (fission/s)
Y – fission yield of the given isotope (atom/fission)
$\lambda$ - decay constant, (1/s)
$\beta$ - purification rate constant (1/s)
$V_L$ –volume of the primary circuit (l)
$T_r$ – transport time between the core and the place of sampling (s)
$C_m$ - activity concentration of the given isotope at the time of sampling (Bq/l)

The number of fissions is calculated considering the amount of $^{235}U$ and $^{239}Pu$ in the fuel. According to plant specific ORIGEN calculations, the average amount of $^{235}U$ varies between 21.5-14 g/kg, while the amount of $^{239}Pu$ between 3.5-5.5 g/kg for an equilibrium core and during a 300-day cycle.

The second basic equation of the model determines the R/B ratio supposing that the primary water activity has two sources: releases from the leaking fuel element and from the tramp Uranium.

$$\frac{R}{B} = \left(\frac{\varepsilon}{\varepsilon + \lambda}\right)\frac{A}{\sqrt{\lambda}}H + c$$

with $A = 3x\sqrt{D}$, (2)

$\varepsilon$ - escape rate from the fuel-to-cladding gap, (1/s)
$D$ – diffusion coefficient inside the fuel pellet,
$x$ – number of leaking fuel elements,
$H$ – precursive diffusion factor.
and $c = F_t/2F$
$F_t$ number of fissions in the tramp uranium
$F$ number of fisisons in the leaking fuel rod

Equation (2) contains three unknown variables:$\varepsilon$ ,$A$ and $c$. Knowing the R/B data from equation (1) the unknown variables can be determined if the data of at least three isotopes of the same element are available. It can be supposed that release of different isotopes of the same element is governed by the same mechanism and is characterized by common parameters. In order to determine the three unknown variables a three-dimensional simplex optimum calculation was applied. The number of failed fuel rods can be estimated according to the following expression: $x = \frac{A}{3\sqrt{D}}$. The diffusion coefficient D is applied for nominal power conditions and its value of iodine and noble gases was determined on the basis of experimental data. The failure size is estimated using $\varepsilon$ escape rate constant. The amount of tramp uranium is calculated if the constant $c$ is known from equation (2).

An example of calculated results is presented in Table 1 and Figs 1 and 2. The measurements were taken from unit 3 of the Paks NPP in July 2000. The activity data indicated the presence of leaking fuel rod(s). The measured data were transformed into R/B values and the optimum calculation fitted the equation (2) type curves on the data. The determined parameters made possible the evaluation of the number of leaking fuel rods, the amount of tramp uranium and

the failure size. The calculations were carried out for both iodine and noble gas data sets and the results showed good agreement between the two calculated cases.

Table 1. Calculated results using NPP measurement data of Unit 3, 2000.07.28

| Number of leaking fuel rods | | Amount of tramp Uranium, kg | | Failure size, $mm^2$ |
|---|---|---|---|---|
| Iodine calculation | Noble gas calculation | Iodine calculation | Noble gas calculation | |
| 1,4 | 1,0 | $2,4\ 10^{-5}$ | $1,5\ 10^{-5}$ | $2,4\ 10^{-1}$ |

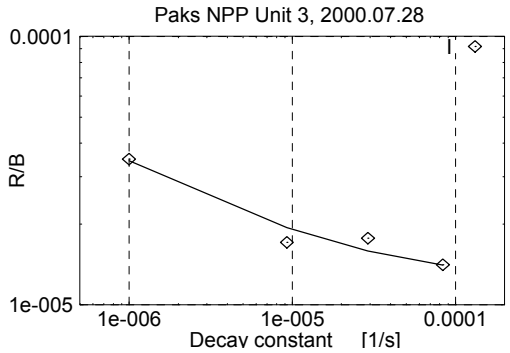


*FIG. 1.*
*Measured (points) and fitted (lines) R/B ratio for iodine isotopes*

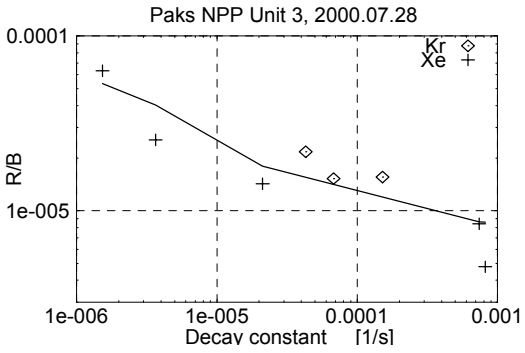


*FIG. 2.*
*Measured (points) and fitted (lines) R/B ratio for noble gas isotopes*

### 3.2. Spiking model

The activity concentration of the $^{131}I$ isotope is calculated according to (3), which was received from equations (1) and (2). Similar approach was used by EPRI.

$$C_m^{calculated} = \frac{FY}{V_L(\lambda+\beta)\exp(\lambda T_r)}\left(\frac{3S\varepsilon x\sqrt{SD}H\sqrt{\lambda}}{\lambda+S\varepsilon}+c\lambda\right) \tag{3}$$

It is supposed that the escape of the fission products from the fuel and their diffusion in the pellet is accelerated during the spiking phenomena due to the change of operating conditions. The effect of power ($Q$), pressure ($P$) and boric acid ($c_{bor}$) concentrations were taken into account in the following expression for $S_s$ spiking factor:

$$S_s = \left(1 + a_1\frac{\Delta Q}{Q^{\max}} + a_2\left(\frac{\Delta P}{P^{\max}}\right)^n + a_3\frac{\Delta c_{bor}}{c_{bor}^{\max}}\right)e^{-T/a_4} \tag{4}$$

The coefficients $a_1$, $a_2$, $a_3$, $a_4$ and exponent $n$ were determined according to four datasets, which were recorded during the shutdown of reactors with leaking fuel elements.

The spiking model uses the variables, $x$ and $c$, which must be determined for steady conditions before the spiking event.

### 3.3. Power plant spiking calculations

For the development and validation of the spiking model the measurements provided by the Paks NPP were used. The data collection covered the first days of the refueling period after reactor shutdown. Activity measurements were taken with high frequency in order to have sufficient number of experimental points for the modeling. The following data were collected and analyzed:

- primary circuit pressure,
- boric acid concentration,
- core power,
- core inlet temperatures,
- activity concentrations.

As an example, measured and calculated data of $^{131}$I concentration during refueling shutdown of reactor#3 at NPP Paks (2001) are shown in the following table.

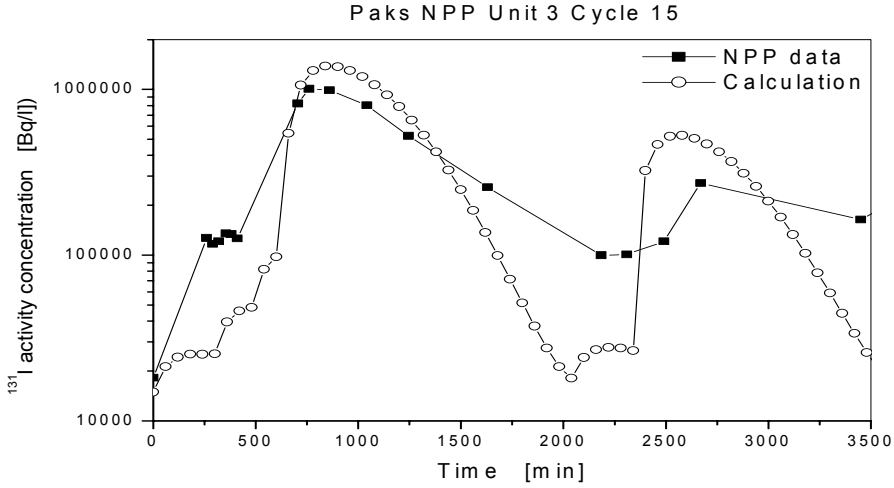


*FIG.3. Measured and calculated data of $^{131}$I concentration during refueling shutdown of reactor#3 at NPP Paks (2001).*

## 4. EXAMINATION OF INDIVIDUAL FUEL PARTICLES

By the identification and analysis of the individual fuel particles from the coolant, the simultaneous examination of several faulty fuel elements becomes possible . The particles, which were released from the leaking fuels into the primary water, were filtered and examined by autoradiography, microanalytical and radioanalytical techniques. The autoradiography was used to identify hot particles, and using microanalytical and radioanalytical methods information were obtained about the morphology, chemical and radiochemical composition of the particles. The determination of the activities of the long-lived and non-volatile transuranium isotopes in the fragments plays important role in the estimation of the burnup of the faulty fuel elements.

### 4.1. Autoradiography examination

The autoradiographic examination of the filters with the fragments of the primary water was carried out using Fortepan 100 black-white film. However, the film was sensitive to alpha, beta and gamma radiation, the method was applicable to the identification of active (hot) particles on the filter. By means of autoradiography, the distribution of the particles was studied, and after identification of the individual particles radiochemical analysis of individual fragments was carried out (see Fig.4 as an example).

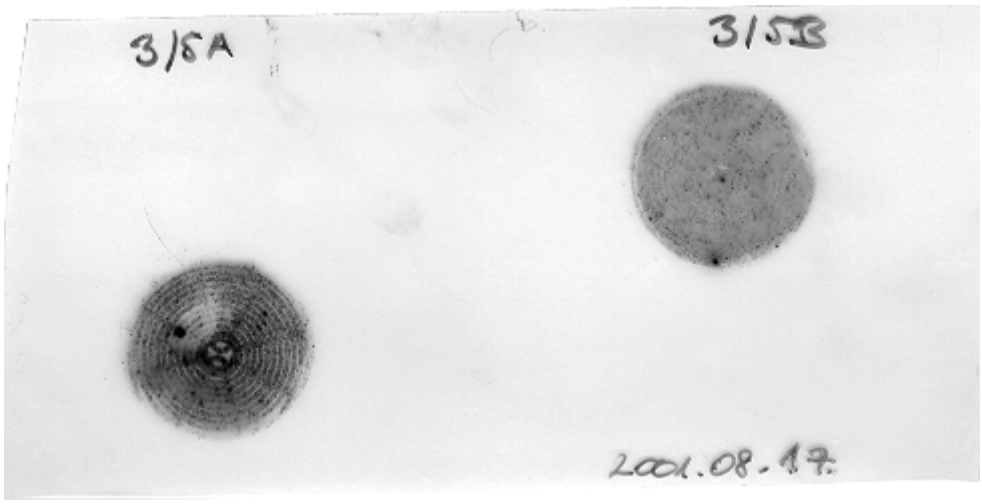


*FIG.4. Autoradiogram of filters by Fortepan film (1 liter primary water of the Unit 3 of NPP Paks was filtered trough the filters, the water was collected in 2001.07. during reactor shutdown).*

### 4.2. Examinations by electron microscopy

The filters were examined by scanning electron microscopy to determine the size, the shape, the structure and the composition of the particles.

The secondary electron image gives a map of the particles. The samples are illuminated with electrons and the sample-emitted secondary electrons are detected. Because these electrons originate from the near-surface layers of the sample, the distribution of the secondary electrons gives a map of the sample surface. The backscattered electron image is in connection with the average atomic number of the sample. By this method the amounts of the elements of high atomic numbers can be determined. The technique is applicable for the semi-quantitative analysis of these elements by using an energy dispersive detector.

After the autoradiographic examinations, individual particles were isolated from the filters. The parts of the filters, which contained particles according to the autoradiographs, were cut out and examined by the electron microscopy. The BEI method has about 0.1m% detection level for an element in a particle of 1micrometer diameter. By means of SEM the quantities of various corrosion products were determined, the amount of uranium and transuranium elements did not reach the detection threshold.

Individual particles in the coolant of reactor unit 3 were examined in 2001.during reactor shutdown. A great variety of particles were distinguished according to SEM examinations, a

lot of particles contained corrosion products, but did not containe uranium or other elements originating from fuels. The mass of uranium in the particles was maximum sometimes 0.1m% in same cases and these particles usually contained zirconium, too. The majority of the particles were rich in Fe-Ni-Cr or in Fe-Ni-Cr-Si-(Mn-Mo). Some exotic particles of fuel origin were also identified which were rich in La-Ce-Nd or Ba-Ce .

### 4.3. Radioanalytical examinations

The individual particles identified by autoradiography were analyzed by alpha spectrometry to determine the activity of actinides and to estimate the burnup of the faulty fuel element with the help of the measured alpha activity of the transuranium isotopes. In same cases not only the particles were examined by alpha spectrometry, but the primary water, too.

The activity concentrations of the Pu and in some cases U isotopes were determined after the radioanalytical separation procedure. Usually these isotopes were separated with extraction using chromatography. The sources for the alpha spectrometry were made by micro-coprecipitation. The spectra were recorded with a multichannel analyzer using semiconductor detector.

From the experimentally determined alpha activity ratio of $^{238}Pu/^{239.240}Pu$ the burnup of the defected fuels was estimated. From the measured mass of Pu the mass of uranium and the maximum size of the released fuel fragments was estimated. The measured activities of the particles were correlated to the measured whole alpha activities of the whole filters.

For example, particles collected during shutdown of the reactor Unit#3 in July 2001 were analysed, the estimated diameter of the uranium particles - according to the measured $^{239.240}Pu$ activity of the particles – was sometimes 1 micrometer. It is likely, that the uranium containing particles can be found in the primary water attached to other particles. The calculated diameters of the above mentioned particles are shown in Table 2.

Table 2. The calculated diameter of the fuel particles

| Code of the sample (of the individual particle) | $^{239,240}Pu$ | U | U | max. | $^{238}Pu/^{239,240}Pu$ |
|---|---|---|---|---|---|
| | Measured activity Bq | Measured mass g | Calculated volume $\mu m^3$ | Calculated diameter μm | Measured activity ratio |
| 3/5A | 0,0075 | 2,62E-10 | 2,62E+01 | 3,7 | 7,96E-01 |
| 3/5B | 0,0138 | 4,85E-10 | 4,85E+01 | 4,5 | 7,12E-01 |
| 3/6B | 0,0020 | 7,06E-11 | 7,06E+00 | 2,4 | 9,90E-01 |
| 3/9A | 0,0194 | 6,81E-10 | 6,81E+01 | 5,1 | 0,46 |
| 3/12A | 0,0185 | 6,50E-10 | 6,50E+01 | 5,0 | 5,7E-01 |
| 3/14A | 0,0018 | 6,32E-11 | 6,32E+00 | 2,3 | 8,9E-01 |
| 3/15A1 | 0,0008 | 2,77E-11 | 2,77E+00 | 1,7 | 6,8E-01 |
| 3/15A2 | 0,0013 | 4,42E-11 | 4,42E+00 | 2,0 | 1,1E+00 |
| 3/15AF | 0,0234 | 8,22E-10 | 8,22E+01 | 5,4 | 8,7E-01 |
| 3/17A | 0,0115 | 4,04E-10 | 4,04E+01 | 4,3 | 1,4E+00 |

The particle-sizes were calculated using the Pu activity for 30GWd/tU burnup. It was supposed, that the whole alpha activity belonged to a single particle. The majority of the measured $^{238}Pu/^{239.240}Pu$ activity ratios varied between 0.6-1.2 referring to burnup values originating from about 2 year-old defected fuel. It is not excluded that particles have been released from surface contamination.

## 5. EVALUATION OF FUEL PERFORMANCES AT PAKS NPP

The determination of the number of the defected fuel elements and of the type of the failures is based on an expert system or on the steady state model. The experimental determination of the fuel performances was carried out using the measured activity concentration ratio of $^{131}I/^{134}I$ and the surface uranium contamination. The estimation with the steady state model based on the measured data all iodine nuclides.

An example, an conservative estimation for the Unit 3 of the NPP Paks by the expert system and the steady state model, is shown in Table 4. The calculations by the expert system and the steady state model were in good agreement.

Table 3. Evaluation of fuel performances at the Unit 3

| Cycle | The type of the failure according to the expert system | The number of the failed fuel elements according to Expert system | The number of the failed fuel elements according to the steady state model |
|---|---|---|---|
| 1. cycle | - | 0 | 0 |
| 2. cycle | - | 0 | 0 |
| 3. cycle | - | 0 | 0 |
| 4. cycle | Macro | 3-4 | 5 |
| 5.cycle | Macro | 4 | 6 |
| 6. cycle | Macro | 2 | 3 |
| 7.cycle | - | 0 | 1 |
| 8. cycle | - | 0 | 0 |
| 9.cycle | - | 0 | 0 |
| 10.cycle | Micro | 1 | 0 |
| 11.cycle | Micro | 1-2 | 1-2 |
| 12. cycle | Micro | 1 | 1 |
| 13. cycle | Micro | 1 | 1 |
| 14. cycle | Macro | 1 | 1 |
| 15. cycle | Macro | 1 | 1 |
| 16.cycle | Macro | 1 | 1 |

The evaluation of the fuel performances by the expert system was carried out for the four units of the NPP Paks. The number of the failures, the type of the failures and the fuel failure rates for the four reactors are summarised in Table 4.

The fuel failure rate for the four reactors together is 0.004% according to a conservative estimation. The average fuel failure rate for the WWER reactors is 0.007%, while this data for other PWR reactors is 0.002%.

Table 4. The evaluation of the fuel performances at the four reactors of the NPP Paks

| | The number of the macro failures (conservative estimation) | The number of the micro failures (conservative estimation) | Fuel failure rate (conservative estimation) |
|---|---|---|---|
| 1#reactor (18cycles) | 1 | 5 | 0.002% |
| 2#reactor (18cycles) | - | 10 | 0.004% |
| 3#reactor (16cycles) | 13 | 5 | 0.008% |
| 4#reactor (14cycles) | 9 | - | 0.005% |

## 6. CONCLUSIONS

The increase of the activities of fission and transmutation products in the primary coolant of the nuclear power plant indicates the presence of fuel rod failures. Methods were developed and improved for the identification and characterisation of the fuel failures in the four reactors of NPP Paks. The examinations of the primary water were carried out during normal and transient operation conditions. To model the behaviour of $^{131}I$ during transient operation conditions a iodine spiking model was adopted for the WWER-440 reactors using measured activity data of Paks NPP. The evaluation of the fuel performances of NPP Paks was carried out by an expert system and by a steady state model. By the microanalitycal and radioanalytical examinations of the fuel particles originated from the primary coolant it can be possible to examine several faulty fuel rods simultaneously.

# DEFECTED FUEL MONITORING AT CERNAVODA NUCLEAR POWER PLANT

E. GHEORGHIU, C. GHEORGHIU
Institute for Nuclear Research,
Pitesti, Romania

**Abstract**

Although the fuel performance at Cernavoda nuclear power plant has been very good, the overall defect rate since 1997 until present being below 0.1%, the management of defected fuel appearing in the core is an important problem with directly implication in the power plant safety. This paper summarizes the defect investigation at unit one of Cernavoda nuclear power plant by the interpretation of signal trends generated by the two independent on – line failed fuel detection and location systems: the Gaseous Fission Product (GFP) Monitoring System and the Delayed Neutron (DN) System. The GFP system monitors four selected isotopes ( Xe – 133, Xe – 135, Kr –88, I – 131 ) continuously and produce signals that form the basis for early warning of a fuel failure. The DN system scans the delayed neutrons emitted by I – 137 and Br – 87 in coolant lines connected to each of the outlet feeders of all fuel channels; the defective bundle is usually found by identifying the fuel channel having the high delayed neutron signal above that of the normal background. The paper will present the coolant gamma activity evolution, the analysis and interpretation of activity data in correlation with DN information and discharge of the defected fuel from the core. During the first 4 years of commercial operation at Cernavoda there have been recorded 13 defects ( 8 in 1997, 4 in 1998, 1 in 1999 and 0 in 2000 ). This gives an overall rate of fuel defects of 0.076% for this period. We appreciated that the main cause of the defects was fretting by debris.

## 1. INTRODUCTION

Fuel performance at Cernavoda nuclear power plant has been very good, the overall defect rate for 1997 - 2000 period being below 0.1%. The on-power refueling capability allows defective fuel to be removed without operation restriction. However, premature refueling lead to an increase in fueling machine demand, loss in fuel burnup and perturbation in fuel management. So, it is an incentive to keep defective fuel in the reactor until reaching the design burnup. On the other hand, this may lead to loss of structural integrity of the defected fuel element or bundle with a possible jamming in the fuel channel, leading to forced reactor shutdown and expensive cleaning operations; it also determines $UO_2$ release from the defected fuel element, $UO_2$ that may deposit on the heat transport system components and increases occupational exposure at the station. For this reason, it is very important to find a compromise between discharging of the defected fuel sooner or later. This paper presents defected fuel monitoring at Cernavoda nuclear power plant during the period 1997-2000.

## 2. CERNAVODA NUCLEAR POWER PLANT PERFORMANCE

### 2.1. General aspects

Cernavoda nuclear power plant is a CANDU-type reactor having a nominal power of 700 MWe. The core contains 380 fuel channels, each channel having 12 fuel bundles [1]. A fuel bundle is 0.5 m long with 37 fuel elements, each element containing natural $UO_2$ pellets (or depleted $UO_2$ pellets) in a Zircaloy-4 sheath. A graphite layer, deposited on the inner surface of the clad, separates the sheath from the pellet to reduce the pellet - sheath interaction. End caps are resistance welded to the sheath extremities to seal the element. End plates are welded to the end caps to hold the elements in a bundle configuration.

Fuel dimensions and material properties have been selected to ensure the integrity of the fuel element and fuel bundle during normal operating conditions. Because the fuel is natural $UO_2$ and the bundles are inexpensive to manufacture, CANDU reactor operate on a once-through fuel cycle; for these reasons, reconstitution of bundles with defected elements is not necessary or practiced in CANDU power station.

## 2.2. Nuclear fuel performance

The first criticality at the Cernavoda Nuclear Power Plant (NPP) has been attained on April 16, 1996 and the commercial operation started in December 1996 [2].

The first fuel charge for Cernavoda NPP consisted of 4,560 bundles supplied by ZPI- Canada; a limited quantity (66 bundles) of domestic fuel, manufactured by the Nuclear Fuel Factory - Pitesti, Romania was included into the first charge for testing purposes.

Reactor refueling started after 100 FPD (Full Power Days), Cernavoda being the first CANDU type reactor having more than 100 days of continuous operation from the commercial start-up. For the refueling scheme, at the beginning, Swing 8 was used (2 bundles are reinserted in the channel for a second irradiation cycle) and then the Standard 8 bundles shift scheme was adopted. In very few cases the 4 bundles shift scheme was used, only in addition to one refueling with 8 bundles to unload the entire channel with supposedly defected fuel.

In 1997 a total of 4,764 fuel bundles have been discharged from the core at an average burnup of 143.8 MWh/kg U, in 1998, an amount of 5,056 fuel bundles were discharged from the core with an average burnup of 170.9 MWh/kg U [3], in 1999, 4,868 fuel bundles with an average burnup of 170.2 MWh/kg U were discharged and in 2000, 5,124 fuel bundles have been discharged from the core at an average burnup of 170.8 MWh/kg U. Thus, at the end of 2000, 19,812 fuel bundles were irradiated in the power plant.

## 2.3. Core monitoring for defected fuel detection and location

Cernavoda power plant has two important systems for failed fuel monitoring: GFP (Gaseous Fission Product) system [2,3,4] and another system to locate the defected fuel: DN (Delayed Neutron) [4,5]. In addition, to confirm or not the information form GFP or DN, it is used GS (Grab Sampling) System [2,3,4].

The Gaseous Fission Products monitor in the CANDU power reactor, computer – controlled, high – resolution gamma – ray spectrometer is shown in Fig. 1. It is designed to operate continuously, repeatedly measuring the gamma activity of the gaseous fission products, Xe-133, Kr-88 and Xe-135 and of I-131 in sample flows from each of the two heat transport system loops. Two sample lines, one from each loop, carry the coolant from the pump discharge to the sample holders. The sample transit time is about 15 minute, which ensures sufficient time to remove unwanted F-17 by radioactive decay. Either loop 1, loop 2 or both loops together can be monitored. This enables the operator to determine which loop contains a defected fuel bundle.

The three gaseous fission products and radioiodine monitored by the GFP system were chosen for the following reasons: Xe-133 is a long – lived fission product which has a high release rate from defected fuel; its concentration, when compared to that of the short – lived fission gas, Kr-88, provides information on the extent of sheath damage (deterioration) and the

buildup of tramp uranium in the core; Xe-135 provides data on iodine release rate when high purification flow to the ion exchange columns are removing the radioiodine from the coolant. I-131 is monitored because of its biological hazard. Since its concentration in the coolant is suppressed by the ion – exchange system, it is not a reliable indicator for assessing fuel damage. However, the "iodine spike" appearing on reactor shutdown, is an indicator of defected fuel presence in the core.

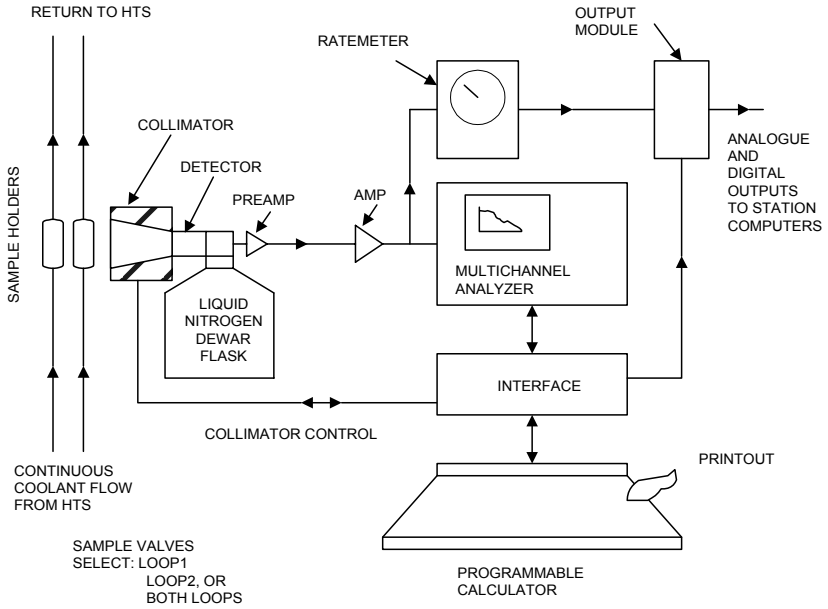


*FIG.1. A schematic diagram of the gaseous fission product monitoring system in a CANDU reactor.*

Delayed Neutron System, shown in Fig. 2, is designed to detect the presence of the delayed neutrons emitted by the fission products I-137 and Kr-87.

DN system has the sampling lines from 380 fuel channels. They carry coolant to the sample coil arrays in two water – filled moderators tanks, one in each scanning room. Six $BF_3$ – filled neutron detectors in each room are positioned by their carriage and lowered into the sample coil dry wells. The data are collected during the preset counting time and analyzed by an on-line computer. The detectors are raised and repositioned in sequence until all channels have been scanned. Computer – controlled or manual operation is done from a separate room in the reactor building. The design incorporates a deliberate 50 seconds delay to eliminate interference from unwanted activation products. These are the photoneutron- producing nitrogen-16 (7 seconds half-life) and neutron emitting nitrogen 17 (4 seconds half-life). All fuel channels normally give a "background" DN signal. Channels containing defected fuel will exhibit a signal above that of normal background, so suspect channels are identified on the basis of their signal to background ratio or Discrimination Ratio (DR); a DR>1.3 indicates the presence of defected fuel in that particular channel. When a defected bundle is suspected in a channel, that channel is subsequently monitored more frequently, until the defected bundle is unloaded. Usually, DN measurements are done once every two weeks.

In a very simple form, DR may have the following expression:

$$DR = 1 + \frac{R\left(1 - r^{1/2}\right)}{R_U}$$

where: R - Fission product release rate from a defect
r - Activity reduction factor {= exp (- λT )}
$R_U$ - Uniform uranium contamination within each loop- half, i.e. $R_a$ for loop – half A and $R_b$ for loop – half B.

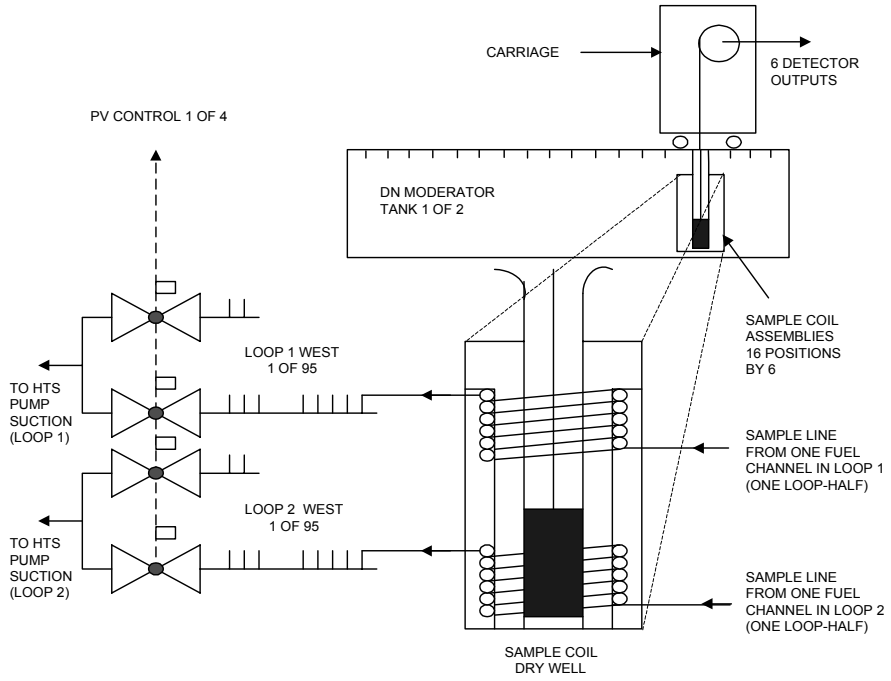


*FIG.2. A schematic diagram of a scanning room for the Delayed Neutron system in a CANDU reactor.*

The magnitude of DR for a suspect channel is a function of defected element power, defect size and amount of coolant exposed uranium which affects R, and uranium contamination level, which affects $R_U$; this means that the discrimination ratio will increase if the hole size increases but decreases if the defect begins to release uranium. When fuel defect is not releasing uranium but has an increasing hole size, the DR increases because the defect hole size is increasing allowing fission products to escape at a higher rate; the loop-half average DN signals will also increase, but at a much slower rate due to both the dilution and mixing effects in the loop and the activity decay during recirculation. In the case, when we have uranium release but stable hole size, the fission products release rate will be constant but the loop half average signal will increase as the tramp uranium builds up in the core.

Grab Sample System involves the collection of small coolant samples taken at selected locations along the HTS (Heat Transport System) while the reactor is at power. The gamma radiation energy spectrum is then analyzed. The measurements are made twice a week or upon request and are provided especially to verify the accuracy of GFP.

After a fuel defect has been detected and located in the core the fueling engineer decides on the refueling scheme to remove it, but he needs confirmation that it has been removed. In this sense Area Alarm Gamma Monitors (AAGM) are used. These monitors are set up at various locations in the fuel handling systems, between the core and the storage bay. The high gamma activity signal associated with the fission products released from the defected fuel above the discharge bay when the bundles were transferred from the fueling machine to the pool, provides the confirmation that a defected bundle was discharged.

During the four years of commercial operation at Cernavoda there have been recorded 13 defects ( 8 in 1997, 4 in 1998 and 1 in 1999 and 0 in 2000 ). This gives an overall rate of fuel defects of 0.076% for this period. If we deduce the Canadian fuel irradiated (4,635 bundles) and the defected Canadian fuel (6 bundles), then the rate of fuel defects for all Romanian fuel irradiated is much smaller. It is to be mentioned that only the first defect has a burnup penalty, the other defected bundles being discharged in time [6].

## 3. DATA ANALYSIS AND INTERPRETATION

### 3.1. Fission products gamma activity evolution

The evolution of the gamma activity, measured by GFP for certain fission products between December 1996 – December 1999, is presented in Figs. 3-6 [6]; in 2000 year, the activity for all fission products measured was all the time at the background level.

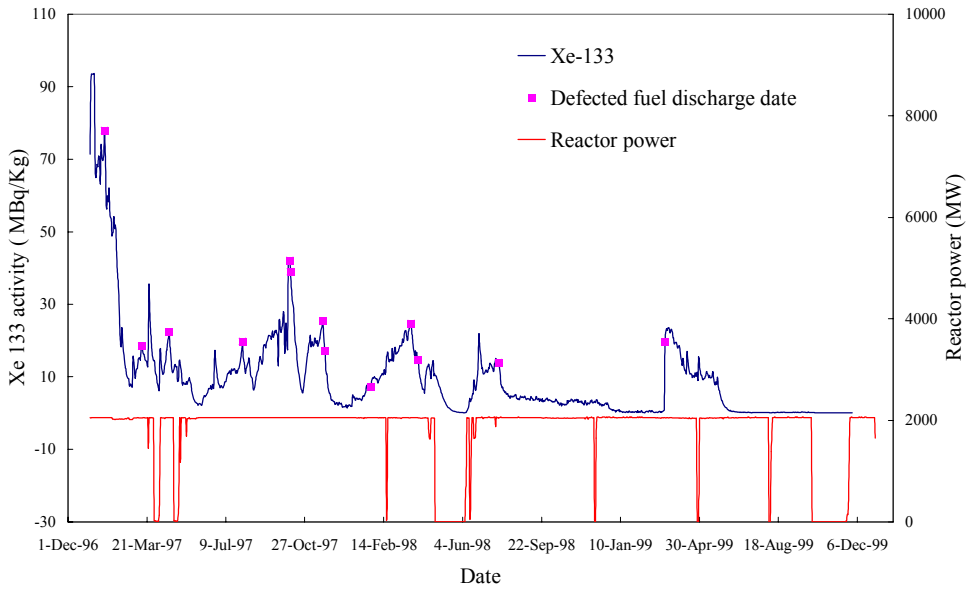


*FIG.3. Xe-133 activity evolution in the coolant and defected fuel discharge dates.*

Figure 3 shows the evolution in time of Xe-133 activity and of the reactor power. The high value of the activity at the beginning of 1997 is a sure proof of the presence of defects in the core. The decrease of the activity is correlated with the discharge of defected fuel. On the other hand, the activity increase when the reactor is operating at constant power means either the occurrence of a new defect, or the evolution of the existing one towards deterioration. On the same figure, we placed the moments when defected fuel was discharged, as it was reported by Cernavoda. From Canadian experience [7], one defected element in the reactor core, operating at 40 KW/m, will account for Xe-133 activity concentrations of 34 to 68 MBq/Kg for a fast release defect (the release mechanism is primarily controlled by the diffusion process of the gases through the fuel matrix with very little holdup inside the fuel element) and 17 to 34 MBq/Kg for a slow release defect ( the release of the fission gases is restricted by a small sized defect and a large fraction of short lived fission products is lost by decay during the delay in the fuel sheath gap). As we can see from this figure, in January 1997, Xe-133 activity was very high; the discharge of one defected fuel bundle cannot explain the decrease of Xe-133 activity from 94 to 8 MBq/Kg; we may suppose that in the same defected bundle we had more defects, or that the next 2 defected bundles discharged in March

and April 1997 already existing in the core in January, 1997; in the same time, defected bundle discharged in April had the biggest contribution to Xe-133 activity because of a high burnup (170 MWh/KgU) and a high power level.

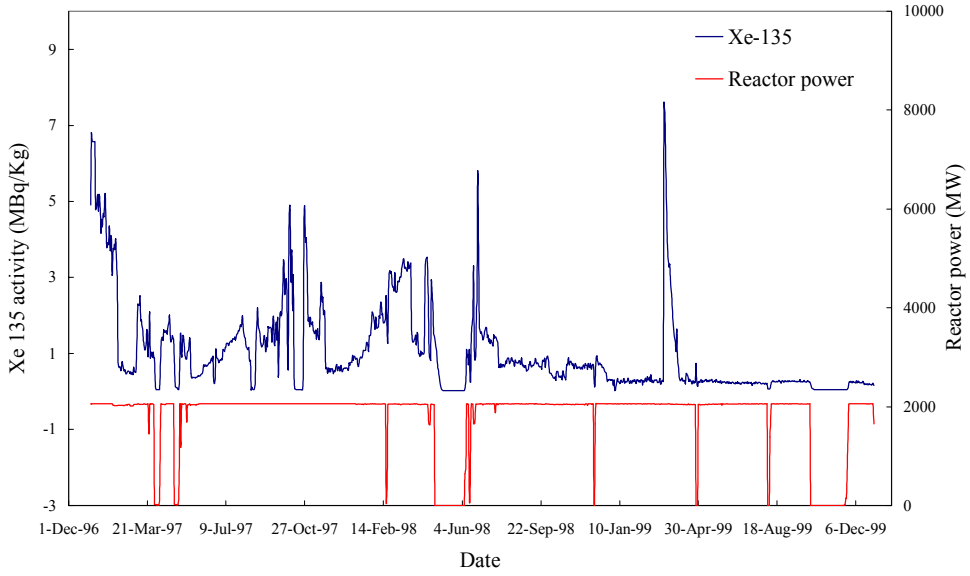


*FIG.4. Xe-135 activity evolution in the coolant.*

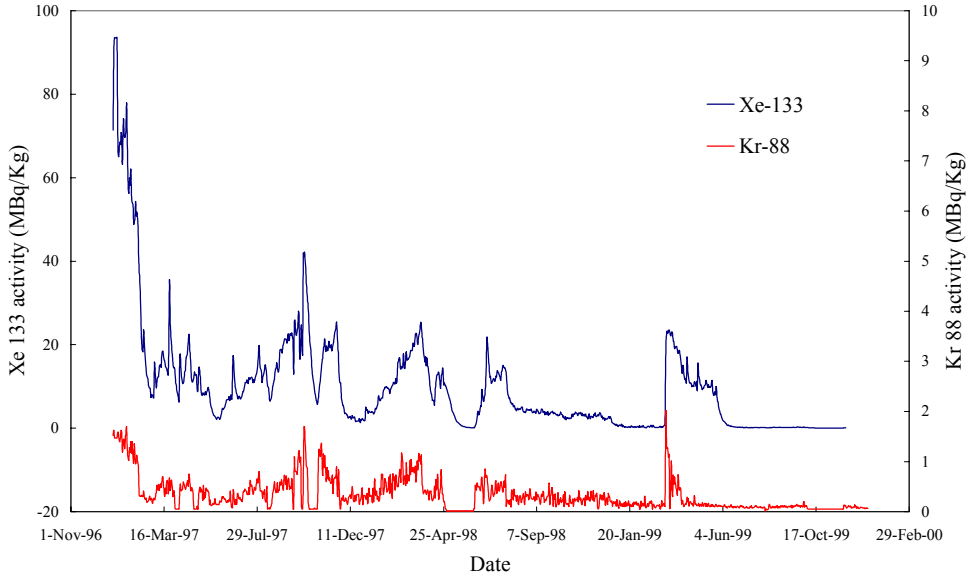


*FIG.5. Comparative evolution in time of Xe-133 and Kr-88 activities.*

The evolution in time of Xe-135 activity and of the reactor power is shown in Fig. 4. We can notice a resemblance of the evolution of this isotope with that of Xe-133, only it is to be mentioned that the values of Xe-135 activities are smaller.

In Fig. 5 we present the comparative time evolution of Xe-133 and Kr-88 activities. This comparison emphasizes the evolution of defects. If, in steady-state power conditions, the increase of Xe-133 activity is accompanied by the increase of Kr-88 activity, then we shall have an evolution of an existing defect towards deterioration. If the activity of Xe-133

increases while that of Kr-88 is approximately constant, then we can suppose that either a new defect occurred, or the degradation of a defect is very slow. For example in May- August 1997, Xe-133 activity increases and Kr-88 activity is constant; we had new defects in this period and this is proved by discharging of 5 defected fuel bundles in the next period. On the other hand, an example of very fast increase of both Xe-133 and Kr-88 activities in 1999 show us un unstable defect going to deterioration.

Fig. 6 presents the I-131 activity and the reactor power evolutions. As we can see, the activity level was small for most of the time because the purification system was operated permanently. The iodine spikes shown after power maneuvers, reactor trips or shutdowns proved the presence of defected fuel inside the core at that time. From this figure we may see that we had defects in the core all the time until May 1999.

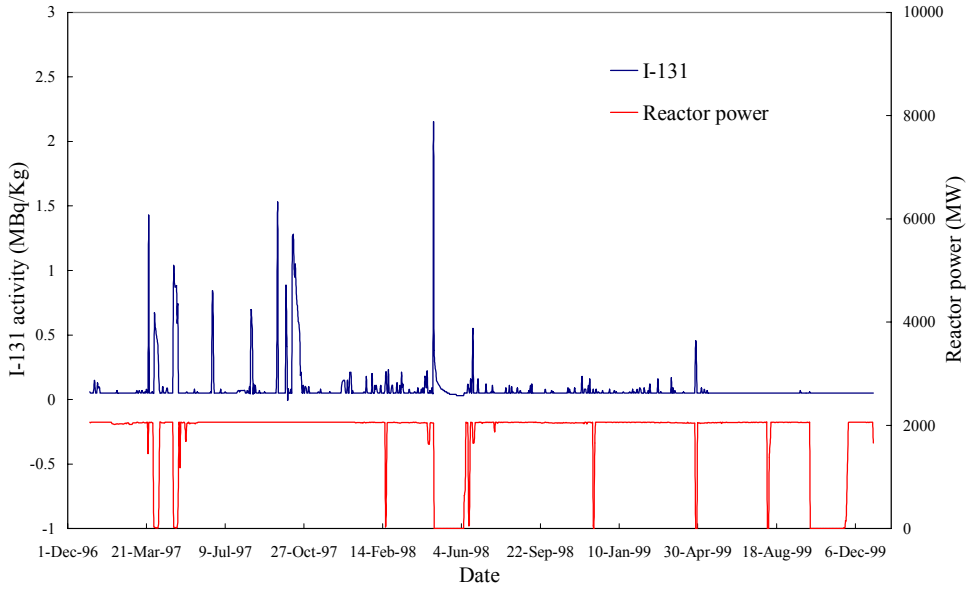


*FIG.6. I-131 activity evolution in the coolant.*

One of the most important issue is to detect in time coolant contamination with uranium released from defected fuel that already deteriorated [4,8] (experiments in Canada have shown that defected elements release uranium when individual grains of $UO_2$ are loosened by oxidation along their boundaries). Uranium released into the coolant deposits on the bundles that are moved by refueling, but also deposits on the pressure tubes and it is trapped there for the entire life of the fuel channel. On the other hand, in-core uranium contamination is not removed by fission; the fissile U-235 is depleted with burnup but fissile Pu-239 builds up from the transmutation of U-238. All the fission products resulting from the fission of U-235 and Pu-239 are released into the coolant. The best solution is to discharge the defected fuel before uranium dioxide is released into the coolant.

### 3.2. Delayed Neutron signals analysis

For defected fuel location it is used DN average count rate for DR calculation. DR is the DN signal of a channel normalized to the average signal of all channels measured by the same detector , for the same loop. To improve the accuracy of the DR values, it was also used DR normalized to its historical value ( HDR). As we already shown, 13 fuel defects where

discharged from the core in the period analyzed. The evolution of the DN average count rate and the evaluation of the discrimination ratio, confirmed 9 defected fuels; four of them were not seen by the DN system, but the Area Alarm Gamma Monitor showed an increase of the background activity above the discharge bay after the bundles were transferred from Fuelling Machine to the pool; these defects could be small, not allowing the release of halogens and causing the DN system inability to detect them [6]. On the other hand, there where situations when a DN signal was high enough to suppose to have a defect but that defect was not confirm by any other monitoring systems. The channels whose DR is more than 1.3 are "suspect channels" and are monitored carefully in order to evidence the trend of the DN signal.

In Fig. 7 we present an example for the evolution in time of the DR for high signal channels; as we may observe from the figure, all the four channels have a DR >1.3, they were monitored and after refueling only channel D15 was confirmed by the other systems to have a defected fuel.

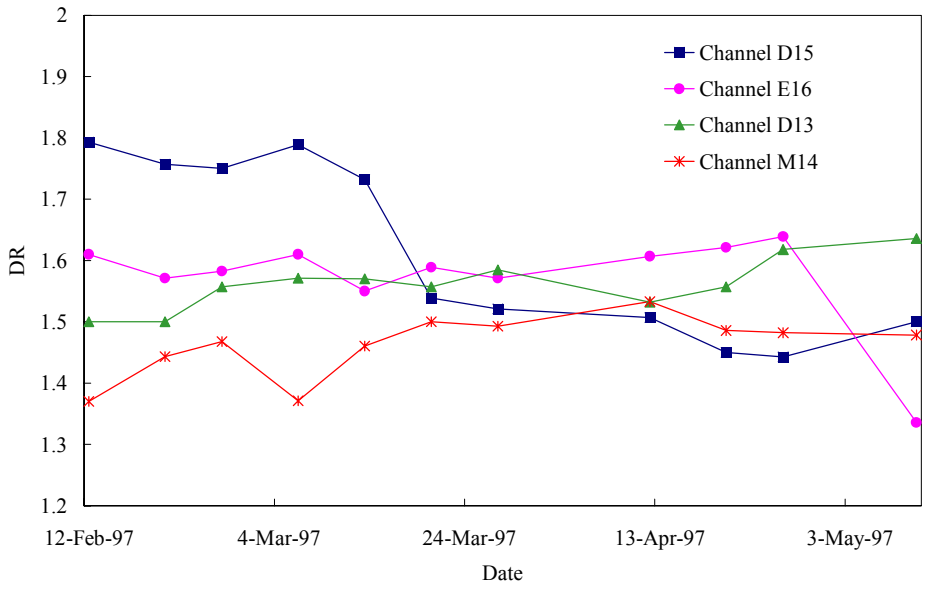


*FIG.7. Discrimination Ratio versus time for high signal channels.*

## 4. CAUSES OF DEFECTS

The most common type of operational defects in CANDU reactors, especially at the beginning of power plant life, is sheath fretting by debris. Debris within the Heat Transport System (HTS) can be circulated through the core by the coolant, which once trapped within the fuel bundle may generate defects by fretting. It has been shown that the majority of defects are in the channels whose feeders are connected to the bottom of the inlet headers near the pump discharge lines. The distribution of defects in the cores is shown to be heavily weighted towards these more susceptible channels. In Fig. 8, it is shown the location of fuel channels that are inclined to collect debris. If we place on this figure the channels with defected fuel at Cernavoda, we notice that 7 defects are in this region and another 6 are very close to this region.

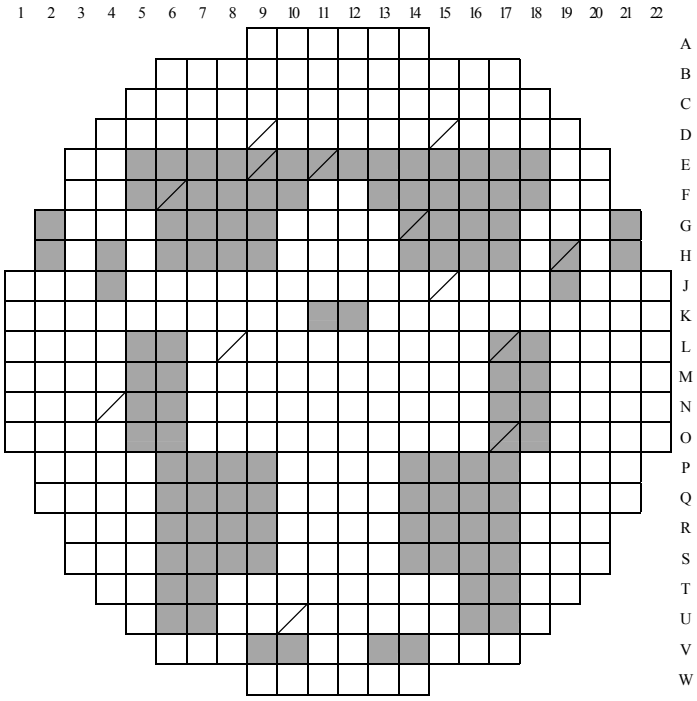


*FIG.8. Location of fuel channels that are inclined to collect debris (■) and the channels with defected fuel at Cernavoda (⧄).*

Another probable defect cause may be due to fuel manufacturing. Unfortunately, at Cernavoda power plant, there is no any kind of tools for inspection of defected bundle in the pool, so no defect was confirmed by post irradiation examination of the fuel in spite of the fact that in INR there is a Hot cell facility.

## 5. CONCLUSIONS

Equipment is installed in Cernavoda power plant to detect and locate even small defects in failed fuel bundles present in the reactor core.

Defected fuel monitored at Cernavoda NPP using this equipment emphasized the following aspects:

- the overall defected fuel rate was very small, i.e. 0.076 %;
- defected fuel bundles did not affect the overall fuel performance;
- the main cause of fuel defects may be fretting by debris.

There is a need to install an underwater examination system at Cernavoda NPP and to provide transport cask allowing detailed post- irradiation examination to confirm defects and establish their causes and remedies.

## REFERENCES


[1] DESIGN MANUAL, "Cernavoda Unit 1 Nuclear Generating Station Core Fuel", 81-37000-DM-000, Revision 1

[2] N. BARAITARU et al., "Core performance at Cernavoda Unit 1 during 1997", Information Report IR - 03310-10,Rev.0, May 1998 (Internal Document)

[3] N. BARAITARU et al., "Core performance at Cernavoda Unit 1 during 1998", Information Report IR - 03310-10,Rev.0, May 1999 (Internal Document)

[4] A. M. MANZER, "Candu Fuel Performance in Nuclear Power Station", IAEA Project, February, 1994

[5] A. M. MANZER and R. W. Sancton, "Detection of defective fuel in an operating CANDU 600 MW(e) reactor", Paper presented at the ANS Meeting, 1984

[6] D. STANILA, "Fuel performance at Cernavoda Unit 1", Paper presented at International Conference on Candu fuel, Ontario, Canada, September 26-30, 1999

[7] R. D. MacDONALD, M. R. FLOYD, B. J. LEWIS, A. M. MANZER and P. T. TRUANT, "Detection, Locating and Identifying Failed Fuel in Canadian Power Reactors", AECL Report No. 9714, 1990

[8] B. J. LEWIS, "Fission product release to the primary coolant of a reactor", AECL Report No. 8975, 1985

# FUEL FAILURE DIAGNOSTICS IN NORMAL OPERATION OF NUCLEAR POWER PLANTS WITH WWER-TYPE REACTORS

L. LUSANOVA, V. MIGLO, P. SLAVYAGIN
Russian Research Center "Kurchatov Institute, Institute of Nuclear Reactors,
Moscow, Russian Federation

**Abstract**

Authentic failed fuel detection is very important for quality operation of NPP, and also for perfecting quality and design of fuel pins and fuel assemblies (FAs). Operative troubleshooting of WWER fuel pins done throughout their service time is mainly based on the data of failed fuel detection (FFD). Therefore, the capability to issue authentic and detailed conclusions on damaged fuel pins is expected to depend significantly on information capacity provided by the applied FFD methods.

## INTRODUCTION

Failed fuel detection on WWER nuclear plants may be carried out at both operating and shut down reactor by means and methods consisting of the following:

- instrumentation systems intended for measuring the activity of reference fission products (hereinafter FPs) in the primary coolant of operating reactor;
- software capable to identify the sources of FP on the basis of isotope contents in the primary coolant;
- FFD system by bottle method with alternating pressure in a shut down reactor.

Nowadays radiation methods are applied on WWER power units at both operating and shut down reactors. Such radiation methods are based on fission products monitoring in fluids (in the primary coolant of operating reactor or in the loop of FFD system of shut down reactor). Damaged fuel pins are the source of such fission products.

FFD radiation methods enable to perform monitoring of penetrating defects in claddings and they are widespread in the international practice due to high sensitivity and simplicity of application on NNPs. In general, to make more or less authentic failed fuel detection during fuel pin operation is only possible with application of radiation methods. Within the framework of nuclear fuel management, which admits operation of damaged FAs, the application of radiation methods in both operating and shut down reactor defines a solution whether to further operate the damaged FAs or not.

Also it is necessary to stress that FFD methods based on radiation monitoring have certain limitations in application, since such methods do not monitor the nature of damage or FP leakage from damaged fuel pins on power operation or during reactor shutdown. The assessment of such characteristics is only performed by an indirect method with application of certain physical and mathematical models enabling to bring them in compliance with radiation levels of fission products, measured in the primary coolant of operating reactor or in FFD system in shut down reactor.

Therefore, the authenticity of assessment made by FFD radiation methods depends upon the degree of how much the adopted model complies with actual parameters which effect the release of FP from the damaged fuel pins.

Moreover, information capacity of FFD radiation methods greatly depends on the number of damaged fuel pins in the core, and on damage size in their claddings.

With achieved safety of WWER fuel pins in normal operation the authenticity of claddings leak-tightness assessment performed by regular FFD methods is high enough. This was demonstrated during verification and certification of calculation techniques for FP release from damaged fuel pins.

In case of frequent depressurization of fuel pins resulting not from the quality of fuel but from some other reasons, such as disparity to normal conditions of fuel operation, the information capacity of FFD radiation methods shall decrease, and inaccuracy of estimations shall increase. This is conditioned by both increase of activity levels in the primary coolant, and extension of parameter range which influence the release of FPs from fuel and damaged fuel pins (operation condition of damaged fuel pins, and also dimensions, nature and location of penetrating defects in claddings of such fuel pins).

At abnormally high levels of depressurization there appear problems even with identification of depressurization moments, since FP activity levels in the primary coolant become so high that the contrast of registration of new damaged fuel pins reduces in their background. In these cases the only correct assessments can be either qualitative assessment, or component assessment of FP leakage from damaged fuel pins only in relation to a registered level of FP activity in the primary coolant.

By concrete examples of NPP operation this report demonstrates the reasons that facilitate authenticity diminishing of FFD methods at increase of fuel pins depressurization.

## 1. PECULIARITIES OF FAILED FUEL DEIECTION AND ITS CAPABILITIES DURING FUEL OPERATION

Failed fuel detection should perform the following tasks:

- identification of depressurization moments;
- monitoring the development tendencies of penetrating defects in claddings;
- perform quantitative assessments of damaged fuel pins in the core.

FFD in WWER power units in operation is carried out by measuring specific activity of reference FPs in the primary coolant and its subsequent analysis. Such analysis covers a comparison of measured absolute values of specific activity of reference FP and different half-lives and also investigation of changes nature of such FP activity levels in the course of certain fuel cycle.

### 1.1. Methodological bases for failed fuel detection in operation and factors of authenticity

Modelling of FP release from damaged fuel pins and of formation the activity levels in the primary coolant has essential importance for developing FFD methods in operating reactor and also for elaboration of algorithms intended for analysis of acquired data.

On the basis of adopted physical models the calculation techniques can be elaborated. Such calculation techniques enable to determine the quantitative characteristics of FP leakage from damaged fuel pins.

Such methods, apparently, determine values or ranges of parameters describing operation conditions (voltage, linear power, density of thermal neutron flux, etc.) and condition of fuel pins for which the calculations of FP leakage are intended (temperature, structure and porosity of fuel, diminishing of radial gap, etc.).

Special research or experimental data from NPP can verify calculation methods of FP release from damaged fuel pins. At that, experimental data used for verification of this or that calculation methods, apparently, should be obtained with such values of parameters and fuel characteristics, which are adopted in the verified calculation methods.

The calculation methods for FP release from damaged fuel pins enable to make a FFD data analysis in operating reactor with the purpose to assess the number of damaged fuel pins and degree of their depressurization. In this analysis the calculation methods will be used for the solution of a reverse problem.

In this case it is essentially important that, if the parameters effecting the FP release from damaged fuel pins are determined at solution of direct problem, the number of damaged fuel pins and degree of depressurization should be assessed for those fuel pins which can operate at parameters different from parameters postulated in calculation models. Such approach, when it is assumed in advance that initial calculation parameters of fuel pin condition are close to actual operation values, contains a primary incorrectness. Particularly this prior assumption is an initial reason for assessment errors to appear.

Due to various reasons calculated and measured parameters may significantly differ. In practice it is rather difficult to register these differences and, moreover, to evaluate them quantitatively. It often happens that the only indicator of any change in fuel rod state (temperature, radial gap, etc.) is the change of ratio between long lived and short lived FP. It is most difficult to make any authentic particular conclusions on their quantitative characteristics which directly influence the FP release from damaged fuel pins by means of registering just the fact of happening changes (i.e. qualitatively).

Also, as it follows both from NPP in-service experience and investigation, in addition to fuel burnup and fuel pin power the following factors essentially influence the FP release from damaged fuel pins into the primary circuit:

- location point of defect [1,2]
- time of fuel pin operation before a defect appeared [1,3];
- availability of water under a cladding [1];
- interaction between fuel and cladding [4];
- fuel pin operation background [4,5];
- change of fuel stoichiometry [6].

The foregoing factors increase the uncertainty degree of parameters (i.e. extend the range of probable values) describing damaged fuel pins, and, consequently, the quantities of FP released out of such damaged fuel pins. Evidently, with increase of degree of fuel pin depressurization such influence should increase. Accordingly, the range of probable values where quantitative assessment of damaged fuel pins will be performed on the basis of FP activity in the coolant of operating reactor, will be also extended. In other words, with the increase of scale of fuel pin depressurization the assessment error increases due to probable increase of parameter range describing damaged fuel pins.

Therefore, in order to increase information capacity and authenticity of assessment in elaboration of FFD methods special attention was given to selection of reference radionuclides by activity of which such assessment is carried out. In particular, the combination of reference FP was made of those radionuclides, which are mostly influenced by separate factors, but not by many of them. For example, the activity in the primary coolant of long-lived Iodine-131 is most sensitive to the number of damaged fuel pins and mode of operation, while the activity of short-lived I-134 is sensitive to the sizes of defects in claddings.

The essential factor that influences FFD in operation is also washing out the fuel from damaged fuel pins to the primary circuit.

The in-service experience demonstrates that this process also takes place even in case of minor penetrating defects in cladding [7]. Naturally, with increase of degree of fuel pin depressurization the quantity of uncovered fuel in the primary circuit increases. It plates out on the surfaces in the primary circuit and the core, and it is also contained in the coolant.

The decrease of quantity of fuel composition delivered to the primary circuit goes slowly in the course of reactor operation. Therefore, in practice when the first damaged fuel pins appear in the core, a so-called residual contamination of the primary circuit by fuel starts. The extent of such contamination depends on the scale of fuel pin depressurization of operating fuel loading.

Finally, the uncovered fuel of the primary loop and damaged fuel pins become an independent source of radioactive FP in the primary coolant, and, practically, in all cases it will make more or less contribution to the activity level of FP in the primary coolant. The amount of such contribution can be calculated by means of algorithms designed especially for this purpose, for example, a algorithm described in publication [8]. But nevertheless, it is possible to state, that the availability of background activity of reference radionuclides in the primary coolant conditioned by residual contamination of the primary circuit with fuel, enhances the error of assessment of damaged fuel pins. In case of high depressurization level such contamination can diminish even the authenticity of registration of new damaged fuel pins in a certain fuel cycle.

## 1.2. Principal philosophy and error of assessment of leakage degree in fuel pins in WWER nuclear plants in operation

### *1.2.1. Principal philosophy*

Isotopes of I-131÷135 will be only used as reference radionuclides in FFD method in operating reactor of WWER type, since we face some problems with registration of effect of unorganized leakage on concentration of xenon-133 in the primary coolant as one of the most informative isotopes out of fission gas (FG).

The selection criteria for calculation data of reference radionuclides activity in the primary coolant of operating WWER reactor were described in Ref. [4]. Such criteria take into account the current and the previous reactor operation mode with the purpose to perform fuel pin troubleshooting.

The basic condition to improve the authenticity of leakage assessment of fuel pins with application of data of FP activity monitoring in the primary coolant is a requirement to use in the analysis of specific activity of reference radionuclides of Iodine as measured in those

reactor operation periods, during which it is possible to assume the following: FP leakage from damaged fuel pins was steady, actual parameters of such leakage were close to the values specified in the adopted calculation methods.

The basic condition for steady leakage of FP from damaged fuel pins is a steady state of reactor operation. However, in practice we may observe the cases when the leakage of FP from damaged fuel pins varies even at constant reactor power. For example, the leakage reduces in the result of radial gap diminishing in damaged fuel pin. Therefore, during selection of FP activity measurement results in the primary coolant in order to perform failed fuel detection it is necessary to analyze the nature of activity changes of reference FP in the primary coolant of the reactor during all the period of the current campaign up to the moment of quantitative assessment. During such analysis in particular it is possible to determine those periods of reactor steady state operation, where the leakage of FP from damaged fuel pins is constant. Pursuant to Ref. [4] in such periods the levels of activity of reference radionuclides in the primary coolant are minimum. It is adopted to use the measurement data of reference FP activity, which were conducted in such periods also for quantitative assessment of WWER fuel pin depressurization.

It is obvious that with such approach to selection of input analysis data, the influence of impulse or non-stationary component of FP leakage upon the level of FP activity in the primary coolant reduces maximally, and hinders achievement of equilibrium state and, consequently, making a correct assessment. In the result, the greatest degree of adequacy of calculated-theoretical model is achieved. Such model depicts the leakage of FP from damaged fuel pins and actual characteristics of FP leakage taking place during reactor operation.

In this connection it is necessary to state, that in order to make a proper selection of reactor operation periods, when the marked condition of adequacy shall be executed, on-line monitoring of activity level for reference FP in the primary coolant of operating reactor will be of great importance. It is obvious that NNPs concerned about information capacity of FFD performed in operating reactor should use engineering facilities enabling to conduct such type of monitoring.

### *1.2.2. Assessment of fuel rod leakage*

It is possible to analyze and demonstrate the capabilities of failed WWER fuel pins detection on the basis of reference isotopes of Iodine activity in the primary coolant of operating reactor of four power units (A, B, C and D) of two NPPs.

FFD in operating reactor was performed in "on-line" mode in these power units, while FFD in reactor shut down for preventive maintenance was conducted for all operating FAs. Activity measurement of reference FP in the primary coolant were not suspended for preventive maintenance and were made for the purpose of registration of «spike-effect" which is known to be an indicator of damaged fuel pins in the core.

With such arrangement of FFD the data comparison acquired by both ways of FFD allows to evaluate most precisely the error of this or that method, and to analyze such error with respect of fuel depressurization degree.

Assessment of quantity of damaged fuel pins in operation of those four power units were performed for 35 fuel cycles by algorithm described in publication [8]. The data of such

assessment are given in Table 1. Table 1 also represents the data of FFD performed in a shut down reactor, particularly, the number of leaking FAs.

Table 1. Results of FFD on a reactor tripped for preventive maintenance and assessment of number of leaking fuel pins on the basis of reference FP activity in the primary coolant of operating reactor

| NPP-1 | | | | | | NPP-2 | | | | | |
|---|---|---|---|---|---|---|---|---|---|---|---|
| Unit A | | | Unit B | | | Unit C | | | Unit D | | |
| 1 | 2 | 3 | 1 | 2 | 3 | 1 | 2 | 3 | 1 | 2 | 3 |
| A-1 | 2-4 | 2 | B-1 | 3-4 | 1 | C-1 | 1 | 1 | D-1 | 6-9 | 3 |
| A-2 | 0 | 0 | B-2 | 4-5 | 2 | C -2 | 0 | 0 | D-2 | 0 | 0 |
| A-3 | 1 | 0 | B-3 | 9-18 | 2 | C-3 | 10-12 | 1 | D-3 | 4-5 | 1[â)] |
| A-4 | 1-2 | 2 | B-4 | 10-20 | 9 | C-4 | 0 | 0 | D-4 | 1 | 1 |
| A-5 | 1 | 1 | B-5 | 10-20 | 4 | C-5 | 1 | 1 | D-5 | 0-10[c)] | 1[d)] |
| A-6 | 1 | 1 | B-6 | 18-36 | 2 | C-6 | 0 | 0 | D-6 | 0 | 0 |
| A-7 | 0 | 0 | B-7 | 10-20 | 1 | C-7 | 3-5 | 1[a)] | | | |
| A-8 | 1 | 1 | B-8 | 10-12 | 1 | C-8 | 10-14 | 2 | | | |
| A-9 | 1 | 1 | B-9 | ≤1 | 1 | C-9 | 5-7 | 3 | | | |
| A-10 | 1-2 | 1 | | | | C- 10 | 0 | 0 | | | |

***Notes.***
a) and c) - as a result of visual inspection a hole was found out in one of the claddings of size (equivalent diameter), comparable with fuel pin diameter;
b) - ratio between the activity of reference isotopes of iodine agreed with their release from uncovered fuel, therefore, a conservative assessment is given on the basis of long-lived iodine-131 activity

Column 1 – No. of campaign; Column 2 - number of leaking fuel pins, assessed on the basis of reference FP activity in the primary coolant of operating reactor by algorithm [8]; Column 3 – number of FA with leaking fuel pins, detected in the result of FFD on a reactor tripped for preventive maintenance.

The comparative analysis of data from Table 1 allows making the following conclusions on probability and value of error of these or those approaches and of FFD method for operating reactor with various degree of fuel depressurization.

First of all, it is necessary to state, that the applied method allows to identify authentically the absence of damaged fuel pins in the core of operating reactor. In-service experience of above mentioned power units during seven fuel cycles: A-1, A-7, C-2, C-4, C-6, C-10, D-2 and D-6 can serve as an example.

Obviously, the primary grounds to make such a conclusion is the absence of "spike-effect" in activity of FPs in the primary coolant, particularly, reference isotopes of Iodine, during reactor operation and during its shutdown.

An additional indication of absence of damaged fuel in the core is the ratio between the activities of reference isotopes of iodine. In this sense such ratio is more informative as contrasted to absolute values of activity.

For example, the values of activity of reference isotopes of I-132-135 registered at the end of campaign D-6 exceeded the time of campaign D-1 by more than an order. Upon completion of this campaign the FFD method performed on a shut down reactor detected 3 damaged fuel

pins. However, the ratio between the values of specific activity of reference isotopes of Iodine in campaign D-6 enabled to assume the absence of damaged fuel pins in the core. This fact was confirmed by FFD data acquired during the reactor shutdown for preventive maintenance.

Thus, the higher levels of activity of reference isotopes of iodine in the primary coolant during campaign D-6 were conditioned not by damaged fuel pins in the core, but by residual contamination of primary loop with fuel.

Assessment of damaged fuel pins in the activity of reference FP in the coolant of operating reactor well agrees with the number of leaking FAs with individual depressurized fuel pins detected during preventive maintenance. For example, when assessment predicts 1 or 2 damaged fuel pins in the core, FFD method also detects 1-2 damaged FAs (campaigns A-1, A-4-6, A-8-10; B-9; C-1, 5; D-4). Consequently, on the average, one fuel pin will be depressurized in each 1-2 FA.

Such situation results from micro flaws of structural nature at crystalline level (dislocations, etc.) in some claddings. Full detection of such defects at the stage of manufacturing, is, of course, impossible. A so to say calibration" of such fuel pins takes place during operation. In such cases it is possible to state quite confidently the absence of operational, structural or manufacturing reasons leading to fuel pin depressurization. Therefore, the acquired quantitative assessment of damaged fuel pins characterizes actual safety and quality of fuel in normal operation.

At depressurization of individual fuel pins it is also possible to troubleshoot with high probability the development of penetrating defects in claddings. As it is known, it is possible to learn about such process by the growth of activity level of short-lived reference isotopes of Iodine, first of all, of I-134.

Campaigns D-3 and D-5 can serve as visual and demonstrative example. During these campaigns we watched a gradual growth of activity levels of short-lived reference isotopes. As a result of visual inspection of unit D inspection facility performed upon completion of such campaigns, penetrating defects of individual claddings were found out. The dimensions of such penetrating defects were comparable with diameter of fuel pins.

As it is known, a direct evidence for the number of damaged fuel pins in the core is specific activity of the most long-lived reference isotope of I-131 in the primary coolant of operating reactor. At depressurization of individual WWER fuel pins the value of specific activity in nominal power reactor operation and specified operational mode of specific water purification system (hereinafter SWPS) does not exceed $10^{-6}$ Ci/kg ($3{,}7 \times 10^{4}$ Bq/kg).

Thus, if NPP operates with such level of specific activity of I-131 in the primary coolant, the assessment of damaged fuel pins performed during reactor operation has a high degree of authenticity.

However, it is necessary to point out that presence of large defects appeared in individual claddings during campaigns D-3 and D-5 has resulted in formation of such residual contamination with fuel in the primary loop which became a source of high activity of reference isotopes of iodine during campaign D-6.

This fact has encomplicated the possibility to state the presence or absence of damaged fuel pins in the core during campaign D-6, and, finally, resulted in significant increase of error in

estimation of probable number of damaged fuel pins in the core of this reactor. For example, at conservative estimation of damaged fuel pins this number could amount to 10. While FFD performed in a shut down reactor did not find out leaking FAs at all.

Obviously, in identification of nature and development of cladding damage the residual contamination of unit D primary loop with fuel was a reason for a long-lived unfavourable factor which increases the uncertainty of both quantitative and qualitative assessment.

With increase of fuel pins depressurization the error of quantitative assessment of damaged fuel pins in operating reactor increases.

This is, first of all, expressed in deterioration of agreement between assessment data of damaged fuel pins detected by FFD during a reactor shutdown for preventive maintenance. The ratio between these two values, typically, becomes larger, as contrasted to the above cases of depressurization of individual fuel pins and its value may lie within rather a broad range of values, the highest of which amounts to 10-20.

In-service experience of unit B may serve a visual evidence for this. In total, judging by FFD data acquired in a shut down reactor, unit B operation had more depressurized fuel pins, as contrasted to other three power units. Finally, as Table 1 shows, the values of damaged fuel pins assessment for different campaigns varied in broad range of values.

A similar picture was also observed during certain campaigns in units C (C-3, C-8, C-9) and D (D-1 and D-3). As Table 1 shows, for these campaigns the range of number of damaged fuel pins in accordance with performed assessment significantly extended as contrasted to the cases of individual fuel pins depressurization.

It is necessary to point out, that in some cases of increase of fuel pin depressurization a good agreement between damaged fuel pins assessment data on operating reactor and FFD data acquired in a shut down reactor may happen. For example, during campaign B-5 the authenticity of assessment of damaged fuel (from 10 to 20 pieces) appeared quite high, since the FFD in a shut down reactor detected such a number of damaged FAs (9 pieces), which corresponded to the lower limit of value range of this assessment. However, this example is an exception, which, nevertheless, also characterizes the increase of uncertainty or assessment errors performed with higher levels of fuel pin depressurization.

In accordance with above mentioned, in cases of higher degree of fuel pin depressurization the deterioration of correlation between FFD data acquired in operating and shut down reactor can be related to a broader range of operational parameters describing damaged fuel pins, and also of types and location of penetrating defects and growth of assessment errors.

### *1.2.3. Activity level and assessment error*

The review of in-service experience of four power units can be related, as a whole, to the category of normal operation. But the FFD data collected on these power units during 35 campaigns visually demonstrate that with rather a small increase of fuel pin depressurization the assessment error in operating reactor increases.

Such increase of error can be related to the activity of reference isotopes of iodine in the primary coolant of operating reactor.

For example, the level of specific activity of the most long-lived reference isotope I-131 in the primary coolant of unit B reactor at its nominal power operation and in specified operation mode of SWPS exceeded $10^{-6}$ Ci/kg ($3{,}7 \times 10^{4}$ Bq/kg) and amounted to ~ $5 \times 10^{-6}$ Ci/kg ($1{,}85 \times 10^{5}$ Bq/kg) in certain campaigns practically during all the operation period (campaigns B-2 - B-8).

As it follows from Table 1, with specific activity of I-131 amounting close to $10^{-5}$ Ci/kg ($3{,}7 \times 10^{5}$ Bq/kg), the uncertainty of acquired assessment data increases so much, that it is possible to consider as correct only such assessment, which is the higher limit of the range of probable values of this assessment.

Informative worth of such assessment is not high, and its practical value significantly diminishes.

Therefore, in order to create favourable conditions for failed fuel detection in operating reactor it is essentially important to operate a power unit in such a manner, that the levels of FP activity in the primary coolant were as small as possible. As it is known, this can be achieved by a set of actions including qualitative operation of power unit in combination with improvement of safety and quality of fuel. Such approach allows using the available nominal methods and engineering facilities of FFD most efficiently. If to make effort in this direction, it will be possible to acquire authentic and more detailed information on the ground of FFD data in order to make decision whether to continue operation of damaged FAs, and, thus, enhance the economical indices of NPP operation.

### *1.2.4. Ratio between assessed damaged fuel and the number of leaking FAs*

The comparative analysis of a large number of FFD data acquired in operating and shut down reactor of WWER power units has shown, that at high degree of depressurization as contrasted to the reached safety of fuel pins the ratio between assessed damaged fuel and the number of leaking FAs, detected by FFD during preventive maintenance, basically, lies within the interval between 4 and 7. These values are successfully used in practice by the staff of WWER type NPPs for prediction of the number of leaking FAs, which are expected to be revealed during FFD in reactor shut down for preventive maintenance.

It is also necessary to mark, that a higher value of this ratio can be an indicator of some construction, operation or manufacturing reasons which lead to depressurization of a larger number of fuel pins within FA. In such cases we face a necessity to perform an additional specific analysis or extended analysis of probable reasons of such phenomenon and to take appropriate actions to improve operation or design and quality of FAs.

## 2. DETECTION OF FAILED FAs AT A SHUT DOWN REACTOR

The detection of leaking FAs and troubleshooting in claddings is to be carried out by FFD methods on a reactor shut down for preventive maintenance.

All FFD methods for FAs, which can be used on shut down reactors of WWER type, can be arranged into two groups of radiation and non-radiation methods.

From the very beginning of operation of WWER type of NPP a radiation bottle method was applied on shut down reactor for WWER type of NPPs, as the basic and most informative FFD method. This method is based on creation of alternating pressure in a special FFD

experimental facility, arranged in cooling pond, during FA testing. Thus, a fission products release from damaged fuel pins into the water of FFD experimental facility is initiated by means of alternating pressure.

The primary goal of FFD in a shut down reactor unit was the detection of those FAs, the further operation of which is either inadmissible in principal (mechanical damages, etc.), or undesirable in the sense of providing normal radiation conditions in NPP in the following campaign.

For FAs of the first group a criterion of advance unloading was established. Should this criterion be reached, these FAs shall be removed from reactor unit irrespective of the reached burnup.

If necessity or feasibility to decrease FP activity in the primary coolant in operating reactor arose, the removal of one or several FAs from the reactor was permitted for those FAs which did not reach the criterion of advance unloading.

The necessity to implement the «criterion of FA group unloading» has always been the liability of NPP staff and, finally, depended on NPP radiation situation unlike the «criterion of advance unloading» of individual FA, which required absolute fulfillment. At such approach the NPP staff gets a chance to plan the fuel loading of the core for the following campaign preceding from actual NPP radiation situation, condition of equipment (first of all, air-tightness of steam generators), and also availability of fuel in NPP (both fresh and fit for further operation).

The application of FFD bottle method in a shut down reactor in combination with established criteria of (advance) unloading allows to ensure high economic indices of NPP operation within the framework of permissible radiation criteria at properly high level. For example, during many hundreds of reactors-years there was no event of advance stop of VVDER power due to non-observance of radiation safety requirements because of making an erroneous decision on further operation of leaking FAs detected by FFD.

It is also necessary to point out, that FFD radiation bottle method likewise all other FFD methods (including non radiation methods), do not ensure a 100 % safety for detection of leaking FAs. For example, it may happen so that identification of FAs with severely damaged claddings will be hindered. This may be facilitated by considerable reduction of FP under claddings due to their removal or washing out through large size penetrating holes.

That is why it is necessary to indicate the initial reasons of principle nature which were used for establishing the criteria of advance FA unloading from WWER reactor, which allow to reach a maximum degree of repeated utilization of leaking FAs within the framework of safety requirements.

Some claddings have micro flaws at crystalline level (dislocations, et.). Full detection of such defects at the stage of manufacturing, is, of course, impossible. It was supposed that one of the main reasons for fuel pin depressurization, pertaining to safety of fuel pins, is bound with such micro flaws.

The second group of fuel pins which theoretically subject to depressurization during operation included fuel pins with production defect of occasional nature (for example, risks and scrapes on claddings, etc.), as well as the above mentioned first probable reason. High quality of issue

control at fuel manufacturing plants allowed to state, that only few fuel pins could depressurize in the course of operation because of production defects.

During normal operation the part of fuel pins falling into both «groups of risk», could depressurize. As a result of such depressurization defects like “gas untightness” appeared in claddings at initial state. Thus, so to say calibration of initially defective fuel pins was taking place.

At further operation by virtue of familiar processes taking place in claddings there could appear secondary defects of larger size. In this case secondary defects appeared in the points of fuel pin greatest power release, typically in joint points of fuel pellets. Therefore, during FA FFD performed by a regular method the created mode of alternating water pressure in FFD test facility facilitated an excursion of reference radionuclides from under the damaged claddings. This fact made a regular FFD method both contrast, and quantitatively representative.

However, if some other original reasons of fuel pin depressurization appear in addition to two reasons mentioned above, a special type of penetrating defects may appear in the claddings. And it will be not reasonable to use the available criteria of calibration for such defects. Penetrating defects are the example of such type of defects. Penetrating defects appear as a result of a fretting –corrosion of claddings with spacer grids. In such cases the delivery of water under the cladding of damaged fuel pin can very problematic or just impossible either because of spacer grid, or because of random arrangement of defect in relation to fuel pile (particularly, joints between pellets). Obviously, in this case the approach to classification of defects in claddings (by size, etc.) should be amended. At that, it seems necessary to expand a set of FFD methods used in shut down reactor, of non-radiation methods (ultrasonic, for example) in particular.

## 3. CONCLUSION

In normal operation at fuel pin depressurization, which corresponds to the reached safety the existing FFD methods allow to diagnose effectively a leakage of fuel pins on operating and shut down reactor, enabling to support favourable radiation conditions in NPP.

At heightened scales of fuel pin depressurization the authenticity of damage assessment of fuel pins significantly reduces due to operation or production reasons, particularly because of considerable uncertainty in types of defects and operational parameters of defective fuel pins, and also because of residual contamination of primary loop with fuel.

## REFERENCES


[1] SCHUSTER E., von JAN R., FISCHER G., " Evaluation of fuel performance from coolant activity data", The Proceedings of International Topical Meeting on LWR Fuel Performance " FUEL FOR THE 90's ", Avignon - France, April 21-24, 1991, V.1, pp. 285-294.

[2] WILLSE J.T., COLEMAN T.A., "Recent results from B&W fuel company's fuel performance improvement program ", ibid., pp. 66-73.

[3] LEUTHROT C., BRISSAUND A., MISSUD J.P. "Relationships between the characteristics of cladding defecte and the activity of the primary coolant circuit and aid for the management of leaking fuel assemblies in PWR ", ibid., the same place, pp. 324-337.

[4] LUZANOVA L.M., MIGLO V.N., SLAVJAGIN P.D., " Experience of identification of damaged fuel pins in operation of nuclear power plant with WWER type reactor ", ibid., there, pp. 488-499.

[5] PORROT E., et al., " Fission gas release during power transients at high burnup ", ibid., 558-566.

[6] LOCKE D.H., “Mechanisms of Deterioration of Defected LWR Fuel”. The Proceedings of International Topical Meeting “The behaviour of defected zirconium alloy clad ceramic fuel in water cooled reactors”. IWGFPT/6. Chalk River, Canada, 1979.

[7] GARZAROLLI F., et al., "Das Verhalten Defekter Brennstabe beiweitergefuhrtem Reaktorbetrieb ", Kerntechnik, V.20 (1978), N 10.

[8] SLAVYAGIN, P., LUSANOVA, L., MIGLO, V., «Regulation of the fission product activity in the primary coolant and assessment of defective fuel rod characteristics in steady state WWER-type reactor operation ». IAEA Technical Meeting on Fuel Failures in Water Reactors: Causes and Mitigation , Bratislava, June 17 - 21, 2002 .

# SUMMARY OF TECHNICAL DEVELOPMENT ON THE ON-LINE MONITORING AND FUEL FAILURE EVALUATING SYSTEM AT THE TEMELIN NPP

M. SEMMLER[1], M. MARTYKAN[2], J. CIZEK[1], M. VALACH[3], J. HEJNA[3]

[1] CHEMCOMEX Praha, a.s.
[2] Nuclear Power Plant Temelin, a.s.
[3] Nuclear Research Institute Rez, a.s.

Czech Republic

## Abstract

The first part of this paper describes primary coolant monitoring system that has been developed by CHEMCOMEX Praha company especially for the Temelin NPP needs. The whole system basic element is the on-line primary coolant monitoring system is placed in the containment – on a by-pass of the 1st steam generator main coolant pump. The monitor is designed to be able to a long-lasting operation without human incidence. The radionuclide spectrum is measured continually by means of the HPGe detector. The whole measuring procedure is remotely operated from the central server that is placed outside the containment in the chemical service area. Full measuring is automatically analyzed and archived at the central server after spectrum measuring which lasts for several hours. By inosculation on technological information systems the whole set input data are ensured for a fuel failure complex analyze from point of view possible of fuel leakages. In the second part of the paper there are described software expert systems PEPA and PES number of fuel rod failures. The PEPA method is based on evaluation of the instantaneous activity level of gaseous fission products, namely Xe and Kr isotopes. The independence of gaseous fission products on the local physical-chemical processes enables to identify defects with various rate of release of cumulated activity. The model works with three types of fuel element defects, which are characterized by the rate constants of the cumulated activity release. The software application PES allows to calculate the on-line PCI margin of critical fuel rod for all assemblies.

## 1. GAMMA SPECTROMETRY PRIMARY COOLANT MONITOR

On-line gamma spectrometry system is identified for continuous monitoring of qualitative and quantitative radionuclides content of the primary circuit coolant at the 1st and 2nd units Temelin NPP (ETE). Results of measurements data form the basis for:

- Identification of nuclear fuel leakages in the cladding
- Monitoring of primary coolant impact (leakage) to a steam generator

The continuous monitoring of primary coolant is working tool for the detection of unfolding leakage defects in the cladding of fuel rods. Energy calibration is performed by etalon sources ($^{60}$Co +$^{241}$Am) for diameter of hole – 80, 26, 8 and 2 mm.

### 1.1. Process measurement description

A general dispositional diagram is given on the Figure 1.

The basic monitor consists of [1], [2]:

- Collimation system
- Computer network switch and UPS

- Detector with cooling
- Gamma spectrometry trace
- Evaluating system

A sampling trace from duct of the primary circuit beyond main coolant pump (MCP) – by-pass of MCP is lead out for measuring. The take-off trace is achieved by sampled stainless-steel pipeline of diameter 14x2 mm. To ensure time delay of the coolant in the sampling trace, thereby conversion high-energy nuclides with a short half-life (e.g. $^{16}N$), seven small pots of the same proportion as the pipe on the sampling trace are located to slow down the coolant flow. The flow is maintained on a constant value by motor-operated valve with the turbine flow meter.
Heat insulated bleeding pipeline with coolant medium of the same pressure and temperature as the primary circuit leads in particular distance from the detector placed in the collimator table. The beams of gamma radiation fall through a collimator hole on the High Pure Germanium detector - HPGe. The detector pulse signal is processed by the electronic gamma-spectrometry trace and digitalized. Measuring spectra are in adjustable time period processed in the superior computational system OPEN VMS. Control system and evaluating of spectra measurement are assured by means of particular application software, which is installed in the superior computational system. This uses a standard routine and algorithm of the GENIE ESP system for its own spectra evaluating. A data presentation is ensured by the CHEMIS informatory system.
Evaluating of an on-line gamma spectrometry monitoring of the primary coolant circuit is operated automatically. Measurement results are stored in the CHEMIS informatory system of chemical service. There is the library of significant and automatically evaluated radionuclides that is served for measurement spectra evaluating.

## 1.2. Collimation system

A collimation system consists of a detector shielding and a control unit [1]. Shielding is made of lead. Inside, towards the detector, 5 mm thick cupriferous plate is lined. The beam falls to the detector that is collimated by the collimation hole. The circular collimation board (100 mm thick lead) has four collimation holes of different sizes for enhancement of the upper range meter and optimal value of impulse frequency by the electronic line processed. The maximum diameter of the collimation board is 80 mm. It is made of lead and from inside is lined 1 mm thick cupriferous plate. The diameters of the other holes are 26 mm, 8 mm and 2 mm.

The control unit allows:

- Temperature and moisture measurement inside the monitor (relative moisture 0..100%,
  temperature from –30 to + 80°C)
- Test point detector voltage measurement (range +/-10V)
- Signal transmission about loss of cooling water flow by compressor
- Signal transmission about collimation hole setting over detector
- Performance setting of collimation hole engaged
- Signal transmission about outage main power supply of coolant unit
- Assuring of power supply detector right sequence

### 1.3. Communication control system

Data transfer between the monitor control system and its supervisor system is given by means of the remote parallel interface model RPI 554. There are 32 TTL inputs and outputs for data transfer in this module.

### 1.4. Switch network and UPS

The monitor is connected to technological network of Chemistry department over CISCO 1912 switch (12 ports 10Mbps, 2 ports 100Mbps). For a backup of the switch power supply and gamma spectrometry trace is used UPS PowerWare (Uninterruptible Power Supply) 1,5kVA with auxiliary batteries [2].

### 1.5. Ge detector with cooling

The base of monitor is a high pure Germanium detector [1], which is placed inside the shielding. Owing to supposed activity measurement the GC1018 HPGe detector with efficiency about 10% and distinction 1,8keV/1332keV is used. The detector has cryostat cooling by the Cryodyn compress system 22C/350C. With respect to room temperature and thermal energy produced by the compressor is eked out unit Cryodyn with a auxiliary water cooling. Non-essential service water is used for cooling (as shown in Figure 1).

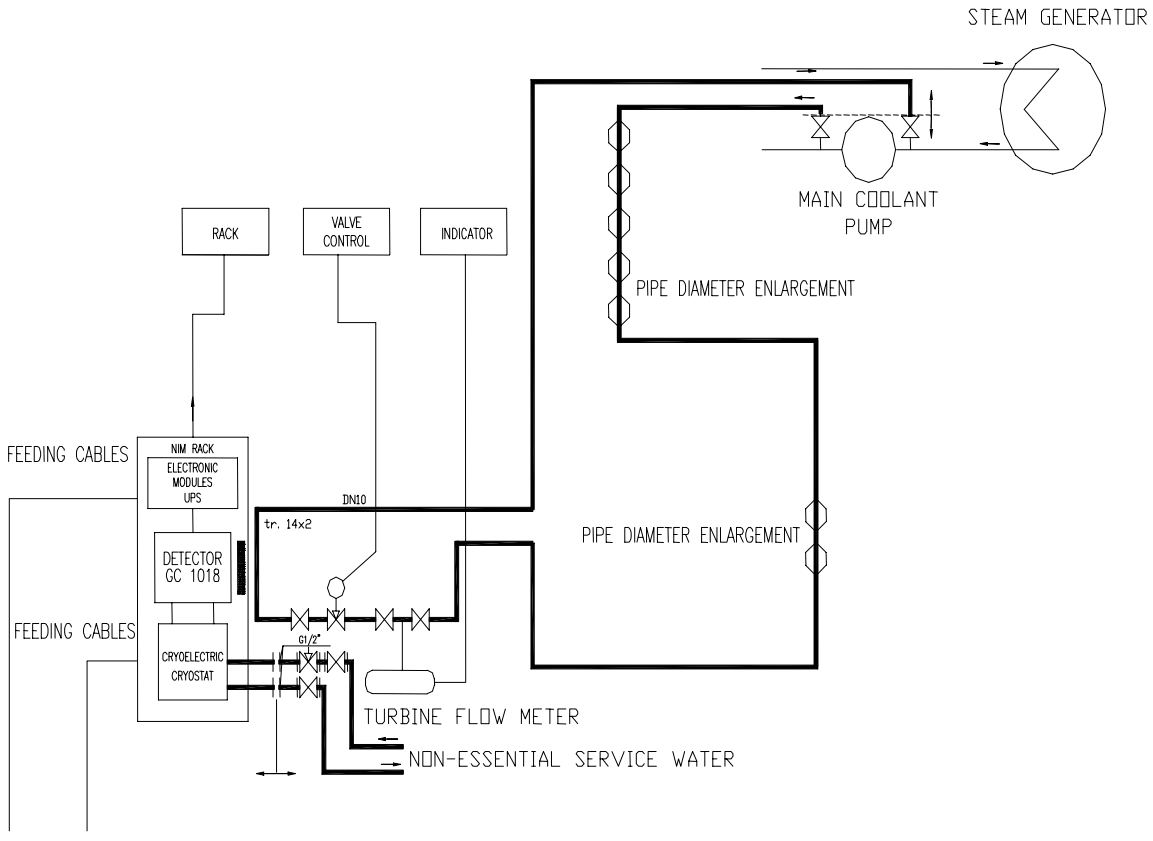


*Figure 1: Technological diagram of primary coolant monitor.*

## 1.6. Gamma spectrometry trace

The hardware part (HW) of the gamma monitoring system was formed by commercially available products of the Canberra-Packard company (see Figure 2). Instead of a standard combination at Amplifier-Analog-to-Digital Converter, the monitor uses the programmable Digital Signal Processor unit DSP 9660 [1]. In connection with Acquisition Interface Module AIM556A the processor offers remote computer controlled treatment of detector signals.
Basic setting of parameters is pursued from the GENIE ESP system and setting-up of the parameters is saved automatically to a spectra measurement file.

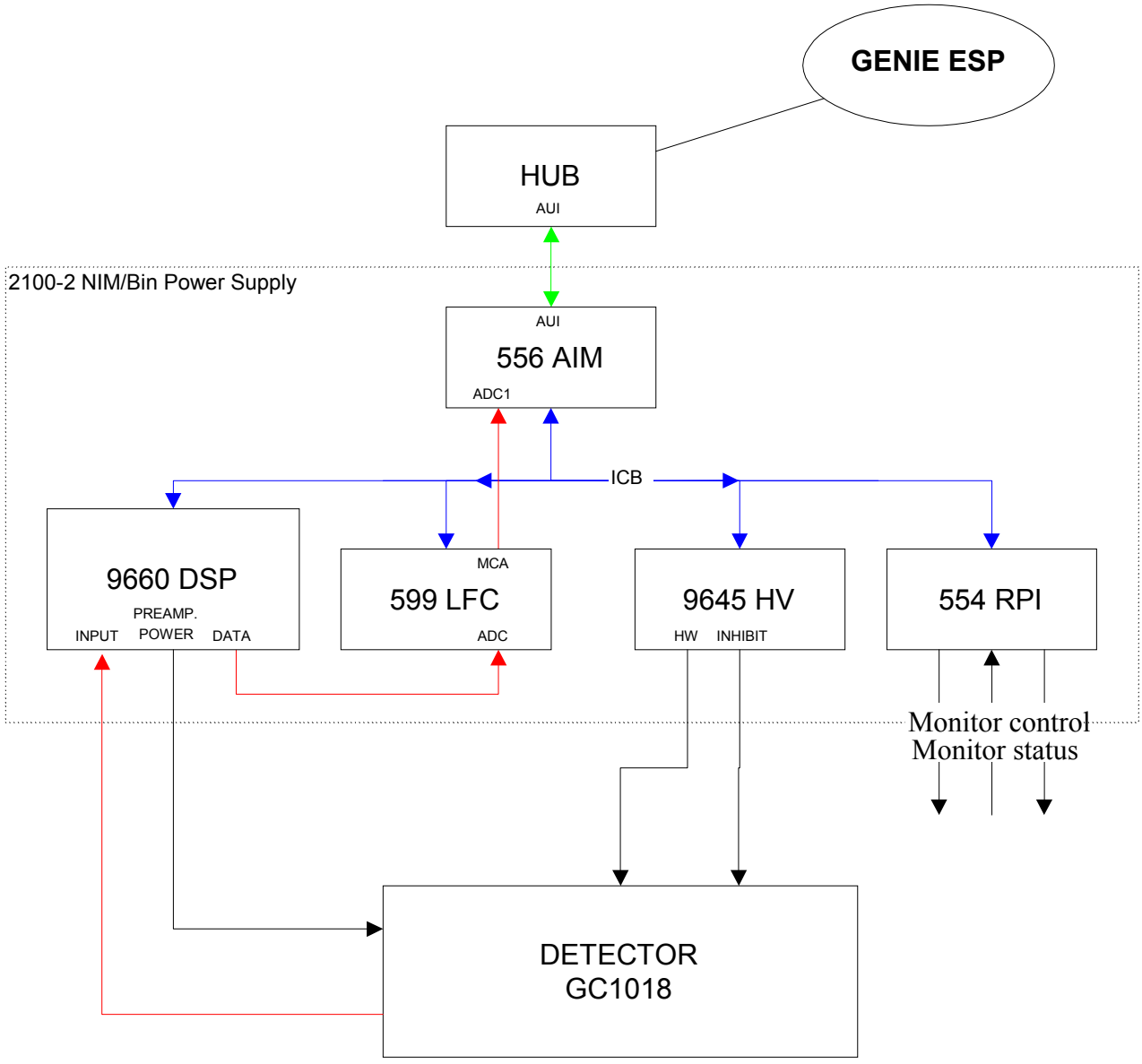


*FIG. 2. Gamma spectrometry system.*

## 1.7. Application software

Measurement, acquisition, analyzing and data transmission run as completely automatic process. Main software features include:

- Set collimation hole according to count of pulses per second (cps)
- Set acquisition live time according to gradient of cps
- Acquisition of spectral data
- Saving and analyzing of spectral data
- Transmission measurement data to the chemistry information system
- Diagnostic of the technology
- Checking humidity in the monitor equipment
- Measurement of the voltage in the detector checking point
- Measurement of the flow cooling water
- Measurement of the temperature compressor cooling medium

Application is divided into two parts, completely automatic technological part and graphic user interface. The technologic module was made for the OPEN VMS 7.2.1 environment (see figure 3). The graphic interface can be used in Windows PC. Whole application is made of independent modules. The communication between modules is solved by means of the TCP packets. Modification or expansion of system is easily done by a modular technology of the system main part of software code was written in the Perl (platform independent on scripting language). For a low level control of technology and analysis spectral data CANBERRA libraries built for VMS was used. A part in MS Windows graphical library TK was used for an external graphical client.

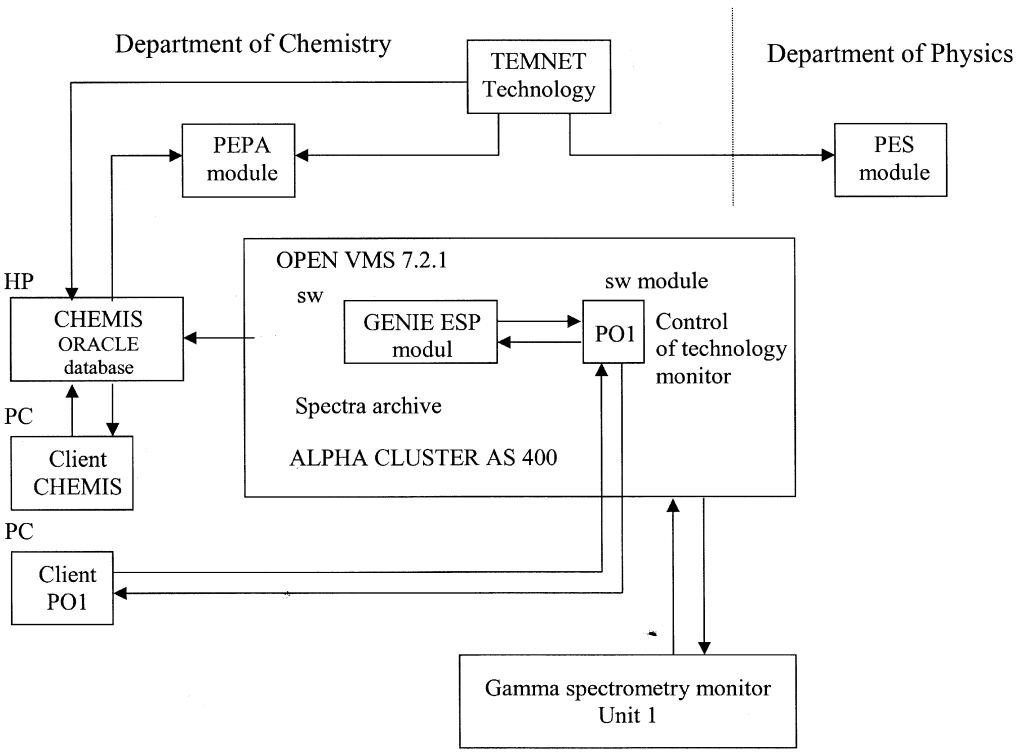


*Figure 3. Fuel monitoring system.*

Application can work in two modes. In the automatic mode all functions are provided automatically without user assistance. The manual mode provides a user control of the technology. A user can select from followed automatic modes:

- AUTO – Fully automatic mode. The collimator hole and live time are set according to cps.
- AUTK - Automatic mode with fixed live time. The collimator hole is set according to cps.
- AUTT - Automatic mode with fixed collimator hole. Live time is set according to cps.
- MANU - Automatic mode with fixed collimator hole and live time.

The module PO1 receives commands from application control in the automatic regime. The way of evaluating of measurement and technology depends on a kind of automatic measurement chosen (regimes AUTO, AUTK, AUTT and MANU).

Diagnostics of equipment and technology is performed in the regime after start. The measuring trace is connected and the high voltage is reached on the detector. Connection is signaled directly on the trace turn on the checking diode IN USE on the module AIM. A cooling control of the detector is carried out.

If any error situation fails, the module PO1 checks on the last calibration test. Calibration checking is performed if the last test is older than 7 days. The energy and efficiency calibration is checked according to an answer of the checking emitter. Energy calibration is tested by the pikes retrieval 59,5 keV $^{241}$Am and 1332,48 keV $^{60}$Co. The efficiency calibration is checked by comparing measurement activity radionuclides on values saved in the PO1_KK.RPT file.

According to automatic regime selected the cycles listed bellow are repeated:

- Spectrum measurement
- Spectrum archiving
- Spectrum evaluating
- Data saving to the CHEMIS
- Calibration checking and measurement of the voltage in the detector checking point if the last test is older than 7 days

Parameters for automatic mode are saved in the file PO1.INI. Radionuclides activity and gradient of activity in the whole spectrum and in the predefined energy areas are checked every 120 seconds. When gradient of activity anywhere in the spectrum or in the predefined areas is higher than limit value the live time is shortened. When activity is higher than limit value collimator is shifted to a lower hole.

When gradient of activity anywhere in the spectrum or in the predefined areas is lower than limit value the live time is set up to a maximum value. When activity is lower than limit value collimator is shifted to a bigger hole.

## 2. DETERMINATION OF FAILURE FUEL NUMBERS - PEPA AND PES MODULES

The principal scheme of the fuel monitoring system is shown on figure 3. It covers two independent parts:

- The PEPA module determines the actual state of elements fuel gladding present in the core during a nuclear reactor operation [4]. This part also enables estimation of the further operation consequence regarding transient parameters.

- The PES module enables assessment of the damage probability as a consequence of fuel-cladding mechanical interaction [3], [4]. On-line version provides continuously information about the local and global power margin to the critical value of stress in the cladding.

### 2.1. PEPA module

The method is based on the evaluation of the instantaneous activity level obtained by direct monitoring of the pipeline (by-pass of the main coolant pump). The monitor consists of spectrometric line with detector that enables to determine activity levels of gaseous fission products, namely Xe and Kr isotopes. The independence of gaseous fission products on the local physical-chemical processes enables to identify defects with various rate of the release of cumulated activity. The model works with three types of fuel element defects, which are characterized by the rate constants of the cumulated activity release during the steady state of the reactor:

- small defects with very slow release rate ($\sim 10^{-6}$ $s^{-1}$);
- medium defects ($\sim 10^{-4.5}$ $s^{-1}$);
- large defects with relatively high release rate ($\sim 10^{-3}$ $s^{-1}$).

The software application PEPA allows to calculate the number of the damage fuel elements. The damage fuel is divided into three groups of gaps – small, middle and large. The code PEPA uses the multiple linear regression method to find such combinations of single types of damaged fuel elements that gives the minimum sum of the squares of differences between the predicted and measured activity level of the selected gaseous fission products group. Verification of the failures predicted number is performed during the reloading shutdown by the on-line sipping test. The assemblies suspected are subjected to the gas-tight canister test (off-line sipping test). In the both procedures statistical treatment is used.

### 2.2. PES module

A number of fuel assembly failures in 1st and 2nd Unit Temelin NPP prompted a study of the potential for pellet-cladding mechanical interaction (PCI) as the principal cause of failure.

PCI fuel failures result from the combined effects of fuel pellet expansion, leading to stresses in the cladding and the presence of an aggressive fission product environment. PCI failures may occur during higher local power ramps after prolonged low power operation. PCI fuel rod failures typically occur in the first row of the bundle closest to the control assembly. For

practical purposes PCI failure is characterized by the following five operational factors associated with a power ramp:

- burnup accumulated prior to the ramp;
- maximum rod power during the ramp;
- power increment during the ramp;
- average power ramp rate;
- dwell time at high power.

For the defect to occur in an LWR, all five parameters have to be in a critical range simultaneously. To show the burnup dependence of PCI failure, correlation between maximum rod power and burnup are most commonly used. It means that a reasonable power ramping restriction could be led to the decrease of the fuel rod damage probability. A typical case of the control system is given in [3]. The similar design for evaluating PCI margin for the WWER-1000 has been developed in the CHEMCOMEX Praha, a.s. The design is based on the following presumptions:

- The equilibrium contact pressure between a fuel pellet and cladding is reached after the long time constant power operation. The value of contact pressure is in the range of 5-10 MPa. In this condition the actual value of local fuel element power "P" is equal to "conditioned" power level "$P_{kond}$".

- The contact pressure rapidly increases after the power ramp as a consequence of the fuel pellet thermal deformation and the stress in cladding slowly relaxes to the new equilibrium value. It corresponds to the gradual increasing of the "conditioned" power $P_{kond}$ to the new actual power level (power "conditioning").

- The contact pressure rapidly falls down after the power drop, which causes the gap opening. During following time the gap is closed and the contact pressure slowly decreases to the new equilibrium value. This process corresponds to the gradual decreasing of the "conditioned" power to the new power level (power "deconditioning").

It means that the "conditioned" power $P_{kond}(t)$ is the power level corresponding to the actual contact pressure in the time "t". Kinetics of conditioning and deconditioning of power is a function of difference ($P - P_{kond}$) and can be describes by the equation:

$$\frac{d(P - P_{kond})}{dt} = a \cdot \exp(b \cdot P)\,(P - P_{kond}) \qquad (1)$$

Analytical solution equation (1) for constant power ramp is done:

$$P_{kond}(t) = \exp(a \cdot t \cdot \exp(b \cdot P)) \cdot (P_{kond0} - P) + P \qquad (2)$$

Where empirical constants "a, b" both for conditioning and deconditioning were estimated using results of two type power ramps calculations by the FEMAXI-V code [8]. This code is able to describe the thermal and mechanical behavior of the fuel rod during transients. Calculated values of contact pressure, tangential strain of cladding and kinetics of the gap closing and reopening were fitted to obtain their empirical time and power dependence.

The probability of fuel cladding failure increases rapidly if the actual value of power exceeds the critical level given as the sum of actual conditioning power and maximum admissible local power ramp. Permissible exceeding of power over the conditioned power is called a critical power ramp $dP_c$. In a typical situation when the power ramp occurs from the stationary state at such burnup level that radiation impact on mechanical properties are saturated and the gap is closed, the $dP_c$ is the only characteristic deciding of breaking of a fuel element. Base on operation WWER-440 units at Bohunice NPP, the statistic dependence of damage occurrence on the power ramp magnitude and burnup was determined. An exponential function of the following type was applied to the experimental data from point of view conservative calculation (see line for PCI threshold on the figure 4):

$$dP_c(Bu) = 75 + 105 .\exp(-0.0779.Bu) \cdot \qquad (3)$$

where: $dP_c$ $W.cm^{-1}$ ;
burnup Bu $MWd.(kgU)^{-1}$.

The maximum power ramps on hot rod during power cycles for all leaking assemblies are showed on the figure 4. There were only two cases crossed the PCI threshold limit given by the equation (3). The worst case was analyzed father by the advanced thermal-mechanical code FEMAXI-V. The results obtained reflected an enclosure gap, but contact pressure was higher than the equilibrium pressure.

### 2.3. Technical realization

Module PES has been developed in the CHEMCOMEX. To calculate conditioned power, which is integral variable, the following input variables have to be obtained from other systems:

- Reactor thermal power;
- Fuel assemblies linear power distribution;
- Fuel burnup distribution;
- Fuel assemblies radial power peaking;
- Previous conditioned power distribution.

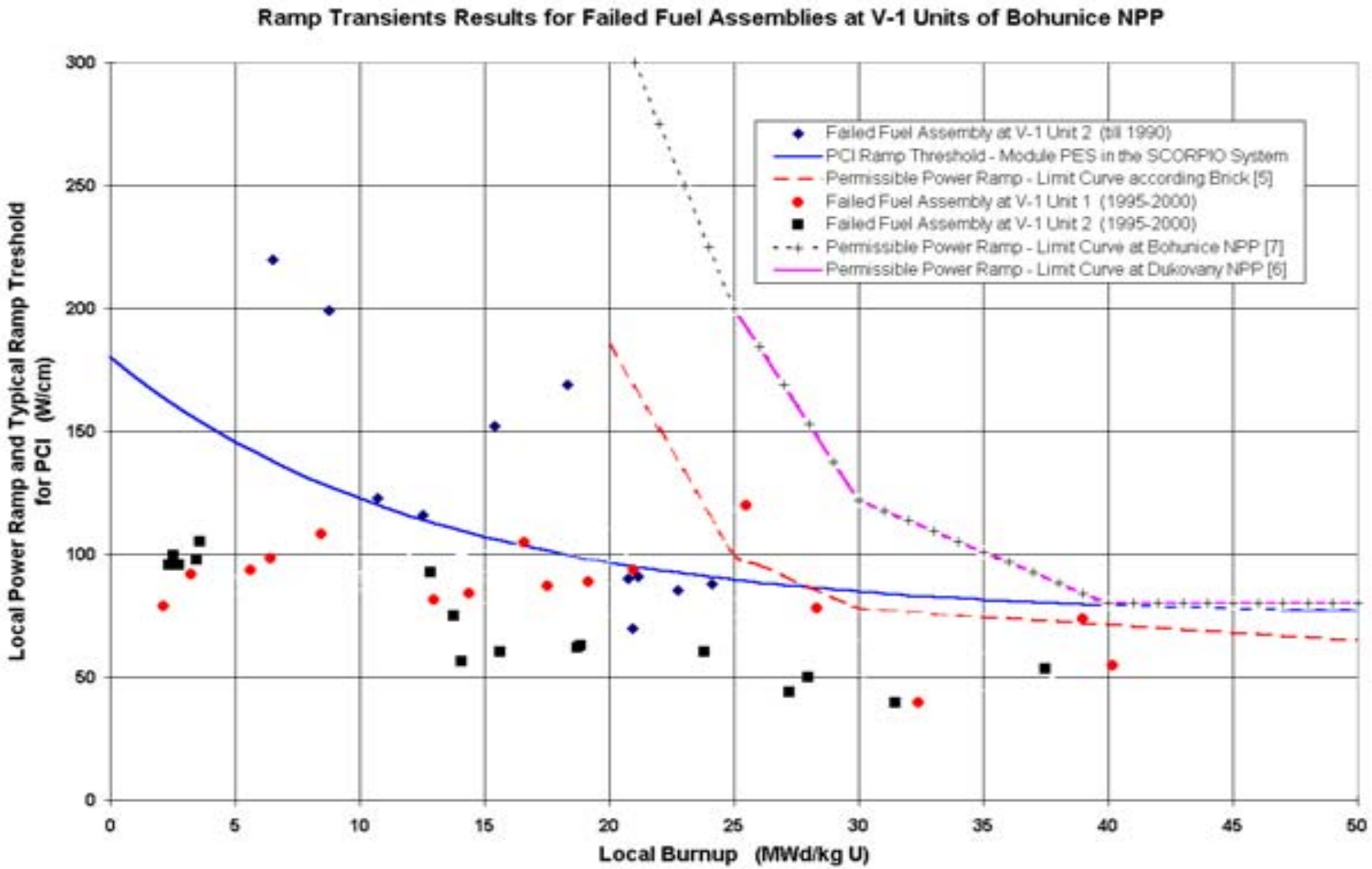


*Figure 4. Theoretical dependence of damage occurrence on the power ramp magnitude and burnup, maximum ramp transient results for failed fuel assemblies WWER.*

The on-line version simulates the probable power load and fuel burnup in 163x40x(6+19) = 163000[float] points of the core, calculated by Beacon system, and checks the values of conditioned power with the local power maximum permissible level.

## 3. CONCLUSION

On-line gamma spectrometry system completely installed at the 1st units Temelin NPP has been functional more than one year. The monitor installed in its final form will be represented an-easy-to-use system that provides complex information on:

- Primary coolant radiation situation in a reactor core during a steady state operation
- Probable number of damage fuel elements present in a reactor core and estimation of their damage scope and a trend
- Probable primary coolant radiation situation development during reactor transient with the possibility to optimize technological parameters during transients
- Instantaneous power local margin to the critical level of a fuel-cladding mechanical interaction
- Power global margin of a reactor unit for every moment of operation.

The PES and PEPA modules key parts have been step by step verified at Bohunice and Dukovany on WWER 440 units. At present is needed to tune computational constants for the modules on Temelin fuel. Further development of the PES and PEPA is directed to design of the modern complex expert systems with user-friendly environment, which assures interactive support for operating personnel.

## REFERENCES


[1] SEMMLER M., et al.: Analysis of technological bindings bearing on transport fission products and appreciation of the fuel state in the ETE. Report CHEMCOMEX Prague, CCE-30-7-00513, Prague, 2000.

[2] Novak L., et al.: Operating rules of gamma spectrometry primary coolant monitor service (MPC). Report CHEMCOMEX Prague, CCE-31-7-00077a, Prague, 2002.

[3] ALEITE, W., von JAN, R.: Germany design for optimum operating flexibility. Nuclear Engineering Int., December 1985.

[4] BARTA O., et al.: The application of the PES-PEPA Expert System at the Dukovany Power NPP, Techn.Comm.Meeting on Fuel Failure in Normal Operation of Water Reactors: Experience, Mechanisms and Management, 26-29 May 1992, Dimitrovgrad, Russian Federation.

[5] BRIK et al.: Local linear heat rate ramps in the WWER-440 transient regimes. Proceedings of the eighth Symposium of AER. p.313, Czech Republic, September 1998.

[6] Operating Conditions of the Dukovany NPP, Czech Republic, 2001.

[7] Operating Conditions of the Bohunice NPP, Slovak Republic, 2001.

[8] SUZUKI, M. UETSUKA, H.: Light Water Reactor Fuel Analysis Code FEMAXI-V, NEA-1080/07, NEA C00K44.

# REGULATION OF THE FISSION PRODUCT ACTIVITY IN THE PRIMARY COOLANT AND ASSESSMENT OF DEFECTIVE FUEL ROD CHARACTERISTICS IN STEADY-STATE WWER-TYPE REACTOR OPERATION

P. SLAVYAGIN, L. LUSANOVA, V. MIGLO
Russian Research Center "Kurchatov Institute, Institute of Nuclear Reactors,
Moscow, Russia Federation

**Abstract**

Regulation of the maximum limiting levels of fuel cladding failure and normalizing of the fission product activity in the primary coolant of WWER-type reactors for steady-state reactor operation is considered. It is shown that for the advanced nuclear power plants with WWER-type reactors the maximum permissible level of fuel rod failure and fission product activity in the primary coolant must be determined taking into account the actual level of the fuel rod reliability, possible failures of other reactor equipment (steam generator tubes) and efficiency of the primary and secondary coolant purification systems. The computer code TIMS developed in RRC "Kurchatov Institute" for the assessment of the number of failed fuel rods and defect characteristics by comparing measured and calculated values of fission product activities in primary coolant is described. The important feature of the code is the increase of reliability of assessment by taking into account the actual errors of fission product activity measurements and possible contamination of primary circuit.

## 1. REGULATION CONCEPT FOR THE MAXIMUM LIMITING LEVELS OF WWER FUEL CLADDING FAILURE

The regulation instruction PBYa-RYu-AS-89 [1] currently in force in Russia specifies the operation limit of fuel rod failure for the WWER-type reactors as 0.2% of fuel rods with microdefects and 0.02% - with serious defects. Should this operation limit be violated, the operating personnel must perform actions for bringing the reactor to normal operation, and in case the normal operation of the reactor cannot be restored the reactor must be shut down.

On the other hand, the advanced NPP designs have a limiting failure level of 0.1% of the total number of fuel rods in the core [1].

It should be noted at this point that normalization of the maximum permissible levels of cladding failures and relevant levels of fission product activity in the reactor coolant is first of all a problem of NPP design. This characteristic is interconnected with such market depend economic factors as fuel cost, electricity and NPP construction costs, assurance of fuel warranty, agreement with current legislation etc. In the end the relation between the actual fuel rod reliability and that specified in the design determines the design cost and commercial risk associated with operation of the NPP.

As far as organization of the normal nuclear power units is concerned, other factors restricting the limiting levels of fuel rod failure may be important (for example, the limiting levels of fission product activity of the primary and secondary circuits as well as restrictions on the reactor coolant leaks into the secondary circuit).

The maximum permissible number of failed fuel rods in the core, as well as type and size of defects, taking into account the efficiency of the coolant purification system and the limiting depressurization degree of other equipment (e.g., steam generators), determines the maximum permissible fission product activity in the coolant during the normal operation of the reactor.

These restrictions must be correlated because otherwise a situation may occur when the NPP bears losses because of electricity underproduction, with no formal grounds for claims to the vendors of the equipment (fuel rods and steam generators).

The coolant activity level depends not only on the number of failed fuel rods and technical characteristics but also on the reactor power whose rise results in increased amount of fission products escaping from the failed fuel rods.

In the normative NPP operation documents, which are now in force in Russia, the following maximum permissible levels are established:

(a) Total specific activity of iodine - 131-135 in the reactor coolant:
  (i) Limits of safe operation:
    $1.85\times10^{8}$Bq/kg for WWER-1000 and $7.4\times10^{7}$Bq/kg for WWER-440;
  (ii) Operational limits:
    $3.7\times10^{7}$Bq/kg for WWER-1000 and $1.48\times10^{7}$Bq/kg for WWER-440;

(b) Specific activity of iodine-131 in the reactor coolant:
  (i) Limits of safe operation:
    $1.85\times10^{7}$Bq/kg for WWER-1000 and $9.25\times10^{6}$Bq/kg for WWER-440;
  (ii) Operational limits:
    $3.7\times10^{6}$Bq/kg for WWER-1000 and $1.85\times10^{6}$Bq/kg for WWER-440;

(c) Specific activity of iodine-131 in the boiler water of one steam generator:
  (i) Limit of safe operation:
    $7.4\times10^{2}$Bq/kg for both types of reactors;
  (ii) Operational limit:
    $3.7\times10^{2}$Bq/kg for both types of reactors;

(d) Permissible value of the reactor coolant leak from the primary into the secondary circuit:
  (i) Limit of safe operation:
    5 kg/hr per steam generator for both types of reactors;
  (ii) Operational limit:
    4 kg/hr per steam generator for both types of reactors.

## 2. COOLANT ACTIVITY EVALUATION MODEL

Fuel reliability is measured usually by monitoring the fission product activity in primary coolant during normal reactor operation. In Russia, for NPPs with WWER-type reactors, such evaluation is based mainly on the levels of I-131, I-132, I-133, I-134 and I-135 in the coolant. Comparing the calculated values of activity of these fission products with the measured ones it is possible to estimate the number of leaking rods and characteristics of defects. In principle, such procedure could be realised using not only activities of iodine isotopes, for instance, using inert gaseous fission products, but choice of iodine isotopes for failed fuel control has some ground reasons.

First, the modelling of iodine behaviour in the primary coolant, as well as behaviour of inert gases, can be performed more comprehensively than the modelling of non-volatile and non-gaseous fission products: all parameters influencing the activity levels in primary coolant (sorption coefficients, for instants), are well known.

Secondly, the absolute values of iodine and gaseous nuclide activities in primary coolant are usually much higher than activities of other fission products; the measurement of activities of iodine and gaseous isotopes in coolant samples do not cause difficulties.
And thirdly, the simplicity of water sampling excludes losses of iodine and provides the highest accuracy of iodine activity measurements in comparison with measurements of gaseous nuclide activity in PWR- and WWER-type reactors.

### 2.1. Modelling of the Migration of Fission Products – RELWWER-2.0 Computer Code

The release of fission products in the primary coolant can be connected quantitatively with the characteristics of the failed fuel rods:

(a) number of leaking rods;
(b) fuel irradiation parameters (linear power, temperature)
(c) type of cladding defects.

The RELWWER-2.0 computer code developed in RRC "Kurchatov Institute" and qualified by Russian authorities, is used to provide these computations. The approach to modelling of fission product behaviour used in the RELWWER-2.0 computer code was initially developed at the end of the 1960's [2] and finally generated in the beginning of the 1980's [3] on the basis of analyses of the data on fission product activities in primary coolants of WWER-type reactors.

Due to difference in WWER fuel rod design in comparison with PWR and BWR fuel rod design (presence of the axial hole in fuel pellets), the migration of fission products released from the fuel through the gap to the primary coolant has multistage character and is described in the RELWWER code as follows.

1st stage. Creation of fission products inside the fuel by heavy metal fission, decay of precursors in decay chains and neutron capture.

2nd stage. Escape of fission products from the fuel through the outer fuel pellet surfaces by various mechanisms: recoil release, knock-out release, thermal and radiation induced diffusion.

As the maximum temperature of uranium dioxide in WWER-type reactors during steady-state operation does not exceed 1000-1100$^0$C and taking into account the existence of the real errors of fission product activity measurements (it permits to "restrict" the number of release models at code verification), it is sufficient to use only two first mechanisms for description of observed activities in primary coolant. It permits us to obtain the value $R_1$ of such release (atoms/s) for each fission product.

*3rd stage.* Accumulation of fission products in the fuel-to-cladding gap (taking into account the own radioactive decay and decay of precursors) and release from the gap to the volume of the axial hole. If we know the release rate $R_{1i}$ of fission product "i" from fuel to the gap, we can write the next set of **I** differential equations (I is a number of radionuclides in considered decay chain) for number $N_{1i}$ of atoms of this fission product in the gap:

$$\frac{dN_{1i}}{dt} = -(\lambda_i + \mu_{3i}) \bullet N_{1i} + R1_i + F_{1i} \qquad (i=1,2\ldots I)$$

where

$\mu_{3i}$ is the gap-to-hole release rate constant of nuclide "i" ($s^{-1}$),
$\lambda_I$ is the radioactive decay constant ($s^{-1}$).

The number of equations is equal to I - number of isotopes in a given decay chain. Here $F_{1i}$ is the additional source of a given nuclide due to radioactive decay of precursors already accumulated in the gap, atoms/s:

$$F_{1i} = \sum_{j=1}^{i-1} \lambda_j B_{ji} N_{1j} ,$$

$B_{ij}$ are the elements of matrix **B**, describing branching of the decay chain considered, rel. units. Numerically element Bji is equal to probability of decay of an isotope with number j in an isotope with number i.

The release of fission products from the fuel-to-cladding gap to the volume of the axial hole occurs through the gaps between fuel pellets or cracks in pellets. The release rate $R_{g\to h}$ is given by formulae:

$$R^{i}_{g\to h} = \mu_3 \times N_{1i}$$

The value of $\mu_3$ used for computations is different for various fission products and depends on their physical and chemical properties. The difference between iodine and gaseous nuclide behaviour is due in principle to chemical sorption of iodine on internal surfaces of the fuel rod: surfaces of uranium dioxide open porosity and of cladding. It is known that some fission products exist at operating temperatures in free volumes of fuel rod only in gaseous form (noble gases), others – in volatile form (halogens, alkaline metals), third - in non-volatile forms (practically all other fission products). The volatile fission products, by virtue of their physical-chemical properties, nevertheless keep their ability to be absorbed on surfaces of uranium dioxide, thus the only part of such fission products exists as gas or vapour. The fission products can migrate inside a fuel rod only in volatile form, and such migration can be described as follows.

The typical geometrical sizes of such fuel elements, as grains, open pores, typical roughness on the fuel surface are very small. Due to this fact, the surface-to-volume ratio in the gap has a relatively high value. Taking into account the relatively high fuel temperature, it is necessary to expect fast kinetic of atom absorption - desorption processes on the surfaces of nuclear fuel.

It results in a fast establishment of equilibrium between concentration of atoms in gas and on a surface of fuel, so the ratio between concentrations can be described by a constant of equilibrium $\nu$ (like the Henry constant), depending on chemical properties of nuclides, temperature and properties of a surface. If $n$ and $m$ - concentrations of atoms of the given nuclide in gas and on surfaces, then

$$\nu = n/m$$

If Q is the number of atoms in the gap, and N and M are the number of atoms in a gas phase and on surfaces accordingly, so Q = N + M, the balance equation for a gap can be written as follows:

$$\frac{dQ}{dt} = -\lambda Q - \mu_3 N + f = -\lambda(N+M) - \mu_3 N + f$$

Here f is the sum of all sources of a nuclide. That, by definition,

$$\frac{N}{M} = \frac{nV_3}{mS} = \nu \frac{V_3}{S}$$

($V_3$ and S - volume of a gap and surface of fuel limiting this volume), and taking into account, that by definition the release rate is equal to $\mu_3 \bullet N$, we obtain the expression for the release rate from the gap:

$$\mu_3 N = \frac{\mu_3^{©}}{\lambda + \mu_3^{©}} f$$

Here $\mu_3^{©}$ is a "visible" mass transfer constant in the gap:

$$\mu_3^{©} = \frac{\mu_3}{1 + \frac{S}{V_3}\frac{1}{\nu}}$$

For chemically inert gaseous fission products the basic mechanism of absorption is the physical absorption. At temperatures of gas in the gap of operating fuel rod of order of $350^0$ C and higher the physical gas absorption is practically negligible, the equilibrium is essentially moved in the gas phase, the value of a constant of equilibrium $\nu$ is very high (practically infinite), and the value of a «visible» mass transfer constant coincides with actual:

$$\mu_3^{©} \text{ (gaseous)} = \mu_3$$

For volatile fission products, the constant of equilibrium is limited, and the ratio of a "visible" mass transfer constant to the actual one depends on the gap surface-to-volume ratio. If a gap ***b*** between fuel and cladding exists, the surface-to-volume ratio is determined by the value of the gap and geometrical surface of fuel:

$$\boldsymbol{S/V_з = 1/b}$$

The value of the non-blocked gap is equal to $(0{,}50\text{-}1)\times 10^{-4}$ m, so $S/V_з = (1\text{-}2)\bullet 10^4$ $m^{-1}$.

If the gap will be closed, the migration of fission products occurs through a porous body, practically through the open pores of fuel, thus the surface-to-volume ratio is equal to

$$S/V_з \cong 1/d_n \cong 10^6 \text{ m}^{-1}$$

($d_n$ is the mean diameter of intergranular pores).

As it is seen from estimations, the surface-to-volume ratio can change practically over two orders of magnitude. This estimation shows that the effect of gap closing can significantly affect on the value of «visible» mass transfer constant for volatile nuclides. Really, the

measurements described in [3] have shown that the reduction of a "visible" mass transfer constant at closing a gap in WWER fuel rods for iodine isotopes has a value of 10 comparing to a the non-closed gap, while the mass transfer constant for noble gases has not changed. Before blocking of the gap the values of mass transfer constant for noble gases and iodine were practically identical.

Further is accepted, that in the event, then during an irradiation of a fuel rod the radial gap between a cladding and fuel is kept open, the value of $\mu_3$ will be identical for radionuclides of gaseous and volatile fission products:

$$\mu_3(\text{volatile}) = \mu_3(\text{gaseous})$$

At blocking of a gap the absolute values of factors will be as following:

$$\mu_3(\text{volatile}) \approx (1 \div 2) \bullet 10^{-6}\ c^{-1}$$
$$\mu_3(\text{gaseous}) \approx 4 \bullet 10^{-5}\ c^{-1}$$

During design calculations the value $4\times10^{-5}s^{-1}$ is used for gaseous nuclides. For iodine the value of $\mu_3$ depends on fuel rod linear power and is accepted equal to $1\times10^{-6}s^{-1}$ for mean linear power ~12 kW/m (typical for WWER-440 reactor) and $2\times10^{-6}\ s^{-1}$ for a mean linear power ~18 kW/m (typical for WWER-1000 reactor).

For non-volatile and non-gaseous nuclides the value of $\mu_3$ is equal to zero.

It is interesting, that the above mentioned $\mu_3$ values, used in the RELWWER-2.0 computer code and obtained from the analysis of the data of operating reactors, practically coincide with the values of escape rate constants, obtained and used, for example, by C.E.Beyer [4] ($\varepsilon>1\times10^{-6}s^{-1}$ for iodine and $\varepsilon>4\times10^{-5}s^{-1}$ for gases) or by B.J.Lewis [5] ("typical" values $\varepsilon=1\times10^{-6}s^{-1}$ for iodine and $\varepsilon=2.1\times10^{-5}s^{-1}$ for gases).

In design calculations the value of $N_1$ is used for assessment of fission product activity in the reactor coolant during operational transients and reactor shutdown (spiking of iodine).

*4th stage.* Accumulation of fission products in the volume of the axial hole and release from the hole through the defect to the coolant. As for radial gap, we can write the set of differential equations for number $N_{2i}$ of atoms in the volume of an axial hole:

$$\frac{dN_{2i}}{dt} = -\left(\lambda_i + \mu_{1i}\right) \bullet N_{2i} + R2_i + R^i_{g\to h} + F_{2i}$$

where

$\mu_{1i}$ is the release rate constant of nuclide "i"($s^1$),
$R_{2i}$ is the direct release rate from fuel to the volume of an axial hole.

In this equation the value of $F_{2i}$ is the additional source of a given nuclide due to radioactive decay of precursors already accumulated in the hole, atoms/s.

The value of $\mu_{1i}$ is defined as the release rate of a given fission product from the axial hole to the coolant. For fuel rods with an axial hole in fuel pellets this parameter seems to be more acceptable for the characteristic of fuel rod failure than $\mu_3$. For such type of fuel rods the mass exchange constant $\mu_3$ practically does not depend on size of defect and is due only to the thermophysical parameters of fuel rod (linear power); in opportunity, the intensity of mass

exchange between the coolant and the volume of the axial hole, a $\mu_{1i}$ constant, directly depends on defect size.

The value of $\mu_{1i}$ is non-zero for volatile and gaseous nuclides and could change in a wide range from $10^{-6}s^{-1}$ for "gaseous untightness" up to $10^{-2}s^{-1}$ for big defects as a fuel rod cross break. For design coolant activity calculations the value $5\times10^{-5}s^{-1}$ is used (expert estimation).

The release rate $R_{h\to c}$ of fission products from failed fuel rod to the coolant is equal to

$$R^i_{h\to c} = \mu_{1i} \bullet N_{2i}$$

*5th stage.* Accumulation of fission products in the primary circuit.

The redistribution of fission products released from failed fuel rods between coolant, ion-exchange filters and internal surfaces of primary circuit is described by the set of next equations:

$$\begin{cases} \dfrac{dMT_i}{dt} = -(\lambda_i + \eta_{fi} + \eta_w + \eta_o + \zeta_i) \bullet MT_i + + R^i_{h\to c} + \chi_i MN_i + \\ + \sum\limits_{j=1}^{i} \left\{ \lambda_j B_{ji} \left[ MT_j + MF_j NG_i + MN_i \right] \right\} + R^i_{cont} \\ \dfrac{dMN_i}{dt} = \zeta_i MT_i - (\lambda_i + \chi_i) \bullet MN_i \\ \dfrac{dMF_i}{dt} = -\lambda_i MF_i + \eta_{fi} MT_i + (1 - NG_i) \bullet \sum\limits_{j=1}^{i} \lambda_j B_{ji} MF_j \end{cases}$$

where

$MT_i$ is the number of atoms in the coolant,
$MF_i$ is the number of atoms, accumulated in ion-exchange filters,
$MN_i$ is the number of atoms on the internal surfaces of primary circuit,
$\eta_{fi}$ is the purification rate constant for ion-exchange filters operation ($s^{-1}$),
$\eta_w$ is the removal rate constant with coolant leakage's ($s^{-1}$),
$\eta_o$ is the purification rate constant for degassing operation ($s^{-1}$),
$\zeta_i$ is the effective sorption constant ($s^{-1}$),
$\chi_i$ is the desorption constant ($s^{-1}$),
$NG_i$ is the constant equal to 1 for gaseous nuclides and 0 for non-gaseous nuclides,
$R^i_{cont}$ is the source of fission products due to surface contamination by uranium (atoms/s).

It is assumed that all nuclides produced after decay of precursors already retained by filters, remain on filters, excepting gaseous nuclides; all nuclides produced after decay of precursors sorbed on surfaces, pass into the coolant.

The equilibrium ($dMT_i/dt = 0$) solution is written as:

$$MT_i = \frac{R^i_{h\to c} + R^i_{cont} + \sum\limits_{j=1}^{i} \lambda_j B_{ji} NG_j \bullet \left[ MT_j + MF_j NG_i + MN_j \right]}{\lambda_i + \eta_{fi} + \eta_w + \eta_o + \dfrac{\varsigma_i \lambda_i}{\lambda_i + \chi_i}}$$

The specific calculated activity $A_{ci}$, Bq/kg, of a given radionuclide – fission product in primary coolant is given by expression:

$$A_{ci} = \frac{\lambda_i M T_i}{M}$$

where M is the mass of coolant (kg).

The value of effective sorption constant $\zeta$ for iodine is equal to $10^{-6}s^{-1}$ and was obtained from activity measurements in special experiments on operating WWER-440 and WWER-1000 reactors with switching-off of the coolant purification system. For gaseous nuclides this constant is equal to zero.

Except for failed fuel rods, there are also other sources of fission products in reactor core. At first, it is natural uranium in cladding material. For zirconium the content of uranium is estimated by value of $5\times10^{-6}$(kg of U)/(kg of Zr) [6]. It provides very low levels of fission product activity, which could be observed only during reactor operation with "pure" core without leaking rods in early period of reactor operation. These levels, as measured in coolant of WWER reactors before appearance of the first failed fuel rod, are due to pure recoil release and are equal typically to (1..5) $\times10^{2}$Bq/kg of coolant and coincide well with theoretical calculations [7]. The main evidence of this type of source is the absence of R/B (release-to-birth ratio) dependence on $\lambda$ (for instance, R/B for I-131 is equal to R/B for I-134).

Second, the contamination of rod surfaces with fuel during fabrication of fuel rods or uranium surface contamination. This contamination is a well-known fact and due mainly to fuel losses from previous failed fuel rods (see, for example, [8]. The main difference from above-mentioned sources is that R/B dependence on $\lambda$ has a slight slope, so R/B for I-131 is 2-3 times greater than R/B for I-134. This difference is due to the fact that fuel released from failed rods exists in the form of particles – grains of uranium dioxide, with dimensions comparable with fission fragments range in fuel, and release rate from particles is due to all mechanisms possible in existing temperature conditions, not only to recoil release. The fission product activity due to tramp contamination varies by two or three orders of magnitude and should be taken into account during evaluations.

The RELWWER-2.0 computer code has been verified using reported primary coolant activity in Loviisa-1,2 with WWER-440 reactors. The irradiation history and power of failed fuel rods and characteristics of defects were known (see, for example, [7]). The comparison of predicted and observed activities is illustrated in Fig.2.

Figure 1 demonstrates the calculated (R/B) dependence on decay constant (relative units) for iodine sources considered above: 1 – iodine release from failed fuel rod (WWER-440, mean linear power, $\mu_l=5\times10^{-5}s^{-1}$), 2 – gaseous nuclide release from failed fuel rod (WWER-440, mean linear power, $\mu_l=5\times10^{-5}s^{-1}$); 3 - natural content of uranium in zirconium, 4 – uranium surface contamination (typical dependence). The measured (R/B) values for iodine and gaseous fission products for uranium in zirconium are plotted too (given in [7]). Calculations have been performed using the RELWWER-2.0 computer code.

The RELWWER-2.0 computer code predicts fission product activity in the primary coolant of WWER-type reactors during normal steady-state operation with a standard deviation of (0.3-0.4).

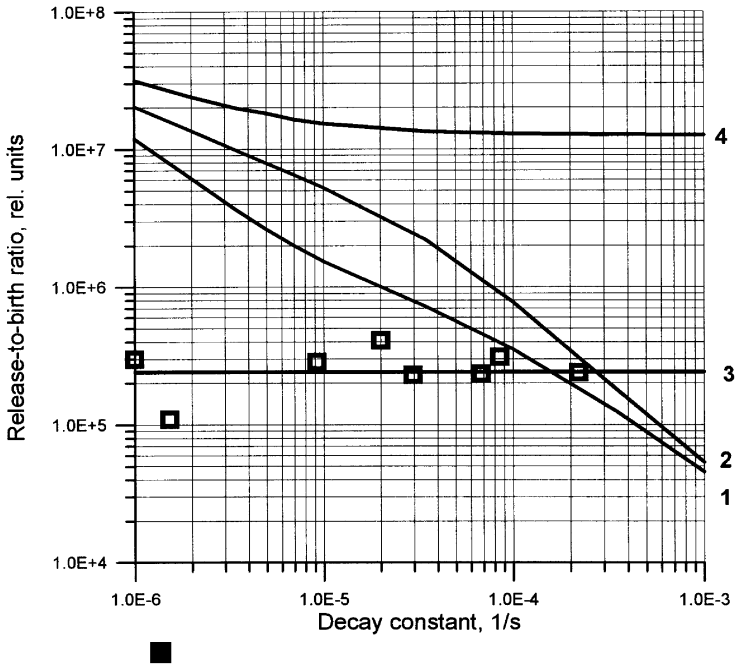


*Figure 1. Release-to-birth ratio for various sources of fission product versus isotope decay constant:*
*1 – iodine from leaking fuel rod;*
*2 – gaseous nuclides from leaking fuel rod;*
*3 – natural uranium in zirconium;*
*4 – uranium surface contamination;*
*- natural uranium in zirconium, measured data.*

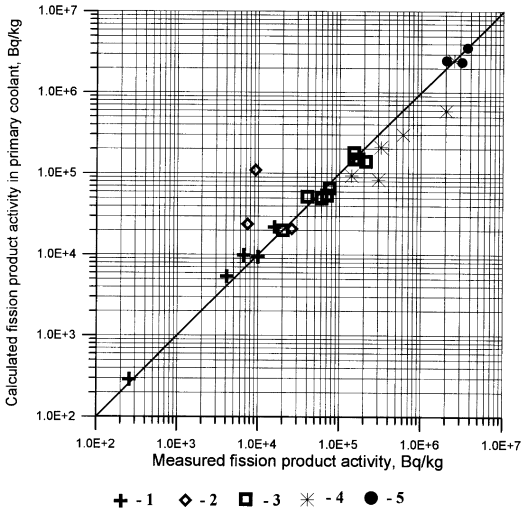


*Figure 2. Comparison of predicted and observed activities of fission products in primary coolant of Loviisa-1,2 NPP*
*Legend:*
*1 – iodine activity due to uranium in zirconium;*
*2 - gaseous activity due to uranium in zirconium;*
*3 - iodine activity due to single leaking rod;*
*4 - gaseous activity due to single leaking rod;*
*5 – iodine spiking due to leaking rods.*

2.2. Evaluation of Failed Fuel Characteristics

The evaluation of leaking rod number and defect characteristics is performed using the well known method of comparison of calculated and measured activities of certain fission products in primary coolant in steady-state reactor operation. The main principle of such estimation is the analysis of ratio between measured activities of radionuclides with identical chemical and physical properties (mainly iodine or noble gas isotopes) but with sufficiently different decay constants. It permits to estimate the main type of defects and after this the number of failed fuel rods. As mentioned above, in Russia, for NPPs with WWER-type reactors, such evaluation is based on steady activities of I-131, I-132, I-133, I-134 and I-135 in the coolant.

The main problem of failed fuel characteristic determination is that *a priori* it is never known that fuel rods are failed and hence what their operation parameters are. For this reason, it is possible to estimate only mean characteristics of the entire failed fuel rod population (excepting, may be, the case with a single leaking rod). Another problem is that the fission product activity in primary coolant is due not only to release from failed fuel rods; there are additional sources of fission products, mainly due to fuel surface contamination. Natural uranium in zirconium provides very low activity levels and does not create problems at evaluation of failures.
The additional problem arising at estimation, is presence of errors of activity measurements. When we compare theoretical and measured ratios of activities of different nuclides and try to estimate the release rate constant of $\mu_1$ using dependence on $\lambda$ even for absolutely adequate modelling, we can obtain situation when the assessed value of $\mu_1$ would be negative for some pairs of isotopes and positive for other pairs, and this effect will be due to existence of errors in activity measurements.

To avoid the above-mentioned problems, a special algorithm was developed and used in elaboration of the TIMS computer code. The main idea of this algorithm is follows.

Let $A_{mi}$ and $\Delta A_{mi}$ be the measured activity of nuclide "i" and an error of the measurement, performed during steady-state reactor operation. Let $A_{ci}(\mu_1 >> \lambda)$ is calculated activity due to single failed fuel rod for $\mu_1 >> \max(\lambda)$, for instance, $\mu_1 = 10^{-1} s^{-1}$.

1st step. We calculate the normalized activities

$$A_{Ni} = \frac{(\lambda_i + \eta_{fi})}{\lambda_i \alpha_{ci}} A_{mi}$$

where $\alpha_{ci}$ is cumulative yield per fission.

If the ratio of $A_N$(I-131)-to-$A_N$(I-134) is less than 3, we should conclude that the main source of iodine activity in core is uranium surface contamination. In this case we can calculate the value of such contamination; for indication of failed fuel rods we should study gaseous fission product behaviour or/and iodine spiking.

If this ratio is more than 3, the coolant activity is due to superposition of two independent sources: failed rods and uranium surface contamination.

2nd step. In this case we calculate four values of $A_i = A_{mi} - A_m$(I-134) and then compute the "partial" values of release rate constant $\mu_1^{il}$:

$$\mu_1^{il} = \frac{\lambda_1 - \omega_{il}\lambda_i}{\omega_{il} - 1},$$

where

$$\omega_{il} = \frac{A_{mi}}{A_{mj}} \times \frac{A_{cj}(\mu_1 >> \lambda_j)}{A_{cj}(\mu_1 >> \lambda_i)},$$

3rd step. From the found values of $\mu_1^{il}$ we exclude negative values and values with pair (i,j) for which the next condition is satisfied:

$$\text{Mod}(1-\omega_{ij}) < \Delta\omega_{ij}$$

$\Delta\omega_{ij}$ values are calculated from known $\Delta A_{mi}$ values.
4th step. For other values of $\mu_1^{il}$ we generate the vector $\mu_r$ (r=1,2..,I) and calculate geometrical average value of $\mu_1$:

$$\overline{\mu_1} = \left\{ \prod_{r=1}^{I} \mu_1^r \right\}^{\frac{1}{I}}$$

as well as top and bottom deviations:

$$\mu_1^t = \overline{\mu_1} \times e^G$$
$$\mu_1^b = \overline{\mu_1} \times e^{-G}$$
$$G = \left[ \frac{1}{I-1} \sum_{r=1}^{I} \ln^2 \left( \frac{\overline{\mu_1}}{\mu_r} \right) \right]^{\frac{1}{2}}$$

5th step. Using found value of $\overline{\mu_1}$, we define calculated values of I-131,132,133,135 activities:

$$A_{ci}(\overline{\mu_1}) = A_{ci}(\mu_1 >> \lambda_i) \times \frac{\overline{\mu_1}}{\lambda_i + \overline{\mu_1}}$$

and estimated mean value of failed fuel rods with deviations:

$$N_T = \frac{1}{4} \times \sum_i \frac{A_{mi}}{A_{ci}(\overline{\mu_1})} \pm \Delta N_T,$$

$$\Delta N_T = \left[ \frac{1}{4} \sum_i \left( N_T - \frac{A_{mi}}{A_{ci}(\overline{\mu_1})} \right)^2 \right]^{\frac{1}{2}}$$

Formulae for $\overline{\mu_1}$ can be used at I>1. For the case when I=1, we use other expressions.

After these calculation we estimate the part of I-134 activity due to surface contamination:

$$A_{m2}(^{134}I) = A_m(^{134}I) - N_T \times A_{cI-134}(\overline{\mu_1})$$

and perform the next iteration returning to the 1st step. As a rule, two iterations are enough.

The last iteration gives the estimation of a number of leaking fuel rods and assessment of mean release rate constant $\mu_1$. The accuracy of leaking rod number estimation is assessed by the value of (-100%) – (+50%).

The described algorithm has been used for estimation of main sources of fission product activity in primary coolant of WWER-type reactors in Russia.

**Conclusion**

Regulation concept for the maximum permissible levels of WWER fuel cladding failure is described. Using verified RELWWER-2.0 computer code, the levels of fission product activity in primary coolant of operating WWER-type reactors appropriate to allowable levels of WWER fuel cladding failure are calculated. These values of activity were included in documents regulating normal operation of NPP's with WWER-type reactors. The conformity of levels, noticed in practice, of fission product activity in the primary coolant of operating reactors to a level of fuel rod damages is defined using the TIMS computer code for definition of the basic sources of fission product release and evaluation of the number of leaking fuel rods and mean defect characteristics.

**REFERENCES**


[1] "Nuclear Safety Rules for NPP Reactors" (PBYa-Ryu-AS-89), PNAE G-1-024-90, Atomnaya Energiya, V.69, Moscow (1990) 409 (in Russian).

[2] L.M. LUSANOVA and B.G. POLOGICH, A method to calculate the fission product activity in primary coolant of a water-cooled and water moderated power reactors. Preprint IAE-1968, Kurchatov Institute of atomic energy, Moscow (1970) (in Russian).

[3] L.M. LUSANOVA and P.D. SLAVYAGIN, Radioactive fission product release from failed fuel rods with sintered uranium dioxide. Preprint IAE-3723/4, Kurchatov Institute of atomic energy, Moscow (1983) (in Russian).

[4] C.E. BEYER, "An analytical model for estimating the number and size of defected fuel rods in an operating reactor", Proceedings of the ANS International Topical Meeting on LWR Fuel Performance, Avignon, France, April 21-24 (1991) 437.

[5] B.J. LEWIS, et al., "An expert system for the monitoring of failed fuel in CANDU reactors", Proceedings of the ANS International Topical Meeting on LWR Fuel Performance, Avignon, France, April 21-24 (1991) 385.

[6] W.N. ZINN, Power Reactor Tech., **3** (1960) 24.

[7] J. MOISIO, et al., "Experience of operation with leaking fuel at Loviisa NPS and examination of leaking assemblies", Proceedings of the ANS International Topical Meeting on LWR Fuel Performance, Avignon, France, April 21-24 (1991) 465.

[8] F. GARZAROLLI, et al., "Das Verhalten defeter Brennstabe bei weitergefuehrten Reactorbetrieb", Kerntechnik, Vol.20, No.10 (1978).

## LIST OF PARTICIPANTS


| | |
|---|---|
| BRAZIL | J.A. Perrotta<br>Nuclear and Energetic Research Institute, IPEN/CNEN-SP,<br>A. Prof. Lineu Prestes, 2242, Cidade Universitária,<br>05508 - 000 São Paulo |
| BULGARIA | V. Tzotcheva<br>Kozloduy NPP Plc,<br>P.B. 103, 3320 Kozloduy |
| CANADA | P. Akhtar<br>Canadian Nuclear Safety Commission,<br>280 Slater Street, P.O. Box 1046 Station "B",<br>Ottawa, Ontario K1P 5S9 |
| | Z. He<br>Atomic Energy of Canada Ltd, Chalk River Laboratories,<br>Chalk River, Ontario K0J 1J0 |
| CZECH REPUBLIC | D. Ernst<br>CEZ, a.s. Jaderna Elektrarna Temeline, 373 05 Temelin |
| | J. Hejna<br>Nuclear Research Institute Řež plc, 25068 Řež |
| | J. Kment<br>CEZ, Inc., NPP Dukovany, 675 50 Dukovany |
| | M. Martykán<br>NPP Temelin, 373 06 Temelin |
| FRANCE | K. Kitagawa<br>Nuclear Fuel Industries, Ltd, 10, rue de Louvois, F-75002 Paris |
| | D. Parrat<br>DEN/DEC/S3C, Centre de Cadarache,<br>F-13108 Saint Paul lez Durances |
| | C. Petit<br>Framatome ANP,<br>10, rue Juliette Récamier, F-69456 Lyon Cedex 06 |
| GERMANY | W. Klinger<br>Framatome ANP GmbH,<br>FGM, Bunsenstrasse 43, D-91058 Erlangen |
| | H.G. Sonnenburg<br>Gesellschaft für Anlagen- und Reaktorsicherheit mbH (GRS),<br>D-85748 Garching |

| | |
|---|---|
| HUNGARY | A. Kerkápoly<br>Budapest University of Technology and Economics,<br>Institute of Nuclear Techniques,<br>P.O. Box 49, H-1521 Budapest |
| | J. Schunk<br>Paks NPP, P.O. Box 71, H-7031 Paks |
| | J. Zsoldos<br>Hungarian Atomic Energy Authority,<br>Nuclear Safety Directorate,<br>Margit Krt 85, H-1024 Budapest |
| JAPAN | H. Hayashi<br>Nuclear Fuel Department,<br>Nuclear Power Engineering Corporation,<br>3-17-1 Toranomon, Minato-ku, Tokyo 105-0001 |
| | M. Susuki<br>Fuel Safety Research Laboratory,<br>Japan Atomic Energy Research Institute,<br>2-4Shirakata Shirane, Tokai-mura, Ibaraki-ken 319-119 |
| REPUBLIC OF KOREA | Je-Geon Bang<br>Korea Atomic Energy Research Institute,<br>Yusung, P.O. Box 105, Taejon |
| | Yong Song Kim<br>Nuclear Engineering Department, Hanyang University,<br>17 Haengdang-Dong, Sungdong-Ku, Seoul 133-791 |
| ROMANIA | E. Gheorghiu<br>Institute for Nuclear Research,<br>Mioveni, Str. Campului nr. 1, Pitesti |
| RUSSIAN FEDERATION | I. Chestakov<br>All-Russian Research Institute of Nuclear Power Plants (VNIIAES),<br>Ferganskaya 25, 109507 Moscow |
| | V. Chirkov<br>JSC “MSZ”, 12, K. Marx st.,<br>Electrostal, Moscow Region |
| | V. Miglo<br>Russian Research Centre “Kurchatov Institute”,<br>Acad. Kurchatov Sq., 1, 123182 Moscow |

B. Kanashov
State Scientific Centre (SSC),
Research Institute of Atomic Reactors (RIAR),
433510 Dimitrovgrad-10, Ulyanovk Region

V.V. Likhanskii
State Research Center of R.F. “TRINITI”,
142190 Troitsk, Moscow Region

V. Novikov
JSC TVEL, 24/26, B. Ordynka st., 109017 Moscow

M. Polozov
JSC “NZHK”, 94, B. Hmelnizki st., 630110 Novosibirsk

A. Sharikov
JSC TVEL, 24/26, B. Ordynka st., 101000 Moscow

V.J. Shishin
State Scientific Centre (SSC),
Research Institute of Atomic Reactors (RIAR),
433510 Dimitrovgrad-10, Ulyanovk Region

P. Slavyagin
Russian Research Centre “Kurchatov Institute”,
Acad. Kurchatov Sq., 1, 123182 Moscow

A.V. Smirnov
State Scientific Centre (SSC),
Research Institute of Atomic Reactors (RIAR),
433510 Dimitrovgrad-10, Ulyanovk Region

SLOVAKIA

J. Beňa
Bohunice NPP, 91931 Jaslovské Bohunice

P. Dařílek
VÚJE Trnava, Inc.,
Engineering, Design and Research Organization,
Okružná 5, 918 64 Trnava

B. Hatala
VÚJE Trnava, Inc.,
Engineering, Design and Research Organization,
Okružná 5, 918 64 Trnava

M. Kačmar
Bohunice NPP, 91931 Jaslovské Bohunice

P. Král
Slovenské elektrárne a.s., Atómové elektrárne Mochovce o.z.,
935 39 Mochovce